รายงานวิจัยฉบับสมบูรณ์

สมบัติทางไฟฟ้าของสารเซรามิกเฟร์โรอิเล็กตริกที่มีตะกั่วเป็นฐานภายใต้ความเค้นอัด

โดย

ผู้ช่วยศาสตราจารย์ ดร. รัตติกร ยิ้มนิรัญ

พฤษภาคม 2552

สัญญาเลขที่ RMU5080021

รายงานวิจัยฉบับสมบูรณ์

สมบัติทางไฟฟ้าของสารเซรามิก เฟร์โรอิเล็กตริกที่มีตะกั่วเป็นฐานภายใต้ความเค้นอัด

ผู้ช่วยศาสตราจารย์ ดร. รัตติกร ยิ้มนิรัญ
ภาควิชาฟิสิกส์และวัสดุศาสตร์ คณะวิทยาศาสตร์
มหาวิทยาลัยเชียงใหม่

สนับสนุนโดยสำนักงานคณะกรรมการการศึกษาอุดมศึกษา
และสำนักงานกองทุนสนับสนุนการวิจัย

กิตติกรรมประกาศ

ผู้วิจัยใคร่ขอขอบพระคุณ สำนักงานคณะกรรมการการศึกษาอุดมศึกษา (สกอ.) และสำนักงานกองทุนสนับสนุนการวิจัย (สกว.) ที่ได้ให้การสนับสนุนงานวิจัยและพัฒนาครั้งนี้ ผ่านทางทุนเพิ่มขีดความสามารถด้านการวิจัยของอาจารย์รุ่นกลาง ประจำปี พ.ศ. 2550 ขอขอบคุณภาควิชาฟิสิกส์และวัสดุศาสตร์ คณะวิทยาศาสตร์ มหาวิทยาลัยเชียงใหม่ ที่ช่วยอำนวยความสะดวกในการใช้เครื่องมือ อุปกรณ์ และ สถานที่ จนทำให้งานวิจัยเรื่องนี้สามารถดำเนินการจนสำเร็จผลได้ด้วยดี ขอขอบคุณผู้ร่วมงานและนักศึกษาทุกท่าน ที่มีส่วนช่วยเหลือผู้วิจัยให้ดำเนินงานชิ้นนี้สำเร็จลุล่วงได้ดี โดยเฉพาะ ดร. อธิพงศ์ งามจารุโรจน์ ดร. สุพัตรา วงศ์แสนใหม่ ดร. อนุรักษ์ ประสาทเขตต์การณ์ ดร. ปิยชนน์ เกษสุวรรณ ดร. เรวดี วงศ์มณีรุ่ง ดร. อรวรรณ คำมั่น ดร. นราธิป วิทยากร ดร. วรรณวิลัย วิทยากร คุณเมืองใจ อุ่นเรือน คุณณัฐพงศ์ วงศ์ดำเนิน คุณธนพงศ์ สารีอินธ์ คุณจิรภา ตั้งศรีตระกูล คุณศศิพร ประเสริฐปาลิฉัตร และคุณนฤทธ์ ตรีอำนรรค ขอขอบคุณผู้ช่วยศาสตราจารย์ ดร.ยงยุทธ เหล่าศิริถาวร สำหรับด้านงานคำนวณและงานด้านฟิสิกส์อื่นๆ ขอขอบคุณรองศาสตราจารย์ ดร.สุพล อนันตา ที่ได้ให้ความช่วยเหลือส่งเสริมเกื้อกูลในการทำงานเสมอมานับตั้งแต่วันเริ่มต้น ตลอดจนเป็นกำลังใจให้กันเสมอที่จะสู้และอยู่รอดในการทำวิจัยในสภาวะที่ยากที่จะกล่าวได้ ผู้วิจัยต้องขอบคุณความร่วมมือที่ได้รับอย่างดีจากนักวิจัยที่ปรึกษาและเพื่อนร่วมงานในต่างประเทศ ได้แก่ Prof. Amar Bhalla แห่ง University of Texas at San Antonio Prof. Xiaoli Tan แห่ง Iowa State University และ Prof. David Cann แห่ง Oregon State University

ท้ายที่สุดนี้ขอมอบความดีทั้งหมดให้แทนคำขอบคุณสำหรับ คุณวิภา ยิ้มนิรัญ ภรรยา และด.ช. รัญชน์ ยิ้มนิรัญ ลูกชาย คงไม่มีความสำเร็จใดๆเกิดขึ้นได้ถ้าปราศจากความรักและความเข้าใจ รอยยิ้มแห่งความสุข คำปลอบเมื่อยามท้อ ตลอดจนกำลังใจและความอดทนที่ครอบครัวมอบให้ผู้วิจัยตลอดมาจนสามารถมาถึง ณ วันนี้ได้

"ขอขอบคุณทุกคนอีกครั้งที่ร่วมสุขและร่วมทุกข์ด้วยกันมาตลอด"

"*Despite all the struggles we have had to face and endure; at last my friends, we still make it to where we have planned all along via our own way*"

This work is dedicated to my two "*teachers*" who have inspired me and recently passed away during the course of this work

Drs. Robert E. Newnham and Anthony J. Moulson

(ผู้ช่วยศาสตราจารย์ ดร. รัตติกร ยิ้มนิรัญ)

หัวหน้าโครงการ

บทคัดย่อ

รหัสโครงการ : RMU5080021

ชื่อโครงการ : สมบัติทางไฟฟ้าของสารเซรามิกเฟร์โรอิเล็กตริกที่มีตะกั่วเป็นฐานภายใต้ความเค้นอัด

ชื่อนักวิจัย : ผศ.ดร. รัตติกร ยิ้มนิรัญ

ภาควิชาฟิสิกส์และวัสดุศาสตร์ คณะวิทยาศาสตร์ มหาวิทยาลัยเชียงใหม่

E-mail Address : rattikornyimnirun@yahoo.com

ระยะเวลาโครงการ : 25 มิถุนายน 2550 ถึง 25 มิถุนายน 2552

ในการวิจัยนี้ได้ทำการศึกษาสมบัติทางไฟฟ้าภายใต้ความเค้นอัดของสารเซรามิกเฟร์โรอิเล็กตริกที่มีตะกั่วเป็นฐานที่สำคัญ กล่าวคือ PT PZT PIN PMN PZN PCoN PNN PZN-PZT PMN-PT PIN-PT PCoN-PZT และ PNN-PZT โดยสามารถแบ่งผลงานที่ได้จากโครงการวิจัยนี้ออกเป็น 4 กลุ่มใหญ่ กล่าวคือ 1. กระบวนการเตรียมผงและเซรามิก 2. สมบัติไดอิเล็กตริกและทางไฟฟ้าอื่นๆของสารเซรามิก 3. อิทธิพลของความเค้นแบบแกนเดี่ยวต่อสมบัติไดอิเล็กตริกและทางไฟฟ้าอื่นๆของสารเซรามิกทั้งหมดที่กล่าวมาข้างต้น และ 4. การศึกษาหาองค์ความรู้ใหม่ด้านอื่นๆที่ถือเป็นการต่อยอดจากผลงานที่ได้ศึกษามาในเบื้องต้น ซึ่งกลุ่มผู้วิจัยได้ประสบความสำเร็จในการเตรียมผงและเซรามิกด้วยการใช้เทคนิคผสมออกไซด์ร่วมกับเทคนิคการบดย่อยละเอียด โดยได้ทราบถึงเงื่อนไขที่เหมาะสมต่อการเตรียมผงให้มีความบริสุทธิ์สูง และพบเงื่อนไขในการเผาที่เหมาะสมต่อการเตรียมเซรามิกแต่ละชนิดที่กล่าวมาเหล่านี้ให้มีความบริสุทธิ์และความหนาแน่นสูง และจากการตรวจสอบคุณลักษณะเฉพาะและคุณสมบัติทางไฟฟ้าต่างๆของเซรามิกที่เตรียมได้ก็พบว่าสารเซรามิกที่เตรียมได้นั้นแสดงคุณลักษณะเฉพาะเป็นสารเซรามิกเฟร์โรอิเล็กตริกแบบปกติ หรือสารเซรามิกเฟร์โรอิเล็กตริกกลุ่มรีแลกเซอร์ หรือสารเซรามิกที่แสดงลักษณะผสมกันระหว่างเซรามิกเฟร์โรอิเล็กตริกแบบปกติและสารเซรามิกเฟร์โรอิเล็กตริกกลุ่มรีแลกเซอร์ ทั้งนี้ขึ้นกับชนิดของสารเซรามิกและอัตราส่วนผสม และจากการศึกษาอิทธิพลของความเค้นแบบแกนเดี่ยวต่อสมบัติไดอิเล็กตริกและทางไฟฟ้าอื่นๆของสารเซรามิกก็พบว่าความเค้นมีผลอย่างชัดเจนในการเปลี่ยนแปลงสมบัติต่างๆในสารเซรามิกทุกระบบ โดยมีทิศทางและอัตราการเปลี่ยนแปลงที่ขึ้นอยู่กับชนิดของสารเซรามิกและอัตราส่วนผสม ท้ายที่สุดนั้นผลการศึกษาในโครงการวิจัยนี้ได้นำไปสู่ผลงานการตีพิมพ์ในระดับนานาชาติแล้วกว่า 50 เรื่อง

คำหลัก: ความเค้นแบบแกนเดี่ยว; สมบัติทางไฟฟ้า; สารเซรามิกเฟร์โรอิเล็กตริก

Abstract

Project Code : RMU5080021

Project Title : Electrical Properties of Lead-Based Ferroelectric Ceramics Under Compressive Stress

Investigators : Asst. Prof. Dr. Rattikorn Yimnirun

Department of Physics and Materials Science, Faculty of Science, Chiang Mai University

E-mail Address : rattikornyimnirun@yahoo.com

Project Period : June 25, 2007 to June 25, 2009

In this study, effects of uniaxial stress on the electrical properties of important ceramics in PT PZT PIN PMN PZN PCoN PNN PZN-PZT PMN-PT PIN-PT PCoN-PZT and PNN-PZT systems were investigated. The outputs of this project can be divided into 4 main groups; namely, 1. powder and ceramic fabrication, 2. dielectric and other electrical properties, 3. effects of uniaxial stress on dielectric and other electrical properties of all the prepared ceramics, and 4. new body of knowledge arised from the above-mentioned studies. We have successfully prepared powders and ceramics by using the mixed-oxide technique in conjunction with the vibro-milling technique and found suitable conditions for preparing high purity powders and for fabricating each ceramic to high purity and density. From the characterization and electrical properties measurements, the prepared ceramics exhibit either normal or relaxor or mixed ferroelectric characteristics, depending upon the type of ceramics and composition ratio. Similarly, the uniaxial stress studies also indicate that the applied stress impose significant influence on the electrical properties with the direction and rate of change depending on the type of ceramics and composition ratio. Finally, the results from this project have resulted in more than 50 international publications.

Keywords : Uniaxial Stress; Electrical Properties; Ferroelectric Ceramics

Executive Summary

แบเรียมไทเทเนต ($BaTiO_3$) หรือ BTเลดไทเทเนต ($PbTiO_3$) หรือ PT เลดเซอร์โคเนตไทเทเนต ($Pb(Zr,Ti)O_3$) หรือ PZT เลดแมกนีเซียมไนโอเบต ($Pb(Mg_{1/3}Nb_{2/3})O_3$) หรือ PMN เลดซิงค์ไนโอเบต ($Pb(Zn_{1/3}Nb_{2/3})O_3$) หรือ PZN เลดนิกเกิลไนโอเบต ($Pb(Ni_{1/3}Nb_{2/3})O_3$) หรือ PNN เลดโคบอลท์ไนโอเบต ($Pb(Co_{1/3}Nb_{2/3})O_3$) หรือ PCoN และ เลดอินเดียมไนโอเบต ($Pb(In_{1/2}Nb_{1/2})O_3$) หรือ PIN ล้วนแล้วแต่เป็นสารซรามิกเฟร์โรอิเล็กตริก (ferroelectrics) ที่ถูกพัฒนาขึ้นมาเพื่อใช้ประโยชน์ในอุปกรณ์อิเล็กทรอนิกส์ประเภทต่างๆ อย่างไรก็ตามโดยทั่วไปแล้ว ในสภาวะการใช้งานจริงของอุปกรณ์อิเล็กทรอนิกส์ที่ผลิตจากสารเซรามิกเฟร์โรอิเล็กตริกดังที่กล่าวมาแล้วนั้น สารเซรามิกมักจะอยู่สภาวะภายใต้ความเค้น ซึ่งอาจจะเกิดจากความเค้นเชิงกลภายนอกระหว่างการใช้งาน หรือความเค้นเชิงกลภายในอันเกิดจากการที่สารเซรามิกเหล่านี้ ดังนั้นข้อมูลเกี่ยวกับสมบัติไดอิเล็กตริกภายใต้อิทธิพลของความเค้น จึงมีความสำคัญอย่างมากต่อการออกแบบ การจัดสร้างและการใช้งานของอุปกรณ์อิเล็กทรอนิกส์ที่ผลิตจากสารเซรามิกเฟร์โรอิเล็กตริกเหล่านี้ ดังนั้นผู้วิจัยจึงทำการศึกษาอย่างเป็นระบบถึงอิทธิพลของความเค้นต่อสมบัติทางไฟฟ้าของสารเซรามิกเฟร์โรอิเล็กตริกที่สำคัญ กล่าวคือ PT PZT PIN PMN PZN PCoN PNN PZN-PZT PMN-PT PIN-PT PCoN-PZT และ PNN-PZT โดยสามารถแบ่งผลงานที่ได้จากโครงการวิจัยนี้ออกเป็น 4 กลุ่มใหญ่ กล่าวคือ 1. กระบวนการเตรียมผงและเซรามิก 2. สมบัติไดอิเล็กตริกและทางไฟฟ้าอื่นๆของสารเซรามิก 3. อิทธิพลของความเค้นแบบแกนเดี่ยวต่อสมบัติไดอิเล็กตริกและทางไฟฟ้าอื่นๆของสารเซรามิกทั้งหมดที่กล่าวมาข้างต้น และ 4. องค์ความรู้ใหม่ด้านอื่นๆที่ถือเป็นการต่อยอดจากผลงานที่ได้ศึกษามาในเบื้องต้น ซึ่งกลุ่มผู้วิจัยได้ประสบความสำเร็จในการเตรียมผงและเซรามิกด้วยการใช้เทคนิคผสมออกไซด์ร่วมกับเทคนิคการบดย่อยละเอียด โดยได้ทราบถึงเงื่อนไขที่เหมาะสมต่อการเตรียมผงให้มีความบริสุทธิ์สูง และพบเงื่อนไขในการเผาที่เหมาะสมต่อการเตรียมเซรามิกแต่ละชนิดที่กล่าวมาเหล่านี้ให้มีความบริสุทธิ์และความหนาแน่นสูง และจากการตรวจสอบคุณลักษณะเฉพาะและคุณสมบัติทางไฟฟ้าต่างๆของเซรามิกที่เตรียมได้ก็พบว่าสารเซรามิกที่เตรียมได้นั้นแสดงคุณลักษณะเฉพาะเป็นสารเซรามิกเฟร์โรอิเล็กตริกแบบปกติ หรือสารเซรามิกเฟร์โรอิเล็กตริกกลุ่มรีแลกเซอร์ หรือสารเซรามิกที่แสดงลักษณะผสมกันระหว่างเซรามิกเฟร์โรอิเล็กตริกแบบปกติและสารเซรามิกเฟร์โรอิเล็กตริก กลุ่มรีแลกเซอร์ ทั้งนี้ขึ้นกับชนิดของสารเซรามิกและอัตราส่วนผสม และจากการศึกษาอิทธิพลของความเค้นแบบแกนเดี่ยวต่อสมบัติไดอิเล็กตริกและทางไฟฟ้าอื่นๆของสารเซรามิกก็พบว่าความเค้นมีผลอย่างชัดเจนในการเปลี่ยนแปลงสมบัติต่างๆในสารเซรามิกทุกระบบ โดยมีทิศทางและอัตราการเปลี่ยนแปลงที่ขึ้นอยู่กับชนิดของสารเซรามิกและอัตราส่วนผสม

เนื้อหางานวิจัย

1. ความสำคัญและที่มาของปัญหาที่ทำการวิจัย

สารเซรามิกเฟร์โรอิเล็กตริกสามารถแบ่งได้เป็น 2 ประเภทใหญ่ๆ จากลักษณะของการเปลี่ยนแปลงเฟสและการตอบสนองต่อความถี่ คือ สารเซรามิกเฟร์โรอิเล็กตริกแบบปกติ (normal ferroelectrics) และสารเซรามิกเฟร์โรอิเล็กตริกกลุ่มรีแลกเซอร์ (relaxor ferroelectrics) ซึ่งในกลุ่มแรกนั้นการเปลี่ยนเฟสจะเกิดขึ้นอย่างรวดเร็ว (sharp transition) บริเวณอุณหภูมิคูรี (Curie temperature: T_C) และมีสมบัติไดอิเล็กตริกที่ไม่ค่อยขึ้นกับความถี่ ในขณะที่สารเซรามิกในกลุ่มที่สองนั้นจะเกิดการเปลี่ยนเฟสแบบช้าๆ (diffuse phass transition) และมีสมบัติไดอิเล็กตริกที่เปลี่ยนแปลงกับความถี่อย่างชัดเจน ตัวอย่างสารเซรามิกเฟร์โรอิเล็กตริกแบบปกติที่สำคัญได้แก่ แบเรียมไทเทเนต ($BaTiO_3$) หรือ BT เลดไทเทเนต ($PbTiO_3$) หรือ PT และเลดเซอร์โคเนตไทเทเนต ($Pb(Zr,Ti)O_3$) หรือ PZT ในขณะตัวอย่างของสารเซรามิกเฟร์โรอิเล็กตริกกลุ่มรีแลกเซอร์ ที่สำคัญประกอบด้วย เลดแมกนีเซียมไนโอเบต ($Pb(Mg_{1/3}Nb_{2/3})O_3$) หรือ PMN เลดซิงค์ไนโอเบต ($Pb(Zn_{1/3}Nb_{2/3})O_3$) หรือ PZN เลดนิกเกิลไนโอเบต ($Pb(Ni_{1/3}Nb_{2/3})O_3$) หรือ PNN เลดโคบอลท์ไนโอเบต ($Pb(Co_{1/3}Nb_{2/3})O_3$) หรือ PCoN และ เลดอินเดียมไนโอเบต ($Pb(In_{1/2}Nb_{1/2})O_3$) หรือ PIN ซึ่งสารเหล่านี้ล้วนแล้วแต่เป็นสารที่ถูกพัฒนาขึ้นมาเพื่อใช้ประโยชน์ในอุปกรณ์อิเล็กทรอนิกส์ประเภทต่างๆ เช่น ตัวเก็บประจุไฟฟ้า ตัวต้านทาน เทอร์มิสเตอร์ เซนเซอร์ แอกทัวเอเทอร์ ทรานสดิวเซอร์ หม้อแปลงไฟฟ้า บัซเซอร์ในลำโพง อุปกรณ์ตรวจสอบตำหนิหรือรอยร้าวในวัสดุแบบไม่ทำลาย ตัวบังคับการสั่นของหัวเข็มในเครื่องมือขูดหินปูน อุปกรณ์ทำความสะอาดเครื่องมือทางการแพทย์ด้วยอัลตร้าโซนิกส์ หัวตรวจวัดอัลตร้าซาวด์ หัวตรวจวัดความดันโลหิต และหุ่นยนต์ขนาดจิ๋วสำหรับใช้ในการตรวจอวัยวะภายในแบบไร้สาย เป็นต้น [1-9] ซึ่งโดยหลักการพื้นฐานแล้ววัสดุที่มีศักยภาพเหมาะสมสำหรับการนำมาประยุกต์ใช้ในงานต่างๆเหล่านี้นั้น จะต้องมีคุณลักษณะที่สำคัญอันได้แก่ การมีค่าสภาพยอมสัมพัทธ์ที่เหมาะสม ในช่วงของอุณหภูมิและความถี่สำหรับการทำงานของอุปกรณ์ มีค่าสัมประสิทธิ์ไฟฟ้าเชิงกลคู่ควบสูง สามารถทำการจัดเรียงไดโพลภายในเนื้อสารได้ง่าย มีการสูญเสียของพลังงานในระหว่างการใช้งานที่ต่ำ มีอายุการใช้งานนานและที่สำคัญต้องสามารถทำการเตรียมได้ง่าย โดยมีค่าใช้จ่ายไม่มากและปลอดภัย สามารถหาวัตถุดิบได้ง่าย และต้องการอุณหภูมิเผาที่ไม่สูงมากนัก เป็นต้น ซึ่งโดยทั่วไปแล้วนั้น การผสมผสานของคุณสมบัติที่ดีต่างๆเหล่านี้ไม่สามารถพบได้ในวัสดุเดี่ยวๆตัวใดตัวหนึ่งที่กล่าวมาในข้างต้นได้ เนื่องจากวัสดุแต่ละชนิดต่างก็มีข้อดีและข้อเสียที่แตกต่างกันไปในลักษณะที่มีความเฉพาะตัวมาก ดังนั้นการศึกษาวิจัยเพื่อค้นหาวัสดุชนิดใหม่ๆ ที่อาศัยหลักการนำเอาวัสดุหลักๆที่มีอยู่เดิมมารวมเข้าด้วยกัน ที่สามารถจะผสมผสานข้อดีและช่วยบรรเทาข้อเสียของแต่ละวัสดุที่เป็นองค์ประกอบหลักได้อย่างลงตัว จึงเป็นวิธีการหนึ่งที่ได้รับความสนใจอย่างมากทั้งในแวดวงวิชาการและในวงการอุตสาหกรรม ทำ

ให้ในปัจจุบันมีสารเซรามิกเฟร์โรอิเล็กตริกชนิดใหม่ๆที่มีความสลับซับซ้อนยิ่งขึ้นจำนวนมากเกิดขึ้นมาเช่น BT-PT, BT-PZT, PZT-PZN, PMN-PT, PMN-PZN, PMN-PZT, PIN-PT, PIN-PMN, PIN-PZN, PNN-PZT, PCoN-PZT, BT-PMN-PZN, PT-PMN-PZN, PMN-PT-BT, PZT-PZN-PMN และ PMN-PT-PIN เป็นต้น [1-3,10-20] และงานวิจัยทางด้านนี้ส่วนใหญ่เน้นถึงการศึกษาถึงอิทธิพลของปัจจัยหลักในกระบวนการผลิตที่มีต่อพฤติกรรมการเกิดเฟส โครงสร้างจุลภาคและสมบัติไดอิเล็กตริก สมบัติเฟร์โรอิเล็กตริกและสมบัติไฟฟ้าเชิงกลของสารเซรามิกที่ผลิตขึ้น [10-24]

เลดไทเทเนต ($PbTiO_3$) หรือ PT นั้นเป็นสารเฟร์โรอิเล็กตริกที่มีสมบัติพิโซอิเล็กตริก (piezoelectrics) และไพโรอิเล็กตริก (pyroelectrics) โดดเด่นมากตัวหนึ่งและเหมาะสำหรับการนำไปใช้ในงานที่ต้องมีอุณหภูมิและความถี่สูงๆอย่างมาก [3-7] แต่ก็ติดอยู่ตรงที่ว่ามีค่าเตตระกอนอลิตี้ (tetragonality) หรือ c/a สูงมากๆ (~ 1.065) [3] ทำให้ PT เป็นสารที่มีความเครียดภายในสูงมากดังนั้นการเตรียมเป็นชิ้นงานเซรามิกจึงกระทำได้ยากมาก เพราะชิ้นงานจะแตกออกเป็นเสี่ยงเสมอ จึงนิยมทำการเติมสารเจือเพื่อลดความเครียดภายในเนื้อสาร หรือไม่ก็นำไปรวมกับสารชนิดอื่นๆก่อนจะนำไปใช้งานต่อไป เช่น BT-PT, PZT, PZN-PT และ PMN-PT เป็นต้น [1,2,25-27]

เลดเซอร์โคเนตไทเทเนต $Pb(Zr,Ti)O_3$ หรือ PZT นั้นเป็นสารละลายของแข็งระหว่าง $PbZrO_3$ กับ $PbTiO_3$ ที่ถูกจัดเป็นต้นแบบของสารเซรามิกพิโซอิเล็กตริกที่มีการศึกษาค้นคว้ากันอย่างกว้างขวางมาก โดยนิยมนำมาใช้ในที่จุดเตาแก๊ส บัซเซอร์ในลำโพง หัวฉีดหมึกในปริ้นส์เตอร์ โซนาร์ และทรานสดิวเซอร์ที่ใช้กันในเครื่องอัลทราโซนิกส์ เป็นต้น [2-5] เนื่องจาก PZT เป็นสารที่มีค่าตัวประกอบไฟฟ้าเชิงกลคู่ควบ (~ 0.65) และอุณหภูมิคูรี (> 400 ^{o}ซ) สูงกว่า BT มาก จึงเหมาะสำหรับการนำไปใช้ในอุปกรณ์ทรานสดิวเซอร์พลังงานสูงที่ต้องมีการใช้งานที่อุณหภูมิสูง นอกจากนี้ PZT ยังเป็นสารที่มีค่าสภาพยอมสัมพัทธ์ใกล้เคียงกับ BT แต่ว่าต้องการอุณหภูมิเผาซินเตอร์ที่ต่ำกว่า (~ 1200 ^{o}ซ) PZT เป็นสารที่สามารถทำการโพลลิ่ง (poling) เพื่อจัดเรียงไดโพลภายในสารได้ง่ายกว่า BT และยังมีช่วงของค่าสภาพยอมสัมพัทธ์กว้างกว่า BT มาก [5,7] นอกจากนี้ สมบัติเฟร์โรอิเล็กตริก พิโซอิเล็กตริก และไพโรอิเล็กตริกที่สำคัญของสาร PZT นั้นสามารถควบคุมได้โดยการปรับเปลี่ยนที่ค่าอัตราส่วนของ Zr ต่อ Ti ทำให้สามารถสร้างสาร PZT ที่มีค่าสภาพยอมสัมพัทธ์ได้หลากหลายมาก ซึ่งค่าอัตราส่วนของZr/Tiที่ 52/48 53/47 และ 55/45 จะเป็นสูตรที่ได้รับความนิยมสูงมากเพราะเป็นสูตรที่อยู่แถวบริเวณแนว Morphotropic Phase Boundary (MPB) ที่มีทั้งเฟสของPZTแบบเตตระกอนอลและรอมโบฮีดรอลอยู่ร่วมกัน ทำให้สาร PZT ที่มีสัดส่วนทางเคมีอยู่แถวบริเวณนี้มีค่าสภาพยอมสัมพัทธ์และค่าสัมประสิทธ์พิโซอิเล็กตริกคู่ควบสูงมาก [1,3] สำหรับข้อด้อยของสาร PZTนั้นก็มีอยู่หลายประการคือ เป็นสารที่มีค่าการสูญเสียทางไดอิเล็กตริกสูง (~ 4.0%) มีความล้า (fatigue) และการสูญเสียของพลังงานสูงมาก (มีสมบัติ Hysteresis ซึ่งไม่เป็นที่ต้องการในการใช้งานที่ต้องการความละเอียดอ่อน) เมื่อผ่านการใช้งานทำให้มีอายุการใช้งานสั้น และที่สำคัญ PZT เป็นสารที่มี

อุณหภูมิคูรีค่อนข้างสูง ($T_C \sim 200 - 400$ °ซ ขึ้นกับค่า Zr/Ti) ทำให้การใช้ประโยชน์สูงสุดของสารถูกจำกัดอยู่ที่อุณหภูมิสูงๆเท่านั้น [1-3]

สารเฟร์โรอิเล็กตริกกลุ่มรีแลกเซอร์ (relaxor ferroelectrics) เช่น เลดแมกนีเซียมไนโอเบต ($Pb(Mg_{1/3}Nb_{2/3})O_3$) หรือ PMN ซึ่งถือว่าเป็นต้นแบบของพวกรีแลกเซอร์นั้นเป็นสารที่พึ่งถูกพัฒนาขึ้นมาภายหลัง PZT แต่ว่ามีค่าสภาพยอมสัมพัทธ์สูงและมีช่วงอุณหภูมิที่เหมาะสำหรับการใช้งานกว้างมากกว่าสาร PZT โดยครอบคลุมถึงช่วงอุณหภูมิห้อง นอกจากนี้ PMN ยังเป็นสารที่ต้องการอุณหภูมิสำหรับเผาซินเตอร์ต่ำกว่า PZT (< 1200 °ซ) ทำให้สามารถใช้วัสดุที่มีจุดหลอมเหลวต่ำเช่น เงิน ทองแดง หรือ เงินผสมปัลลาเดียม ซึ่งมีราคาถูกมาทำเป็นขั้วไฟฟ้าได้ [3,28] PMN เป็นสารที่มีลักษณะเฉพาะทางจุลภาคที่ส่งผลทำให้มีการสูญเสียพลังงานต่ำเมื่อผ่านการใช้งานและไม่มีสมบัติ Hysteresis ทำให้มีประสิทธิภาพในการส่งถ่ายพลังงานสูงกว่าสาร PZT ในปัจจุบันจึงนิยมนำสาร PMN มาใช้ในพวกตัวเก็บประจุไฟฟ้าแบบหลายชั้นและอุปกรณ์อิเล็กทรอนิกส์ที่ต้องการความละเอียดอ่อนสูงๆเช่น หัววัดทรานสดิวเซอร์ทางการแพทย์ และตัวขับเร้า (acturtors) เป็นต้น [5-7] แต่อย่างไรก็ตาม PMN ก็เป็นสารที่มีค่าสัมประสิทธิ์ไฟฟ้าเชิงกลคู่ควบต่ำกว่า PZT มาก และยังมีพฤติกรรมทางไดอิเล็กตริกที่เปลี่ยนแปลงตามความถี่ของสัญญาณอีกด้วย [3,5] และที่สำคัญการเตรียมสาร PMN ให้มีความบริสุทธิ์สูงนั้นกระทำได้ยากกว่าการเตรียมสาร PZT เนื่องจากจะพบว่ามีการเกิดเฟสไพโรคลอร์ (pyrochlores) ที่เป็นสารประกอบของ $PbO\text{-}Nb_2O_5$ เกิดขึ้นปะปนอยู่เสมอ และส่งผลในแง่ลบต่อสมบัติทางไฟฟ้าของเซรามิก PMN [29-31]

ในช่วงสองทศวรรษที่ผ่านมา เลดซิงค์ไนโอเบต ($Pb(Zn_{1/3}Nb_{2/3})O_3$) หรือ PZN เป็นสารเฟร์โรอิเล็กตริกกลุ่มรีแลกเซอร์ที่ได้รับความสนใจมากเป็นพิเศษ เนื่องจากมีสมบัติไดอิเล็กตริก สมบัติพิโซอิเล็กตริก และสมบัติอิเล็กโทรสตริกทีฟที่โดดเด่นมาก โดยผลึกเชิงเดี่ยวของ PZN มีค่าสัมประสิทธิ์สมบัติพิโซอิเล็กตริก (d_{33}) ค่าความเครียดที่ถูกเหนี่ยวนำจากสนามไฟฟ้า (s) และค่าคงที่ไฟฟ้าเชิงกลคู่ควบ (k_{33}) ที่สูงถึง 2500 pm/V 1.7% และ 90% ตามลำดับ ทำให้เกิดความสนใจอย่างกว้างขวางในการที่จะนำสาร PZN ไปประยุกต์ใช้ในแอกทัวเอเทอร์และหัวตรวจวัดอัลตร้าซาวด์ [9,14,15,32,33] อย่างไรก็ตาม สาร PZN ในรูปแบบที่เป็นเซรามิกก็มีความยากลำบากในการเตรียมมากเนื่องจากจะเกิดเฟสไพโรคลอร์ที่มีผลทำให้สมบัติทางไฟฟ้าของเซรามิก PZN ลดลง และโดยทั่วไปจะต้องการทำให้เกิดเสถียรภาพของเฟสเพอรอฟสไกด์ด้วยการเติมสารอื่น เช่น BT หรือ PZT ลงไป หรือการเตรียมสารด้วยวิธีเคมีกล (mechanochemical) [34] นอกจากนี้ ยังได้มีการพบว่า นอกจาก PZN แล้ว เลดนิกเกิลไนโอเบต ($Pb(Ni_{1/3}Nb_{2/3})O_3$) หรือ PNN เลดโคบอลท์ไนโอเบต ($Pb(Co_{1/3}Nb_{2/3})O_3$) หรือ PCoN ซึ่งก็เป็นสารเฟร์โรอิเล็กตริกกลุ่มรีแลกเซอร์ก็ได้รับความสนใจมากเป็นพิเศษ เนื่องสารละลายของแข็งระหว่าง PZT และ PZN PNN และ PCoN นั้นมีมีสมบัติไดอิเล็กตริก สมบัติพิโซอิเล็กตริก และสมบัติอิเล็กโทรสตริกทีฟที่โดดเด่นมาก ทำให้ได้รับการศึกษาอย่างกว้างขวาง [35-39]

เลดอินเดียมไนโอเบต ($Pb(In_{1/2}Nb_{1/2})O_3$) หรือ PIN เป็นสารเฟร์โรอิเล็กตริกกลุ่มรีแลกเซอร์ที่ได้รับความสนใจเนื่องจากความพิเศษที่ว่า PIN สามารถเปลี่ยนลักษณะของโครงสร้างไปมาระหว่างแบบมีระเบียบ (order) และแบบไม่มีระเบียบ (disorder) ด้วยการอบอุ่น (annealing) ที่อุณหภูมิที่เหมาะสม โดยเมื่อ PIN อยู่ในสถานะแบบไม่มีระเบียบนั้นจะมีสมบัติเฟร์โรอิเล็กตริกและมีโครงสร้างแบบ pseudo-cubic โดยอุณหภูมิที่ค่าคงที่ไดอิเล็กตริกมีค่าสูงสุด (T_m) อยู่ที่ 66 °ซ ในขณะที่ในสถานะแบบมีระเบียบนั้น PIN จะเปลี่ยนไปเป็นสารแอนตีเฟร์โรอิเล็กตริกที่มีโครงสร้างแบบออทรอรอมบิค (orthorhombic) ซึ่งมีอุณหภูมิการเปลี่ยนเฟสที่ 190 °ซ [15,17,40]

โดยทั่วไปแล้วนั้น เนื่องจากวัสดุแต่ละชนิดต่างก็มีข้อดีและข้อเสียที่แตกต่างกันไปในลักษณะที่มีความเฉพาะตัวมาก ดังนั้นการศึกษาวิจัยเพื่อค้นหาวัสดุชนิดใหม่ๆ ที่อาศัยหลักการนำเอาวัสดุหลักๆที่มีอยู่เดิมมารวมเข้าด้วยกัน ที่สามารถจะผสมผสานข้อดีและช่วยบรรเทาข้อเสียของแต่ละวัสดุที่เป็นองค์ประกอบหลักได้อย่างลงตัว จึงเป็นวิธีการหนึ่งที่ได้รับความสนใจอย่างมากทั้งในแวดวงวิชาการและในวงการอุตสาหกรรม โดยเฉพาะการรวมกันระหว่างสารเซรามิกเฟร์โรอิเล็กตริกแบบปกติ เช่น PT และ PZT และสารเซรามิกเฟร์โรอิเล็กตริกกลุ่มรีแลกเซอร์ เช่น PMN PZN PNN PCoN และ PIN นั้นจะได้รับความสนใจเป็นพิเศษ เนื่องจากมีสมบัติที่โดดเด่นมาก ทำให้ในปัจจุบันมีสารเซรามิกเฟร์โรอิเล็กตริกชนิดใหม่ๆที่มีความสลับซับซ้อนยิ่งขึ้นจำนวนมากเกิดขึ้น [10-24]

ในช่วงหลายปีที่ผ่านมานี้การพัฒนาสารเฟร์โรอิเล็กตริกชนิดใหม่ๆที่มี PMN เป็นองค์ประกอบหลักเริ่มได้รับความสนใจเพิ่มมากขึ้นเรื่อยๆนับตั้งแต่มีการค้นพบว่าสารในระบบ PMN-PT สูตรที่มีปริมาณของ PT ไม่เกิน 30% นั้นมีค่าสภาพยอมสัมพัทธ์ที่สูงมาก (~ 24000) และมีศักยภาพเหมาะสำหรับการพัฒนาไปใช้ในพวกตัวขับเร้าจุลภาค (microactuators) หรือตัวเก็บประจุไฟฟ้าได้ [41-43] แต่ก็ยังมีข้อด้อยอยู่ที่การมีค่าการสูญเสียทางไดอิเล็กตริกที่สูงใกล้เคียงกับสาร PZT และมีค่าตัวประกอบคุณภาพเชิงกลที่ต่ำ นอกจากนี้ยังต้องใช้เวลาในการเผาซินเตอร์ที่นานมาก [41,42]

สารเซรามิกเฟร์โรอิเล็กตริก PZN-PZT นอกจากจะมีเสถียรภาพของเฟสเพอรอพสไกต์ที่ดีแล้วนั้น ยังมีสมบัติไดอิเล็กตริกและสมบัติพิโซอิเล็กตริกที่ดี โดยมีค่าสัมประสิทธิ์สมบัติพิโซอิเล็กตริก (d_{33}) ค่าความเครียดที่ถูกเหนี่ยวนำจากสนามไฟฟ้า (2 kV/mm) (s) และค่าคงที่ไฟฟ้าเชิงกลคู่ควบ (k_p) ที่สูงถึง 430 pC/N 0.24% และ 67% ตามลำดับ ซึ่งเหมาะสมที่จะนำไปประยุกต์ใช้ในแอกทัวเอเทอร์ หม้อแปลงไฟฟ้า และมอเตอร์กำลังสูง ทั้งนี้สารเซรามิกเฟร์โรอิเล็กตริก PZN-PZT ยังสามารถซินเตอร์ได้ที่อุณหภูมิที่ต่ำกว่า 1100 °ซ [44,45] นอกจากนี้ ยังพบว่าสารเฟร์โรอิเล็กตริกในกลุ่มเดียวกันกล่าวคือ PNN-PZT และ PCoN-PZT ก็ยังสมบัติไดอิเล็กตริกและสมบัติพิโซอิเล็กตริกที่โดดเด่นไม่แพ้ PZN-PZT จึงมีการศึกษาอย่างแพร่หลายเช่นกัน [35-39] อย่างไรก็ตาม ถึงแม้ว่าสารที่มีพื้นฐานมาจาก PZN นั้นจะมีสมบัติที่น่าสนใจมาก แต่สารเหล่านั้นมักจะไม่สารถใช้งานที่อุณหภูมิที่สูงเกิน 85 °ซ ทั้งนี้เนื่องจากอุณหภูมิคูรีที่ค่อนข้างต่ำ [15]

ดังนั้นจึงมีความต้องการสารที่มีค่าคงที่ไฟฟ้าเชิงกลคู่ควบที่มากและอุณหภูมิคูรีที่สูงกว่า 250 °ซ สาร PIN-PT เป็นหนึ่งในสารที่ได้รับความสนใจเป็นพิเศษเนื่องจากเป็นสารเฟร์โรอิเล็กตริกกลุ่มรีแลกเซอร์ที่มีอุณหภูมิคูรีที่สูงกว่า 250 °ซ [15]

อย่างไรก็ตามโดยทั่วไปแล้ว ในสภาวะการใช้งานจริงของอุปกรณ์อิเล็กทรอนิกส์ที่ผลิตจากสารเซรามิกเฟร์โรอิเล็กตริกดังที่กล่าวมาแล้วนั้น สารเซรามิกมักจะอยู่สภาวะภายใต้ความเค้น ซึ่งอาจจะเกิดจากความเค้นเชิงกลภายนอกระหว่างการใช้งาน เช่น แอกทัวเอเทอร์และทรานสดิวเซอร์ เป็นต้น หรือความเค้นเชิงกลภายในอันเกิดจากการที่สารเซรามิกเหล่านี้ซึ่งมีสมบัติพิโซอิเล็กตริกจะเกิดการเปลี่ยนแปลงรูปร่างภายใต้อิทธิพลของสนามไฟฟ้าซึ่งส่งผลให้เกิดความเค้นกระทำต่อสารเซรามิก เช่น ตัวเก็บประจุไฟฟ้า เทอร์มิสเตอร์ เซนเซอร์ หม้อแปลงไฟฟ้า และหัวตรวจวัดอัลตร้าซาวด์ เป็นต้น ดังนั้นข้อมูลเกี่ยวกับสมบัติทางไฟฟ้าต่างๆ โดยเฉพาะ สมบัติไดอิเล็กตริก สมบัติเฟร์โรอิเล็กตริก และสมบัติไฟฟ้าเชิงกล ภายใต้อิทธิพลของความเค้น จึงมีความสำคัญอย่างมากต่อการออกแบบ การจัดสร้างและการใช้งานของอุปกรณ์อิเล็กทรอนิกส์ที่ผลิตจากสารเซรามิกเฟร์โรอิเล็กตริกเหล่านี้ ซึ่งการศึกษาเหล่านี้นอกจากจะช่วยเสริมข้อมูลที่จำเป็นในการพัฒนาและการนำไปประยุกต์ใช้ของสารเซรามิกเฟร์โรอิเล็กตริกแล้ว ยังสามารถเสริมองค์ความรู้พื้นฐานในเรื่องโครงสร้างของโดเมน (domain structure) และการเคลื่อนที่ของโดเมน (domain motion) [46,47] ซึ่งเป็นกลไกที่สำคัญที่มีอิทธิพลต่อสมบัติไดอิเล็กตริกและสมบัติไฟฟ้าเชิงกลในสารเซรามิกเฟร์โรอิเล็กตริก ส่งผลให้ในช่วงที่ผ่านมาได้เริ่มมีการศึกษาถึงอิทธิพลของความเค้นต่อสมบัติทางไดอิเล็กตริก สมบัติเฟร์โรอิเล็กตริก และไฟฟ้าเชิงกลของสารเซรามิกในระบบต่างๆ เช่น PZT PMN-PT PZT-BT PIN-PT PZN-PZT และ PMN-PZT เป็นต้น แต่ยังคงอยู่ในวงที่จำกัดเมื่อเปรียบเทียบกับจำนวนของสารเซรามิกเฟร์โรอิเล็กตริกใหม่ๆที่ได้รับการพัฒนาขึ้นมา ทำให้งานวิจัยที่เป็นระบบในประเด็นของอิทธิพลของความเค้นต่อสมบัติต่างๆของสารเซรามิกเฟร์โรอิเล็กตริกที่สำคัญที่ปรากฏในวารสารงานวิจัยในระดับนานาชาติยังมีจำนวนที่ค่อนข้างน้อย [20,46-54]

ด้วยเหตุผลดังกล่าวมาข้างต้น ดังนั้นในช่วงระยะเวลา 7 ปีที่ผ่านมาทางผู้วิจัยจึงได้ทำการศึกษาอย่างเป็นระบบถึงอิทธิพลของความเค้นต่อสมบัติทางไฟฟ้าของสารเซรามิกเฟร์โรอิเล็กตริกที่สำคัญ กล่าวคือ สารเซรามิกเฟร์โรอิเล็กตริกระบบเดี่ยว เช่น BT PT PZT PZN PMN PIN เป็นต้น สารเซรามิกเฟร์โรอิเล็กตริกระบบคู่ที่สำคัญที่เกิดจากการผสมสารในระบบเดี่ยว เช่น PZT-BT PMN-PT PZN-PZT PIN-PT เป็นต้น และ สารเซรามิกเฟร์โรอิเล็กตริกที่มีความซับซ้อนมากและไม่เป็นที่ปรากฏมาก่อน คือ PZTBT-PMNT โดยโครงการวิจัยแรกที่ได้รับทุนส่งเสริมนักวิจัยรุ่นใหม่ ประจำปี 2545 (TRG-4580054) มุ่งเน้นความสำคัญไปที่การศึกษาถึงสมบัติไดอิเล็กตริกและไฟฟ้าเชิงกลของสารเซรามิกในระบบ PMN-PZT ภายใต้อิทธิพลของความเค้นแบบแกนเดี่ยว ซึ่งผลการศึกษาที่ได้มีการนำไปสู่การสร้างองค์ความรู้พื้นฐานใหม่ซึ่งนำไปสู่การตีพิมพ์ผลงานในระดับนานาชาติถึง 5 เรื่อง และต่อมาในโครงการศึกษาต่อเนื่องที่ได้รับทุนพัฒนานักวิจัย (เมธีวิจัย สกว) ประจำปี 2547 (RSA-4780002) ผู้วิจัยได้ทำการศึกษา

เพื่อสร้างองค์ความรู้พื้นฐานใหม่ที่จำเป็นสำหรับการทำความเข้าใจในธรรมชาติของสมบัติไดอิเล็กตริกของสารเซรามิกเฟร์โรอิเล็กตริกภายใต้ความเค้นของสารเซรามิกในระบบที่มีที่สำคัญกล่าวคือ สารเซรามิกเฟร์โรอิเล็กตริกระบบเดี่ยว เช่น BT PT PZT PZN PMN PIN เป็นต้น สารเซรามิกเฟร์โรอิเล็กตริกระบบคู่ที่สำคัญที่เกิดจากการผสมสารในระบบเดี่ยว เช่น PZT-BT PMN-PT PZN-PZT PIN-PT เป็นต้น และ สารเซรามิกเฟร์โรอิเล็กตริกที่มีความซับซ้อนมากและไม่เป็นที่ปรากฏมาก่อน คือ PZTBT-PMNT ทั้งนี้มีผลการศึกษาเป็นที่น่าพอใจและเป็นที่ยอมรับโดยทั่วไปในระดับนานาชาติ โดยในโครงการดังกล่าวนี้ได้มีการการตีพิมพ์ผลงานในระดับนานาชาติถึง 45 เรื่อง อย่างไรก็ตาม ด้วยระยะเวลาที่จำกัดทำให้ยังไม่ได้มีการศึกษาถึงอิทธิพลของความเค้นต่อสมบัติเฟร์โรอิเล็กตริกของสารเซรามิกทั้งหมดที่ได้ศึกษามา (ยกเว้นเพียง PMN-PZT) เพื่อเป็นการสร้างองค์ความรู้ที่สมบูรณ์แบบมากขึ้นผู้วิจัยจึงมีความประสงค์ที่จะทำการศึกษาถึงอิทธิพลของความเค้นต่อสมบัติเฟร์โรอิเล็กตริกของสารเซรามิกที่ได้กล่าวมาข้างต้น และนอกจากนี้ยังจะได้ขยายการศึกษาเพื่อครอบคลุมสารเซรามิกเฟร์โรอิเล็กตริกที่สำคัญที่ได้รับการศึกษาอย่างกว้างขวางในช่วงที่ผ่านมาเนื่องจากมีคุณลักษณะทางไฟฟ้าที่โดดเด่นกล่าวคือสารเซรามิกในระบบ PCoN-PZT และ PNN-PZT

กล่าวโดยสรุปในโครงการวิจัยปัจจุบันที่ดำเนินการนี้ จะเป็นการพัฒนาองค์ความรู้ใหม่แบบรวบยอดของอิทธิพลของความเค้นต่อสมบัติทางไฟฟ้าของสารเซรามิกเฟร์โรอิเล็กตริกที่สำคัญ เพื่อเป็นแนวทางในการนำองค์ความรู้ที่ได้รับจากการวิจัยนี้ไปใช้ในภาคปฏิบัติเพื่อพัฒนาการออกแบบ การจัดสร้างและการใช้งานของอุปกรณ์อิเล็กทรอนิกส์ที่ผลิตจากสารเซรามิกเฟร์โรอิเล็กตริกเหล่านี้ให้มีประสิทธิภาพสูงขึ้น นอกจากนี้แล้ว โครงการวิจัยนี้ยังเป็นการสร้างผลงานวิจัยแบบต่อเนื่องซึ่งมุ่งเน้นการใช้องค์ความรู้ที่ได้รับจากโครงการวิจัยจากทุนส่งเสริมนักวิจัยรุ่นใหม่และทุนพัฒนานักวิจัยของผู้วิจัยเองมาประยุกต์ใช้ และยังเป็นการส่งเสริมให้เกิดการเชื่อมโยงด้านการวิจัยระหว่างนักวิจัยในประเทศโดยการนำผลการวิจัยจากนักวิจัยท่านอื่นที่มีความร่วมมืออย่างใกล้ชิดซึ่งได้รับทุนส่งเสริมนักวิจัยรุ่นใหม่และทุนพัฒนานักวิจัยมาใช้ประโยชน์ในโครงการวิจัยนี้ [55-57] ซึ่งโครงการทั้งสองดังกล่าวนั้นได้มุ่งเน้นไปที่การการศึกษาถึงอิทธิพลของปัจจัยหลักในกระบวนการผลิตที่มีต่อพฤติกรรมการเกิดเฟส โครงสร้างจุลภาคและสมบัติไดอิเล็กตริกของสารเซรามิกในระบบ PZN PMN PNN และ PCoN ซึ่งผลการศึกษาเหล่านี้สามารถนำมาใช้โดยตรงในการเลือกเงื่อนไขที่เหมาะสมในการเตรียมสารเซรามิกที่มีความบริสุทธิ์และความหนาแน่นสูง รวมทั้งสมบัติไดอิเล็กตริกที่ดี มาใช้ในการศึกษาในโครงการวิจัยนี้ จะเห็นได้ว่าโครงการวิจัยนี้ นอกจากจะให้องค์ความรู้ที่สามารถนำไปใช้ในภาคปฏิบัติแล้ว ยังจะนำไปสู่ความรู้ความเข้าใจพื้นฐานใหม่ๆเกี่ยวกับสารเซรามิกเฟร์โรอิเล็กตริกที่สำคัญอันจะเป็นพื้นฐานในการพัฒนาประเทศและผลงานที่ได้ยังสามารถที่จะตีพิมพ์ในวารสารวิชาการระดับนานาชาติได้ นอกจากนี้ยังเป็นการพัฒนาวิชาชีพอาจารย์ให้มีศักยภาพในการผลิตนักศึกษาระดับปริญญาเอกได้

2. วัตถุประสงค์ของการวิจัย

1. เพื่อศึกษากระบวนการเตรียมผงและเซรามิกในระบบ PCoN PNN PZT PCoN-PZT และ PNN-PZT
2. เพื่อศึกษาอิทธิพลของความเค้นอัดต่อสมบัติไดอิเล็กตริกและสมบัติเฟร์โรอิเล็กตริกของสารเซรามิกระบบเดี่ยว PCoN และ PNN
3. เพื่อศึกษาอิทธิพลของความเค้นอัดต่อสมบัติไดอิเล็กตริกและสมบัติเฟร์โรอิเล็กตริกของสารเซรามิกระบบคู่ PCoN-PZT และ PNN-PZT
4. เพื่อศึกษาอิทธิพลของความเค้นอัดต่อสมบัติเฟร์โรอิเล็กตริกของสารเซรามิกระบบเดี่ยว PT PZT PIN PMN และ PZN
5. เพื่อศึกษาอิทธิพลของความเค้นแบบแกนเดี่ยวต่อสมบัติเฟร์โรอิเล็กตริกของสารเซรามิก ระบบคู่ PZN-PZT PMN-PT และ PIN-PT
6. เพื่อศึกษาความสัมพันธ์ระหว่างสมบัติไดอิเล็กตริกและสมบัติเฟร์โรอิเล็กตริกภายใต้ความเค้นอัดของแต่ละองค์ประกอบและสมบัติดังกล่าวของสารเซรามิกระบบคู่

3. ระเบียบวิธีวิจัย

ขั้นตอนการวิจัยในโครงการนี้จะถูกแบ่งออกเป็น 3 ส่วนหลัก คือ 1) การศึกษาการเตรียมผงและเซรามิกในระบบ PZT PNN PCoN PNN-PZT และ PCoN-PZT ด้วยการใช้เทคนิคผสมออกไซด์ เพื่อหาเงื่อนไขในการเตรียมผงและสารเซรามิกที่มีความบริสุทธิ์และความหนาแน่นสูง โดยใช้องค์ความรู้บางส่วนจากโครงการของ รองศาสตราจารย์ ดร. สุพล อนันตา และ ดร. นราธิป วิทยากร 2)การศึกษาอิทธิพลของความเค้นอัดต่อสมบัติเฟร์โรอิเล็กตริกของสารเซรามิกระบบ PMN-PT PIN-PT และ PZN-PZT โดยเป็นการศึกษาต่อเนื่องจากโครงการวิจัยที่ได้รับทุนพัฒนานักวิจัย ปี 2547 ของผู้วิจัยเอง ซึ่งเน้นเฉพาะการศึกษาอิทธิพลของความเค้นอัดต่อสมบัติไดอิเล็กตริกของสารเซรามิกดังกล่าว และ 3) การศึกษาอิทธิพลของความเค้นอัดต่อสมบัติไดอิเล็กตริกและสมบัติเฟร์โรอิเล็กตริกของสารเซรามิกระบบของสารเซรามิกระบบเดี่ยว PZT PNN และ PCoN และสารเซรามิกระบบคู่ PNN-PZT และ PCoN-PZT ที่เตรียมขึ้นได้

ดังนั้นเพื่อให้เกิดความต่อเนื่องของการดำเนินการวิจัยระหว่างโครงการนี้และโครงการที่เกี่ยวข้อง จึงต้องมีการวางแผนงานการวิจัยโดยมีรายละเอียดของระเบียบวิธีวิจัยดังนี้ (โดยใช้ระยะเวลารวม 2 ปีในการดำเนินการทั้งหมด (จากที่วางแผนไว้ในเบื้องต้น 3 ปี))

1 ศึกษาค้นคว้ารวบรวมข้อมูลจากผลงานวิจัยและเอกสารทางวิชาการที่เกี่ยวข้อง

2 ทำการติดตั้งและตรวจสอบเครื่องมืออัดแรงเพื่อใช้ในการวัดสมบัติไดอิเล็กตริกและสมบัติเฟร์โรอิเล็กตริกของสารเซรามิกภายใต้ความเค้นอัด และทำการติดตั้งและตรวจสอบอุปกรณ์อื่นๆที่จะใช้งานให้มีความพร้อม

3 เตรียมผงและเซรามิกในระบบ $Pb(Ni_{1/3}Nb_{2/3})O_3$ หรือ PNN ด้วยการใช้เทคนิคผสมออกไซด์ โดยศึกษาหาเงื่อนไขที่เหมาะสมต่อการเตรียมผงให้มีความบริสุทธิ์สูง และศึกษาหาเงื่อนไขในการเผาที่เหมาะสมต่อการเตรียมเซรามิกเหล่านี้ให้มีความบริสุทธิ์และความหนาแน่นสูง

4 เตรียมผงและเซรามิกในระบบ $Pb(Co_{1/3}Nb_{2/3})O_3$)หรือ PCoN ด้วยการใช้เทคนิคผสมออกไซด์ โดยศึกษาหาเงื่อนไขที่เหมาะสมต่อการเตรียมผงให้มีความบริสุทธิ์สูง และศึกษาหาเงื่อนไขในการเผาที่เหมาะสมต่อการเตรียมเซรามิกเหล่านี้ให้มีความบริสุทธิ์และความหนาแน่นสูง

5 เตรียมผงและเซรามิกในระบบ $Pb(Zr_{1/2}Ti_{1/2})O_3$ หรือ PZT ด้วยการใช้เทคนิคผสมออกไซด์ โดยศึกษาหาเงื่อนไขที่เหมาะสมต่อการเตรียมผงให้มีความบริสุทธิ์สูง และศึกษาหาเงื่อนไขในการเผาที่เหมาะสมต่อการเตรียมเซรามิกเหล่านี้ให้มีความบริสุทธิ์และความหนาแน่นสูง

6 ทำการตรวจสอบคุณลักษณะเฉพาะและคุณสมบัติของผงและเซรามิกที่เตรียมได้

7 ทดสอบอิทธิพลของความเค้นอัดต่อสมบัติเฟร์โรอิเล็กตริก (Polarization-Electric Field (P-E) Loops) ของสารเซรามิกระบบเดี่ยว PT และ PMN ด้วยเครื่องมืออัดแรงแบบแกนเดี่ยว

8 ทดสอบอิทธิพลของความเค้นอัดต่อสมบัติเฟร์โรอิเล็กตริก (Polarization-Electric Field (P-E) Loops) ของสารเซรามิกระบบคู่ PMN-PT ด้วยเครื่องมืออัดแรงแบบแกนเดี่ยว

9 สรุปความสัมพันธ์ระหว่างสมบัติเฟร์โรอิเล็กตริกภายใต้ความเค้นอัดของ PT และ PMN และสมบัติดังกล่าวของสารเซรามิกระบบ PMN-PT

10 อภิปรายผลการศึกษา และการเตรียมผลงานเพื่อการตีพิมพ์

11 เตรียมผงและเซรามิกในระบบ (1-x)PZT-xPNN เมื่อ x มีค่าเป็น 0.0, 0.1, 0.2, 0.3, 0.4, และ 0.5 ด้วยเทคนิคผสมออกไซด์โดยใช้สารที่เตรียมได้จาก ข้อ 8.3 และ 8.5 ที่มีความบริสุทธิ์สูงเป็นสารตั้งต้น โดยศึกษาหาเงื่อนไขที่เหมาะสมต่อการเตรียมผง

ให้มีความบริสุทธิ์สูง และศึกษาหาเงื่อนไขในการเผาที่เหมาะสมต่อการเตรียมเซรามิกเหล่านี้ให้มีความบริสุทธิ์และความหนาแน่นสูง

12 เตรียมผงและเซรามิกในระบบ (1-x)PZT-xPCoN เมื่อ x มีค่าเป็น 0.0, 0.1, 0.2, 0.3, 0.4, และ 0.5 ด้วยเทคนิคผสมออกไซด์โดยใช้สารที่เตรียมได้จาก ข้อ 8.4 และ 8.5 ที่มีความบริสุทธิ์สูงเป็นสารตั้งต้น โดยศึกษาหาเงื่อนไขที่เหมาะสมต่อการเตรียมผงให้มีความบริสุทธิ์สูง และศึกษาหาเงื่อนไขในการเผาที่เหมาะสมต่อการเตรียมเซรามิกเหล่านี้ให้มีความบริสุทธิ์และความหนาแน่นสูง

13 ทำการตรวจสอบคุณลักษณะเฉพาะและคุณสมบัติของผงและเซรามิกที่เตรียมได้

14 ทดสอบอิทธิพลของความเค้นอัดต่อสมบัติเฟร์โรอิเล็กตริก (Polarization-Electric Field (P-E) Loops) ของสารเซรามิกระบบเดี่ยว PT และ PIN ด้วยเครื่องมืออัดแรงแบบแกนเดี่ยว

15 ทดสอบอิทธิพลของความเค้นอัดต่อสมบัติเฟร์โรอิเล็กตริก (Polarization-Electric Field (P-E) Loops) ของสารเซรามิกระบบคู่ PIN-PT ด้วยเครื่องมืออัดแรงแบบแกนเดี่ยว

16 สรุปความสัมพันธ์ระหว่างสมบัติเฟร์โรอิเล็กตริกภายใต้ความเค้นอัดของ PT และ PIN และสมบัติดังกล่าวของสารเซรามิกระบบ PIN-PT

17 ทดสอบอิทธิพลของความเค้นอัดต่อสมบัติเฟร์โรอิเล็กตริก (Polarization-Electric Field (P-E) Loops) ของสารเซรามิกระบบเดี่ยว PZT และ PZN ด้วยเครื่องมืออัดแรงแบบแกนเดี่ยว

18 ทดสอบอิทธิพลของความเค้นอัดต่อสมบัติเฟร์โรอิเล็กตริก (Polarization-Electric Field (P-E) Loops) ของสารเซรามิกระบบคู่ PZN-PZT ด้วยเครื่องมืออัดแรงแบบแกนเดี่ยว

19 สรุปความสัมพันธ์ระหว่างสมบัติเฟร์โรอิเล็กตริกภายใต้ความเค้นอัดของ PZT และ PZN และสมบัติดังกล่าวของสารเซรามิกระบบ PZN-PZT

20 อภิปรายผลการศึกษาและการเตรียมผลงานเพื่อการตีพิมพ์

21 ทดสอบอิทธิพลของความเค้นอัดต่อสมบัติไดอิเล็กตริก (ค่าคงที่ไดอิเล็กตริก (ε_r) และการสูญเสียทางไดอิเล็กตริก (tan δ)) ของสารเซรามิกระบบเดี่ยว PZT และ PNN ด้วยเครื่องมืออัดแรงแบบแกนเดี่ยว

22 ทดสอบอิทธิพลของความเค้นอัดต่อสมบัติไดอิเล็กตริก (ค่าคงที่ไดอิเล็กตริก (ε_r) และการสูญเสียทางไดอิเล็กตริก (tan δ)) ของสารเซรามิกระบบคู่ PNN-PZT ด้วยเครื่องมืออัดแรงแบบแกนเดี่ยว

23 ทดสอบอิทธิพลของความเค้นอัดต่อสมบัติไดอิเล็กตริก (ค่าคงที่ไดอิเล็กตริก (ε_r) และการสูญเสียทางไดอิเล็กตริก (tan δ)) ของสารเซรามิกระบบเดี่ยว PZT และ PCoN ด้วยเครื่องมืออัดแรงแบบแกนเดี่ยว

24 ทดสอบอิทธิพลของความเค้นอัดต่อสมบัติไดอิเล็กตริก (ค่าคงที่ไดอิเล็กตริก (ε_r) และการสูญเสียทางไดอิเล็กตริก (tan δ)) ของสารเซรามิกระบบคู่ PCoN-PZT ด้วยเครื่องมืออัดแรงแบบแกนเดี่ยว

25 สรุปความสัมพันธ์ระหว่างสมบัติไดอิเล็กตริกภายใต้ความเค้นอัดของ PZT PNN และ PCoN และสมบัติดังกล่าวของสารเซรามิกระบบ PNN-PZT และ PCoN-PZT

26 ทดสอบอิทธิพลของความเค้นอัดต่อสมบัติเฟร์โรอิเล็กตริก (Polarization-Electric Field (P-E) Loops) ของสารเซรามิกระบบเดี่ยว PZT และ PNN ด้วยเครื่องมืออัดแรงแบบแกนเดี่ยว

27 ทดสอบอิทธิพลของความเค้นอัดต่อสมบัติเฟร์โรอิเล็กตริก (Polarization-Electric Field (P-E) Loops) ของสารเซรามิกระบบคู่ PNN-PZT ด้วยเครื่องมืออัดแรงแบบแกนเดี่ยว

28 ทดสอบอิทธิพลของความเค้นอัดต่อสมบัติเฟร์โรอิเล็กตริก (Polarization-Electric Field (P-E) Loops) ของสารเซรามิกระบบเดี่ยว PZT และ PCoN ด้วยเครื่องมืออัดแรงแบบแกนเดี่ยว

29 ทดสอบอิทธิพลของความเค้นอัดต่อสมบัติเฟร์โรอิเล็กตริก (Polarization-Electric Field (P-E) Loops) ของสารเซรามิกระบบคู่ PCoN-PZT ด้วยเครื่องมืออัดแรงแบบแกนเดี่ยว

30 สรุปความสัมพันธ์ระหว่างสมบัติสมบัติเฟร์โรอิเล็กตริกภายใต้ความเค้นอัดของ PZT PNN และ PCoN และสมบัติดังกล่าวของสารเซรามิกระบบ PNN-PZT และ PCoN-PZT

31 อภิปรายผลการศึกษาและสรุปผลการวิจัย ตลอดจนข้อเสนอแนะในรูปแบบการเขียนรายงานฉบับสมบูรณ์ และการเตรียมผลงานเพื่อการตีพิมพ์

4. ประโยชน์ที่ได้รับจากโครงการวิจัยนี้

1 องค์ความรู้ใหม่ในเรื่องกระบวนการเตรียมผงและเซรามิกในระบบ PNN PCoN PZT PNN-PZT และ PCoN-PZT

2 องค์ความรู้ใหม่ในเรื่องของอิทธิพลของความเค้นอัดต่อสมบัติไดอิเล็กตริกของสารเซรามิกระบบเดี่ยว PZT PNN และ PCoN

3 องค์ความรู้ใหม่ในเรื่องของอิทธิพลของความเค้นอัดต่อสมบัติไดอิเล็กตริกของสารเซรามิกระบบคู่ PNN-PZT และ PCoN-PZT

4 ความรู้ความเข้าใจถึงความสัมพันธ์ระหว่างสมบัติไดอิเล็กตริกภายใต้ความเค้นอัดของแต่ละองค์ประกอบและสมบัติดังกล่าวของสารเซรามิกระบบคู่

5 องค์ความรู้ใหม่ในเรื่องของอิทธิพลของความเค้นอัดต่อสมบัติเฟร์โรอิเล็กตริกของสารเซรามิกระบบเดี่ยว PMN PT PIN PZN PZT PNN และ PCoN

6 องค์ความรู้ใหม่ในเรื่องของอิทธิพลของความเค้นอัดต่อสมบัติเฟร์โรอิเล็กตริกของสารเซรามิกระบบคู่ PMN-PT PIN-PT PZN-PZT PNN-PZT และ PCoN-PZT

7 ความรู้ความเข้าใจถึงความสัมพันธ์ระหว่างสมบัติเฟร์โรอิเล็กตริกภายใต้ความเค้นอัดของแต่ละองค์ประกอบและสมบัติดังกล่าวของสารเซรามิกระบบคู่

8 ผลงานวิจัยในรูปของสิ่งตีพิมพ์ ได้แก่สิ่งตีพิมพ์ในวารสารทางวิชาการต่างๆ การนำเสนอผลงานในการประชุมวิชาการและสัมมนา หรือหนังสือตำราวิชาการ เพื่อเป็นการพัฒนาวิชาชีพอาจารย์ให้มีศักยภาพในการผลิตนักศึกษาระดับปริญญาเอกได้

9 องค์ความรู้ใหม่ที่จะนำไปใช้ประกอบการเรียนการสอนและการปรับปรุงกระบวนวิชาในหลักสูตรวัสดุศาสตร์ทั้งในระดับปริญญาตรีและระดับบัณฑิตศึกษาที่ผู้วิจัยรับผิดชอบอยู่ต่อไป

10 นักวิจัยรุ่นกลางที่มีความรู้ทางด้านสารเซรามิกเฟร์โรอิเล็กตริกกลุ่มเพอรอพสไกต์และแนวทางในการกำหนดหัวข้อวิทยานิพนธ์สำหรับการพัฒนาบุคลากรทางด้านวัสดุศาสตร์ที่เกี่ยวข้องทั้งในระดับปริญญาโท และเอก สาขาวัสดุศาสตร์อย่างต่อเนื่อง

11 การเชื่อมโยงด้านการวิจัยระหว่างนักวิจัยในประเทศท่านอื่นซึ่งได้รับทุนผู้รับทุนพัฒนาศักยภาพในการทำงานวิจัยของอาจารย์รุ่นใหม่และรุ่นกลางที่มีความร่วมมือกันอย่างใกล้ชิด รวมทั้งกับนักวิจัยชั้นนำในระดับนานาชาติ

12 แนวทางการพัฒนาชุดโครงการวิจัยและการสร้างความร่วมมือของกลุ่มนักวิจัยภายในสถาบันต้นสังกัดและระหว่างกลุ่มวิจัยต่างๆที่สนใจในเรื่องที่เกี่ยวข้องกันทั้งในและต่างประเทศ

5. สรุปผลที่ได้จากโครงการวิจัยนี้

เมื่อพิจารณาจากวัตถุประสงค์ของโครงการวิจัยทั้ง 6 ข้อแล้ว โดยสรุปสามารถแบ่งองค์ความรู้ใหม่ที่ได้จากโครงการวิจัยนี้ออกเป็น 4 กลุ่มใหญ่ กล่าวคือ

1. องค์ความรู้ใหม่ในเรื่องกระบวนการเตรียมผงและเซรามิกในระบบ PNN PCoN PZT PNN-PZT และ PCoN-PZT และความสัมพันธ์ระหว่างสมบัติไดอิเล็กตริกและสมบัติเฟร์โรอิเล็กตริกของสารเซรามิกระบบดังกล่าว
2. องค์ความรู้ใหม่ในเรื่องอิทธิพลของความเค้นอัดต่อสมบัติเฟร์โรอิเล็กตริกของสารเซรามิกระบบเดี่ยว PT PZT PIN PMN และ PZN และสารเซรามิกระบบคู่ PZN-PZT PMN-PT และ PIN-PT พร้อมทั้งความสัมพันธ์ระหว่างสมบัติเฟร์โรอิเล็กตริกภายใต้ความเค้นอัดของแต่ละองค์ประกอบและสมบัติดังกล่าวของสารเซรามิกระบบคู่
3. องค์ความรู้ใหม่ในเรื่องอิทธิพลของความเค้นอัดต่อสมบัติไดอิเล็กตริกและสมบัติเฟร์โรอิเล็กตริกของสารเซรามิกระบบเดี่ยว PCoN และ PNN และ สารเซรามิกระบบคู่ PCoN-PZT และ PNN-PZT พร้อมทั้งความสัมพันธ์ระหว่างสมบัติไดอิเล็กตริกและสมบัติเฟร์โรอิเล็กตริกภายใต้ความเค้นอัดของแต่ละองค์ประกอบและสมบัติดังกล่าวของสารเซรามิกระบบคู่
4. องค์ความรู้ใหม่ด้านอื่นๆที่ถือเป็นการต่อยอดจากผลงานที่ได้ศึกษามาในเบื้องต้น

ซึ่งผลงานที่ได้ใน 4 กลุ่มนั้น ถือเป็นผลงานที่เกี่ยวข้อง*โดยตรง*กับโครงการวิจัยนี้ ดังจะได้กล่าวถึงในรายละเอียดต่อไป

ส่วนที่ 1: สำหรับองค์ความรู้ใหม่ในเรื่องกระบวนการเตรียมผงและเซรามิกในระบบ PNN PCoN PZT PNN-PZT และ PCoN-PZT นั้น กลุ่มผู้วิจัยได้ประสบความสำเร็จในการเตรียมผงและเซรามิกในระบบ $Pb(Ni_{1/3}Nb_{2/3})O_3$ หรือ PNN $Pb(Zr_{0.52}Ti_{0.48})O_3$ $Pb(Co_{1/3}Nb_{2/3})O_3$)หรือ PCoN และ $Pb(Zr_{1/2}Ti_{1/2})O_3$ หรือ PZT ด้วยการใช้เทคนิคผสมออกไซด์ โดยศึกษาหาเงื่อนไขที่เหมาะสมต่อการเตรียมผงให้มีความบริสุทธิ์สูง และศึกษาหาเงื่อนไขในการเผาที่เหมาะสมต่อการเตรียมเซรามิก เหล่านี้ให้มีความบริสุทธิ์และความหนาแน่นสูง นอกจากนี้ก็ได้เตรียมผงและเซรามิกในระบบ (1-x)PZT-xPNN และ (1-x)PZT-xPCoN เมื่อ x มีค่าเป็น 0.1, 0.2, 0.3, 0.4 และ 0.5 ด้วยการใช้เทคนิคผสมออกไซด์เช่นกัน ส่วนองค์ความรู้ใหม่ในเรื่องของสมบัติไดอิเล็กตริกและทางไฟฟ้าอื่นๆของสารเซรามิกในทุกระบบนั้น ได้รับโดยตรงจากการทำการตรวจสอบคุณลักษณะเฉพาะและคุณสมบัติต่างๆของเซรามิกที่เตรียมได้ ผลงาน

ที่ได้รับนั้นได้ถูกนำไปตีพิมพ์ในวารสารทางวิชาการต่างๆ ดังต่อไปนี้ (ทั้งนี้ รายละเอียดได้ถูกนำเสนอในแต่ละผลงานแล้ว และในกรณีที่เป็นผลงานตีพิมพ์ในวารสารวิชาการนานาชาติสามารถค้นคว้าเพิ่มเติมได้ในภาคผนวก)

ผลงานตีพิมพ์ในวารสารวิชาการนานาชาติ (จำนวน 11 เรื่อง)

1. O. Khamman, **R. Yimnirun**, and S. Ananta, "Effect of calcination conditions on phase formation and particle size of lead nickel niobate powders synthesized by using $Ni_4Nb_2O_9$ precursor" *Materials Letters,* 61, pp 4466-4470 (2007)
2. N. Vittayakorn, S. Wirunchit, S. Traisak, **R. Yimnirun**, G. Rujijanagul, "Development of Perovskite and Phase Transition in Lead Cobalt Niobate Modified Lead Zirconate Titanate System" *Current Applied Physics,* 8, pp 128-133 (2008)
3. Anurak Prasatkhetragarn, Naratip Vittayakorn, Supon Ananta, **Rattikorn Yimnirun** and David P. Cann, "Synthesis, dielectric and ferroelectric properties of ceramics in the *(1-x)*$Pb(Zr_{1/2}Ti_{1/2})O_3$ – *(x)*$Pb(Co_{1/3}Nb_{2/3})O_3$ system" *Japan Journal of Applied Physics*, 47(2), pp 998-1002 (2008).
4. O. Khamman, **R. Yimnirun**, and S. Ananta, "Effect of vibro-milling time on phase formation and particle size of nickel niobate nanopowders" *Materials Science and Engineering B*, 150(1), pp 12-17 (2008)
5. Orawan Khamman, **Rattikorn Yimnirun**, Supon Ananta, "Effect of Niobate B-Site Precursor of Phase Formation of PNN Powders" *J. Alloys and Compounds*, 465, pp522-526 (2008).
6. Muangjai Unruan, Naratip Vittayakorn, Rewadee Wongmaneeruang, Anurak Prasatkhetragarn, Supon Ananta and **Rattikorn Yimnirun**, "Synthesis and Properties of $Pb(Co_{1/3}Nb_{2/3})O_3$ Ceramics" *J. Alloys and Compounds*, 466, pp 264-267 (2008).
7. S. Ananta,, **R. Yimnirun**, and O. Khamman "Effect of nickel niobate B-site precursors on phase formation, microstructure and dielectric properties of perovskite PNN ceramics" *Functional Materials Letters*, 1(3), pp 229-233 (2008)
8. P. Ketsuwan, Y. Laosiritaworn, S. Ananta, **R. Yimnirun**, "Electrical Properties of Nb-Doped $Pb(Zr_{0.52}Ti_{0.48})O_3$ Ceramics" *International Journal of Modern Physics B*, 23, pp 105-111 (2009)

9. Anurak Prasatkhetragarn, Athipong Ngamjarurojana, Yongyut Laosiritaworn, Supon Ananta, **Rattikorn Yimnirun**, and David Cann, “Effects of Zr/Ti ratio on phase formation and electrical properties of $0.8Pb(Zr_{1/2}Ti_{1/2})O_3$-$0.2Pb(Co_{1/3}Nb_{2/3})O_3$ ceramics” *Current Applied Physics*, 9, pp 802-806 (2009)
10. Anurak Prasatkhetragarn, Piyachon Ketsuwan, Supon Ananta, **Rattikorn Yimnirun**, and David Cann “Phase Formation, Microstructure and Dielectric Properties of $(1-x)Pb(Zr_{1/2}Ti_{1/2})O_3–xPb(Co_{1/3}Nb_{2/3})O_3$ Ceramics” *Materials Letters,* 63, pp 1281-1284 (2009)
11. Anurak Prasatkhetragarn, Athipong Ngamjarurojana, Yongyut Laosiritaworn, Supon Ananta, **Rattikorn Yimnirun**, and David Cann, “Effects of sintering conditions on phase formation and electrical properties of $0.8Pb(Zr_{1/2}Ti_{1/2})O_3$-$0.2Pb(Co_{1/3}Nb_{2/3})O_3$ ceramics” *Current Applied Physics* (2009) *in press*

ผลงานตีพิมพ์ในวารสารประกอบการประชุมวิชาการระดับนานาชาติ (จำนวน 1 เรื่อง)

1. W. Laosiritaworn, O. Khamman, S. Ananta, **R. Yimnirun** and Y. Laosiritaworn, “Artificial Neural Network Modeling of Ceramics Powder Preparation: application to $NiNb_2O_6$” *Ceramics International,* 34(4), pp 809-812 (2008).

ส่วนที่ 2: ในส่วนนี้นั้นถือเป็นผลงานหลักของโครงการวิจัยนี้ โดยเป็นองค์ความรู้ใหม่ในเรื่องของอิทธิพลของความเค้นแบบแกนเดี่ยวต่อสมบัติเฟร์โรอิเล็กตริกของสารเซรามิกระบบเดี่ยว PT PZT PIN PMN และ PZN และสารเซรามิกระบบคู่ PZN-PZT PMN-PT และ PIN-PT ซึ่งได้จากการใช้เครื่องมืออัดแรงแบบแกนเดี่ยวประกอบในการวัดสมบัติไดอิเล็กตริก เช่น ค่าคงที่ไดอิเล็กตริก (ε_r) และการสูญเสียทางไดอิเล็กตริก (tan δ) และสมบัติอื่นๆ เช่น สมบัติเฟร์โรอิเล็กทริกฮิสเทอรีซิส (วงวน P-E) ของสารเซรามิกในทุกระบบที่กล่าวมาภายใต้ความเค้นแบบแกนเดี่ยว และผลงานที่ได้นั้นก็ได้ถูกนำไปตีพิมพ์ในวารสารทางวิชาการต่างๆ ดังต่อไปนี้ (รายละเอียดได้ถูกนำเสนอในแต่ละผลงานแล้ว และในกรณีที่เป็นผลงานตีพิมพ์ในวารสารวิชาการนานาชาติสามารถค้นคว้าเพิ่มเติมได้ในภาคผนวก)

ผลงานตีพิมพ์ในวารสารวิชาการนานาชาติ (จำนวน 20 เรื่อง)

1. S. Wongsaenmai, W. Qu, S. Ananta, **R. Yimnirun**, and X. Tan, “Effect of Ba-substitution on the structure and properties of $Pb_{0.8}Ba_{0.2}In_{0.5}Nb_{0.5}O_3$ ceramics” *Applied Physics A,* 88, pp 757-761 (2007).

2. S. Wongsaenmai, **R. Yimnirun,** S. Ananta, R. Guo, and, A. Bhalla, "Thermal Expansion Measurement in the Relaxor Ferroelectric PIN-PT System" *Materials Letters*, 62, pp 352-356 (2008)
3. M. Unruan, S. Wongsaenmai, Y. Laosiritaworn, S. Ananta, and **R. Yimnirun**, "Changes in Dielectric Properties of $Pb(In_{1/2}Nb_{1/2})O_3$-$PbTiO_3$ Ceramics Under Compressive Stress Applied Parallel and Perpendicular to Electric Field" *J. Phys. D: Appl. Phys.,* 41*,* pp 541-545 (2008)*.*
4. Supattra Wongsaenmai, Xiaoli Tan, Supon Ananta, and **Rattikorn Yimnirun**, "Dielectric and Ferroelectric Properties of Fine Grains $Pb(In_{1/2}Nb_{1/2})O_3$–$PbTiO_3$ Ceramics" *Journal of Alloys and Compounds*, 454, pp 331-339 (2008).
5. **R. Yimnirun**, N. Wongdamnern, N. Triamnak, M. Unruan, A. Ngamjarurojana, S. Ananta, and Y. Laosiritaworn, "Stress-Dependent Scaling Behavior of Sub-Coercive Field Dynamic Ferroelectric Hysteresis in $Pb(Zn_{1/3}Nb_{2/3})O_3$-Modified $Pb(Zr_{1/2}Ti_{1/2})O_3$ Ceramic" *J. Applied. Physics,* 103 (8)*,* pp 086105-1-3 (2008).
6. R. Wongmaneerung, **R. Yimnirun,** S. Ananta,. A. Bhalla, and R. Guo, "Thermal Expansion Measurement in the PMN-PT Ceramic Systems" *J. Alloys and Compounds,* 461, pp 565-569 (2008)*.*
7. Muangjai Unruan, Athipong Ngamjarurojana, Yongyut Laosiritaworn, Supon Ananta, and **Rattikorn Yimnirun**, "Influences of Perpendicular Compressive Stress on Ferroelectric Properties of Electrostrictive and Piezoelectric $Pb(Mg_{1/3}Nb_{2/3})O_3$-$PbTiO_3$ Ceramics" *J. Applied Physics.* 104, 034101 (2008).
8. M. Unruan, R. Wongmaneerung, A. Ngamjarurojana, S. Ananta, Y. Laosiritaworn, and **R. Yimnirun,** "Changes of Ferroelectric Properties of Lead Magnsium Niobate-Lead Titanate Ceramics Under Compressive Stress" *J. Applied Physics.* 104, 064107 (2008)
9. **R. Yimnirun**, N. Wongdamnern, N. Triamnak, M. Unruan, A. Ngamjarurojana, S. Ananta, and Y. Laosiritaworn, "Stress-Dependent Scaling Behavior of Sub-Coercive Field Dynamic Ferroelectric Hysteresis in $0.4Pb(Zn_{1/3}Nb_{2/3})O_3$-$0.6Pb(Zr_{1/2}Ti_{1/2})O_3$ Ceramic" *J. Physics: Condensed Matters.* 20, 415202 (2008)
10. **R. Yimnirun**, N. Wongdamnern, N. Triamnak, T. Sareein, M. Unruan, A. Ngamjarurojana, S. Ananta, and Y. Laosiritaworn, "Power-law Scaling of Sub-Coercive Field Dynamic Ferroelectric Hysteresis in $0.3Pb(Zn_{1/3}Nb_{2/3})O_3$-

$0.7Pb(Zr_{1/2}Ti_{1/2})O_3$ Ceramic" *J. Physics D: Applied. Physics,* 41, 205415 (2008)

11. **R. Yimnirun**, N. Wongdamnern, N. Triamnak, M. Unruan, A. Ngamjarurojana, S. Ananta, and Y. Laosiritaworn, "Stress-Dependent Scaling Behavior of Sub-Coercive Field Dynamic Ferroelectric Hysteresis in $0.5Pb(Zn_{1/3}Nb_{2/3})O_3$-$0.5Pb(Zr_{1/2}Ti_{1/2})O_3$ Ceramic" *J. Applied. Physics,* **104***,* pp 104103-1-4 (2008)
12. **Rattikorn Yimnirun**, Narit Triamnak, Muangjai Unruan, Athipong Ngamjarurojana, Yongyut Laosiritaworn, and Supon Ananta, "Ferroelectric Properties of $Pb(Zr_{1/2}Ti_{1/2})O_3$—$Pb(Zn_{1/3}Nb_{2/3})O_3$ Ceramics Under Compressive Stress" *Current Applied Physics*, 9, pp 249-252 (2009)
13. R. Wongmaneerung, **R. Yimnirun**, S. Ananta, "Processing and Properties of $Pb(Mg_{1/3}Nb_{2/3})O_3$-$PbTiO_3$ Based Ceramics" *Current Applied Physics*, 9, pp 268-273 (2009).
14. **R. Yimnirun**, S. Wongsaenmai, S. Ananta, N. Triamnak, "Dielectric Properties of PIN-PT Ceramics Under Compressive Stress" *Current Applied Physics,* 9, pp 422-425 (2009).
15. **R. Yimnirun** "Dielectric Properties of PMN-PT Prepared by Mixed Oxide Method" *International Journal of Modern Physics B*, 23(3), pp 403-410 (2009)
16. R. Wongmaneerung, **R. Yimnirun**, and S. Ananta, "Effect of two-stage sintering on phase formation, microstructure and dielectric properties of perovskite PMN ceramics derived from a corundum $Mg_4Nb_2O_9$ precursor" *Materials Chemistry and Physics*, 114, pp 569-575 (2009)
17. S. Wongsaenmai, S. Ananta, and **R. Yimnirun**, "Effects of Addition of BT on Structural Phase Formation and Electrical Properties of Relaxor Ferroelectric $Pb(In_{0.5}Nb_{0.5})_{(1-x)}Ti_{(x)}O_3$ ceramics" *J. Alloys and Compounds,* 474, pp 241-245 (2009)
18. R. Wongmaneerung, A. Rujiwatra, **R. Yimnirun**, and S. Ananta, "Fabrication and Dielectric Properties of Self-reinforced Lead Titanate Nanocomposites" *J. Alloys and Compounds,* 475, pp 473-478 (2009)
19. R. Wongmaneerung, P. Singjai, **R. Yimnirun** and S. Ananta, "Effects of SiC nanofibers Addition on Microstructure and Dielectric Properties of Lead Titanate Ceramics" *J. Alloys and Compounds,* 475, pp 456-462 (2009)
20. R. Wongmaneerung, **R. Yimnirun**, and S. Ananta, "Effect of Magnasium Niobate Precursors on Phase Formation, Microstructure and Dielectric

Properties of Perovskite Lead Magnesium Niobate Ceramics" *J. Alloys and Compounds* (2008) *in press*

ผลงานตีพิมพ์ในวารสารประกอบการประชุมวิชาการระดับนานาชาติ (จำนวน 2 เรื่อง)

1. **R. Yimnirun**, S. Wongsaenmai, R. Wongmaneerung, N. Wongdamnern, A. Ngamjarurojana, S. Ananta, and Y. Laosiritaworn, " Stress- and Temperature-Dependent Scaling Behavior of Dynamic Hysteres-is in Soft PZT Bulk Ceramics" *Physica Scripta*, T129, pp 184-189 (2007)
2. A. Ngamjarurojana, S. Ural, S.H. Park, S. Ananta, **R. Yimnirun**, and K. Uchino, "Piezoelectric Properties of Low Temperature Sintering in $Pb(Zr,Ti)O_3$ - $Pb(Zn,Ni)_{1/3}Nb_{2/3}O_3$ Ceramics for Piezoelectric Transformer Applications" *Ceramics International,* 34(4), pp 705-708 (2008).

ส่วนที่ 3: เช่นเดียวกับส่วนที่ 2 ในส่วนนี้นั้นถือเป็นผลงานหลักของโครงการวิจัยนี้ โดยองค์ความรู้ใหม่ในเรื่องอิทธิพลของความเค้นอัดต่อสมบัติไดอิเล็กตริกและสมบัติเฟร์โรอิเล็กตริกของสารเซรามิกระบบเดี่ยว PCoN และ PNN และ สารเซรามิกระบบคู่ PCoN-PZT และ PNN-PZT พร้อมทั้งความสัมพันธ์ระหว่างสมบัติไดอิเล็กตริกและสมบัติเฟร์โรอิเล็กตริกภายใต้ความเค้นอัดของแต่ละองค์ประกอบและสมบัติดังกล่าวของสารเซรามิกระบบคู่นั้น ได้จากการใช้เครื่องมืออัดแรงแบบแกนเดี่ยวประกอบในการวัดสมบัติไดอิเล็กตริก เช่น ค่าคงที่ไดอิเล็กตริก (ε_r) และการสูญเสียทางไดอิเล็กตริก ($\tan \delta$) และสมบัติอื่นๆ เช่น สมบัติเฟร์โรอิเล็กทริกฮิสเทอรีซิส (วงวน P-E) ของสารเซรามิกในทุกระบบที่กล่าวมาภายใต้ความเค้นแบบแกนเดี่ยว และผลงานที่ได้นั้นก็ได้ถูกนำไปตีพิมพ์ในวารสารทางวิชาการต่างๆ ดังต่อไปนี้ (รายละเอียดได้ถูกนำเสนอในแต่ละผลงานแล้ว และในกรณีที่เป็นผลงานตีพิมพ์ในวารสารวิชาการนานาชาติสามารถค้นคว้าเพิ่มเติมได้ในภาคผนวก)

ผลงานตีพิมพ์ในวารสารวิชาการนานาชาติ (จำนวน 3 เรื่อง)

1. Muangjai Unruan, Anurak Prasatkhetragarn, Yongyut Laosiritaworn, Supon Ananta, and **Rattikorn Yimnirun**, "Dielectric Properties of PZT-PCN Ceramics Under Compressive Stress" *Physica Scripta,* 77, pp 571-574 (2008).
2. Muangjai Unruan , Anurak Prasatkhetragarn, Yongyut Laosiritaworn, Supon Ananta, and **Rattikorn Yimnirun**, "Changes in Dielectric Properties of $Pb(Zr_{1/2}Ti_{1/2})O_3$-$Pb(Co_{1/3}Nb_{2/3})O_3$ Ceramics Under Compressive Stress

Applied Perpendicular to Electric Field" to *J. Phys. D:Applied Physics,* **41**, pp 245405 (2008)

3. Muangjai Unruan , Anurak Prasatkhetragarn, Athipon Ngamjarurojana, Yongyut Laosiritaworn, Supon Ananta, and **Rattikorn Yimnirun**, "Changes in Dielectric and Ferroelectric Properties of $Pb(Zr_{1/2}Ti_{1/2})O_3$-$Pb(Ni_{1/3}Nb_{2/3})O_3$ Ceramics Under Compressive Stress" *J. Applied Physics,* **105***,* (2009)

ส่วนที่ 4: ในส่วนนี้ เป็นการศึกษาหาองค์ความรู้ใหม่ด้านอื่นๆที่ถือเป็นการต่อยอดจากผลงานที่ได้ศึกษามาในเบื้องต้น ซึ่งผลงานที่ได้มีความหลากหลายและเป็นจุดเริ่มต้นในการวิจัยอีกหลายๆโครงการของผู้ที่มีส่วนร่วมในโครงการวิจัยนี้ และผลงานที่ได้นั้นก็ได้ถูกนำไปตีพิมพ์ในวารสารทางวิชาการต่างๆ ดังต่อไปนี้ (รายละเอียดได้ถูกนำเสนอในแต่ละผลงานแล้ว และในกรณีที่เป็นผลงานตีพิมพ์ในวารสารวิชาการนานาชาติสามารถค้นคว้าเพิ่มเติมได้ในภาคผนวก)

ผลงานตีพิมพ์ในวารสารวิชาการนานาชาติ (จำนวน 12 เรื่อง)

1. Yongyut Laosiritaworn, Supon Ananta**,** and **Rattikorn Yimnirun**, "Effects of Temperature Gradient of Magnetic Properties of Ising Thin-Film", *Physical Review B,* 75, pp 054417 (2007)
2. Prasit Thongbai, Chivalrat Masingboon, Santi Maensir, T. Yamwong, S. Wongsaenmai, and **R. Yimnirun**, "Giant dielectric behavior of $CaCu_3Ti_4O_{12}$ subjected to post-sintering annealing and uniaxial stress" *J. Phys.: Condensed Matter,* 19, pp 236208-1-10 (2007).
3. R. Wongmaneerung, X. Tan, R.W. McCullum, S. Ananta, and **R. Yimnirun**, Cation-, dipole-, and spin-order in $Pb(Fe_{2/3}W_{1/3})O_3$-based magnetoelectric multiferroic compounds" *Applied Physics Letters,* 90, 242905 (2007)
4. **R. Yimnirun**, R. Wongmaneerung, S. Wongsaenmai, A. Ngamjarurojana, S. Ananta, and Y. Laosiritaworn, "Temperature Scaling of Dynamic Hysteresis in Hard Lead Zirconate Titanate Bulk Ceramic" *Applied Physics A*, 89, pp 737-741 (2007).
5. Prasit Thongbai, Santi Maensiri, Teerapon Yamwong, and **Rattikorn Yimnirun** "Giant dielectric properties of $CaCu_3Ti_4O_{12}$/(Li, Ti)-doped NiO composites subjected to post-sintering annealing and compressive stress" *J. Applied Physics*, 103, pp 114107-1-6 (2008).

6. **Rattikorn Yimnirun,** "Scaling Behavior of Dynamic Hysteresis in PZT-Based Ferroelectric Bulk Ceramics" *Functional Materials Letters*, 1(2), pp 133-137 (2008).
7. M. Unruan, T. Sareein, J. Tangsritrakul, S. Prasertpalichatr, A. Ngamjarurojana, S. Ananta, and **R. Yimnirun**, "Changes in Dielectric and Ferroelectric Properties of Fe^{3+}/Nb^{5+} Hybrid-Doped Barium Titanate Ceramics Under Compressive Stress" *J. Applied Physics,* **104**, pp 124102-1-5 (2008)
8. N. Wongdamnern, A. Ngamjarurojana, Y. Laosiritaworn, S. Ananta, and **R. Yimnirun**, "Dynamic Ferroelectric Hysteresis Scaling in $BaTiO_3$ Single Crystals" *Journal of Applied Physics,* 105, 044109 (2009)
9. O. Khamman, X. Tan, S. Ananta, and **R. Yimnirun**, "The morphotropic phase boundary and electrical properties of $(1-x)Pb(Zn_{1/2}W_{1/2})O_3$—$xPb(Zr_{0.5}Ti_{0.5})O_3$ ceramics" *J. Materials Science*, 44, pp 1868-1872 (2009)
10. T. Sareein, M. Unruan, A. Ngamjarurojana, S. Jiansirisomboon, A. Watcharapasorn, and **R. Yimnirun**, "Influences of Compressive Stress and Aging on Dielectric Properties of Sodium Bismuth Titanate Ceramics" *Physics Letters A,* 373, pp 1583-1587 (2009)
11. **Rattikorn Yimnirun**, Muangjai Unruan, Rewadee Wongmaneerung, Orawan Khamman, Wanwilai Chaisan, and Supon Ananta, "Dielectric Properties of Complex Perovskite PZBT-PMNT Ceramic Under Compressive Stress" *International Journal of Modern Physics B* (2009) *accepted*
12. A. Chaipanich, N. Jaitanong and **R. Yimnirun**, "Ferroelectric Hysteresis Behavior in 0-3 PZT-Cement Composites: Effects of Frequency and Electric Field" *Ferroelectric Letters* (2009) *accepted*

ผลงานตีพิมพ์ในวารสารประกอบการประชุมวิชาการระดับนานาชาติ (จำนวน 5 เรื่อง)

1. W. Chaisan, **R. Yimnirun**, S. Ananta, " Effects of Compressice Stress of Ferroelectric Properties of BT Ceramics" *Physica Scripta*, T129, pp 205-208 (2007)
2. N. Wongdamnern, N. Triamnak, A. Ngamjarurojana, Y. Laosiritaworn, S. Ananta, and **R. Yimnirun**, "Comparative Studies of Dynamic Hysteresis Responses in Hard and Soft PZT Ceramics" *Ceramics International,* 34(4), pp 731-734 (2008).

3. Y. Laosiritaworn, S. Ananta, J. Poulter, and **R. Yimnirun**, “Monte Carlo investigation of hysteresis properties in ferroelectric thin-films under the effect of uniaxial stresses” *Ceramics International*, 35*,* pp 181-184 (2009)
4. W. Chaisan, **R. Yimnirun**, and S. Ananta, “Preparation and characterization of ceramic nanocomposites in the PZT–BT system” *Ceramics International,* 35*,* pp 121-124 (2009)
5. W. Chaisan, **R. Yimnirun**, and S. Ananta, “Effect of vibro-milling time on phase formation and particle size of barium titanate nanopowders” *Ceramics International*, 35*,* pp 173-176 (2009)

เอกสารอ้างอิง

1. B. Jaffe, W.R. Cook Jr., and H. Jaffe, *Piezoelectric Ceramics*, Academic Press, 1971.
2. Y. Xu, *Ferroelectric Materials and Their Applications*, North-Holland, 1991.
3. A.J. Moulson and J.M. Herbert, *Electroceramics*, Chapman and Hall, 1993.
4. R.E. Newnham and G.R. Ruschau, *Am. Ceram. Soc. Bull*. **75**[10] 51 (1996).
5. K. Uchino, *Piezoelectric Actuators and Ultrasonic Motors*, Kluwer Academic, 1997.
6. J.F. Scott, *Ferroelectrics*, **206/207**, 365 (1998).
7. G.H. Haertling, *J. Am. Ceram. Soc.* **82**[4] 797 (1999).
8. A.S. Bhalla, R. Guo and R. Roy, Mat. Res. Innovat. **4**, 3 (2000)
9. S.E.E Park and W. Hackenberger, *Current Opinion Sol. State Mat. Sci.* **6**, 11 (2002).
10. H. Chen, X. Guo and Z. Meng, *Mater. Chem.Phys.* **75**, 202 (2002).
11. R. Zuo, L. Li, X. Hu and Z. Gui, *Mater. Lett*. **54**, 185 (2002).
12. Y. H. Chen, K. Uchino, M. Shen and D. Viehland, *J. Appl. Phys.* **90(3)**, 1455 (2001).
13. H. Chen, J. Long and Z. Meng, *Mater. Sci. Eng*. **B99**, 433 (2003).
14. S. Priya, K. Uchino and D. Viehland, *Appl. Phys. Lett*. **81(13)**, 2430 (2002).
15. N. Yasuda, H. Ohwa, M. Kume, K. Hayashi, Y. Hosono and Y. Yamashita, *J. Cryst. Growth*. **229**, 299 (1999).
16. E. F. Alberta and A. S. Bhalla, *Mater. Lett*. **40**, 114 (1999).
17. E. F. Alberta and A. S. Bhalla, *Mater. Lett*. **29**, 127 (1996).
18. H. Ouchi, *J. Am. Ceram. Soc.* **51** 169 (1968).
19. C.H. Wang, *J. Eur. Ceram. Soc*. **22** 2033 (2002).

20. R. Yimnirun, S. Ananta, E. Meechoowas and S. Wongsaenmai, *J. Phys. D: Appl. Phys*. **36,** 1615 (2003).
21. R. Yimnirun, S. Ananta and P. Laoratanakul, *Mater. Sci. Eng. B* **112,** 79 (2004).
22. W. Chaisan, R. Yimnirun, S. Ananta and D. Cann, *Mater. Lett.*, **59,** 3732 (2005).
23. R. Yimnirun, S. Ananta and P. Laoratanakul, *J. Eur. Ceram. Soc* **25,** 3225 (2005).
24. R. Tipakontitikul, S. Ananta, and R. Yimnirun, *Curr. Appl. Phys.* **6**, 307 (2006).
25. H. Cai, Z. Gui and L.T. Li, *Mat. Sci. Eng. B-Solid* **83**, 137 (2001).
26. A.S. Bhalla, R. Guo and E.F. Alberta, *Mater. Lett.* **54**, 264 (2002).
27. R. Yimnirun, R. Tipakontitikul, and S. Ananta, *Int. J. Mod. Phys. B* **20**, 2415 (2006).
28. T.R. Shrout and J.P. Dougherty, *Ceramic Transactions: Ceramic Dielectrics*, American Ceramic Society, Westerville, O.H. **8**, 3 (1990).
29. S. Ananta and N.W. Thomas, *J. Eur. Ceram. Soc*. **19**, 1873 (1999).
30. S. Wongsaenmai, Y. Laosiritaworn, S. Ananta, and R. Yimnirun, *Mater. Sci. Eng. B* **128**, 83 (2006).
31. A.L. Costa, C. Galassi, G. Fabbri, E. Roncari and C. Capiani, *J. Eur. Ceram. Soc*. **21**, 1165 (2001).
32. J. Kuwata, K. Uchino and S. Nomura, *Jpn. J. Appl. Phys., Part 1*, **21**, 1298 (1982).
33. S.E. Park and T.R. Shrout, *J. Appl. Phys.* **82**, 1804 (1997).
34. B.D. Stojanovic, *J. Mater. Proc. Tech.* **143-144**, 78 (2003).
35. N. Vittayakorn, G. Rujijanagul, T. Tunkasiri, X. Tan, and D. P. Cann, *Mat. Sci. Eng. B* **108**, 258 (2004).
36. N. Vittayakorn, G. Rujijanagul, T. Tunkasiri, X. Tan and D. P. Cann, *J. Mat. Res.* **18**, 2882 (2003)
37. N. Vittayakorn, G. Rujijanagul, X, Tan, M. A. Marquardt, and D. P. Cann, *J. Appl. Phys.* **96(9)**, 5103 (2004)
38. N. Vittayakorn, G. Rujijanagul, X, Tan, and D. P. Cann, *J. Electroceramics* (*in press)*
39. N. Vittayakorn, G. Rujijanagul, X, Tan, and D. P. Cann, *Curr. Appl. Phys.* (*in press*).
40. E.F. Alberta and A.S. Bhalla, *J. Phys. Chem. Solids*, **63**, 1759 (2002).
41. H.K. Guo, X.G. Tang, J.X. Zhang, S.W. Shan, M.M. Wu and Y.J. Luo, *J. Mater. Sci. Lett.* **17**, 1567 (1998).
42. M. Lejeune and J.P. Boilot, *Mater. Res. Bull*. **17**, 1245 (1982).
43. K. Chen, C. Li, X. Zhang and Y. Huang, *Mater. Lett*. **57**, 20 (2002).
44. H. Fan and H.E. Kim, *J. Appl. Phys.* **91(1)**, 317 (2002).

45. N. Vittayakorn, S. Uttiya, G. Rujijanagul, and D. P. Cann, *J. Phys. D: Appl. Phys.*, **38**, 2942 (2005)
46. R. Yimnirun, Y. Laosiritaworn, and S. Wongsaenmai, *J. Phys. D: Appl. Phys.* **39,** 759 (2006).
47. Q.M. Zhang, J. Zhao, K. Uchino and J. Zheng, *J. Mater. Res.* **12[1],** 226 (1997).
48. D. Viehland, J.F. Li, E. McLaughlin, J. Powers, R. Janus and H. Robinson, *J. Appl. Phys.* **95(4)**, 1969 (2004).
49. I.J. Fritz, *J. Appl. Phys.* **49(9)**, 4922 (1978).
50. D. Viehland and J. Powers, *Appl. Phys. Lett.* **78(20)**, 3112 (2001).
51. R. Yimnirun, *Ferroelectrics* **331**, 9 (2006).
52. J. Zhao, A.E. Glazounov and Q.M. Zhang, *Appl. Phys. Lett.* **74(3)**, 4362 (1999).
53. R. Yimnirun, M. Unruen, Y. Laosiritaworn, and S. Ananta, *J. Phys. D: Appl. Phys.* **39**, 3097 (2006).
54. R. Yimnirun, S. Wongsaenmai, A. Ngamjarurojana, and S. Ananta, *Curr. Appl. Phys,* **6** 520 (2006).
55. รัตติกร ยิ้มนิรัญ, อิทธิพลของความเค้นแบบแกนเดี่ยวต่อสมบัติไดอิเล็กตริกและไฟฟ้าเชิงกลของสารเซรามิกในระบบ PMN-PZT, รายงานฉบับสมบูรณ์ โครงการทุนส่งเสริมนักวิจัยรุ่นใหม่, สนับสนุนโดยสำนักงานกองทุนสนับสนุนการวิจัย (สกว.) พ.ศ. 2545.
56. สุพล อนันตา, อิทธิพลของปัจจัยในกระบวนการเตรียมต่อการเกิดเฟส โครงสร้างจุลภาค และสมบัติไดอิเล็กตริกของสารเซรามิก PBZT-PMNT, รายงานฉบับสมบูรณ์ โครงการทุนพัฒนานักวิจัย, สนับสนุนโดยสำนักงานกองทุนสนับสนุนการวิจัย (สกว.) พ.ศ. 2546.
57. รัตติกร ยิ้มนิรัญ, อิทธิพลของความเค้นแบบแกนเดี่ยวต่อสมบัติไดอิเล็กตริกของสารเฟร์โรอิเล็กตริกเซรามิก, รายงานฉบับสมบูรณ์ โครงการทุนพัฒนานักวิจัย, สนับสนุนโดยสำนักงานกองทุนสนับสนุนการวิจัย (สกว.) พ.ศ. 2547.

Output จากโครงการวิจัยที่ได้รับทุนจาก สกอ. และ สกว.

1. ผลงานตีพิมพ์ในวารสารวิชาการนานาชาติ จำนวนทั้งสิ้น 46 เรื่องได้แก่ (*รายละเอียดในภาคผนวก*)

1. Yongyut Laosiritaworn, Supon Ananta**,** and **Rattikorn Yimnirun**, "Effects of Temperature Gradient of Magnetic Properties of Ising Thin-Film", *Physical Review B,* 75, pp 054417 (2007).
2. Prasit Thongbai, Chivalrat Masingboon, Santi Maensir, T. Yamwong, S. Wongsaenmai, and **R. Yimnirun**, "Giant dielectric behavior of $CaCu_3Ti_4O_{12}$ subjected to post-sintering annealing and uniaxial stress" *J. Phys.: Condensed Matter,* 19, pp 236208-1-10 (2007).
3. R. Wongmaneerung, X. Tan, R.W. McCullum, S. Ananta, and **R. Yimnirun**, Cation-, dipole-, and spin-order in $Pb(Fe_{2/3}W_{1/3})O_3$-based magnetoelectric multiferroic compounds" *Applied Physics Letters,* 90, 242905 (2007)
4. S. Wongsaenmai, W. Qu, S. Ananta, **R. Yimnirun**, and X. Tan, "Effect of Ba-substitution on the structure and properties of $Pb_{0.8}Ba_{0.2}In_{0.5}Nb_{0.5}O_3$ ceramics" *Applied Physics A,* 88, pp 757-761 (2007).
5. O. Khamman, **R. Yimnirun**, and S. Ananta, "Effect of calcination conditions on phase formation and particle size of lead nickel niobate powders synthesized by using $Ni_4Nb_2O_9$ precursor" *Materials Letters,* 61, pp 4466-4470 (2007)
6. **R. Yimnirun**, R. Wongmaneerung, S. Wongsaenmai, A. Ngamjarurojana, S. Ananta, and Y. Laosiritaworn, "Temperature Scaling of Dynamic Hysteresis in Hard Lead Zirconate Titanate Bulk Ceramic" *Applied Physics A*, 89, pp 737-741 (2007).
7. N. Vittayakorn, S. Wirunchit, S. Traisak, **R. Yimnirun**, G. Rujijanagul, "Development of Perovskite and Phase Transition in Lead Cobalt Niobate Modified Lead Zirconate Titanate System" *Current Applied Physics,* 8, pp 128-133 (2008)
8. S. Wongsaenmai, **R. Yimnirun,** S. Ananta, R. Guo, and, A. Bhalla, "Thermal Expansion Measurement in the Relaxor Ferroelectric PIN-PT System" *Materials Letters*, 62, pp 352-356 (2008)

9. Anurak Prasatkhetragarn, Naratip Vittayakorn, Supon Ananta, **Rattikorn Yimnirun** and David P. Cann, "Synthesis, dielectric and ferroelectric properties of ceramics in the *(1-x)*$Pb(Zr_{1/2}Ti_{1/2})O_3$ – *(x)*$Pb(Co_{1/3}Nb_{2/3})O_3$ system" *Japan Journal of Applied Physics*, 47(2), pp 998-1002 (2008).
10. M. Unruan, S. Wongsaenmai, Y. Laosiritaworn, S. Ananta, and **R. Yimnirun**, "Changes in Dielectric Properties of $Pb(In_{1/2}Nb_{1/2})O_3$-$PbTiO_3$ Ceramics Under Compressive Stress Applied Parallel and Perpendicular to Electric Field" *J. Phys. D: Appl. Phys.,* 41*,* pp 541-545 (2008)*.*
11. Supattra Wongsaenmai, Xiaoli Tan, Supon Ananta, and **Rattikorn Yimnirun**, "Dielectric and Ferroelectric Properties of Fine Grains $Pb(In_{1/2}Nb_{1/2})O_3$–$PbTiO_3$ Ceramics" *Journal of Alloys and Compounds*, 454, pp 331-339 (2008).
12. Muangjai Unruan, Anurak Prasatkhetragarn, Yongyut Laosiritaworn, Supon Ananta, and **Rattikorn Yimnirun**, "Dielectric Properties of PZT-PCN Ceramics Under Compressive Stress" *Physica Scripta,* 77, pp 571-574 (2008).
13. **R. Yimnirun**, N. Wongdamnern, N. Triamnak, M. Unruan, A. Ngamjarurojana, S. Ananta, and Y. Laosiritaworn, "Stress-Dependent Scaling Behavior of Sub-Coercive Field Dynamic Ferroelectric Hysteresis in $Pb(Zn_{1/3}Nb_{2/3})O_3$-Modified $Pb(Zr_{1/2}Ti_{1/2})O_3$ Ceramic" *J. Applied. Physics,* 103 (8)*,* pp 086105-1-3 (2008).
14. O. Khamman, **R. Yimnirun**, and S. Ananta, "Effect of vibro-milling time on phase formation and particle size of nickel niobate nanopowders" *Materials Science and Engineering B*, 150(1), pp 12-17 (2008)
15. Prasit Thongbai, Santi Maensiri, Teerapon Yamwong, and **Rattikorn Yimnirun** "Giant dielectric properties of $CaCu_3Ti_4O_{12}$/(Li, Ti)-doped NiO composites subjected to post-sintering annealing and compressive stress" *J. Applied Physics*, 103, pp 114107-1-6 (2008)*.*
16. R. Wongmaneerung, **R. Yimnirun,** S. Ananta,. A. Bhalla, and R. Guo, "Thermal Expansion Measurement in the PMN-PT Ceramic Systems" *J. Alloys and Compounds,* 461, pp 565-569 (2008)*.*
17. Muangjai Unruan, Athipong Ngamjarurojana, Yongyut Laosiritaworn, Supon Ananta, and **Rattikorn Yimnirun**, "Influences of Perpendicular Compressive Stress on Ferroelectric Properties of Electrostrictive and

Piezoelectric $Pb(Mg_{1/3}Nb_{2/3})O_3$-$PbTiO_3$ Ceramics" *J. Applied Physics.* 104, 034101 (2008).

18. Orawan Khamman, **Rattikorn Yimnirun**, Supon Ananta, "Effect of Niobate B-Site Precursor of Phase Formation of PNN Powders" *J. Alloys and Compounds*, 465, pp522-526 (2008).
19. Muangjai Unruan, Naratip Vittayakorn, Rewadee Wongmaneeruang, Anurak Prasatkhetragarn, Supon Ananta and **Rattikorn Yimnirun**, "Synthesis and Properties of $Pb(Co_{1/3}Nb_{2/3})O_3$ Ceramics" *J. Alloys and Compounds*, 466, pp 264-267 (2008).
20. M. Unruan, R. Wongmaneerung, A. Ngamjarurojana, S. Ananta, Y. Laosiritaworn, and **R. Yimnirun,** "Changes of Ferroelectric Properties of Lead Magnsium Niobate-Lead Titanate Ceramics Under Compressive Stress" *J. Applied Physics.* 104, 064107 (2008)
21. **R. Yimnirun**, N. Wongdamnern, N. Triamnak, M. Unruan, A. Ngamjarurojana, S. Ananta, and Y. Laosiritaworn, "Stress-Dependent Scaling Behavior of Sub-Coercive Field Dynamic Ferroelectric Hysteresis in $0.4Pb(Zn_{1/3}Nb_{2/3})O_3$-$0.6Pb(Zr_{1/2}Ti_{1/2})O_3$ Ceramic" *J. Physics: Condensed Matters.* 20, 415202 (2008)
22. **R. Yimnirun**, N. Wongdamnern, N. Triamnak, T. Sareein, M. Unruan, A. Ngamjarurojana, S. Ananta, and Y. Laosiritaworn, "Power-law Scaling of Sub-Coercive Field Dynamic Ferroelectric Hysteresis in $0.3Pb(Zn_{1/3}Nb_{2/3})O_3$-$0.7Pb(Zr_{1/2}Ti_{1/2})O_3$ Ceramic" *J. Physics D: Applied. Physics,* 41, 205415 (2008)
23. **Rattikorn Yimnirun,** "Scaling Behavior of Dynamic Hysteresis in PZT-Based Ferroelectric Bulk Ceramics" *Functional Materials Letters*, 1(2), pp 133-137 (2008).
24. S. Ananta,, **R. Yimnirun**, and O. Khamman "Effect of nickel niobate B-site precursors on phase formation, microstructure and dielectric properties of perovskite PNN ceramics" *Functional Materials Letters*, 1(3), pp 229-233 (2008)
25. Muangjai Unruan , Anurak Prasatkhetragarn, Yongyut Laosiritaworn, Supon Ananta, and **Rattikorn Yimnirun**, "Changes in Dielectric Properties of $Pb(Zr_{1/2}Ti_{1/2})O_3$-$Pb(Co_{1/3}Nb_{2/3})O_3$ Ceramics Under Compressive Stress

Applied Perpendicular to Electric Field" to *J. Phys. D:Applied Physics,* **41**, pp 245405 (2008)

26. **R. Yimnirun**, N. Wongdamnern, N. Triamnak, M. Unruan, A. Ngamjarurojana, S. Ananta, and Y. Laosiritaworn, "Stress-Dependent Scaling Behavior of Sub-Coercive Field Dynamic Ferroelectric Hysteresis in $0.5Pb(Zn_{1/3}Nb_{2/3})O_3$-$0.5Pb(Zr_{1/2}Ti_{1/2})O_3$ Ceramic" *J. Applied. Physics,* **104***,* pp 104103-1-4 (2008)
27. M. Unruan, T. Sareein, J. Tangsritrakul, S. Prasertpalichatr, A. Ngamjarurojana, S. Ananta, and **R. Yimnirun**, "Changes in Dielectric and Ferroelectric Properties of Fe^{3+}/Nb^{5+} Hybrid-Doped Barium Titanate Ceramics Under Compressive Stress" *J. Applied Physics,* **104**, pp 124102-1-5 (2008)
28. **Rattikorn Yimnirun**, Narit Triamnak, Muangjai Unruan, Athipong Ngamjarurojana, Yongyut Laosiritaworn, and Supon Ananta, "Ferroelectric Properties of $Pb(Zr_{1/2}Ti_{1/2})O_3$—$Pb(Zn_{1/3}Nb_{2/3})O_3$ Ceramics Under Compressive Stress" *Current Applied Physics*, 9, pp 249-252 (2009)
29. R. Wongmaneerung, **R. Yimnirun**, S. Ananta, "Processing and Properties of $Pb(Mg_{1/3}Nb_{2/3})O_3$-$PbTiO_3$ Based Ceramics" *Current Applied Physics*, 9, pp 268-273 (2009).
30. **R. Yimnirun**, S. Wongsaenmai, S. Ananta, N. Triamnak, "Dielectric Properties of PIN-PT Ceramics Under Compressive Stress" *Current Applied Physics,* 9, pp 422-425 (2009).
31. P. Ketsuwan, Y. Laosiritaworn, S. Ananta, **R. Yimnirun**, "Electrical Properties of Nb-Doped $Pb(Zr_{0.52}Ti_{0.48})O_3$ Ceramics" *International Journal of Modern Physics B*, 23, pp 105-111 (2009)
32. **R. Yimnirun** "Dielectric Properties of PMN-PT Prepared by Mixed Oxide Method" *International Journal of Modern Physics B*, 23(3), pp 403-410 (2009)
33. R. Wongmaneerung, **R. Yimnirun**, and S. Ananta, "Effect of two-stage sintering on phase formation, microstructure and dielectric properties of perovskite PMN ceramics derived from a corundum $Mg_4Nb_2O_9$ precursor" *Materials Chemistry and Physics*, 114, pp 569-575 (2009)

34. N. Wongdamnern, A. Ngamjarurojana, Y. Laosiritaworn, S. Ananta, and **R. Yimnirun**, "Dynamic Ferroelectric Hysteresis Scaling in $BaTiO_3$ Single Crystals" *Journal of Applied Physics,* 105, 044109 (2009)
35. S. Wongsaenmai, S. Ananta, and **R. Yimnirun**, "Effects of Addition of BT on Structural Phase Formation and Electrical Properties of Relaxor Ferroelectric $Pb(In_{0.5}Nb_{0.5})_{(1-x)}Ti_{(x)}O_3$ ceramics" *J. Alloys and Compounds,* 474, pp 241-245 (2009)
36. R. Wongmaneerung, A. Rujiwatra, **R. Yimnirun**, and S. Ananta, "Fabrication and Dielectric Properties of Self-reinforced Lead Titanate Nanocomposites" *J. Alloys and Compounds,* 475, pp 473-478 (2009)
37. R. Wongmaneerung, P. Singjai, **R. Yimnirun** and S. Ananta, "Effects of SiC nanofibers Addition on Microstructure and Dielectric Properties of Lead Titanate Ceramics" *J. Alloys and Compounds,* 475, pp 456-462 (2009)
38. Anurak Prasatkhetragarn, Athipong Ngamjarurojana, Yongyut Laosiritaworn, Supon Ananta, **Rattikorn Yimnirun**, and David Cann, "Effects of Zr/Ti ratio on phase formation and electrical properties of $0.8Pb(Zr_{1/2}Ti_{1/2})O_3$-$0.2Pb(Co_{1/3}Nb_{2/3})O_3$ ceramics" *Current Applied Physics*, 9, pp 802-806 (2009)
39. O. Khamman, X. Tan, S. Ananta, and **R. Yimnirun**, "The morphotropic phase boundary and electrical properties of (1-*x*)$Pb(Zn_{1/2}W_{1/2})O_3$—*x*$Pb(Zr_{0.5}Ti_{0.5})O_3$ ceramics" *J. Materials Science*, 44, pp 1868-1872 (2009)
40. T. Sareein, M. Unruan, A. Ngamjarurojana, S. Jiansirisomboon, A. Watcharapasorn, and **R. Yimnirun**, "Influences of Compressive Stress and Aging on Dielectric Properties of Sodium Bismuth Titanate Ceramics" *Physics Letters A,* 373, pp 1583-1587 (2009)
41. Anurak Prasatkhetragarn, Piyachon Ketsuwan, Supon Ananta, **Rattikorn Yimnirun**, and David Cann "Phase Formation, Microstructure and Dielectric Properties of $(1-x)Pb(Zr_{1/2}Ti_{1/2})O_3$–$xPb(Co_{1/3}Nb_{2/3})O_3$ Ceramics" *Materials Letters,* 63, pp 1281-1284 (2009)
42. Muangjai Unruan , Anurak Prasatkhetragarn, Athipon Ngamjarurojana, Yongyut Laosiritaworn, Supon Ananta, and **Rattikorn Yimnirun**, "Changes in Dielectric and Ferroelectric Properties of $Pb(Zr_{1/2}Ti_{1/2})O_3$-

$Pb(Ni_{1/3}Nb_{2/3})O_3$ Ceramics Under Compressive Stress" *J. Applied Physics* (2009)

43. R. Wongmaneerung, **R. Yimnirun**, and S. Ananta, "Effect of Magnasium Niobate Precursors on Phase Formation, Microstructure and Dielectric Properties of Perovskite Lead Magnesium Niobate Ceramics" *J. Alloys and Compounds* (2008) *in pres*
44. Anurak Prasatkhetragarn, Athipong Ngamjarurojana, Yongyut Laosiritaworn, Supon Ananta, **Rattikorn Yimnirun**, and David Cann, "Effects of sintering conditions on phase formation and electrical properties of $0.8Pb(Zr_{1/2}Ti_{1/2})O_3$-$0.2Pb(Co_{1/3}Nb_{2/3})O_3$ ceramics" *Current Applied Physics* (2009) *in press*
45. **Rattikorn Yimnirun**, Muangjai Unruan, Rewadee Wongmaneerung, Orawan Khamman, Wanwilai Chaisan, and Supon Ananta, "Dielectric Properties of Complex Perovskite PZBT-PMNT Ceramic Under Compressive Stress" *International Journal of Modern Physics B* (2009) *accepted*
46. A. Chaipanich, N. Jaitanong and **R. Yimnirun**, "Ferroelectric Hysteresis Behavior in 0-3 PZT-Cement Composites: Effects of Frequency and Electric Field" *Ferroelectric Letters* (2009) *accepted*

2. การนำผลงานวิจัยไปใช้ประโยชน์

2.1 เชิงพาณิชย์

ในการวิจัยนี้ถึงแม้ไม่ได้มุ่งหวังในด้านการนำผลงานไปใช้ประโยชน์ในเชิงพาณิชย์ แต่มุ่งเน้นในการสร้างองค์ความรู้ใหม่ แต่อุปกรณ์ที่ถูกพัฒนาขึ้นมาใช้ประกอบการศึกษา ซึ่งได้แก่ ชุดอุปกรณ์ในการวัดสมบัติทางไฟฟ้าภายใต้ความเค้นนั้น สามารถนำไปประยุกต์ใช้ในการวัดสมบัติดังกล่าวทั้งในกรณีที่ไม่มีความเค้นและกรณีที่มีความเค้นในวัสดุตัวอื่นๆได้ ซึ่งสามารถที่จะลดการสั่งซื้ออุปกรณ์ที่มีความคล้ายคลึงจากต่างประเทศได้

2.2 เชิงนโยบาย

ผลการวิจัยที่ได้จากโครงการนี้ได้ถูกนำไปใช้ในการกำหนดแผนและทิศทางการวิจัยของกลุ่มผู้วิจัยที่ชัดเจนขึ้น ดังจะเห็นได้จากการเสนอหัวข้อวิจัยเพื่อขอรับทุนพัฒนาศักยภาพการทำงานวิจัยของอาจารย์รุ่นใหม่และรุ่นกลาง ประจำปี 2550-2551 ของ

อดีตผู้ร่วมวิจัยหลายท่าน จากสำนักงานกองทุนสนับสนุนการวิจัยและสำนักงานคณะกรรมการการอุดมศึกษา ซึ่งเป็นการวิจัยต่อเนื่องจากโครงการวิจัยนี้ เพื่อเป็นการส่งเสริมให้เกิดการวิจัยแบบมีทิศทางมากขึ้น

2.3 เชิงสาธารณะ

โครงการวิจัยนี้ได้ก่อให้เกิดเครือข่ายความร่วมมือในการวิจัยมากขึ้นระหว่างนักวิจัยรุ่นกลางและนักวิจัยรุ่นใหม่ทั้งในและต่างประเทศ เช่นความร่วมมืออย่างใกล้ชิดในการวิจัยกับ รศ. ดร. สุพล อนันตา ภาควิชาฟิสิกส์และวัสดุศาสตร์ คณะวิทยาศาสตร์ มหาวิทยาลัยเชียงใหม่ ซึ่งเน้นการวิจัยด้านกระบวนการผลิตเซรามิก ในขณะที่ผู้วิจัยได้มีส่วนร่วมในการวัดสมบัติทางไฟฟ้าของเซรามิกที่ผลิตขึ้น นอกจากนี้ก็มีความร่วมมือกับ ผศ. ดร. ยงยุทธ เหล่าศิริถาวร ภาควิชาฟิสิกส์และวัสดุศาสตร์ คณะวิทยาศาสตร์ มหาวิทยาลัยเชียงใหม่ ที่นำความรู้เรื่องฟิสิกส์คณานามาประกอบการคำนวณหลายๆอย่าง และการร่วมมืออย่างเหนียวแน่นกับ อ.ดร. อธิพงศ์ งามจารุโรจน์ ในการพัฒนาอุปกรณ์และเครื่องมือในการวัดต่างๆ นอกจากนี้ยังได้มีการสร้างความร่วมมือด้านการวิจัยกับนักวิจัยในต่างประเทศคือ Prof. David Cann แห่ง Oregon State University และ Prof. Xiaoli Tan แห่ง Iowa State University สหรัฐอเมริกา และที่สำคัญที่สุดผู้วิจัยได้รับความรู้ในการวิจัยจากนักวิจัยอาวุโสจากต่างประเทศคือ Prof. Robert Newnham Prof. L. Eric Cross Prof. Kenji Uchino แห่ง The Pennsylvania State University สหรัฐอเมริกา และ Prof. Amar Bhalla แห่ง University of Texas at San Antonio สหรัฐอเมริกา

2.4 เชิงวิชาการ (พัฒนาการเรียนการสอน/สร้างนักวิจัยใหม่)

ผลงานที่ได้จากการวิจัยนี้ได้ถูกนำไปใช้ประกอบการเรียนการสอนในหลายๆ กระบวนวิชาของสาขาวิชาวัสดุศาสตร์ ในระดับบัณฑิตศึกษา เช่น MATS 701 Characterization and Properties of Materials MATS 703 Fabrication Processes of Materials MATS 723 Ferroelectric Materials MATS 743 Electroceramics และ MATS 745 Physical Properties of Crystals นอกจากนี้ผู้วิจัยยังนำผลงานบางส่วนไปประกอบการเขียนตำราเรื่อง สมบัติทางไฟฟ้าของเซรามิกเฟร์โรอิเล็กทริก (Electrical Properties of Ferroelectric Ceramics) สำหรับในส่วนของการสร้างนักวิจัยใหม่นั้น นอกจากประโยชน์โดยตรงที่เกิดกับผู้วิจัยเองแล้ว โครงการวิจัยนี้ได้มีส่วนในการฝึกฝนทักษะการวิจัยและการเผยแพร่ผลงานให้กับนักศึกษาทั้งในระดับปริญญาตรีและระดับบัณฑิตศึกษาในฐานะผู้ช่วยวิจัยร่วมกับหัวหน้าโครงการ และผลงานวิจัยที่ได้สามารถนำไปตีพิมพ์ในวารสาร

ทางวิชาการทั้งในและต่างประเทศ รวมทั้งการนำเสนอผลงานในที่ประชุมทางวิชาการระดับนานาชาติ (ดังแสดงใน output และผลงานอื่น ๆ) ซึ่งมีผลให้เกิดการพัฒนานักวิจัยรุ่นใหม่และรุ่นกลางมากขึ้น

3. อื่น ๆ (ผลงานตีพิมพ์ในวารสารวิชาการและการเสนอผลงานในที่ประชุมวิชาการนานาชาติ)

3.1 ผลงานตีพิมพ์ในวารสารประกอบการประชุมวิชาการระดับนานาชาติ (Proceedings of International Conferences) จำนวนทั้งสิ้น 8 เรื่องได้แก่

1 **R. Yimnirun**, S. Wongsaenmai, R. Wongmaneerung, N. Wongdamnern, A. Ngamjarurojana, S. Ananta, and Y. Laosiritaworn, " Stress- and Temperature-Dependent Scaling Behavior of Dynamic Hysteres-is in Soft PZT Bulk Ceramics" *Physica Scripta*, T129, pp 184-189 (2007)

2 W. Chaisan, **R. Yimnirun**, S. Ananta, " Effects of Compressice Stress of Ferroelectric Properties of BT Ceramics" *Physica Scripta*, T129, pp 205-208 (2007)

3 N. Wongdamnern, N. Triamnak, A. Ngamjarurojana, Y. Laosiritaworn, S. Ananta, and **R. Yimnirun**, "Comparative Studies of Dynamic Hysteresis Responses in Hard and Soft PZT Ceramics" *Ceramics International,* 34(4), pp 731-734 (2008).

4 W. Laosiritaworn, O. Khamman, S. Ananta, **R. Yimnirun** and Y. Laosiritaworn, "Artificial Neural Network Modeling of Ceramics Powder Preparation: application to $NiNb_2O_6$" *Ceramics International,* 34(4), pp 809-812 (2008).

5 A. Ngamjarurojana, S. Ural, S.H. Park, S. Ananta, **R. Yimnirun**, and K. Uchino, "Piezoelectric Properties of Low Temperature Sintering in $Pb(Zr,Ti)O_3$ - $Pb(Zn,Ni)_{1/3}Nb_{2/3}O_3$ Ceramics for Piezoelectric Transformer Applications" *Ceramics International,* 34(4), pp 705-708 (2008).

6 Y. Laosiritaworn, S. Ananta, J. Poulter, and **R. Yimnirun**, "Monte Carlo investigation of hysteresis properties in ferroelectric thin-films under the effect of uniaxial stresses" *Ceramics International*, 35*,* pp 181-184 (2009)

7 W. Chaisan, **R. Yimnirun**, and S. Ananta, "Preparation and characterization of ceramic nanocomposites in the PZT–BT system" *Ceramics International,* 35*,* pp 121-124 (2009)

8 W. Chaisan, **R. Yimnirun**, and S. Ananta, “Effect of vibro-milling time on phase formation and particle size of barium titanate nanopowders” *Ceramics International*, 35, pp 173-176 (2009)

3.2 การเสนอผลงานในที่ประชุมวิชาการนานาชาติจำนวนทั้งสิ้น 49 เรื่องได้แก่

1. **R. Yimnirun**, S. Wongsaenmai, R. Wongmaneerung, N. Wongdamnern, A. Ngamjarurojana, S. Ananta, and Y. Laosiritaworn, “ Stress- and Temperature-Dependent Scaling Behavior of Dynamic Hysteresis in Soft PZT Bulk Ceramics” ISFM-2007, Hangzhou, China (May 2007). ***Invited Talk***
2. S. Wongsaenmai, S. Ananta, **R. Yimnirun**, R. Guo, A. Bhalla, “Correlation of Ordered-Disordered State and Electrical Properties of BT and PT Substituted PIN Systems” ICMAT-2007, Singapore (July 2007)
3. **R. Yimnirun**, S. Wongsaenmai, R. Wongmaneerung, M. Unruan, N. Wongdamnern, A. Ngamjarurojana, Y. Laosiritaworn, and S. Ananta, “Temperature- and Stress-Dependent Scaling of Ferroelectric Hysteresis in Soft and Hard PZT Bulk Ceramics” MS&T 2007, Detroit, USA (September 2007) ***Invited Talk***
4. R. Wongmaneerung, **R. Yimnirun**, and S.Ananta, “Dielectric Properties of PMN-PT Ceramics” Thailand’s First Nano Conference, Chiang Mai, Thailand (August 2007)
5. **R. Yimnirun**, “Scaling Behavior of Dynamic Hysteresis in PZT Ceramics”, *The 2nd Progress in Advances in Materials and Technology in Thailand Meeting*, Khon Kaen, (2008) ***Invited Talk***
6. **Rattikorn Yimnirun**, Jirapa Tangsritrakul, Saroj Rujirawat, and Sukit Limpijumnong, “Experimental Identification of Mn Site in $BaTiO_3$ by Synchrotron X-Ray Absorption Near-Edge Structure” *The 6th Asian Meeting of Ferroelectrics (AMF-6)*, Taiwan (August 2008) ***Invited Talk***
7. **R. Yimnirun**, N. Triamnak, M. Unruan, S. Wongsaenmai, A. Ngamjarurojana, Y. Laosiritaworn, and S. Ananta, “Dielectric and Ferroelectric Properties of Complex Perovskite Ceramics Under Compressive Stress” ISFM-2007, Hangzhou, China (May 2007).
8. W. Chaisan, **R. Yimnirun**, S. Ananta, “ Effects of Compressive Stress of Ferroelectric Properties of BT Ceramics” ISFM-2007, Hangzhou, China (May 2007).

9. Muangjai Unruan , Anurak Prasatkhetragarn, Yongyut Laosiritaworn, Supon Ananta, and **Rattikorn Yimnirun**, “Effects of Compressive Stress on Dielectric Properties of PZT-PCN Ceramics” ICMAT-2007, Singapore (July 2007)
10. N. Wongdamnern, S. Ananta, Y. Laosiritaworn, and **R. Yimnirun**, “Stress-Dependent Scaling Behavior of Dynamic Hysteresis in Hard Lead Zirconate Titanate Ceramic” ICMAT-2007, Singapore (July 2007)
11. R. Wongmaneerung, **R. Yimnirun,** S. Ananta,. A. Bhalla, and R. Guo, “Thermal Expansion Measurement in the 0.9PMN-0.1PT Ceramics” ICMAT-2007, Singapore (July 2007)
12. O. Khamman, **R. Yimnirun**, and S. Ananta, “A Two-Stage Solid State Reaction of Lead Nickel Niobate Powders” MS&T 2007, Detroit, USA (September 2007)
13. P. Ketsuwan, Y. Laosiritaworn, S. Ananta, **R. Yimnirun**, and D. P. Cann, “Effect of Nb-Doping on Electrical Properties of $Pb(Zr_{0.52}Ti_{0.48})O_3$ Ceramics” MS&T 2007, Detroit, USA (September 2007)
14. P. Ketsuwan, A. Prasatkhetragarn, N. Vittayakorn, C. C. Huang, S. Ananta, **R. Yimnirun**, B. J. Gibbons, D. P. Cann, “$Bi(Zn_{1/2}Ti_{1/2})O_3$-ABO_3 effect for alkaline base perovskite” ISAF 2008, Santa Fe, NM, USA (February 2008)
15. P. Ketsuwan, S. Ananta, Y. Laosiritaworn, **R. Yimnirun**, David P. Cann, “Impedance and Dielectric Properties of Nb-Doped $Pb(Zr_{0.52}Ti_{0.48})O_3$ Ceramics” *The International Conference on Smart Materials: Smart/Intelligent Materials and Nanotechnology-2008 (SmartMat’08 and* IWOFM-2), April 22-25. 2008, Chiang Mai, Thailand.
16. A. Ngamjarurojana , S. Ananta, **R. Yimnirun**, “Effect of Al_2O_3 Addition on Dielectric, Piezoelectric and Ferroelectric Properties of $0.2Pb(Zn_{1/3}Nb_{2/3})O_3$–$0.8Pb(Zr_{1/2}Ti_{1/2})O_3$ Ceramics” *The International Conference on Smart Materials: Smart/Intelligent Materials and Nanotechnology-2008 (SmartMat’08 and* IWOFM-2), April 22-25. 2008, Chiang Mai, Thailand.
17. S. Prasertpalichatr, M. Unruan, S. Rujirawat, S. Limpijumnong, **R. Yimnirun**, “Dielectric and Ferroelectric Aging Effect of Fe^{3+}/Nb^{5+} Hybrid-Doped Barium Titanate Ceramics” *The International Conference on Smart Materials: Smart/Intelligent Materials and Nanotechnology-2008 (SmartMat’08 and* IWOFM-2), April 22-25. 2008, Chiang Mai, Thailand.

18. M. Unruan, R. Wongmaneerung, Y. Laosiritaworn, S. Ananta, **R. Yimnirun**, "Changes in Ferroelectric Properties of 0.7PMN–0.3PT Ceramics with Compressive Stress" *The International Conference on Smart Materials: Smart/Intelligent Materials and Nanotechnology-2008 (SmartMat'08 and* IWOFM-2), April 22-25. 2008, Chiang Mai, Thailand.
19. N. Wongdamnern, A. Ngamjarurojana, S. Ananta, Y. Laosiritaworn, **R. Yimnirun**, "Scaling Behavior of Dynamic Hysteresis in Hard PZT Bulk Ceramics Under Influence of Compressive Stress and Temperature" *The International Conference on Smart Materials: Smart/Intelligent Materials and Nanotechnology-2008 (SmartMat'08 and* IWOFM-2), April 22-25. 2008, Chiang Mai, Thailand.
20. A. Prasatkhetragarn, S. Ananta, **R. Yimnirun**, David P. Cann, "Effect of Temperature Treatment on Dielectric Properties of $0.8Pb(Zr_{1/2}Ti_{1/2})O_3$ - $0.2Pb(Co_{1/3}Nb_{2/3})O_3$ Ceramics" *The International Conference on Smart Materials: Smart/Intelligent Materials and Nanotechnology-2008 (SmartMat'08 and* IWOFM-2), April 22-25. 2008, Chiang Mai, Thailand.
21. C. Silawongsawat, T. Sareein, A. Ngamjarurojana, S. Maensiri**, R. Yimnirun**, S. Ananta, "Effect of Calcination Conditions on Phase Formation and Characterization of $BiFeO_3$ Powders Synthesized By a Solid-State Reaction" *The International Conference on Smart Materials: Smart/Intelligent Materials and Nanotechnology-2008 (SmartMat'08 and* IWOFM-2), April 22-25. 2008, Chiang Mai, Thailand.
22. S. Chandarak, T. Sareein, A. Ngamjarurojana, S. Maensiri, S. Ananta, **R. Yimnirun**, "Effect of Calcination Conditions on Phase Formation and Characterization of $BiFeO_3$-$BaTiO_3$ Powders Synthesized By a Solid-State Reaction" *The International Conference on Smart Materials: Smart/Intelligent Materials and Nanotechnology-2008 (SmartMat'08 and* IWOFM-2), April 22-25. 2008, Chiang Mai, Thailand.
23. Muangjai Unruan , Athipong Ngamjarurojana, Yongyut Laosiritaworn, Supon Ananta, And **Rattikorn Yimnirun**, "Dielectric Properties of $Pb(Zr_{1/2}Ti_{1/2})O_3$-$Pb(Zn_{1/3}Nb_{2/3})O_3$ Ceramics Under Compressive Stress Applied Perpendicular to Electric Field" *The 6th Asian Meeting of Ferroelectrics (AMF-6)*, Taiwan (August 2008)

24. M. Unruan, A. Prasatkhetragarn, A. Ngamjarurojana, Y. Laosiritaworn, S. Ananta and **R. Yimnirun**, "Ferroelectric Properties of $Pb(Zr_{1/2}Ti_{1/2})O_3$-$Pb(Zn_{1/3}Nb_{2/3})O_3$ Ceramics under Compressive Stress Applied Perpendicular to Electric Field" *The 6th Asian Meeting of Ferroelectrics (AMF-6)*, Taiwan (August 2008)
25. irapa Tangsritrakul, Muangjai Unruan, Piyachon Ketsuwan, Narit Triamnak, Saroj Rujirawat, Tanawadee Dechakupt, Supon Ananta, And **Rattikorn Yimnirun**," Effects Of Iron Addition On Electrical Properties And Aging Behavior Of Barium Titanate Ceramics" *The 6th Asian Meeting Of Ferroelectrics (Amf-6)*, Taiwan (August 2008)
26. Anurak Prasatkhetragarn, Supon Ananta, and **Rattikorn Yimnirun**, "Effect of Zr/Ti Ratio on Phase Formation and Electrical Properties of $0.2Pb(Co_{1/3}Nb_{2/3})O_3 - 0.8Pb(Zr_xTi_{1-x})O_3$ Ceramics" *The 6th Asian Meeting of Ferroelectrics (AMF-6)*, Taiwan (August 2008)
27. Anurak Prasatkhetragarn, Supon Ananta, and **Rattikorn Yimnirun**, "Effects of Sintering Conditions on Phase Formation and Electrical Properties of $0.2Pb(Co_{1/3}Nb_{2/3})O_3 - 0.8Pb(Zr_{1/2}Ti_{1/2})O_3$ Ceramics" *The 6th Asian Meeting of Ferroelectrics (AMF-6)*, Taiwan (August 2008)
28. P. Ketsuwan, C. C. Huang, S. Ananta, **R. Yimnirun**, D. P. Cann, "Electrical Conductivity And Dielectric And Ferroelectric Properties Of Chromium Doped Lead Zircronate Titanate Ceramic" *The 6th Asian Meeting of Ferroelectrics (AMF-6)*, Taiwan (August 2008)
29. P. Ketsuwan, C. C. Huang, S. Ananta, **R. Yimnirun**, D. P. Cann, "Effects Of Niobium Doping On Dielectric And Ferroelectric Properties Of Chromium Modified Lead Zircronate Titante Ceramics" *The 6th Asian Meeting of Ferroelectrics (AMF-6)*, Taiwan (August 2008)
30. Sasiporn Prasertpalichatr, Muangjai Unruan, Jirapa Tangsritrakool, Supon Ananta, and **Rattikorn Yimnirun**, "Dielectric and Ferroelectric Aging Effect of Fe^{3+}/Nb^{5+} Hybrid-Doped Barium Titanate Ceramics" *The 6th Asian Meeting of Ferroelectrics (AMF-6)*, Taiwan (August 2008)
31. N. Wongdamnern, Y. Laosiritaworn, A. Ngamjarurojana, S. Ananta, and **R. Yimnirun**, "Stress-Dependent Scaling Behavior of PZT-PZN Ceramics Under Sub-Coercive Field Condition" *The 6th Asian Meeting of Ferroelectrics (AMF-6)*, Taiwan (August 2008)

32. Thanapong Sareein, Athipong Ngamjarurojana, Supon Ananta, and **Rattikorn Yimnirun**, "Dielectric and Ferroelectric Properties of KNN-BNT Ceramic Systems" *The 6th Asian Meeting of Ferroelectrics (AMF-6)*, Taiwan (August 2008)
33. A.Ngamjarurojana, **R. Yimnirun**, S. Ananta"Effect of. VibroMilling Time on Phase Formation and Particle Size of $ZnNb_2O_6$ Nano- powders" *The 6th Asian Meeting on Electroceramics (AMEC-6)*, Japan (October 2008)
34. M. Unruan, A. Prasatkhetragarn, A. Ngamjarurojana, Y. Laosiritaworn, S. A nanta, **R. Yimnirun** "Ferroelectric Properties of $Pb(Zr_{1/2}Ti_{1/2})O_3$-$Pb(Zn_{1/3}Nb_{2/3})O_3$ Ceramics under compressive stress applied perpendicular to electric field" *The 6th Asian Meeting on Electroceramics (AMEC-6)*, Japan (October 2008)
35. L. Srisombat, O. Khamman, **R. Yimnirun**, S. Ananta, T.R. Lee "XPS Chara cterization of Relaxor Perovskite PNN Ceramics Prepared By Corundum Pr ecursor Method" *The 6th Asian Meeting on Electroceramics (AMEC-6)*, Japan (October 2008)
36. Wimalin S. Laosiritaworn, **Rattikorn Yimnirun**, Yongyut Laosiritaworn "Artifi cial Neural Network Modeling of Ferroelectric Hysteresis: An Application to Soft Lead Zirconate Titanate Ceramics" *The 6th Asian Meeting on Electroceramics (AMEC-6)*, Japan (October 2008)
37. W. C. Vittayakorn, **R. Yimnirun**, S. Ananta"Composition, Structure and Pro perties of PZT-BT Ceramics Prepared by Two-stage Sintering" *The 6th Asian Meeting on Electroceramics (AMEC-6)*, Japan (October 2008)
38. Jirapa Tangsritrakul, Muangjai Unruan, Piyachon Ketsuwan, Narit Triamna k, Tanawadee Dechakupt, Supon Ananta, **Rattikorn Yimnirun**, Saroj Rujira wat"Effects of Iron Addition on Aging Behavior of Barium Titanate Ceramics " *The 6th Asian Meeting on Electroceramics (AMEC-6)*, Japan (October 2008)
39. Piyachon Ketsuwan, Supon Ananta, **Rattikorn Yimnirun**, Chien-Chih Huang,David P. Cann "Dielectric Properties of Lidoped $Bi_{0.2}K_{0.8}(Zn_{0.1}Ti_{0.1})Ta_{0.8}O_3$ Ceramics"
40. S. Prasertpalichatr, J. Tangsritrakul, T. Sareein, M. Unruan, A. Ngamjaruroj ana, **R. Yimnirun**"Effect of Compressive Stress on Aging Behavior of

Hybrid-doped Fe^{3+}/Nb^{5+} $BaTiO_3$ Ceramics" *The 6th Asian Meeting on Electroceramics (AMEC-6)*, Japan (October 2008)

41. S. Ananta, R. Wongmaneerung, L. Srisombat, **R. Yimnirun**"Potential of M icrostructural Engineering Technique for Fabrication of Highly Dense Perov skite Lead Titante Ceramics" *The 6th Asian Meeting on Electroceramics (AMEC-6)*, Japan (October 2008)
42. T. Sareein, M. Unruan, A. Ngamjarurojana, S. Ananta, **R. Yimnirun**"Effects of Compressive Stress on Dielectric and Ferroelectric Properties.of Lead-Free $(Bi_{1/2}Na_{1/2})TiO_3$-$(K_{1/2}Na_{1/2})NbO_3$ Ceramic Systems" *The 6th Asian Meeting on Electroceramics (AMEC-6)*, Japan (October 2008)
43. A. Thongon, S. Ananta, **R. Yimnirun**, S. Choopun, Y. Laosiritaworn "Monte Carlo simulations of nanopowders from mechanical milling" *The 6th Asian Meeting on Electroceramics (AMEC-6)*, Japan (October 2008)
44. A. Thongon, S. Ananta, **R. Yimnirun**, S. Choopun, Y. Laosiritaworn "Modeling of Nano Structure via a Spinodal Decomposition" *The 6th Asian Meeting on Electroceramics (AMEC-6)*, Japan (October 2008)
45. Sukrit Sucharitakul, Sasiporn Prasertpalichat, Yongyut Laosiritaworn, **Rattikorn Yimnirun** "Pinched Hysteresis Scaling in HybridDoped $BaTiO_3$" *The 6th Asian Meeting on Electroceramics (AMEC-6)*, Japan (October 2008)
46. Yongyut Laosiritaworn, **Rattikorn Yimnirun**, Ruyan Guo, Amar S. Bhalla " Stress Dependence of Dielectric Properties in Relaxor Ferroelectric : Monte Carlo Investigation" *The 6th Asian Meeting on Electroceramics (AMEC-6)*, Japan (October 2008)
47. Sukrit Sucharitakul, **Rattikorn Yimnirun**, Yongyut Laosiritaworn,"Hybrid-Doped Ferroelectric Modeling via Monte Carlo Simulation" *The 6th Asian Meeting on Electroceramics (AMEC-6)*, Japan (October 2008)
48. Piyachon Ketsuwan, Supon Ananta, **Rattikorn Yimnirun**, Chien-Chih Huang, David P. Cann "Dielectric and Ferroelectric Properties of (Cr,N b) doped Lead Zircronate Titanate Ceramics" *The 6th Asian Meeting on Electroceramics (AMEC-6)*, Japan (October 2008)
49. N. Wongdamnern, A. Ngamjarurojana, S. Ananta, Y. Laosiritaworn, **R. Yim nirun**,"ScalingBehavior of SubCoercive Field Dynamic Hysteresis in $BaTiO_3$ Single Crystal" *The 6th Asian Meeting on Electroceramics (AMEC-6)*, Japan (October 2008)

ภาคผนวก

Re-Print หรือ Pre-Print หรือ Accepted Manuscript

ของ

ผลงานตีพิมพ์ในวารสารวิชาการนานาชาติ

(จำนวน 46 เรื่อง)

และ

ผลงานที่ตีพิมพ์ในวารสารประกอบการประชุมวิชาการระดับนานาชาติ (Proceedings of International Conferences)

(จำนวน 8 เรื่อง)

Temperature effects in the magnetic properties of two-dimensional Ising square lattices: A Monte Carlo investigation

Yongyut Laosiritaworn,* Supon Ananta, and Rattikorn Yimnirun
Department of Physics, Faculty of Science, Chiang Mai University, Chiang Mai 50200, Thailand
(Received 3 November 2006; revised manuscript received 5 January 2007; published 22 February 2007)

The magnetic behavior of a two-dimensional nearest-neighbor Ising model with the presence of linear temperature variation in a thermal steady state was studied using the Wolff Monte Carlo simulation. The technique consists of fixing the temperatures of boundary spins, while the temperature field in the interior linearly varies with distance. It is found that with increasing the temperature difference between the two boundaries, the magnetization greatly reduces in magnitude while the susceptibility peaks tend to spread out over a temperature range. The detailed descriptions of these magnetization and susceptibility behaviors are elucidated from their spatial variation. The extraction of the "critical temperatures" is taken via the fourth-order cumulant of the magnetization. The critical temperatures are found to reduce slightly with increasing the temperature difference. This implies the vulnerability of the magnetization and susceptibility properties to the temperature variation in ferromagnetic materials, and to use such materials in temperature variation environments must be done with caution.

DOI: 10.1103/PhysRevB.75.054417 PACS number(s): 75.10.Dg, 05.10.Ln, 75.40.Cx

I. INTRODUCTION

Magnetic thin films have been known to be very important in terms of fundamental and technological interest, especially in the magnetic recording technology.[1,2] Many contributions have been taken to provide understanding of these systems in detail.[3,4] However, there are still incomplete pictures describing their magnetic properties especially in nonequilibrium states. For instance, the theoretical studies usually investigate the thin-film problems by considering the system in contact with only a single heat bath, which means that the temperature of the whole system is fixed. As a result, the conventional thermal equilibrium investigation may not be useful in understanding the magnetic materials used in some applications, which operate at some fluctuating temperatures. For instance, in heat-assisted magnetic recording, the media temperature is nonuniformly raised by laser irradiation.[5] In such applications, there occurs a heat flux flowing among regions from high to low temperatures, resulting in local variation in temperature. Therefore, the approximation on using a single (average) temperature in the calculation is clearly inadequate since important thermodynamics is missing. On the other hand, magnetic properties strongly depend on thermal fluctuation. Therefore, the variation in temperatures makes the problem very complex, so experimental and theoretical investigations of this issue cannot be taken trivially. Consequently, it is of great interest and challenge to find how magnetic properties respond to the variation in temperature field. To date, there are few studies on this effect of temperature variation on magnetic systems; i.e., they are mainly restricted to the thermal properties such as heat conductivity.[6,7] A particular study on the field uses nonequilibrium simulations to calculate thermal conductivity in a two-dimensional (2D) Ising system based on microcanonical algorithm,[8] which was later extended to include external magnetic field.[9]

Therefore, in this study, the understanding of the effect of temperature variation, but restricted only to thermal steady state, on magnetic system has been extended by performing Monte Carlo simulation to investigate magnetic properties, i.e., the magnetization and the magnetic susceptibility including their spatial resolution. The simulation considers the use of Ising model, which has been proven to be useful in many areas starting from biological systems[10,11] to financial problems[12,13] and statistical mechanics, with the ultrathin film or 2D structure. Also, in magnetic material problems, both theoretical[14,15] and experimental investigations[16–18] have also shown, in terms of critical exponents, that the 2D Ising system is very useful for the study of magnetic behavior in thin ferromagnetic films. To outline, the study investigates how the overall average magnetic properties, such as the magnetization and the magnetic susceptibility, depend on temperature supplied to the boundary spins from the heat baths and heat bath temperature differences by means of Monte Carlo simulations. Next, the study investigates the variation of these magnetic properties in terms of spatial resolution to observe how local magnetic behavior plays a part in overall average magnetic properties. Then, the "critical temperature," which is defined to be the temperature (of a lower temperature heat bath) where the order parameter of the system vanishes at thermodynamic limit, is extracted to examine how the temperature variation affects the critical phenomena. These are followed by a conclusion, which summarizes a prominent finding from the study, and a suggestion on how the topic would benefit the community.

II. METHODOLOGY

In this study, we consider the Ising Hamiltonian

$$H = -J\sum_{\langle ij\rangle} S_i S_j, \tag{1}$$

where the spins $S_{i(j)}$ take on the values ± 1 and the sum includes only first nearest-neighbor pairs. The units J and J/k_B are used for temperatures and energies, respectively. The

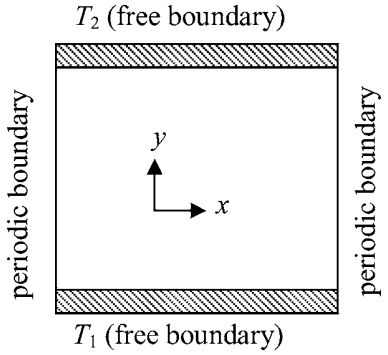

FIG. 1. The setup system structure showing its boundary conditions and its temperature constraint on the free boundaries, i.e., T_1 at $y=1$ and T_2 at $y=L$, where $T_1 \leqslant T_2$.

considered system is a 2D structure where periodic and free boundary conditions are used for the x and y directions, respectively. The simulations are carried out with total number of spins $N=L_x \times L_y$, where L_x and L_y represent the number of magnetic (atomic) sites along the x and y directions of the system. A rule of thumb in performing Monte Carlo simulations is to choose L_x and L_y as large as possible to minimize finite-size effect. Therefore, in this study we use $L_x=L_y=L$ ranging from 40 to 100 in steps of 10, which are still computationally feasible and fairly large. Actually, these chosen L are picked from the L that the correction to scaling is not significantly needed in the investigation of critical properties.[19] In fact, the finite-size effect causes the deviation in any physical properties between those of the finite system and of the infinite system especially close to critical point. This can be described using the critical behavior of the magnetic interaction. For instance, in a paramagnetic phase, the correlation length of the same spin is small. However, on approaching the critical point from above, the correlation length starts to grow and blows up if the considered system is very large (L tends to infinity). Nevertheless, for finite L, the divergence of the correlation length is not permitted since the largest value of the correlation length itself is L. Furthermore, due to finite-size effect, which arises from the free surfaces (if there are any), or the periodic image (if the periodic boundary condition is chosen), the rate of correlation growing in the finite-size system and the infinite system is different, and this alters the magnetic properties in the finite system from the infinite system. For example, it is very obvious that the magnetization in the finite system does not cease down to zero at the critical point.

Next, in applying temperatures to the system, along the y direction, at $y=1$ and L_y, the fixed temperatures T_1 and T_2 where $T_1 < T_2$ (see Fig. 1) are supplied to the boundary spins. Due to the temperature variation, starting from the $y=1$ side, the temperature steadily increases from T_1 and reaches T_2 at the opposite side. In this nonequilibrium state, the heat flux passes from the T_2 side to the T_1 side, while local temperatures along the pathway can be determined from the heat conduction formula,

$$\frac{1}{A}\frac{dQ}{dt} = -K\frac{dT}{dx}, \tag{2}$$

where K is the thermal conductivity and dT/dx refers to the one-dimensional temperature gradient. However, when the system relaxes to its steady state, the ratio dQ/dt is maintained and the resulting temperature gradient becomes a constant. As a result, at this steady state, the temperature T is linearly proportional to the distance away from the T_1 side and it can be estimated that

$$T_y = T_1 + \left(\frac{T_2 - T_1}{L_y - 1}\right)y, \tag{3}$$

where y is the distance away from T_1 and T_y is the local temperature at y. Because the study considers the system only in its steady state, the local temperature T_y is therefore fixed at the distance y throughout the simulation, giving rise to various local thermal equilibria for each specific distance y in the system.

In this study, we consider the temperature difference between the two heat baths $\Delta T=T_2-T_1$ ranging from 0.0 to 2.8 J/k_B with steps of 0.4 J/k_B, and T_1 ranging from 0.1 to 3.4 J/k_B with steps of 0.1 J/k_B. With these ΔT and T_1 ranges, it is possible to investigate the system in several cases. For instance, both T_1 and T_2 are in ferromagnetic phase, T_1 is in ferromagnetic but T_2 is in paramagnetic phase, and both T_1 and T_2 are in paramagnetic phase. Note that without temperature variation, the 2D Ising critical temperature T_C, which splits paramagnetic out of ferromagnetic phase, is $T_C=2/\ln(1+\sqrt{2}) \approx 2.269\ J/k_B$.[20]

Next, in updating the spin configurations during Monte Carlo simulations, a series of successive spin configurations are chosen via importance sampling under the condition of ergodicity and detailed balance. A very popular algorithm, which satisfies these conditions, is the Metropolis algorithm,[21] where a particular spin configuration is different from its previous configuration by only a single spin flip. The probability in accepting a new spin configuration, which is generated from the previous study, is $p=\exp(-\Delta E/k_B T_y)$, where ΔE is the energy difference associated with the flip and T_y is the local temperature attached to the flipped spin. However, instead of using the conventional Metropolis algorithm, we consider the Wolff algorithm[22] because the Wolff greatly reduces the correlation time τ. This is due to the fact that the updated probability in Metropolis algorithm depends only on an energy difference from a single spin flip. Therefore, this results in a large correlation time τ among successive spin configurations.[23,24] In the following, the large τ brings a large statistical error of the magnetization $\langle(\delta m)^2\rangle$ because[23,24]

$$\langle(\delta m)^2\rangle = \frac{1}{n}(\langle m^2\rangle - \langle m\rangle^2)\left(1 + 2\frac{\tau}{\delta t}\right), \tag{4}$$

where, at large enough n, $\tau=\Sigma(\langle m_0 m_i\rangle - \langle m^2\rangle)/(\langle m^2\rangle - \langle m\rangle^2)$ is the integrated correlation time and δt is the time interval between two successive configurations, and n is the number of configurations being sampled. As can be seen from the above equation, the smaller the τ, the lower the statistical

error. Therefore, one can see the benefit of using the Wolff algorithm upon the Metropolis algorithm since the Wolff provides a smaller τ in the same system. For example, close to critical temperature in 2D Ising model, the correlation time τ scales with the system size L as $\tau \propto L^z$, and the gives $z=0.25\pm0.01$,[25] while the Metropolis gives $z=2.1665\pm0.0012$.[26]

In using the Wolff algorithm to make configuration updates, a cluster of the same direction spins is made and flipped. In creating the cluster, a seed spin is randomly chosen and then its neighboring spins, at temperature T_y, are added to form a group with a probability

$$p = 1 - \exp\left(-\frac{2J}{k_B T_y}\right). \tag{5}$$

Then, the procedure is repeated for the just added spins until no more spins are added to the cluster. Next all the spins in the cluster are flipped to their opposite directions, i.e., S_i to $-S_i$.

In this Monte Carlo study, with the chosen Wolff algorithm, we first waited for each simulation at least for 1000 Monte Carlo steps per site (MCS) from its initial state (disordered state) to allow the system to relax to its steady state before taking any measurements. After that, during the simulation, the magnetization and the energy are measured when the number of flipped spins exceeds or is equal to N. The global average of the magnetization per spin is defined as $m=(1/N)\Sigma_i S_i$, and in each simulation, $N'=50\,000$ configurations are used to calculate the expectation of the magnetization per spin, i.e.,

$$\langle m \rangle = \frac{1}{N'} \sum_{t}^{N'} |m_t|. \tag{6}$$

It is also of interest to observe how the free boundaries play their roles on the microscopic magnetic properties. This is so since the effect of average exchange interaction on a single magnetic spin strongly depends on its neighboring. At the free boundary, the smaller number of nearest-neighbor sites causes the smaller magnitude of average exchange interaction, whereas in the interior the spin feels more bulklike (homogeneously). So the variation of magnetic properties from the free boundary to the interior of the system is expected. Therefore, the spatial dependence of the magnetic properties, i.e., m_y and χ_y, for distance y away from the T_1 side, is calculated to observe the free boundary effect (for which the temperature variation is not yet turned on) and the temperature variation effects on the local magnetic properties. Specifically, the study considers the variation of m_y and χ_y as a function of the distance y away from the T_1 side to the direction toward the T_2 side. For convenience, only y that is a multiple of lattice spacing unit is considered, and all spins at the same distance y are defined to have local magnetization and local susceptibility per spins in the absence of external field as $m_y=(1/L)\Sigma_{i\in y}S_i$ and $\chi_y=L(\langle m_y^2\rangle - \langle m_y\rangle^2)/k_B T_y$. Note that we have applied the thermal equilibrium formalism to microscopically investigate the thermal steady state because all spins at the same distance y are virtually attached to the same heat bath at temperature T_y. In this way, it means that we first consider the region to be small enough to experience only a single and stable temperature, and then the thermal equilibrium technique is applied to study this microscopic region. After that, the dependence of the magnetic properties on the spatial temperature is calculated and the overall magnetic properties are extracted by averaging the microscopic properties. Note that if the system has not yet arrived at the steady state, everywhere except at the boundary the spins we will notice the spatial temperatures to change in time and the thermal equilibrium technique cannot be applied to such case.

Next, based on the local magnetic susceptibility χ_y, the global (average) magnetic susceptibility at zero field is defined as

$$\chi \equiv \left.\frac{\partial m}{\partial h}\right|_{h\to 0} = \frac{1}{L}\sum_y \left.\frac{\partial m_y}{\partial h}\right|_{h\to 0} = \frac{1}{L}\sum_y \chi_y$$
$$= \sum_y \frac{1}{k_B T_y}(\langle m_y^2\rangle - \langle m_y\rangle^2). \tag{7}$$

Also in this study, the critical behavior is investigated via the critical temperature T_C. Note that the term critical temperature used in this context is the temperature that the magnetization of the whole system vanishes at the thermodynamic limit. In this temperature variation study, at a particular temperature, some parts of the system may already lie in paramagnetic state, but if there are still some other parts residing in ferromagnetic state, the whole system is categorized to be ferromagnetic since there still exists finite magnetization. Then, T_C is defined if and only if the magnetization is completely destroyed by the thermal fluctuation that spreads throughout the system (in the infinite sized system). However, due to computational limitation, the simulations have to be performed in finite sizes where their finite-size effects must be taken into account. Therefore, in this study, the temperature T_C is phenomenologically located via the fourth-order cumulant U_L of the magnetization per spin,[27]

$$U_L = 1 - \frac{\langle m^4\rangle}{3\langle m^2\rangle^2}, \tag{8}$$

where, at critical point, U_L should be independent of L; i.e., for differing sizes L and L', $(U_L/U_{L'})_{T=T_C}=1$. The reason in using Eq. (8), which was created to study thermal equilibrium systems to extract the critical temperature T_C, is based on the fact that the correlation length of the magnetization diverges (or the spontaneous symmetry breaking occurs throughout the system) at the critical point. Thus, no matter how large the system size L is, U_L should be the same at the critical point. Therefore, in this study of thermal steady state, for a specific value of ΔT, the critical temperature is defined in terms of T_1 (the lower temperature heat bath), which allows the correlation length of global magnetization to diverge at the thermodynamic limit and results in $(U_L/U_{L'})_{T=T_C}=1$. In fact, instead of T_1, one may define the critical temperature in terms of T_2 if it is desired. However, in this study, the lower temperature of the two heat baths is

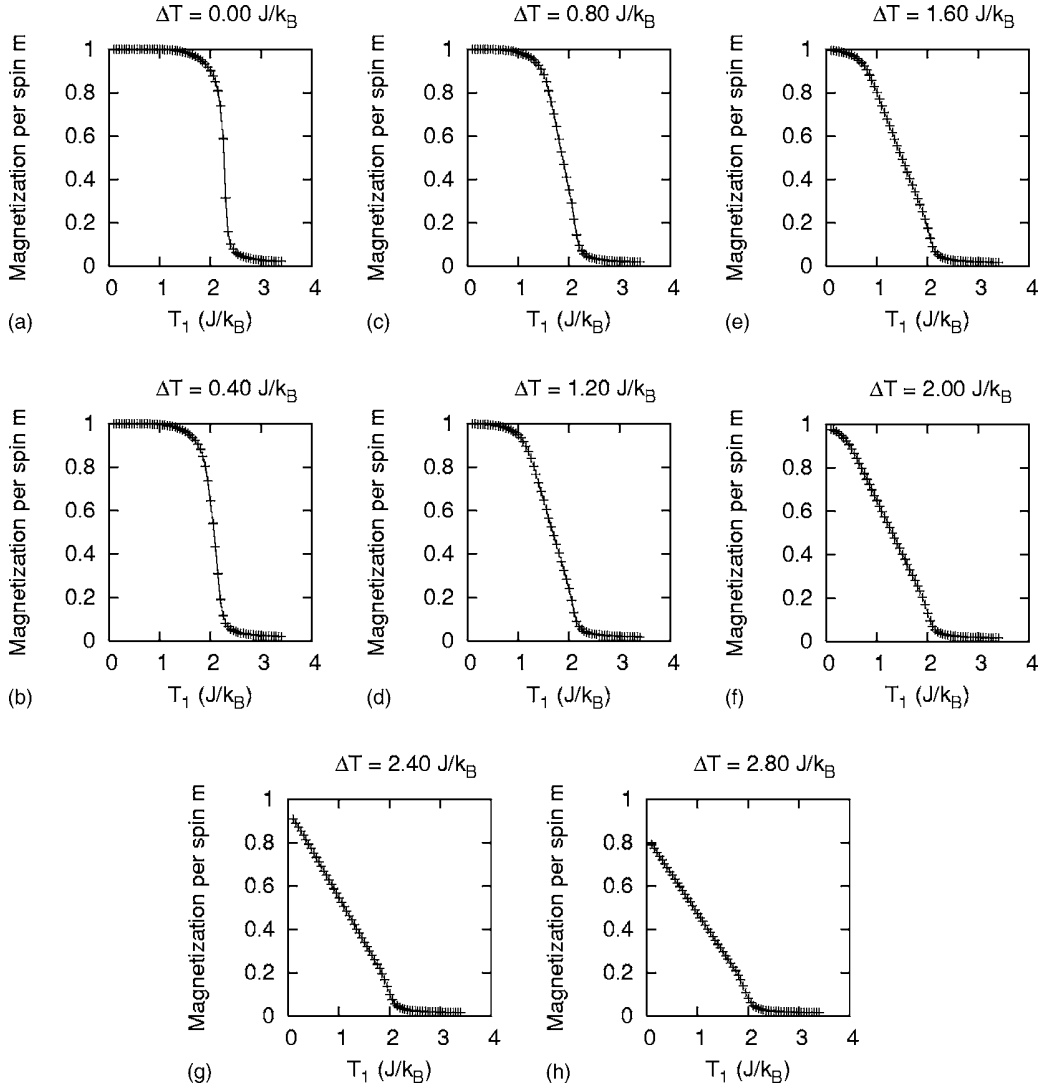

FIG. 2. Magnetization per spin m as a function of temperature T_1 for various $\Delta T = T_2 - T_1$.

preferred to define the critical temperature.

Nevertheless, owing to finite-size effects, the cumulant curves obtained from Eq. (8) for different L's do not exactly cross at the same temperature. Therefore, the critical temperature is estimated from $T_C(b=L/L')$ at the limit $(\ln b)^{-1} \rightarrow 0$.[24,27] To maximize the efficiency of this T_C calculation, for each system, a single long simulation is only performed at a temperature T_0 and the histogram method[28,29] is used to extrapolate U_L to a temperature nearby in order to find the cumulant crossing points on a fine scale. The temperature T_0 is guessed from the temperature at the center of the cumulant crossing points. Approximately 2×10^5 spin configurations, which are found to compromise between calculation time and statistical error, are used to create the histograms. To exclude the data obtained from temperatures too far from the simulated temperature T_0, the range of the extrapolation obeys $|U(T) - U(T_0)| \leq \sigma_E$, where $U = \langle E \rangle$ is the average of the energy and σ_E is a standard deviation of E at T_0.[30]

III. RESULTS AND DISCUSSIONS

A. Overall magnetization and magnetic susceptibility profiles

From the simulations, the magnetization m and susceptibility χ profiles for various T_1 and temperature difference $\Delta T = T_2 - T_1$ are obtained and shown in Figs. 2 and 3. As can be seen from Fig. 2, with increasing ΔT, the magnetization m tends to decrease. This is because the larger ΔT is, the greater the temperature is at the hotter part of the system (close to the T_2 side). Then, at this hotter part, the magnetic spins experience larger thermal fluctuation, resulting in smaller local magnetization magnitude. Consequently, on the overall average, the magnetization reduces with increasing ΔT. Note that even the magnetization significantly reduces in magnitude at large ΔT, the critical point (the temperature where magnetization curve has the maximum slope) only slightly changes. This is due to the fact that there are still some parts of the system, connecting to lower temperature T_1, which reside in ferromagnetic phase even magnetic order

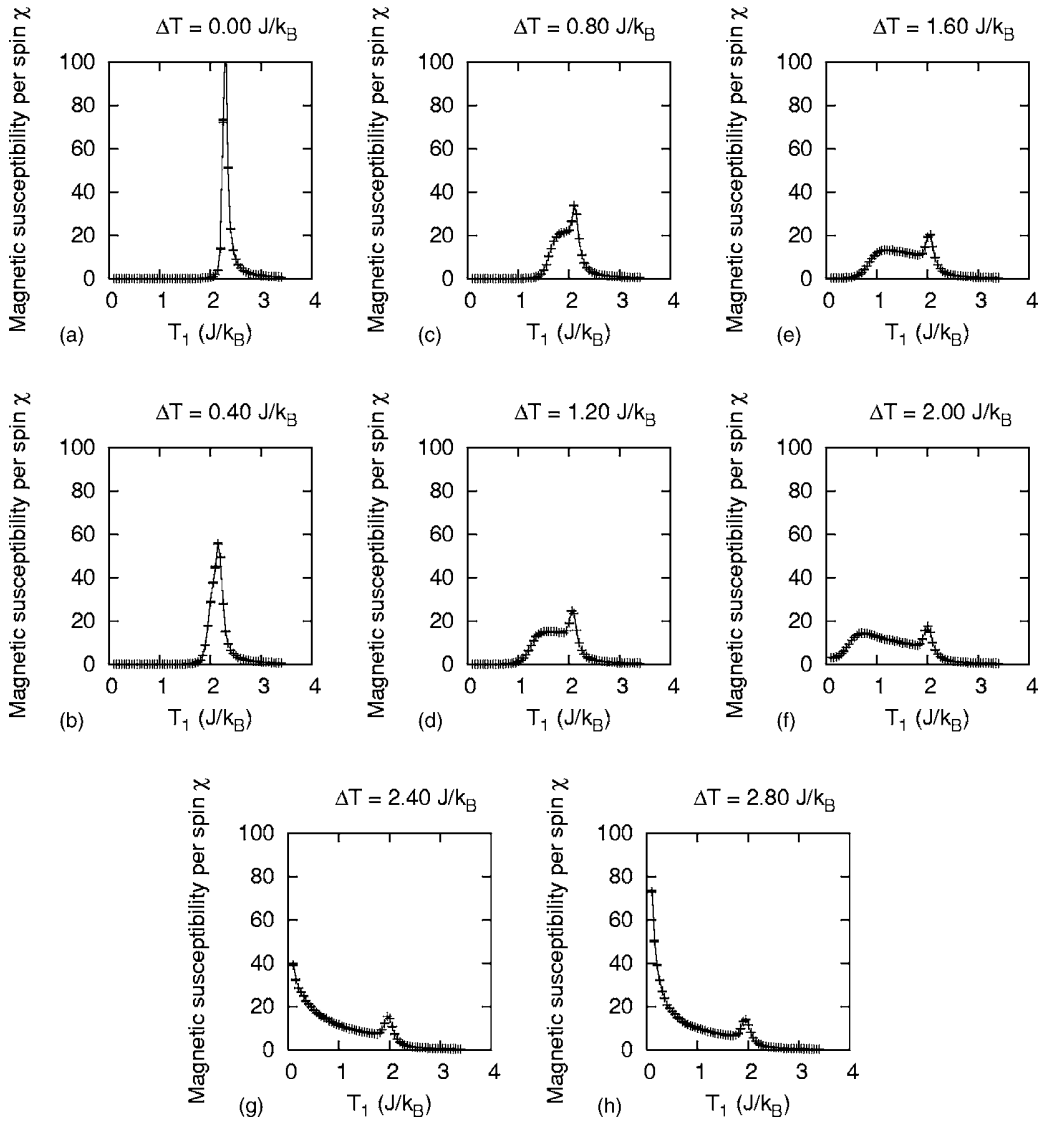

FIG. 3. Magnetic susceptibility per spin χ as a function of temperature T_1 for various $\Delta T = T_2 - T_1$.

of the other parts has already been destroyed. Therefore, the whole system presents some finite magnetization and preserves the overall ferromagnetic behavior. This phenomenon is similar to those found in magnetic thin films where exchange interaction varies from layer to layer.[31] In Ref. 31, because of the differences in exchange interaction magnitude, the magnetic orders from different layers are not destroyed at the same temperature. Therefore, the true critical temperature is defined to be the largest eigenvalue (temperature) that allows the susceptibility to diverge (under the framework of mean-field theory), which is the first encounter of temperature in which the overall magnetization is completely destroyed by the thermal fluctuation if the system is heated from its ferromagnetic phase.

On the other hand, the results for magnetic susceptibility χ, as in Fig. 3, show a broader range of phase transition for $\Delta T > 0$. This is very different from the case $\Delta T = 0$ where the susceptibility blows up only at the normal 2D Ising critical temperature $T_C \approx 2.269\ J/k_B$. This is due to the fact that the susceptibility is representative of magnetization fluctuation which severely increases in magnitude at the critical point. As for $\Delta T > 0$, there is temperature variation, making the temperature field rise in magnitude from T_1 to T_2. Consequently, different parts of the system experience different local temperatures. Some parts may already reach the critical point where others may not. Each part of the system will not highlight the critical behavior at the same temperature T_1. For example, at $T_1 = 1.60\ J/k_B$ and $\Delta T = 0.6\ J/k_B$, the spins close to the T_1 boundary are lying in ferromagnetic state and their local susceptibility will be very small. On the other hand, the spins close to the $T_2 = 2.00\ J/k_B$ boundary will start to exhibit large thermal induced magnetization fluctuation since this temperature T_2 is close to T_C. Therefore, the local susceptibility for spins close to T_2 will be fairly large. Another example is the case where $T_1 = 2.20\ J/k_B$ and $\Delta T = 0.2\ J/k_B$. The local susceptibility will be large for spins close to T_1, but will be small for spins close to T_2 because these spins are already lying in paramagnetic state. These two examples

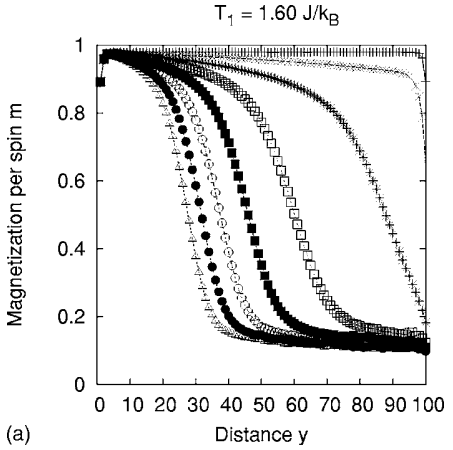

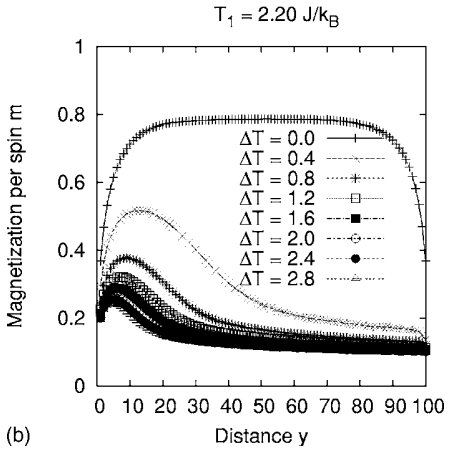

FIG. 4. Spatial variation of magnetization per spin m as a function of distance y away from the T_1 boundary for various ΔT at (a) $T_1=1.60\ J/k_B$ and at (b) $T_1=2.20\ J/k_B$. The legends to symbols in (a), which are the same as those in (b), are removed for visual aids.

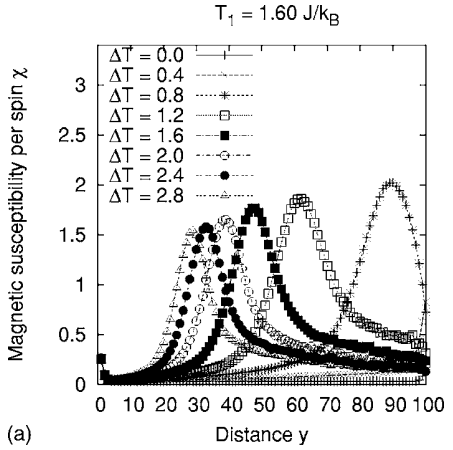

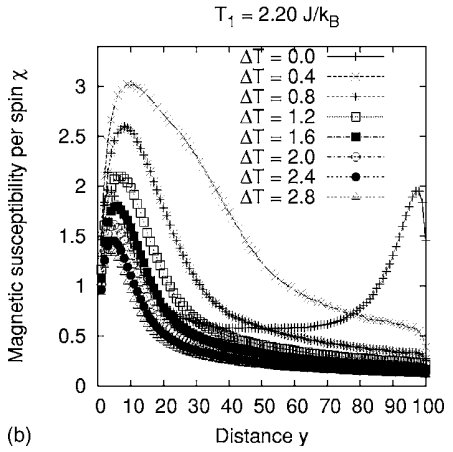

FIG. 5. Spatial variation of magnetic susceptibility per spin χ as a function of distance y away from the T_1 boundary for various ΔT at (a) $T_1=1.60\ J/k_B$ and at (b) $T_1=2.20\ J/k_B$.

can be used to describe the susceptibility phenomena in Fig. 3. Even T_1 is smaller than the normal 2D T_C, but with help from ΔT, there will be some interior parts of the system which will exhibit critical behavior. This results in a broader range of the susceptibility peak on the temperature T_1 scale. Nevertheless, the peak is not as sharp as the $\Delta T=0\ J/k_B$ system because in the case of $\Delta T=0\ J/k_B$, all spins contribute in magnetization fluctuation at the same temperature, i.e., T_C. A more detailed description of this broader range can be given by looking at spatial variation of the magnetic properties (see Figs. 4 and 5).

B. Spatial variation of magnetization and magnetic susceptibility

The study has found that the temperature variation has a strong effect on the local (spatial) magnetic properties. For example, Fig. 4 shows the spatial variation of magnetization per spin m as a function of distance y away from the T_1 boundary for various temperature differences $\Delta T=0.0$, 0.4, 0.8, 1.2, 1.6, 2.0, 2.4, and 2.8 J/k_B at (a) $T_1=1.60\ J/k_B$ and at (b) $T_1=2.20\ J/k_B$. Starting with $\Delta T=0\ J/k_B$, all spins experience the same temperature throughout the system. All parts of the system have the same magnetic behavior; i.e., all local magnetization and local susceptibility show the critical behavior at the same T_C, which is about 2.269 J/k_B for normal infinite size 2D Ising system. The spins on both T_1 and T_2 boundaries have a lower magnetization magnitude than those from other spins in the interior (see Fig. 4). This is due to the fact that the spins inside are coupled with four nearest-neighbor spins, while spins at the edges ($y=1$ and $y=L$) experience the free boundary and are coupled with only three nearest-neighbor spins. Therefore, the spins close to the T_1 and T_2 boundaries are more susceptible to the thermal fluctuation and result in a smaller magnetization magnitude. On the other hand, the spins which reside in the interior experience a higher level of ferromagnetic interaction, causing more spins to point to the same direction and yield a higher magnitude of magnetization. These results agree well with previous Ising model investigations that the spins at the free boundaries have smaller magnetization magnitudes compared with those in the interior.[32,33]

However, with increasing $\Delta T>0$, the temperature variation induced by temperature gradient in the system linearly raises the temperature T from the T_1 boundary to T_2 boundary. This makes the local magnetic properties vary, which is

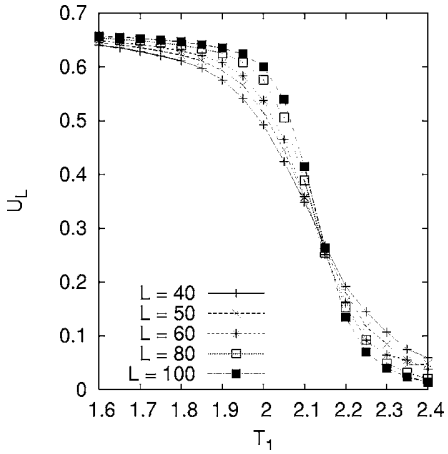

FIG. 6. The fourth-order cumulant of the magnetization for $\Delta T=1.20\ J/k_B$ system as a function of T_1. From the figure, it can be estimated that the crossing points take place between $T_1=2.10$ and $2.20\ J/k_B$, therefore, the critical temperature will lie in this region.

very different from the $\Delta T=0$ case. Looking at Fig. 4(a) as an example, at $T_1=1.60\ J/k_B$ and $\Delta T<0.669\ J/k_B$, both T_1 and T_2 are smaller than the normal $T_C\approx 2.269\ J/k_B$, and the whole system experiences ferromagnetic coupling. Therefore, finite magnetization behavior can be found throughout the system. Nevertheless, the magnetization reduces in magnitude from the T_1 boundary to the T_2 boundary due to a higher level of thermal fluctuation. On the other hand, for $\Delta T>0.669\ J/k_B$, the spins at and close to the T_2 boundary experience paramagnetic interaction because T_2 is greater than the normal 2D Ising T_C. Consequently, the magnetization reduces very sharply from the T_1 to the T_2 boundary. This detailed description can also be applied to understand the magnetization behavior in Fig. 4(b). Therefore, these are the reasons why the magnetization declines with increasing ΔT (e.g., see Fig. 2), which could be very useful in designing sensor applications such as the temperature sensor from magnetic materials.[34] In addition, as one may see in Fig. 4, the distance y away from the T_1 boundary is a "thermometer," which indicates the rise of temperature from T_1 to T_2. This is why the results in Fig. 4 are more or less similar to some subfigures in Fig. 2. Note that the magnetization does not completely reduce to zero because of the finite-size effect.

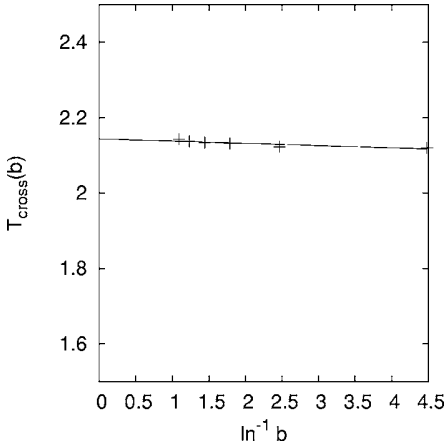

FIG. 7. The extraction of critical temperature T_C for $\Delta T=1.20\ J/k_B$ via the extrapolation of $T_{cross}(b)$ to the limit $\ln^{-1}(b)\rightarrow 0$, where T_{cross} is the temperature that $U_L=U_{L'}$ where $L'=40$ and $L=50$, 60, 70, 80, 90, and 100, and $b=L/L'$. The line is drawn from linear least-squares fit, which gives $T_C=2.14393\pm 0.00393\ J/k_B$.

TABLE I. Critical temperature T_C obtained from Monte Carlo simulation for various temperature differences between the two free boundaries.

$\Delta T=T_2-T_1$	T_C
0.0	2.26926±0.00018
0.4	2.19187±0.00312
0.8	2.16802±0.00273
1.2	2.14393±0.00393
1.6	2.13046±0.00367
2.0	2.11466±0.00406
2.4	2.09977±0.00640
2.8	2.08514±0.00510

Apart from the magnetization results, the temperature variation has a similar effect on the spatial magnetic susceptibility. For instance, at $\Delta T=0$ in Fig. 5(a), the whole system experiences the same temperature $T=T_1=T_2=1.60\ J/k_B$, which is smaller than T_C. The system is then far from the critical point and the thermally induced magnetization fluctuation (the susceptibility) is small. However, for $\Delta T=0$ in Fig. 5(b), the temperature $T=T_1=T_2=2.20\ J/k_B$ is close to T_C, so the magnetization starts to fluctuate strongly and the susceptibility starts growing (resulting in peaks) near the boundary T_1 and T_2 ends. In this $\Delta T=0$ case, the interior spins have a smaller susceptibility because there are more (average) number of neighbor spins which provides a higher magnetic interaction, and this interaction behaves as a buffer to the magnetization fluctuation. Similar to magnetization results, for $\Delta T>0$, the distance y indicates the rise of temperature. In Fig. 5, with increasing ΔT, the susceptibility peaks move toward the T_1 boundary since some parts inside the system have already reached T_C and this T_C moves towards the T_1 end with increasing ΔT.

C. Critical temperatures

On the other hand, in looking at the critical property, i.e., T_C, the fourth-order cumulant in Eq. (8) is found useful. The crossing of U_L is found for the whole range $\Delta T=0.0$–$2.8\ J/k_B$ in this study. An example for the cumulant crossing for $\Delta T=1.2\ J/k_B$ is shown in Fig. 6. As mentioned earlier, to minimize the finite-size effect, an extrapolation of $T_C(b=L/L')$ to the limit $(\ln b)^{-1}\rightarrow 0$ is performed (e.g., see Fig. 7). The critical temperatures T_C at this thermodynamic limit are presented in Table I and plotted as a function of temperature difference $\Delta T=T_2-T_1$ (see Fig. 8). As can been seen, for $\Delta T=0$ which is in the absence of temperature variation, the value of T_C agrees well with the exact solution, which is about $2.269\ J/k_B$ for normal infinite size 2D Ising model. This definitely assures the validity of the simulation codes.

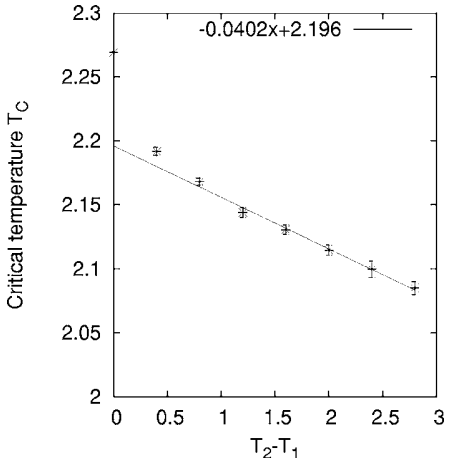

FIG. 8. Critical temperatures T_C obtained from 2D Ising simulations for various $\Delta T=T_2-T_1$. The straight line is a linear least-squares fit to the data for $T_2-T_1 \geqslant 0.8\ J/k_B$.

However, for $\Delta T>0$, T_C reduces very sharply from $\Delta T=0$ to $\Delta T=0.8\ J/k_B$ and afterward reduces slightly for $\Delta T>0.8\ J/k_B$. As can be seen in Fig. 8, it is possible to assign a linear fit to T_C for the range $\Delta T>0.8\ J/k_B$, which gives $T_C(\Delta T)=-0.0402(\Delta T)+2.196$. As evident from the linear fit in Fig. 8, the slope to the fitted function $dT_C/d(\Delta T)=-0.0402$ is rather small. This indicates that even if T_C reduces with increasing ΔT, it does not significantly change in magnitude. This implies that the temperature variation has some minor effects on the critical point by shifting T_C to a smaller value with increasing ΔT. This is so since the greater temperature difference brings more thermal fluctuation into the system so the transition from a ferromagnetic state to the parameter magnetic state occurs at a lower temperature. However, the change is not substantial because the paramagnetic state is defined for a magnetic state that all finite magnetizations are destroyed. Nevertheless, though the temperature variation brings a higher thermal fluctuation to the T_2 boundary causing the spins to align randomly and the local average magnetization close to this T_2 ceases down to zero, the spins close to the lower temperature side T_1 is still intact to the heat bath T_1 with a temperature smaller than the normal T_C. Therefore, some parts of the system still lie in ferromagnetic state. Hence, the overall average magnetization is not completely destroyed resulting in finite magnetization. As a result, unlike other magnetic properties, such as the sharp reduction in magnetization magnitude and the spreading out of susceptibility peaks over a temperature range, T_C changes very slightly.

IV. CONCLUSION

In this study, the effects of linear temperature variation on magnetic properties, i.e., the magnetization, the magnetic susceptibility, and the critical temperature, in the thermal steady state are investigated. In the absence of temperature difference ($\Delta T=0$ or $T_1=T_y=T_2$), the result (e.g., T_C) was found to agree well with the theoretical exact solution of the thermal equilibrium 2D Ising problem. This assures the validity of the simulation codes. However, when the temperature variation is turned on, the temperature difference at the boundaries supplies thermal fluctuation to the spins in the system with different magnitudes, and this makes the magnetization and the susceptibility become spatially dependent. The hotter and the colder parts of the system tend to show paramagnetic and ferromagnetic behaviors, respectively. The interference between these two behaviors turns out to be the reason why the average magnetization sharply reduces and the susceptibility peak becomes broader, while the critical temperature slightly decreases with increasing the temperature difference. The detailed descriptions of the phenomena are given via the investigation of spatial variation of the corresponding magnetic properties. To conclude, the study provides a detailed understanding of how the magnetic properties behave in response to the temperature variation in thermal steady state in ultrathin film, which may be another step closer in modeling real magnetic materials.

ACKNOWLEDGMENTS

The authors would like to acknowledge the Commission on Higher Education (Thailand) and the Thailand Research Fund for financial support.

*Corresponding author. FAX: +66 53 943445. Email address: yongyut_laosiritaworn@yahoo.com

[1] A. Moser, K. Takano, D. T. Margulies, M. Albrecht, Y. Sonobe, Y. Ikeda, S. Sun, and E. E. Fullerton, J. Phys. D **35**, r157 (2002).
[2] T. Osaka, T. Asahi, J. Kawaji, and T. Yokoshima, Electrochim. Acta **50**, 4576 (2005).
[3] P. J. Jensen and K. H. Bennemann, Surf. Sci. Rep. **61**, 129 (2006).
[4] F. Aguilera-Granja and J. L. Morán-López, Solid State Commun. **74**, 155 (1990).
[5] Shengbin Hu, Baoxi Xu, Hongxing Yuan, Yunjie Chen, Jun Zhang, and Rong Ji, J. Magn. Magn. Mater. **303**, e62 (2006).
[6] R. Harris and M. Grant, Phys. Rev. B **38**, 9323 (1988).
[7] M. Neek-Amal, R. Moussavi, and H. R. Sepangi, Physica A **371**, 424 (2006).
[8] M. Creutz, Phys. Rev. Lett. **50**, 1411 (1983).
[9] S. S. Mak, Phys. Lett. A **196**, 318 (1995).
[10] S. V. Buldyrev, N. V. Dokholyan, A. L. Goldberger, S. Havlin, C.-K. Peng, H. E. Stanley, and G. M. Viswanathan, Physica A **249**, 430 (1998).
[11] H. E. Stanley, S. V. Buldyrev, A. L. Goldberger, Z. D. Goldberger, S. Havlin, R. N. Mantegna, S. M. Ossadnik, C.-K. Peng, and M. Simons, Physica A **205**, 214 (1994).
[12] D. Horváth, M. Gmitra, and Z. Kuscsik, Physica A **361**, 589 (2006).
[13] A. Krawiecki and J. A. Hołyst, Physica A **317**, 597 (2003).

[14] K. Binder and P. C. Hohenberg, Phys. Rev. B **9**, 2194 (1974).
[15] M. Bander and D. L. Mills, Phys. Rev. B **38**, 12015 (1988).
[16] Y. Li and K. Baberschke, Phys. Rev. Lett. **68**, 1208 (1992).
[17] H. J. Elmers, J. Hauschild, H. Höche, U. Gradmann, H. Bethge, D. Heuer, and U. Köhler, Phys. Rev. Lett. **73**, 898 (1994).
[18] M. J. Dunlavy and D. Venus, Phys. Rev. B **69**, 094411 (2004).
[19] A. M. Ferrenberg and D. P. Landau, Phys. Rev. B **44**, 5081 (1991).
[20] B. M. McCoy and T. T. Wu, *The Two-Dimensional Ising Model* (Harvard University Press, Cambridge, MA, 1973).
[21] N. Metropolis, A. W. Rosenbluth, M. N. Rosenbluth, A. H. Teller, and E. Teller, J. Chem. Phys. **21**, 1087 (1953).
[22] U. Wolff, Phys. Rev. Lett. **62**, 361 (1989).
[23] H. Müller-Krumbhaar and K. Binder, J. Stat. Phys. **8**, 1 (1973).
[24] K. Binder and D. W. Heermann, *Monte Carlo Simulation in Statistical Physics* (Springer-Verlag, Berlin, 1992).
[25] P. D. Coddington and C. F. Baillie, Phys. Rev. Lett. **68**, 962 (1992).
[26] M. P. Nightingale and H. W. J. Blöte, Phys. Rev. Lett. **76**, 4548 (1996).
[27] K. Binder, Z. Phys. B: Condens. Matter **43**, 119 (1981).
[28] A. M. Ferrenberg and R. H. Swendsen, Phys. Rev. Lett. **61**, 2635 (1988).
[29] A. M. Ferrenberg and D. P. Landau, Phys. Rev. B **44**, 5081 (1991).
[30] M. E. J. Newman and G. T. Barkema, *Monte Carlo Methods in Statistical Physics* (Clarendon, Oxford, 1999).
[31] S. S. A. Razee, J. B. Staunton, L. Szunyogh, and B. L. Györffy, Phys. Rev. B **66**, 094415 (2002).
[32] Q. Hong, Phys. Rev. B **41**, 9621 (1990).
[33] Y. Laosiritaworn, J. Poulter, and J. B. Staunton, Phys. Rev. B **70**, 104413 (2004).
[34] H. Osada, S. Chiba, H. Oka, H. Hatafuku, N. Tayama, and K. Seki, J. Magn. Magn. Mater. **272-276**, e1761 (2004).

IOP PUBLISHING JOURNAL OF PHYSICS: CONDENSED MATTER

J. Phys.: Condens. Matter **19** (2007) 236208 (10pp) doi:10.1088/0953-8984/19/23/236208

Giant dielectric behaviour of $CaCu_3Ti_4O_{12}$ subjected to post-sintering annealing and uniaxial stress

Prasit Thongbai[1], Chivalrat Masingboon[1], Santi Maensiri[1,4], Teerapon Yamwong[2], Supattra Wongsaenmai[3] and Rattikorn Yimnirun[3]

[1] Integrated Nanotechnology Research Center (INRC) and Small & Strong Materials Group (SSMG), Department of Physics, Faculty of Science, Khon Kaen University, Khon Kaen, 40002, Thailand
[2] National Metals and Materials Technology Center (MTEC), Thailand Science Park, Pathumthani, 12120, Thailand
[3] Department of Physics, Faculty of Science, Chiang Mai University, Chiang Mai, 50200, Thailand

E-mail: sanmae@kku.ac.th and santimaensiri@gmail.com

Received 21 March 2007, in final form 18 April 2007
Published 8 May 2007
Online at stacks.iop.org/JPhysCM/19/236208

Abstract

This paper reports the influences of the post-sintering annealing in argon and uniaxial compressive pre-stress on the giant dielectric properties of the $CaCu_3Ti_4O_{12}$ ceramics sintered at 1100 °C in air for 6 and 16 h. The $CaCu_3Ti_4O_{12}$ ceramic sintered at 1100 °C for 6 h exhibited high ε' of $\sim 1 \times 10^4$ whereas the $CaCu_3Ti_4O_{12}$ ceramic sintered at 1100 °C for 16 h possessed one order of magnitude higher dielectric constant ($\varepsilon' \sim 2 \times 10^4$). The dielectric behaviour of both samples exhibits Debye-like relaxation, and can be explained based on a Maxwell–Wagner model. Post-sintering annealing in argon for 5 h leads to a significant increase in ε' for $CaCu_3Ti_4O_{12}$ ceramic sintered at 1100 °C for 16 h but a slight decrease in ε' for the $CaCu_3Ti_4O_{12}$ ceramic sintered at 1100 °C for 6 h. The ε' of the 16 h sintered $CaCu_3Ti_4O_{12}$ ceramic after annealing in argon increases with increasing temperatures, and exhibits a peak at about 150 °C, which is closely related to the oxygen vacancies. The dielectric behaviour of this argon-annealed sample follows the UDR law. The dielectric properties of the argon-annealed samples change significantly with the applied compressive stress (the absolute change can reach 25% at a maximum stress of 130 MPa). However, the changes in dielectric properties with the stress in the samples subjected to different sintering times follow opposing trends. The mechanisms responsible for this difference are discussed.

(Some figures in this article are in colour only in the electronic version)

[4] Author to whom any correspondence should be addressed.

1. Introduction

Dielectric materials that have high dielectric constant and good thermal stability and are Ba/Pb free have particularly attracted ever-increasing attention for their practical applications in microelectronics such as capacitors and memory devices. Recently, calcium copper titanate ($CaCu_3Ti_4O_{12}$), a non-ferroelectric material with a cubic perovskite-related crystal structure, has generated considerable interest because it exhibits a giant dielectric constant of $\varepsilon \sim 10^4$ for polycrystalline ceramics [1–8] and $\varepsilon \sim 10^5$ for single crystals [9] in the kilohertz region over a large temperature range (from 100 to 600 K). This material does not undergo any structural change over the same temperature range, although its dielectric constant abruptly decreases to less than 100 below 100 K, showing a Debye-type relaxation [1, 2, 9]. It has also been reported [6] that the colossal dielectric constant of close to 10^6 at room temperature can be obtained in $CaCu_3Ti_4O_{12}$ after annealing in flowing argon at 1000 °C for 6 h, and was attributed to the increase in concentration of oxygen vacancies and hence charge carriers. Fang and his co-worker [10] also studied the effects of post-annealing conditions on the dielectric properties of $CaCu_3Ti_4O_{12}$ thin films deposited on $Pt/Ti/SiO_2/Si$ substrates by pulsed laser deposition. They observed that post-sintering annealing in nitrogen atmosphere produced strong low-frequency dielectric relaxation as the annealing temperature increases, whereas annealing in oxygen atmosphere at high temperature suppressed the relaxation and decreased the dielectric constant of the thin films. Most recently, the influence of post-sintering annealing on dielectric properties of $CaCu_3Ti_4O_{12}$ was further investigated by Wang and Zhang [11, 12]. They showed that the annealing treatments on $CaCu_3Ti_4O_{12}$ in reducing (nitrogen) and oxidizing (oxygen) atmospheres have significant changes in dielectric properties near room temperature. These results support the results reported in [6] and strongly suggest that the concentration of oxygen plays an important role in the dielectric properties of $CaCu_3Ti_4O_{12}$.

So far, several explanations for the origin of the colossal dielectric property of $CaCu_3Ti_4O_{12}$ material have been proposed to be due to either intrinsic or extrinsic effects. Since the giant dielectric response of this material was found to be very sensitive to the microstructure (such as grain size) and processing conditions (such as sintering temperature and time, cooling rate, and partial pressure) [3, 5–8], more investigations tend to indicate that the high dielectric constant originates from the extrinsic effect such as internal barrier layer capacitor (IBLC) [3–5], contact-electrode effect [13, 14], and special inhomogeneity of local dielectric response [15]. Although still unclear, the IBLC explanation of the extrinsic mechanism is widely accepted at the present stage [16–21].

In addition to its interesting dielectric property, $CaCu_3Ti_4O_{12}$ has remarkably strong linear current–voltage characteristics without the addition of dopants [22]. These excellent properties render this material particularly attractive for a wide range of applications. However, in some practical applications, dielectric ceramics may be subjected to mechanical or thermal stresses, causing changes in their properties. A prior knowledge of how the material properties change under different load conditions is therefore crucial for proper design of a device and for suitable selection of materials for a specific application. Despite this fact, material constants used in many design calculations are often obtained from a stress free measuring condition, which in turn may lead to incorrect or inappropriate device designs. However, the stress dependence of the permittivity in this highly dielectric material has not been thoroughly studied. It is therefore important to determine the properties of $CaCu_3Ti_4O_{12}$ material as a function of applied stress.

In the present study, we investigate the influences of the post-sintering annealing in argon and uniaxial compressive pre-stress on the giant dielectric properties of the $CaCu_3Ti_4O_{12}$ ceramics sintered at 1100 °C in air for 6 and 16 h. The mechanisms responsible for the giant dielectric properties are discussed.

2. Experiment details

$CaCu_3Ti_4O_{12}$ powders were prepared by a conventional mixed oxide technique using the powders of $CaCO_3$ (99.95% purity; CERAC, USA), CuO (99.9% purity; CERAC, USA) and TiO_2 (99.5% purity; CERAC, USA). A stoichiometric mixture of the starting materials was ball-milled in ethanol for 24 h with a polyethylene bottle and zirconia balls. The mixed slurry was dried and then calcined at 950 °C in air for 8 h. The calcined powders were ground and passed through a 106 μm sieve to break up large agglomerates. Green bodies were prepared from the sieved powders using uniaxial pressing in a 16 mm die with an applied pressure of 100 MPa. The compacts were pressureless-sintered at 1100 °C in air for 6 and 16 h. The final dimensions of the samples were ∼12 mm in diameter and ∼3 mm in height. A post-annealing process was carried out in flowing argon (99.999% purity) at 1000 °C for 5 h. Throughout this paper, we assign symbols of CCTO-6 and CCTO-16 for the bulk samples of $CaCu_3Ti_4O_{12}$ sintered at 1100 °C in air for 6 and 16 h, respectively, and assign symbols of CCTO-6–Ar and CCTO-16–Ar for the bulk samples of CCTO-6 and CCTO-16 after post-sintering annealing under flowing argon at 1000 °C for 5 h.

The $CaCu_3Ti_4O_{12}$ ceramics were characterized by x-ray diffraction (XRD) (Philips PW3710, The Netherlands), and scanning electron microscopy (SEM) (LEO 1450VP, UK). The dielectric response of the samples was measured using a Hewlett Packard 4194A impedance gain phase analyser over the frequency ranges from 100 Hz to 1 MHz and at an oscillation voltage of 1 V. The measurements were performed over the temperature ranges from −30 to 160 °C using an inbuilt cooling–heating system. Each measured temperature was kept constant with an accuracy of ±1 °C. Silver paint was coated on both surfaces of the samples and dried overnight. The dielectric properties of the samples after post-sintering annealing were measured under the influence of the compressive stress through spring-loaded pins connected to an LCZ-meter (Hewlett Packard 4276A) at the frequency of 1 kHz and room temperature (25 °C). The details of the system are described in elsewhere [23].

3. Results and discussion

The microstructure of all the sintered ceramics revealed by scanning electron microscopy (figures 1(a) and (b)) shows polycrystalline grains with estimated grain sizes of 7.7 ± 1.9 and 9.0 ± 1.9 μm for CCTO-6 and CCTO-16. Figure 1(c) shows XRD patterns of the sintered ceramics before and after post-sintering annealing, confirming a main phase of $CaCu_3Ti_4O_{12}$ (JCPDS card no 75-2188) in all the samples. The values of lattice parameter a calculated from the XRD spectra are 0.7387 ± 0.000 03, 0.7385 ± 0.000 04, 0.7389 ± 0.000 03, and 0.7391 ± 0.000 07 nm for CCTO-6, CCTO-16, CCTO-6–Ar, and CCTO-16–Ar, respectively. The values of a for CCTO-6 and CCTO-16 are slightly lower than the 0.7391 nm reported by Subramanian *et al* [1]. Post-annealing in argon results in an increase in the values of a for CCTO-6–Ar and CCTO-16–Ar, which are close to 0.7391 nm.

Figures 2(a) and (b) show the real and imaginary parts of dielectric dispersion for the samples of CCTO-6 and CCTO-16, measured using a Hewlett Packard 4194A impedance gain phase analyser at the frequency ranges from 100 Hz to 1 MHz with an oscillation voltage of 1 V at various temperatures. It is clearly seen from figure 2(a) that both samples exhibit the giant dielectric permittivity of $\sim 1 \times 10^4$ for CCTO-6 and $\sim 2 \times 10^4$–2.5×10^4 for CCTO-16 at low frequencies and each sample has a similar dielectric behaviour. First, all of the samples exhibit the Debye-like relaxation [2, 9, 14, 16]. This behaviour is similar to that observed in CCTO ceramics reported in the literature [3, 4, 7, 8, 17, 24, 25]. Second, ε' has little frequency dependence below the relaxation frequency. Third, the relaxation peak in both samples shifts to higher frequency at higher temperature.

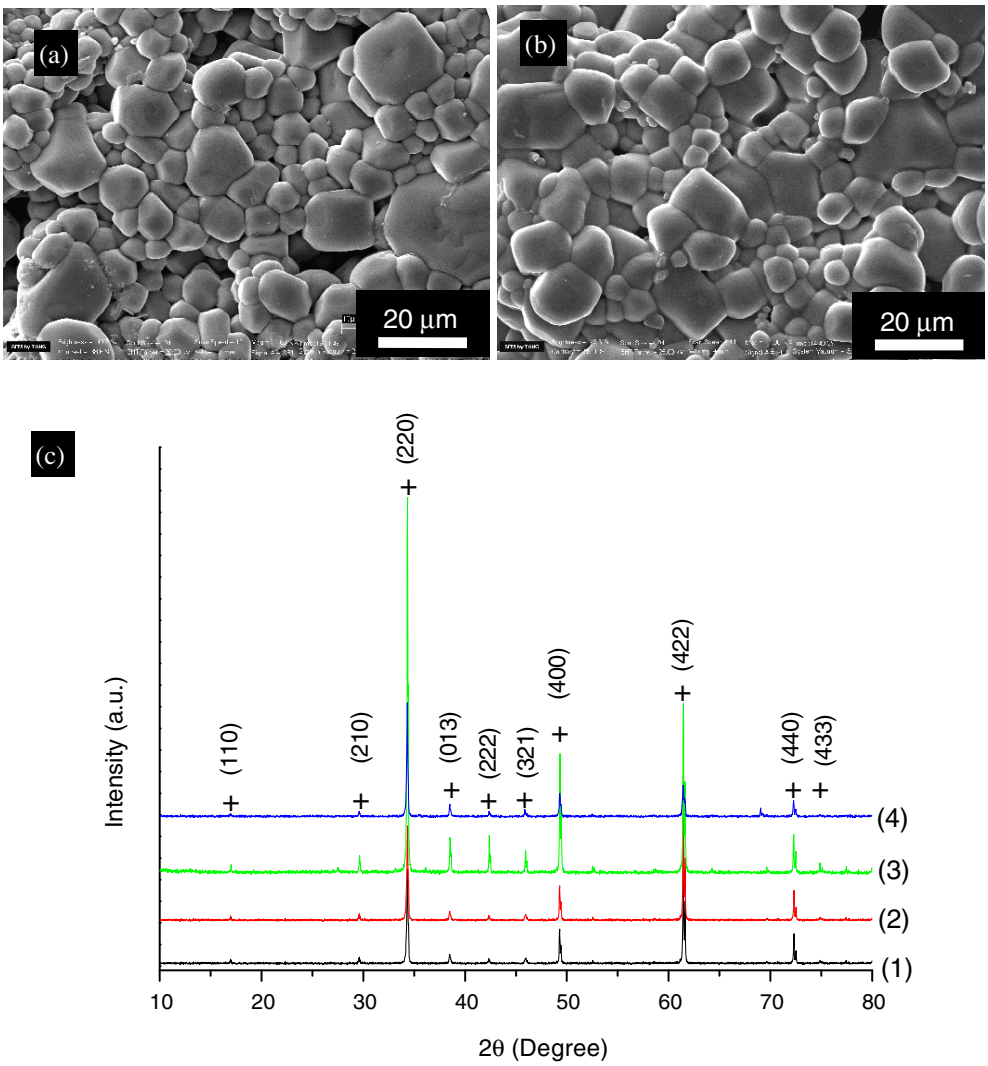

Figure 1. (a) and (b) SEM micrographs of sintered CCTO-6 and CCTO-16, respectively. (c) XRD patterns of the sintered materials of CCTO-6 and CCTO-16 before and after annealing at 1000 °C for 5 h under flowing argon. (1) CCTO-6, (2) CCTO-16, (3) CCTO-6–Ar, and (4) CCTO-16–Ar.

The Debye-like relaxation for CCTO-6 and CCTO-16 (figures 2(a) and (b)) can be fitted to the empirical Cole–Cole equation [26]:

$$\varepsilon^*(\omega) = \varepsilon'(\omega) - \mathrm{i}\varepsilon''(\omega) = \varepsilon_\infty + [(\varepsilon_\mathrm{s} - \varepsilon_\infty)/1 + (\mathrm{i}\omega\tau)^\alpha] \quad (1)$$

where ε_s and ε_∞ are the static and high-frequency limits of the dielectric constant, respectively, τ is the most probable relaxation time, and α is a constant with values between zero and unity. For an ideal Debye relaxation $\alpha = 1$. If $\alpha < 1$, this implies that the relaxation has a distribution of relaxation times, leading to a broader peak shape than a Debye peak as shown in figure 2(b). The solid lines in figures 2(a) and (b) are the fitted results with $\alpha = 0.92$ for CCTO-6 and $\alpha = 0.91$ for CCTO-16. Figure 2(c) shows the plot of log τ versus $1/T$, in which the solid line

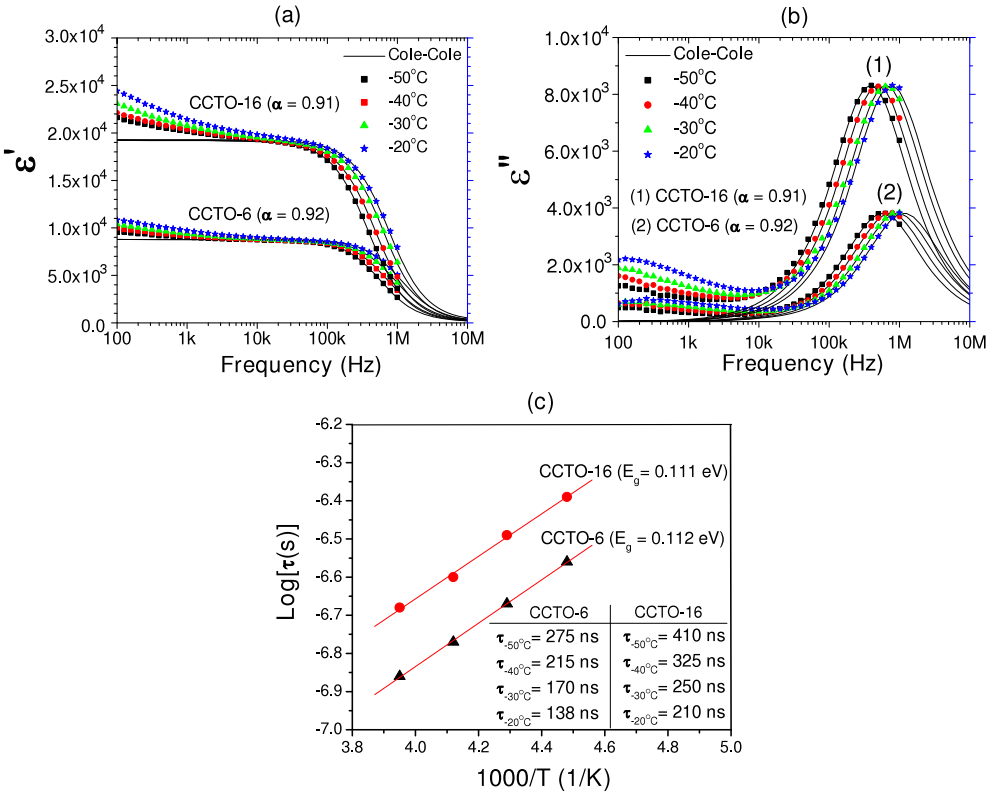

Figure 2. (a) Frequency dependence of the dielectric dispersion showing ε' at several temperatures for the sintered materials of CCTO-6 and CCTO-16. (b) Frequency dependence of the dielectric dispersion showing ε'' at several temperatures for the sintered materials of CCTO-6 and CCTO-16. (c) Arrhenius plot of dielectric relaxation time for the CCTO-6 and CCTO-16 samples. Solid lines in (a) and (b).

is the fitted result obeying the Arrhenius law, i.e.

$$\tau = \tau_0 \exp(E/k_B T) \tag{2}$$

where τ_0 is the pre-exponential factor, E is the activation energy for the relaxation, k_B is the Boltzmann constant, and T is the absolute temperature. τ is calculated from the relations $\omega\tau = 1$ and $\omega = 2\pi f_p$, where ω is the angular frequency and f_p is the characteristic frequency corresponding to the peak of ε''. Activation energies of the low-frequency relaxation determined from the slopes of the graphs (figure 2(c)) were obtained to be 0.112 for CCTO-6 and 0.111 eV for CCTO-16. Both values are comparable to the reported values of 0.067 eV [16], 0.08 eV [3, 17], 0.093 eV [18], 0.059–0.076 eV [19], and 0.084–0.132 eV [7] for the grains of $CaCu_3Ti_4O_{12}$.

Since the dielectric response in both CCTO-6 and CCTO-16 shows the Debye-like relaxation which is approximately equal to the pure Debye functional form of a Maxwell–Wagner relaxation, the giant dielectric behaviour of both samples can be explained by using the Maxwell–Wagner relaxation model. The Maxwell–Wagner relaxation can be described by an equivalent circuit consisting of a series array of two subcircuits, one representing grain effects and one grain boundaries [8]. In each subcircuit, the resistor and capacitor are in parallel. From this equivalent circuit, the static permittivity (ε'_s) and dielectric relaxation time (τ) can

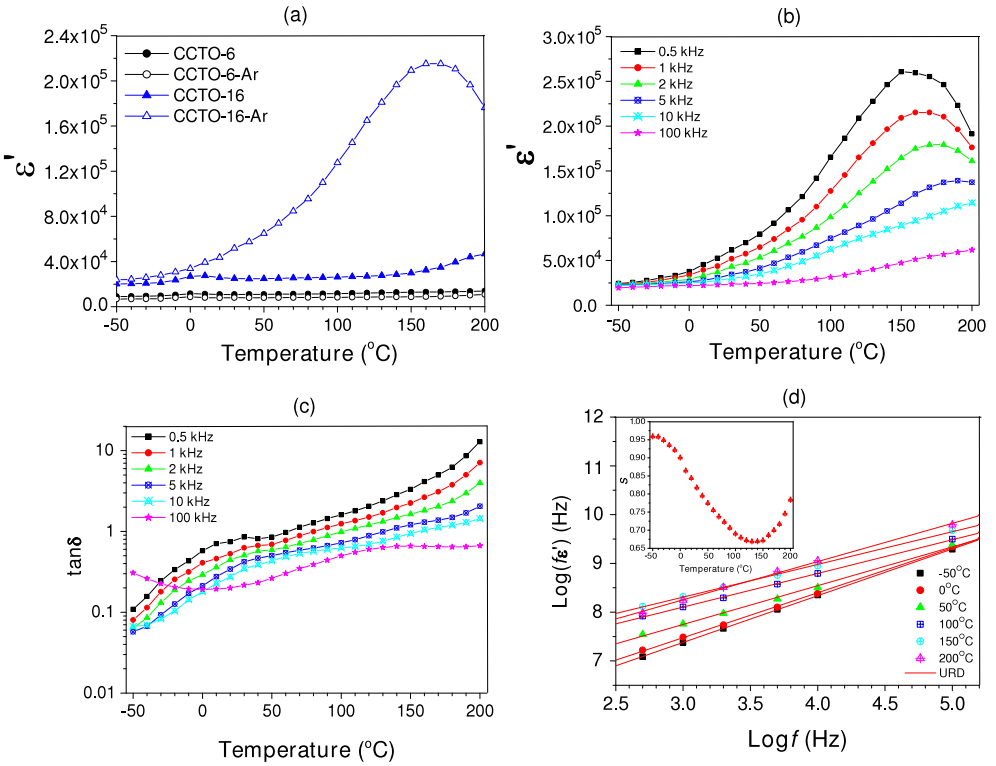

Figure 3. (a) Temperature dependence of ε' at frequency of 100 Hz for the sintered materials of CCTO-6 and CCTO-16 before and after annealing at 1000 °C for 5 h under flowing argon. (b) Temperature dependence of ε' at various frequencies for the CCTO-16 after annealing at 1000 °C for 5 h under flowing argon. (c) Temperature dependence of $\tan\delta$ at various frequencies for the CCTO-16 after annealing at 1000 °C for 5 h under flowing argon.

be calculated as

$$\varepsilon'_{\mathrm{s}} = (R_{\mathrm{g}}^2 C_{\mathrm{g}} + R_{\mathrm{gb}}^2 C_{\mathrm{gb}})/[C_0(R_{\mathrm{g}} + R_{\mathrm{gb}})^2] \tag{3}$$

and

$$\tau = [R_{\mathrm{g}} R_{\mathrm{gb}}(C_{\mathrm{g}} + C_{\mathrm{gb}})]/(R_{\mathrm{g}} + R_{\mathrm{gb}}), \tag{4}$$

where R_{g}, R_{gb} and C_{g}, C_{gb} are the resistance and capacitance of grains and grain boundaries, respectively [27]. Since $R_{\mathrm{gb}} \gg R_{\mathrm{g}}$, and C_{gb} is also much larger than C_{g} [3, 8], the effective dielectric permittivity ($\varepsilon'_{\mathrm{s}}$) of the sample at frequencies much lower than the relaxation frequency $1/(2\pi\tau)$ can therefore be obtained approximately from equation (3),

$$\varepsilon'_{\mathrm{s}} = C_{\mathrm{gb}}/C_0 \tag{5}$$

and we can approximate τ from equation (4) using

$$\tau \approx R_{\mathrm{g}} C_{\mathrm{gb}} = \tau_{\mathrm{g}}(C_{\mathrm{gb}}/C_{\mathrm{g}}) \tag{6}$$

where $\tau = R_{\mathrm{g}} C_{\mathrm{g}}$ is the response time of the grains [8]. Since C_{g} and C_{gb} have been reported to be independent of temperature [3, 8], τ and τ_{g} have the same temperature dependence and the electrical response of grains has the same activation energy as that of the observed dielectric relaxation (figure 3(c)). On the basis of this analysis, we conclude that the activation

energies for the response of the grains in the samples of CCTO-6 and CCTO-16 are 0.112 and 0.111 eV, respectively. It is noted that the relation $\varepsilon'_s = C_{gb}/C_0$ implies that ε'_s is determined only by the ratio between the grain boundary capacitance C_{gb} and the vacuum capacitance of the sample C_0, and ε'_s is constant when C_{gb} is unchanged with temperature and frequency. Liu *et al* [28] observed a constant dielectric permittivity in wide temperature and frequency ranges in $Bi_{2/3}Cu_3Ti_4O_{12}$ because of its constant C_{gb}. Therefore, we attribute the differences in dielectric response observed in CCTO-6 and CCTO-16 to the differences in their grain boundary capacitances.

Figure 3(a) compares dielectric constant ε' of CCTO-6 and CCTO-16 before and after post-sintering annealing, showing a significant increase in ε' for the CCTO-16 after post-sintering annealing (CCTO-16–Ar) but a slight decrease in ε' for the CCTO-6 after post-sintering annealing (CCTO-6–Ar). The ε' of CCTO-16–Ar increases with increasing temperatures, and interestingly exhibits a peak at about 150 °C. This behaviour is important in explaining the effect of post-sintering annealing under a reducing atmosphere in the $CaCu_3Ti_4O_{12}$ system, and thus we further consider the dielectric behaviour of the CCTO-16 in detail. Figures 3(b) and (c) show temperature dependences of ε' and $\tan\delta$ over the frequencies of 500 Hz–100 kHz. ε' exhibits a peak around 150 °C (at 1 kHz) (figure 3(a)), whereas $\tan\delta$ increases near-exponentially with increasing temperature without a visible anomaly in the vicinity of 150 °C (figure 3(b)). This implies that the peak in ε' is not likely caused by the relaxation process. From figure 3(b), upon increasing the measured frequency, the peak position of ε' is shifted to higher temperatures and the peak height decreases, which is typical of a thermally activated Debye-like behaviour. The obvious upturn in $\tan\delta$ at low temperatures for the curves of high frequencies (at 100 kHz) shown in figure 3(c) is due to the relaxation widely studied before in the $CaCu_3Ti_4O_{12}$ system. This dielectric behaviour observed in CCTO-16–Ar is similar to that of the $CaCu_3Ti_4O_{12}$ sample after post-sintering annealing under nitrogen at 920 °C for 2 h, reported by Wang and Zhang [12]. In their report, the dielectric peak was observed at around 67 °C (340 K) (hereafter referred to as the 67 °C peak) and can be eliminated by annealing in oxidizing (O_2) atmosphere and created by annealing in reducing (N_2) atmosphere. This strongly suggests that the 67 °C peak is closely related to oxygen vacancies which made the grains of the $CaCu_3Ti_4O_{12}$ ceramic more conductive. Therefore, Wang and Zhang [12] proposed that the 67 °C peak was linked with the conductivity, the dielectric behaviour of the $CaCu_3Ti_4O_{12}$ after annealing in N_2 atmosphere followed the universal dielectric law (UDR) [29], and ε' can be calculated as

$$\varepsilon' = [\tan(s\pi/2)\sigma_0 f^{s-1}]/\varepsilon_0, \tag{7}$$

where σ_0 and the frequency exponent s are temperature dependent and ε_0 is the electric permittivity of free space. This equation can be rewritten as $f\varepsilon' = A(T)f^s$ with the temperature-dependent constant $A(T) = \tan(s\pi/2)\sigma_0/\varepsilon_0$. Hence, at a given temperature, a straight line with a slope of s should be obtained if $\log_{10}(f\varepsilon')$ is plotted as a function of $\log_{10} f$. Since the URD-law model is typically valid for materials with hopping localized charge carriers, Wang and Zhang [12] confirmed that the charge carriers in the $CaCu_3Ti_4O_{12}$ after annealing in N_2 atmosphere are localized and not free charge carriers. This rules out the space-charge polarization as the origin of the 67 °C peak. To confirm this model, we plotted $\log_{10}(f\varepsilon')$ as a function of $\log_{10} f$ for the CCTO-16–Ar as shown in figure 3(c). As expected, straight lines with slopes of s were obtained. The values of the parameter s deduced from linear fitting are presented in the inset of figure 3(c). It is seen from figure 3(c) that with increasing temperature the slope of the linear temperature dependence changes from a negative to a positive value at the transition temperature ~150 °C. This result is consistent with that observed in $CaCu_3Ti_4O_{12}$ after annealing in N_2 atmosphere with the transition temperature

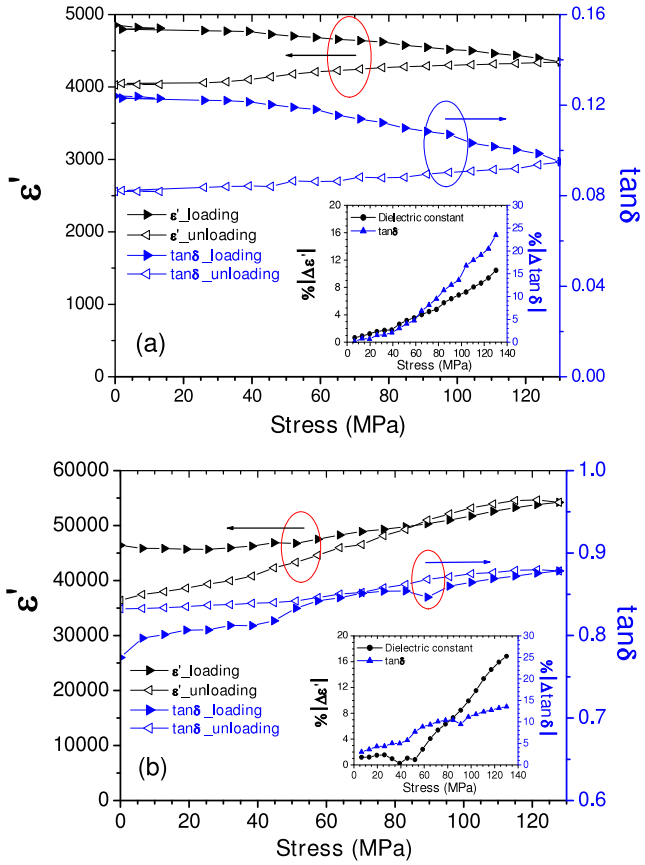

Figure 4. Uniaxial stress dependence of ε' and $\tan\delta$ at a frequency of 100 Hz for the samples of (a) CCTO-6 and (b) CCTO-16 after annealing at 1000 °C for 5 h under flowing argon.

at ∼67 °C. The change in slope implies an alternation of the polarization mechanism [12]. According to our post-sintering annealing results, we conclude that the ε' peak is unlikely to be caused by a relaxation process. The ∼150 °C peak is closely related to the oxygen vacancies and the dielectric behaviour follows the UDR law. Annealing the $CaCu_3Ti_4O_{12}$ sample in argon atmosphere at high temperatures would increase the concentration of the oxygen vacancies as obtained in the nitrogen-annealed $CaCu_3Ti_4O_{12}$ reported by Wang and Zhang [12].

Figures 4(a) and (b) show the stress dependent dielectric properties for CCTO-6–Ar and CCTO-16–Ar, respectively. It is clearly observed that the dielectric properties of both samples change significantly with the applied compressive stress (the absolute change can reach 25% at the maximum stress of 130 MPa). However, the changes in dielectric properties with the stress in the samples subjected to different sintering times follow opposing trends. For the CCTO-6–Ar, both ε' and $\tan\delta$ decrease with increasing stress, and, interestingly, continue to decrease upon the reduction of the applied stress (figure 4(a)). On the other hand, the dielectric properties of the CCTO-16–Ar sample increase when the stress is increased and decrease when the stress is gradually reduced, as shown in figure 4(b). To explain these observations, at least qualitatively, one needs to consider the different bases in the dielectric behaviours of the two ceramics. Clearly, the very high dielectric constant observed in CCTO ceramics is attributable to highly resistive grain boundaries [18, 30]. Interestingly, the CCTO-

16–Ar ceramic, which has been subjected to longer sintering (16 h), also possessed one order of magnitude higher dielectric constant, possibly due to higher concentration of the acceptor state (oxygen vacancies) available in the grain boundaries of the ceramic [31]. With lower concentrations of acceptor states, the CCTO-6–Ar should contain more mobile dipoles that can easily be activated by the applied stress. Hence, this leads to a stress-induced ageing mechanism, as reported previously [32–34], that results in the decrease in the dielectric constant and dielectric loss. This stress-induced ageing is irreversible, as the dielectric properties continue to decrease even upon reduction of the applied stress (figure 4(a)). On the other hand, in the case of the CCTO-16–Ar ceramic, with higher concentration of the acceptor states, there are competing mechanisms between the stress-induced ageing and the elastic deformation. Initially, with the stress-induced ageing mechanism still dominating, most of the acceptor states come to rest at the grain boundaries and stabilize the stress influence, as it is observed that the dielectric properties are rather stable at lower stress level [32–34]. A further increase in the compressive stress may result in a slight decrease in the grain boundary thickness. The effective dielectric properties of this ceramic, which can be regarded as the boundary layer capacitor (BLC) [16–21, 31], therefore increase, and the decrease in the effective dielectric properties follows with the reduction of the stress, as observed in figure 4(b).

4. Conclusion

The giant dielectric behaviour of polycrystalline $CaCu_3Ti_4O_{12}$ ceramics subjected to post-sintering annealing and under uniaxial stress was investigated. The dielectric behaviour of both CCTO-6 and CCTO-16 samples exhibits Debye-like relaxation, and can be explained based on the Maxwell–Wagner model. A significant increase in ε' was observed for the CCTO-16 after post-sintering annealing in argon (CCTO-16–Ar), whereas a slight decrease in ε' was observed for the CCTO-6 after post-sintering annealing in argon (CCTO-6–Ar). The ε' of CCTO-16–Ar increases with increasing temperatures, and interestingly exhibits a peak at about 150 °C. The ε' peak at 150 °C is unlikely to be caused by a relaxation process but is closely related to the oxygen vacancies. The dielectric properties of both CCTO-6–Ar and CCTO-16–Ar samples change significantly with the applied compressive stress, and this can be explained by the stress-induced ageing mechanism.

Acknowledgments

The authors would like to thank the Electron Microscopy Unit, Faculty of Science, Khon Kaen University, for providing SEM facilities. This work is supported by The Integrated Nanotechnology Research Center (INRC), Khon Kaen University, and The Postgraduate Education Development (PED) in Physics Program, The Commission on Higher Education, The Ministry of Education, Thailand.

References

[1] Subramanian M A, Li D, Duan N, Reisner B A and Sleight A W 2000 *J. Solid State Chem.* **151** 323
[2] Ramirez A P, Subramanian M A, Gardela M, Blumberg G, Li D, Vogt T and Shapiro S M 2000 *Solid State Commun.* **115** 217
[3] Sinclair D C, Adams T A, Morrison F D and West A R 2002 *Appl. Phys. Lett.* **80** 2153
[4] Adams T B, Sinclair D C and West A R 2002 *Adv. Mater.* **18** 1321
[5] Fang T T and Shiau H K 2004 *J. Am. Ceram. Soc.* **87** 2072
[6] Bender B A and Pan M J 2005 *Mater. Sci. Eng.* B **117** 339

[7] Shao S F, Zhang J L, Zheng P, Zhong W L and Wang C L 2006 *J. Appl. Phys.* **99** 084106
[8] Liu J, Sui Y, Duan C G, Mei W N, Smith R W and Hardy J R 2006 *Chem. Mater.* **18** 3878
[9] Homes C C, Vogt T, Shapiro S M, Wakimoto S and Ramirez A P 2001 *Science* **293** 673
[10] Fang L, Shen M and Cao W 2004 *J. Appl. Phys.* **95** 6483
[11] Wang C C and Zhang L W 2006 *Appl. Phys. Lett.* **88** 042906
[12] Wang C C and Zhang L W 2006 *Phys. Rev.* B **74** 024106
[13] Lunkenheimer P, Bobnar V, Pronin A V, Ritus A I, Volkov A A and Loidl A 2002 *Phys. Rev.* B **66** 052105
[14] Lunkenheimer P, Fichtl R, Ebbinghaus S G and Loidl A 2004 *Phys. Rev.* B **70** 172102
[15] Cohen M H, Neaton J B, He L X and Vanderbilt D 2003 *J. Appl. Phys.* **94** 3299
[16] Zhang L and Tang Z J 2004 *Phys. Rev.* B **70** 174306
[17] West A R, Adams T B, Morrison F D and Sinclair D C 2004 *J. Eur. Ceram. Soc.* **24** 1439
[18] Chiodeli G, Massarotti V, Capsoni D, Bini M, Azzoni C B, Mozzati M C and Lupotto P 2004 *Solid State Commun.* **132** 241
[19] Capsoni D, Bini M, Massarotti V, Chiodelli G, Mozzatic M C and Azzoni C B 2004 *J. Solid State Chem.* **177** 4494
[20] Kalinin S V, Shin J, Veith G M, Baddorf A P, Lobanov M V, Runge H and Greenblatt M 2005 *Appl. Phys. Lett.* **86** 102902
[21] Fang T T, Mei L T and Ho H F 2006 *Acta Mater.* **54** 2867
[22] Chung S, Kim I and Kang S 2004 *Nat. Mater.* **3** 774
[23] Yimnirun R, Moses P J, Mayer R J and Newnham R E 2003 *Rev. Sci. Instrum.* **74** 3429
[24] Aygun S, Tan X, Maria J P and Cann D 2005 *J. Electroceram.* **15** 203
[25] Zhang J L, Zheng P, Wang C L, Zhao M L, Li J C and Wang J F 2005 *Appl. Phys. Lett.* **87** 142901
[26] Cole K S and Cole R H 1941 *J. Chem. Phys.* **9** 341
[27] Hippel V 1954 *Dielectrics and Waves* (New York: Wiley)
[28] Liu J, Duan C, Yin W, Mei W N, Smith R W and Hardy J R 2004 *Phys. Rev.* B **70** 144106
[29] Jonscher A K 1983 *Dielectric Relaxation in Solids* (London: Chelsea Dielectric Press)
[30] Chen W P, Xiang W, Guo M S, You W C, Zhao X Z and Chan H L W 2006 *J. Alloys Compounds* **422** L9–12
[31] Moulson A J and Herbert J M 2003 *Electroceramics* (Chichester: Wiley)
[32] Yimnirun R, Ananta S, Ngamjarurojana A and Wongsaenmai S 2006 *Curr. Appl. Phys.* **6** 520
[33] Yimnirun R, Unruan M, Laosiritaworn Y and Ananta S 2006 *J. Phys. D: Appl. Phys.* **39** 3097
[34] Yimnirun R 2006 *Int. J. Mod. Phys.* B **20** 3409

Cation, dipole, and spin order in $Pb(Fe_{2/3}W_{1/3})O_3$-based magnetoelectric multiferroic compounds

R. Wongmaneerung and X. Tan[a)]
Department of Materials Science and Engineering, Iowa State University, Ames, Iowa 50011

R. W. McCallum
Materials and Engineering Physics Program, Ames Laboratory, U.S. DOE, Ames, Iowa 50011

S. Ananta and R. Yimnirun
Department of Physics, Faculty of Science, Chiang Mai University, Chiang Mai 50200, Thailand

(Received 6 March 2007; accepted 17 May 2007; published online 11 June 2007)

Long range 1:1 cation order was developed in $Pb(Fe_{2(1-x)/3}Sc_{2x/3}W_{1/3})O_3$ solid solution compounds by high temperature solid state reaction. It is found that the degree of cation order directly influences the saturation magnetization in these single phase compounds. A high saturation magnetization ($\sim 0.61\mu_B$/f.u.) was observed for $x=0.15$ at 10 K under 5 T. A ferrimagnetic structure was suggested to take into account for the observed magnetic behavior. These compounds also display a saturated electrical polarization of $\sim 15\ \mu C/cm^2$ at 40 kV/cm at 120 K. © *2007 American Institute of Physics*. [DOI: 10.1063/1.2748098]

Magnetoelectric multiferroic compounds, combining a spontaneous electrical polarization with a net magnetization, have attracted worldwide interest recently due to their great potentials for fundamental research and practical applications.[1–3] However, all the known magnetic ferroelectric oxides either have a low transition temperature or display an extremely small polarization/magnetization. Among these multiferroic compounds, those with the ABO_3 perovsite structure show the highest magnetic transition temperatures and the largest electrical polarizations.[3] Considering the fact that most magnetic perovskite oxides have an antiferromagnetic order due to a superexchange coupling between magnetic ions on the *B* site,[4] Baettig and Spaldin[5] and Baettig *et al.*[6] proposed to introduce spontaneous magnetization via *ferrimagnetism* and predicted that $Bi(Fe_{1/2}Cr_{1/2})O_3$ would display an electrical polarization of 80 $\mu C/cm^2$ and a saturation magnetization of $1\mu_B/ABO_3$ f.u. if Fe^{3+} and Cr^{3+} occupy separate *B* sublattices (B' and B'') to form a double perovskite structure. The Neel temperature was calculated to be low (<100 K), though. However, such a double perovskite structure with long range *B*-site cation order is not likely to form since Fe^{3+} and Cr^{3+} have the same charge and close ionic sizes. $Bi(Fe_{1/2}Cr_{1/2})O_3$ is, thus, expected to adopt a simple perovskite structure with random occupancy of Fe^{3+} and Cr^{3+} on *B* site. Recent experimental work confirmed that the $Bi(Fe_{1/2}Cr_{1/2})O_3$ epitaxial thin film is isostructural to $BiFeO_3$ with a rhombohedral distortion.[7] A saturation magnetization of only $0.26\mu_B$/f.u. was measured at room temperature due to the absence of long range cation order. In addition, the film was found to be very leaky with an induced polarization of only 2.8 $\mu C/cm^2$ at 82 kV/cm. In the bulk form, $Bi(Fe_{1/2}Cr_{1/2})O_3$ shows neither *B*-site cation order nor any ferri—or ferromagnetic order down to 2 K.[8]

In contrast, a few ferroelectric Pb-based complex perovskite oxides have been reported to display long range 1:1 *B*-site cation order, such as $Pb(Sc_{1/2}Ta_{1/2})O_3$,[9] La-doped $Pb(Mg_{1/3}Nb_{2/3})O_3$,[10,11] and $Pb(Sc_{2/3}W_{1/3})O_3$.[12] The multiferroic $Pb(Fe_{2/3}W_{1/3})O_3$ compound also shows 1:1 cation order, however, the chemical order is very weak and the cation ordered domains are limited to the nanometer scale (<5 nm).[13–15] Developing long range cation order in $Pb(Fe_{2/3}W_{1/3})O_3$ for large saturation magnetization has been experimentally attempted previously with Mg^{2+} doping[16] and Co^{2+} doping.[17] The present work aims to enhance cation order in $Pb(Fe_{2/3}W_{1/3})O_3$ through solid solution with $Pb(Sc_{2/3}W_{1/3})O_3$, both of which have a *B*-cation ratio of 2:1. Magnetic as well as ferroelectric properties are assessed as a function of the degree of *B*-site cation order.

Ceramics in the solid solution $(1-x)Pb(Fe_{2/3}W_{1/3})O_3-xPb(Sc_{2/3}W_{1/3})O_3$($x=0.09, 0.15, 0.21$), or $Pb(Fe_{2(1-x)/3}Sc_{2x/3}W_{1/3})O_3$, were prepared via a solid state reaction method with high purity powders (better than 99.9%). Proportional amount of Fe_2O_3, WO_3, and Sc_2O_3 powders were mixed and calcined at 900 °C for 24 h. Then appropriate amount of PbO powder was mixed and a second calcination was carried out at 850 °C for 2 h. Ceramic pellets were formed by sintering at 890 °C for 2 h followed by a slow cooling procedure at 9 °C/h to 800 °C. The surface layers of the sintered disks were removed before x-ray diffraction experiments. Dielectric characterization was performed with a *LCR* meter (HP-4284A, Hewlett-Packard) in conjunction with an environmental chamber (9023, Delta Design). A heating rate of 3 °C/min was used during measurement. The polarization hysteresis measurement was carried out with a standardized ferroelectric test system (RT-66A, Radiant technologies). A Quantum Design 5T MPMS was used for magnetic characterization.

X-ray diffraction indicates that the as-sintered ceramics are phase pure and display a pseudocubic perovskite structure, as shown in Fig. 1. The lattice parameters increase with Sc^{3+} content and were determined to be 3.9760, 3.9837, and 4.0004 Å for ceramics of $x=0.09$, 0.15, and 0.21, respectively. This is consistent with the fact that Sc^{3+} has a larger ionic radius than both Fe^{3+} and W^{6+}. Furthermore, $(\frac{1}{2}\frac{1}{2}\frac{1}{2})$-type superlattice peaks get strengthened as Sc^{3+} content increases, as revealed clearly by the inset in Fig. 1. In

[a)]Electronic mail: xtan@iastate.edu

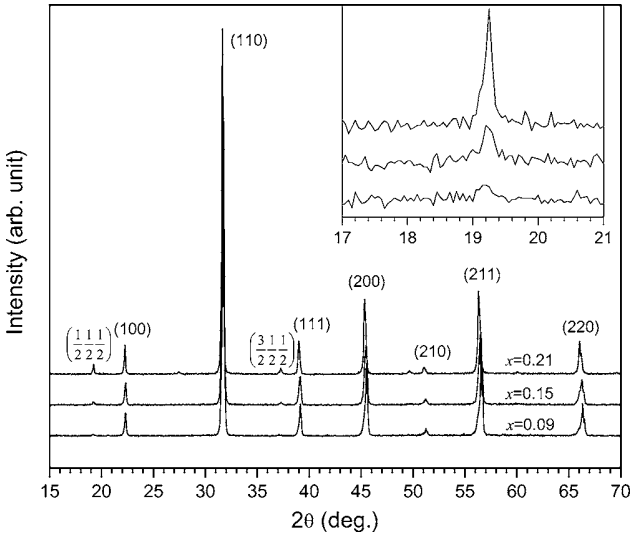

FIG. 1. X-ray diffraction pattern of the sintered $Pb(Fe_{2(1-x)/3}Sc_{2x/3}W_{1/3})O_3$ ceramics. Major peaks are indexed on the basis of a simple cubic perovskite structure. The $(\frac{1}{2}\frac{1}{2}\frac{1}{2})$-type superlattice peaks due to *B*-site cation order are also indexed. The inset shows the close view of the $(\frac{1}{2}\frac{1}{2}\frac{1}{2})$ superlattice peak.

complex perovskite oxides, the presence of the $(\frac{1}{2}\frac{1}{2}\frac{1}{2})$ superlattice peak is an indication of the development of 1:1 *B*-site cation order and the intensity of this superlattice peak has been routinely used to calculate the ordering parameter *S*.[10,11] This parameter ranges from 0 to 1, with 0 marking the complete disorder and 1 marking the complete order. The ordering parameters *S* are calculated to be 0.26, 0.55, and 0.81 for ceramics of $x=0.09$, 0.15, and 0.21, respectively. The double perovskite model,

$$Pb[Sc_{2x/3}Fe_{(1/2-2x/3)}][Fe_{1/6}W_{1/3}]O_3,$$

was used for the calculation.

The dielectric response of these ceramic pellets was examined and the result is shown in Fig. 2. It is noted that broad peaks appear for all three compositions. At 100 kHz, the maximum relative permittivities ε_m were measured to be 5130 at 198 K, 5460 at 206 K, and 4160 at 198 K for ceramics of $x=0.09$, 0.15, and 0.21, respectively. It appears that the ceramic with $x=0.15$ behaves slightly abnormally. The

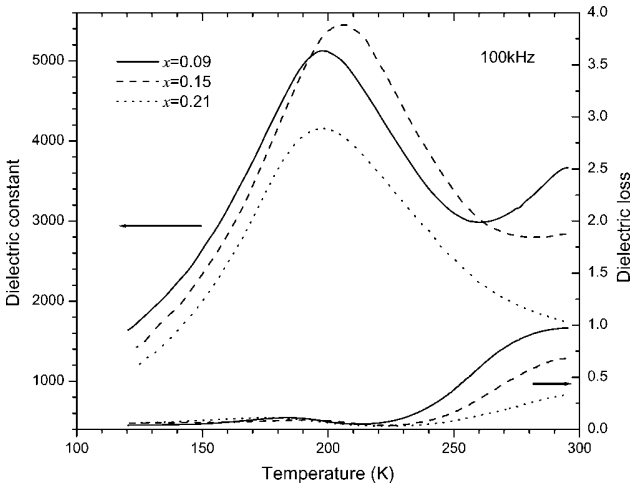

FIG. 2. Relative dielectric permittivity and dielectric loss of the $Pb(Fe_{2(1-x)/3}Sc_{2x/3}W_{1/3})O_3$ ceramics as a function of temperature at 100 kHz.

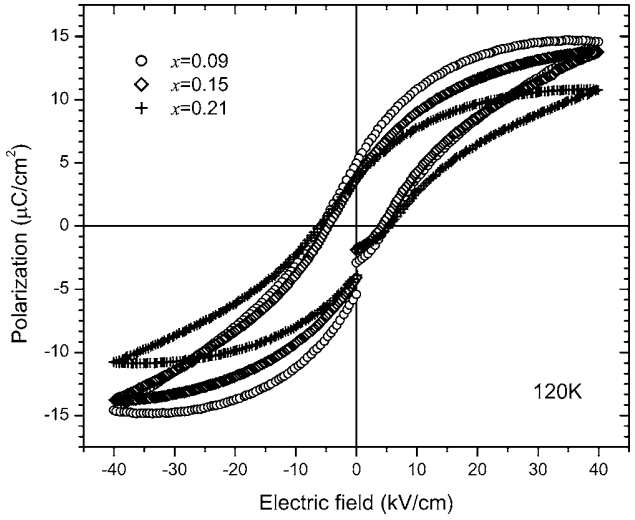

FIG. 3. Polarization vs electric field hysteresis loops measured at 4 Hz at 120 K in the $Pb(Fe_{2(1-x)/3}Sc_{2x/3}W_{1/3})O_3$ ceramics. Well defined saturated loops are observed.

dielectric loss is relatively low for all three ceramics, especially under 230 K. Compared to pure $Pb(Fe_{2/3}W_{1/3})O_3$ ($\varepsilon_m=11\,700$ at $T_m=190$ K at 100 kHz),[13] solid solution with $Pb(Sc_{2/3}W_{1/3})O_3$ leads to a slight higher T_m but a much lower ε_m value.

The low dielectric loss at low temperatures allows the electric field-induced polarization measurement under quasistatic fields. The electrical polarization versus electric field hysteresis loop was evaluated at 4 Hz at 120 K. As shown in Fig. 3, saturated loops were recorded for all three compositions. Saturation polarizations of 14.6, 13.8, and 10.9 $\mu C/cm^2$ for ceramics of $x=0.09$, 0.15, and 0.21, respectively, were measured at the peak electric field of 40 kV/cm at this temperature. Remanent polarizations of 5.2, 4.0, and 3.8 $\mu C/cm^2$ for $x=0.09$, 0.15, and 0.21, respectively, were recorded. The coercive fields were determined to be 5.5, 4.5, and 5.5 kV/cm for $x=0.09$, 0.15, and 0.21, respectively. Therefore, strong ferroelectricity with large electrical polarizations and low coercive fields is demonstrated in the $Pb(Fe_{2(1-x)/3}Sc_{2x/3}W_{1/3})O_3$ solid solution.

The magnetization under weak field indicates a clear transition from paramagnetic to ferrimagnetic at ~224, ~245, and ~222 K for the ceramics of $x=0.09$, 0.15, and 0.21, respectively. Compared to pure $Pb(Fe_{2/3}W_{1/3})O_3$ ($T_N=370$ K),[13–15] incorporating Sc decreases the transition temperature, which can be attributed to the dilution of the magnetic cations. The magnetization under a strong magnetic field of 5 T for the three ceramics is shown in Fig. 4. Interestingly, the ceramic of $x=0.15$ shows the highest magnetization. The saturation magnetizations at 10 K under 5 T were determined to be $0.22\mu_B/ABO_3$ f.u., $0.61\mu_B/ABO_3$ f.u., and $0.48\mu_B/ABO_3$ f.u. for $x=0.09$, 0.15, and 0.21, respectively. The saturation magnetizations observed in these ceramics are about one order of magnitude higher than disordered perovskite compounds[3,15] and are even two times as high as single crystalline $Bi(Fe_{1/2}Cr_{1/2})O_3$ epitaxial thin films.[7]

We believe that the observed magnetic behavior is dictated by the *B*-site cation order in the ceramics. As mentioned previously, the solid solution can be expressed as a double perovskite compound $Pb[Sc_{2x/3}Fe_{(1/2-2x/3)}]$

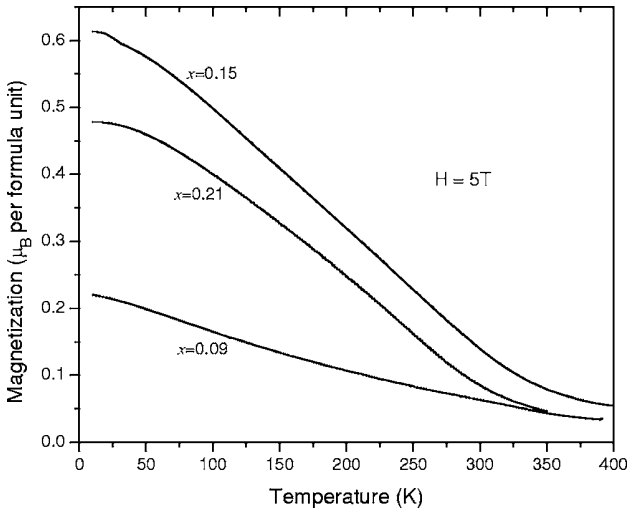

FIG. 4. Magnetization vs temperature during cooling under 5 T in the $Pb(Fe_{2(1-x)/3}Sc_{2x/3}W_{1/3})O_3$ ceramics.

$\times[Fe_{1/6}W_{1/3}]O_3$ when it is fully ordered. We denote the sublattice occupied by $[Sc_{2x/3}Fe_{(1/2-2x/3)}]$ as B', while the one occupied by $[Fe_{1/6}W_{1/3}]$ as B''. Due to the superexchange coupling between the Fe^{3+} cations, an antiferromagnetic order is developed on the magnetic moment of Fe^{3+} between the two *B*-site sublattices. Therefore, the measured magnetization depends on the partition of the Fe^{3+} cations on the two sublattices. For $0.00 \leqslant x \leqslant 0.50$, the double perovskite model $Pb[Sc_{2x/3}Fe_{(1/2-2x/3)}][Fe_{1/6}W_{1/3}]O_3$ indicates that the B' sublattice has more Fe^{3+} cations than the B'' sublattice and the difference is $(1-2x)/3$ Fe^{3+} ions/f.u. The magnetization data above T_c indicate that the magnetic moment for each Fe^{3+} in the paramagnetic state is roughly $3\mu_B$. Therefore, we estimate that in the ordered state, the saturation magnetization of our double peroskite model for the composition series will be $(1-2x)\mu_B$/f.u. for a fully ordered structure. This is a straight line with respect to x and is plotted in Fig. 5.

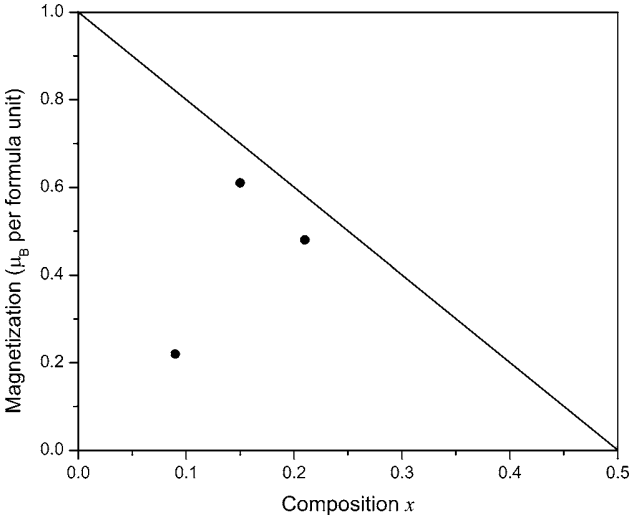

FIG. 5. Predicted linear relation between the saturation magnetization and the composition x in the $Pb(Fe_{2(1-x)/3}Sc_{2x/3}W_{1/3})O_3$ solid solution system based on the ferrimagnetic double perovskite model. The dark dots mark the measured saturation magnetizations.

The three dark dots in Fig. 5 are the measured saturation magnetization at 10 K under 5 T for the ceramics of $x=0.09$, 0.15, and 0.21, respectively. The experimental values of the saturation magnetization correspond to 27%, 87%, and 83% of the predicted values from the straight line for each composition, respectively. For the ceramics of $x=0.15$ and 0.21, it is clear that the experimental data match the ferrimagnetic double perovskite model quite well. The large discrepancy between the experimental data and the ferrimagnetic model for $x=0.09$ is due to the weak long range *B*-site cation order. As mentioned in the x-ray diffraction section, the cation ordering parameters *S* are 0.26, 0.55, and 0.81 for the ceramics of $x=0.09$, 0.15, and 0.21, respectively. It is interesting to note that the values of the chemical order parameter *S* are in good agreement with the percentage of the predicted saturation magnetization in these ceramics, especially for $x=0.09$ and $x=0.21$. Clearly there is a direct correlation between the degree of the long range cation order and the achieved saturation magnetization. The low saturation magnetization measured in the ceramic of $x=0.09$ is due to antisite occupancy of the *B*-site cations. For the ceramic of $x=0.15$, we believe that the ordering parameter *S* is under estimated due to the small size of cation ordered domains.

In summary, long range cation order is developed in ceramics of $Pb(Fe_{2(1-x)/3}Sc_{2x/3}W_{1/3})O_3$ solid solution prepared with a simple solid state reaction method. Saturated polarization versus electric field hysteresis loops were observed for all three ceramics under quasistatic electric fields. Large electrical polarizations (14.6 $\mu C/cm^2$ for $x=0.09$) were measured at 40 kV/cm at 120 K. Direct correlation between the measured saturation magnetization and the degree of *B*-site cation order is observed. Ultrahigh saturation magnetization ($0.61\mu_B/ABO_3$ f.u.) was measured in the ceramic of $x=0.15$.

This work was supported by the Short Term Innovative Research (STIR) program at the Army Research Office through Grant No. W911NF-06-1-0417. Research at Ames Laboratory (RWM) is supported by the U.S. Department of Energy, Basic Energy Sciences, under Contract No. DE-AC02-07CH11358. Three of the authors (R.W., S.A., and R.Y.) are grateful to the Thailand Research Fund.

[1] S. W. Cheong and M. Mostovoy, Nat. Mater. **6**, 13 (2007).
[2] N. A. Spaldin and M. Fiebig, Science **309**, 391 (2005).
[3] M. Fiebig, J. Phys. D **38**, R123 (2005).
[4] J. Kanamori, J. Phys. Chem. Solids **10**, 87 (1959).
[5] P. Baettig and N. A. Spaldin, Appl. Phys. Lett. **86**, 012505 (2005).
[6] P. Baettig, C. Ederer, and N. A. Spaldin, Phys. Rev. B **72**, 214105 (2005).
[7] R. Nechache, C. Harnagea, A. Pignolet, F. Normandin, T. Veres, L. P. Carignan, and D. Menard, Appl. Phys. Lett. **89**, 102902 (2006).
[8] M. R. Suchomel, C. I. Thomas, M. Allix, M. J. Rosseinsky, A. M. Fogg, and M. F. Thomas, Appl. Phys. Lett. **90**, 112909 (2007).
[9] N. Setter and L. E. Cross, J. Appl. Phys. **51**, 4356 (1980).
[10] J. Chen, H. M. Chan, and M. P. Harmer, J. Am. Ceram. Soc. **72**, 593 (1989).
[11] M. A. Akbas and P. K. Davies, J. Am. Ceram. Soc. **80**, 2933 (1997).
[12] P. Juhas, I. Grinberg, A. M. Rappe, W. Dmowski, T. Egami, and P. K. Davies, Phys. Rev. B **69**, 214101 (2004).
[13] P. M. Vilarinho and J. L. Baptista, J. Eur. Ceram. Soc. **11**, 407 (1993).
[14] L. Zhou, P. M. Vilarinho, and J. L. Baptista, J. Eur. Ceram. Soc. **18**, 1383 (1998).
[15] W. Qu, X. Tan, R. W. McCallum, D. P. Cann, and E. Ustundag, J. Phys.: Condens. Matter **18**, 8935 (2006).
[16] G. A. Smolenskii, V. A. Isupov, N. N. Krainik, and A. I. Agranovskaya, Izv. Akad. Nauk SSSR, Ser. Fiz. **25**, 1333 (1961).
[17] K. Uchino and S. Nomura, Ferroelectrics **17**, 505 (1978).

Appl. Phys. A 88, 757–761 (2007)
DOI: 10.1007/s00339-007-4064-z

Applied Physics A
Materials Science & Processing

S. WONGSAENMAI[1]
W. QU[2]
S. ANANTA[1]
R. YIMNIRUN[1]
X. TAN[2,✉]

Effect of Ba-substitution on the structure and properties of $Pb_{0.8}Ba_{0.2}[(In_{1/2}Nb_{1/2})_{1-x}Ti_x]O_3$ ceramics

[1] Department of Physics, Faculty of Science, Chiang Mai University, Chiang Mai 50200, Thailand
[2] Department of Materials Science and Engineering, Iowa State University, Ames, IA 50011, USA

Received: 29 December 2006/Accepted: 14 April 2007
Published online: 14 June 2007 •

ABSTRACT Ferroelectric ceramics with formula $Pb_{0.8}Ba_{0.2}[(In_{1/2}Nb_{1/2})_{1-x}Ti_x]O_3$ (PBINT) ($x = 0.0, 0.1, 0.2, 0.3, 0.4$ and 0.5) were prepared via a two-step solid state reaction method. It was found that ceramics with compositions in the range of $x = 0.0 \sim 0.3$ showed a pseudo-cubic structure, whereas the ceramic with $x = 0.5$ displayed a tetragonal structure. All compositions showed significant frequency dispersion in their dielectric properties. The remanent polarization P_r as well as the coercive field E_c, measured at room temperature, increases with the Ti content. The experimental results obtained in this system are summarized into a phase diagram, with the morphotropic phase boundary (MPB) located at $x = 0.4$. Compared with the $Pb[(In_{1/2}Nb_{1/2})_{1-x}Ti_x]O_3$ solid solution system, incorporating Ba in the A-site leads to a significant decrease in the dielectric maximum temperature T_{max}, a suppression of the dielectric relaxation parameter γ, and a shift of the MPB composition to a higher Ti content.

PACS 77.84.Dy; 77.80.Bh; 77.22.Ch

1 Introduction

Lead-based relaxor ferroelectric compounds have been extensively investigated because of their unique dielectric, ferroelectric and piezoelectric properties [1–3]. One of these compounds is $Pb(In_{1/2}Nb_{1/2})O_3$ (PIN), which can be prepared as crystals with different degrees of cation order [4–10]. Due to the charge and size difference between the In^{3+} (0.800 Å) and Nb^{5+} (0.64Å) [11], long range In/Nb cation order on the B-site in the ABO_3 perovskite structure can be developed by extended thermal annealing. Most importantly, the cation order was observed to have significant impact on the ferroelectric property of PIN. Disordered PIN is a relaxor ferroelectric with a pseudo-cubic structure and a broad dielectric maximum [4–7]. In contrast, ordered PIN shows an antiferroelectric behavior with an orthorhombic structure [6–8]. A sharp peak in the dielectric constant vs. temperature relation is observed around 145 °C [8]. Compared to other relaxor compounds, such as the extensively studied $Pb(Mg_{1/3}Nb_{2/3})O_3$, the high transition temperature of PIN is very attractive, offering better thermal stability in transducer applications [12].

Synthesis of phase pure PIN ceramic with the solid state reaction method has been a challenge due to its small tolerance factor ($t = 0.964$) [13–15]. The presence of a minor amount of cubic pyrochlore phases is detrimental to the dielectric and ferroelectric properties. The wolframite method, as used by Grove [13] for the preparation of perovskite PIN ceramic, is not effective in suppressing the pyrochlore phase formation. The addition of excess In_2O_3 was found to be capable of improving the perovskite phase yield [13, 14]. The perovskite phase can also be stabilized with the solid solution method, where the B-site ($In_{1/2}Nb_{1/2}$) is substituted with Ti to form the $Pb(In_{1/2}Nb_{1/2})O_3$-$PbTiO_3$ (PIN-PT) solid solution [16–20] or the A-site Pb is substituted with Ba to form the $Pb(In_{1/2}Nb_{1/2})O_3$-$Ba(In_{1/2}Nb_{1/2})O_3$ (PIN-BIN) solid solution [21]. It is interesting to notice that In/Nb cation order is often observed in PIN single crystals but not polycrystalline ceramics [4–10], while complete cation order is present in the compound of $Ba(In_{1/2}Nb_{1/2})O_3$ [22–24]. In addition, $BaTiO_3$ is also known to be effective at stabilizing the perovskite phase for compounds with small tolerance factors [25].

The present study was initially intended to introduce long range In/Nb cation order in PIN ceramics by forming solid solutions with BIN and, at the same time, to stabilize the perovskite phase. Alternatively, Ti substitution at B-site is known to disrupt the long range cation order [26]. For that reason, the degree of cation order in PIN ceramics may be manipulated by controlling the amount of Ba and Ti addition. Therefore, the ultimate goal is to investigate the effect of the B-site cation order on the electric dipole order in the ceramics. In addition, the role of Ba substitution may be elucidated by comparing the data with our recent work on the PIN-PT solid solution [20].

2 Experimental

$Pb_{0.8}Ba_{0.2}[(In_{1/2}Nb_{1/2})_{1-x}Ti_x]O_3$ ($x = 0.0, 0.1, 0.2, 0.3, 0.4$ and 0.5, abbreviated as PBINT hereafter) powders were synthesized by a two-step solid state reaction method. The wolframite $InNbO_4$ was first prepared from oxide powders of Nb_2O_5 and In_2O_3. Mixed powders were milled with a vibratory mill for 6 h in isopropanyl alcohol. After drying, the mixture was calcined at 1100 °C for 2 h to obtain the intermediate precursor $InNbO_4$. The wolframite precursor was

✉ Fax: +1-515-2945444, E-mail: xtan@iastate.edu

then mixed with appropriate amounts of PbO, $BaCO_3$, and TiO_2. Excess amounts of PbO (2 wt. %) and In_2O_3 (2 wt. %) were added at this stage. The mixture was milled again for 6 h. After drying, the mixture was calcined in air at temperatures between 1050 and 1250 °C with dwell time of 2 hours and a heating/cooling rate of 20 °C/min inside closed alumina crucibles. Pellets 12.7 mm in diameter and ∼ 1 mm thick were pressed with 1 wt. % PVA binder. The pressed pellets were sintered in a double crucible configuration at temperatures 1300 °C (for $x = 0.0$) and 1250 °C (for $x = 0.1 \sim 0.5$) for 2 h with a heating/cooling rate of 5 °C/min. To minimize PbO loss, the pellets were buried in protective powders of the same composition.

The crystal structure of the sintered ceramics and the degree of cation order was analyzed with X-ray diffraction (XRD) at a step size of 0.05° and a duration time of 1 s. The grain morphology of the ceramics was examined with scanning electron microscopy (SEM). The ferroelectric domain structure was observed with transmission electron microscopy (TEM). The density of ceramics was determined with the Archimedes method. The dielectric properties were measured with an LCR meter (HP-4284A, Hewlett-Packard) in conjunction with an environmental chamber (9023, Delta Design). A heating rate of 2 °C/min and frequencies of 100, 1000 and 10 000 Hz were used during measurement. Ferroelectric hysteresis loops were evaluated at ±30 kV/cm at temperatures of 25, −20, −50 and −80 °C with a standardized ferroelectric test system (RT-66A, Radiant Technologies).

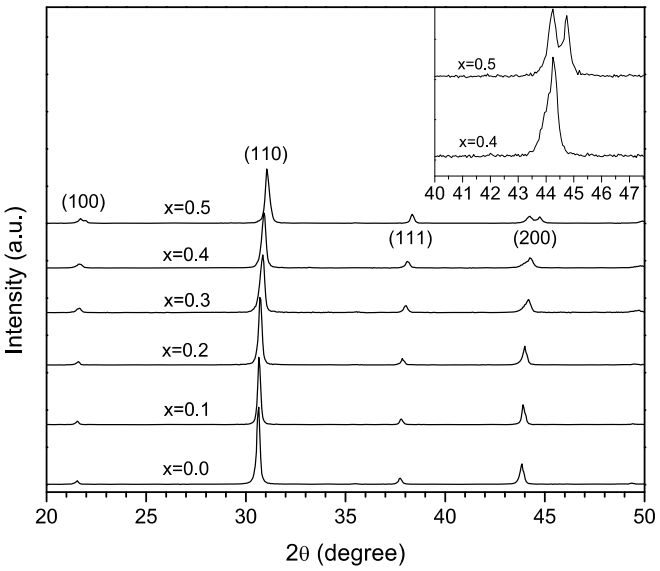

FIGURE 1 X-ray diffraction spectra of the $Pb_{0.8}Ba_{0.2}[(In_{1/2}Nb_{1/2})_{1-x}Ti_x]O_3$ ceramics. The *inset* shows the close view of the (200) peak in ceramics of $x = 0.4$ and 0.5

3 Results and discussion

3.1 *Structure of the PBINT ceramics*

Figure 1 shows the X-ray diffraction pattern of the $Pb_{0.8}Ba_{0.2}[(In_{1/2}Nb_{1/2})_{1-x}Ti_x]O_3$ ceramics. It is evident that the as-sintered ceramics are in pure perovskite phase within the detection limit of X-ray powder diffraction, indicating that the addition of Ba and Ti stabilizes the perovskite structure. The splitting of the (200) peak in the composition of $x = 0.5$ indicates a tetragonal symmetry. For compositions of $x = 0.0$ through 0.3, a pseudo-cubic structure was observed. For the ceramic with $x = 0.4$, a broad (100) peak and a distorted (200) peak were noticed. A closer view of the (200) peak for the ceramics with $x = 0.4$ and 0.5 is shown in the inset. It, therefore, appears that the morphotropic phase boundary (MPB) which separates the pseudo-cubic phase from the tetragonal phase in this system is located around $x = 0.4$. Increase in the Ti content leads not only to a structural transition from pseudo-cubic to tetragonal, but also to a decrease in the lattice parameters and the unit cell volume. The decrease in lattice parameter is expected since the radius of Ti^{4+} (0.605 Å) is much smaller than the average radius 0.72 Å for $(1/2In^{3+} + 1/2Nb^{5+})$ [11]. These observations are similar to those of our recent work on the PIN-PT ceramics [20]. It is interesting to notice that the substitution of 20 at. % Pb with Ba on the A-site pushes the MPB composition from $x = 0.3$ to $x = 0.4$.

The X-ray diffraction pattern was collected with 2θ starting from 15° in order to detect a possible superlattice peak $(\frac{1}{2}\ \frac{1}{2}\ \frac{1}{2})$ between 18.5° and 19.0° (spectra with $2\theta < 20°$ were not shown in Fig. 1). This extra peak is the signature of the B-site In/Nb 1 : 1 order. Unfortunately, the $(\frac{1}{2}\ \frac{1}{2}\ \frac{1}{2})$ peak is absent for all as-sintered ceramics. Since Ti is known to disrupt B-site cation order in complex perovskite [26], additional attempts were made to the $Pb_{0.8}Ba_{0.2}(In_{1/2}Nb_{1/2})O_3$ composition (with no Ti addition). Another pellet of this composition was sintered at 1250 °C for 2 h (a lower temperature was used

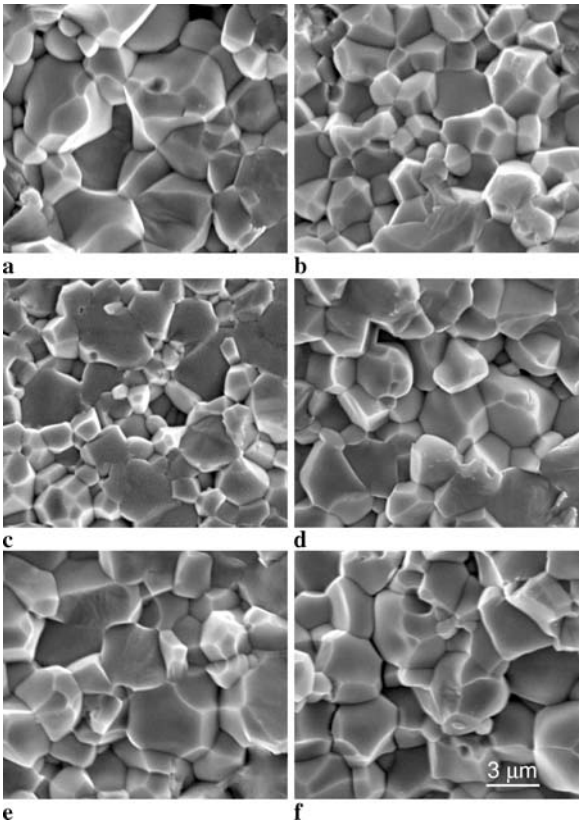

FIGURE 2 SEM micrographs of the $Pb_{0.8}Ba_{0.2}[(In_{1/2}Nb_{1/2})_{1-x}Ti_x]O_3$ ceramics. (**a**) $x = 0.0$, (**b**) $x = 0.1$, (**c**) $x = 0.2$, (**d**) $x = 0.3$, (**e**) $x = 0.4$, (**f**) $x = 0.5$

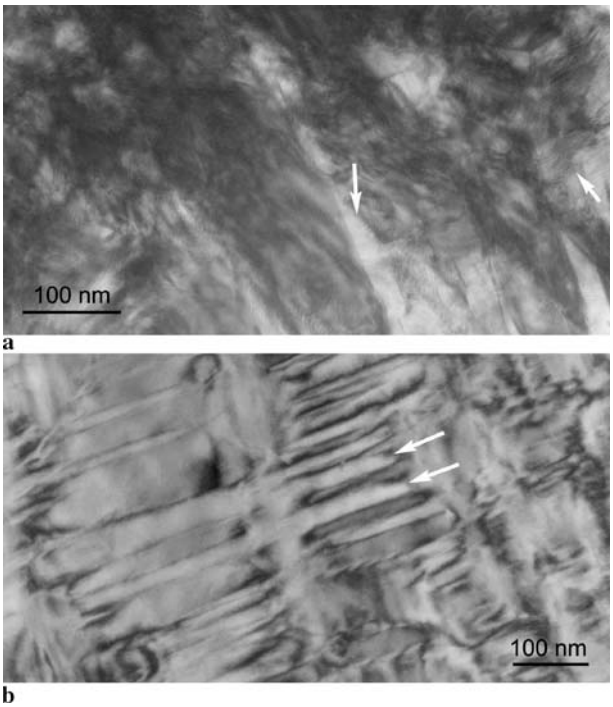

FIGURE 3 TEM bright field micrographs of the $Pb_{0.8}Ba_{0.2}[(In_{1/2}Nb_{1/2})_{1-x}Ti_x]O_3$ ceramics with [110] zone axis. (**a**) $x = 0.3$. The bright *arrow* in the right points at the disrupted domains while the one in the middle points at a large ferroelectric domain. (**b**) $x = 0.5$. The two bright *arrows* point at two parallel 90° ferroelectric domains

hoping that it was below the order/disorder transition temperature), cooled at a slow rate of 12 °C/h to 830 °C, followed by furnace cool to room temperature. Slow scan (step size 0.05, duration time 2 s) X-ray diffraction was performed for 2θ in the range of 15° to 20°. Again, no superlattice $(\frac{1}{2}\frac{1}{2}\frac{1}{2})$ peak was detected, indicating that long range In/Nb cation order was not developed under the present processing conditions. The absence of long range chemical order, even with the presence of 20 at. % Ba on the A-site, was further confirmed by TEM observations. We speculate that the absence of cation order may be attributed to the fact that In/Nb order is hard to develop in PIN polycrystalline ceramics [4–10]. The results indicate that Ba substitution is effective in stabilizing the perovskite phase but not in enhancing the In/Nb cation order.

The grain morphology of the sintered ceramics was examined by SEM and is shown in Fig. 2. Dense microstructure with uniform grains is evident for all ceramics. The average grain size, determined with the linear intercept method, and the relative density are listed in Table 1. It is found that all the ceramics have a grain size of $2 \sim 3$ μm and a relative density above 90%. The ceramic with $x = 0.0$ (Fig. 2a) shows large grain size and high relative density as a result of a higher sintering temperature (1300 °C). For ceramics with $x = 0.1$ through 0.5, which were sintered at 1250 °C, increase in the Ti content substituting for $(In_{1/2}Nb_{1/2})$ on the B-site leads to an increase in both grain size and relative density, indicating an increasing sinterability of the ceramics.

Composition (x)	Average grain size (μm)	Relative density (%)
0.0	3.5	97
0.1	2.3	90
0.2	2.4	93
0.3	2.5	94
0.4	3.0	97
0.5	3.2	99

TABLE 1 Average grain size and relative density of the $Pb_{0.8}Ba_{0.2}[(In_{1/2}Nb_{1/2})_{1-x}Ti_x]O_3$ ceramics

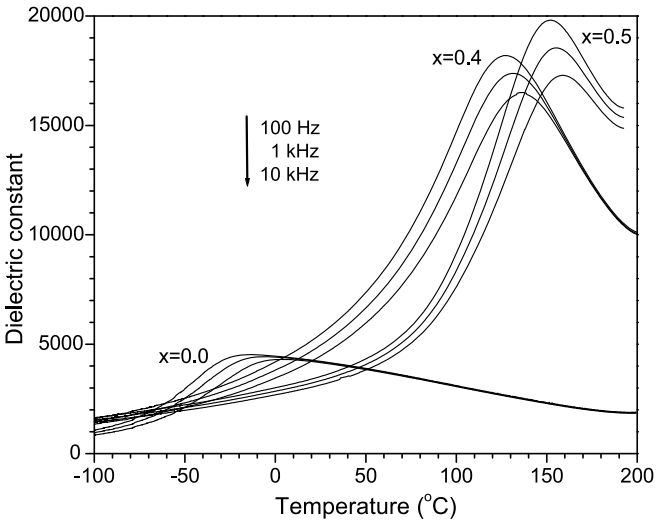

FIGURE 4 The frequency dispersion of the dielectric constant of the $Pb_{0.8}Ba_{0.2}[(In_{1/2}Nb_{1/2})_{1-x}Ti_x]O_3$ ceramics with $x = 0.0$, 0.4, and 0.5

The subgrain structure of the ceramics was further analyzed with TEM (Fig. 3). Selected area electron diffraction did not show any $(\frac{1}{2}\frac{1}{2}\frac{1}{2})$-type superlattice spots, even in the slowly cooled $Pb_{0.8}Ba_{0.2}(In_{1/2}Nb_{1/2})O_3$ ceramic. The absence of In/Nb cation order revealed by X-ray diffraction was, therefore, further confirmed. The ferroelectric domain structure shows dramatic change over the composition range. For the $Pb_{0.8}Ba_{0.2}(In_{1/2}Nb_{1/2})O_3$ ceramic, a faint contrast was observed in the bright field image for the polar nanodomains (not shown). For the ceramic with $x = 0.3$, a mixture of large ferroelectric domains (a couple of hundred nanometers) and disrupted domains with complicated contrast were observed (Fig. 3a). For the ceramic with $x = 0.5$, large regular lamellar ferroelectric domains were found (Fig. 3b). They have similar morphologies as those in other tetragonal ferroelectric crystals [27] and are, therefore, ferroelectric 90° domains.

3.2 *Dielectric and ferroelectric properties*

The temperature dependence of the dielectric constant in the PBINT system was measured and is shown in Fig. 4. All of the compositions show a broad peak at T_{max} and very low dielectric loss. The properties measured at 1 kHz are listed in Table 2. It is found that T_{max} generally increases with increasing Ti content. The maximum dielectric permittivity ε_{max} also follows this trend. Compared with our recent work on PIN-PT ceramics [20], it is evident that substituting Pb with Ba leads to a significant decrease in T_{max}. For example, T_{max} is 155 °C for $Pb_{0.8}Ba_{0.2}[(In_{1/2}Nb_{1/2})_{0.5}Ti_{0.5}]O_3$ while 375 °C for $Pb[(In_{1/2}Nb_{1/2})_{0.5}Ti_{0.5}]O_3$. This indicates that Ba on the A-site is much weaker than Pb for ferroelectricity.

Figure 4 also shows a considerable frequency dispersion in the dielectric behavior. The results are quite similar to those in PIN-PT ceramics [20]. The relative permittivity ε_r vs. temperature T in ferroelectrics generally obeys the relation

$$\frac{1}{\varepsilon_r} - \frac{1}{\varepsilon_{max}} = B(T - T_{max})^{\gamma} \quad (1)$$

at temperatures above the dielectric peak [28–30]. Equation (1) corresponds to the Curie–Weiss law observed in normal ferroelectrics such as $BaTiO_3$ when $\gamma = 1$. Equation (1) becomes the quadratic relationship suggested for ideal relaxor ferroelectrics when γ equals to 2 [1]. Therefore, the parameter γ has been used as an indicator of the degree of dielectric relaxation. For all of the ceramics studied in this work, fitting the 1 kHz dielectric constant data leads to the quantitative variation of γ with composition, as listed in Table 2. Compared to PIN-PT ceramics [20], the PBINT ceramics show a lower dielectric relaxation parameter at the same Ti content (e. g., 1.52 vs. 1.62 at $x = 0.5$).

The ferroelectric hysteresis loops of the PBINT ceramics were measured at a series of temperature at and below room temperature. Figure 5 shows the observed P vs. E loops at 25 °C and −80 °C. It is found that the hysteresis loops open up as Ti content increases at both temperatures. The ceramics with $x = 0.4$ and 0.5 show well-defined hysteresis loops at both temperatures, indicating the presence of a normal ferroelectric state with long range polar order. For the ceramic with the composition of $x = 0.3$, a slim loop was observed at room temperature while a fairly square loop was found at −80 °C. For the ceramics with $x = 0.0$ through 0.2, nonlinear curves were observed at 25 °C, while slim loops were observed at the low temperature. Measurements of the remanent polarization (P_r) and coercive field (E_c) from the hysteresis loops indicate that increasing Ti content from $x = 0.3$ to 0.4 leads to a significant jump in P_r at both temperatures. In contrast, this composition change shows almost no increase in E_c at room temperature. Therefore, the ceramic with $x = 0.4$ exhibits a high P_r and a moderate E_c, indicating that it is the composition with the best ferroelectric properties in this system. This result also suggests that $x = 0.4$ is the morphotropic phase boundary composition, consistent with the X-ray diffraction analysis.

The monotonic increase in both P_r and E_c with Ti content at room temperature in the present PBINT system is in sharp contrast to that in the PIN-PT ceramics. The P_r at room temperature in the PIN-PT ceramics was observed to reach a peak at the MPB composition of $x = 0.3$ and then decrease sharply with further increase in Ti content in the tetragonal phase [20].

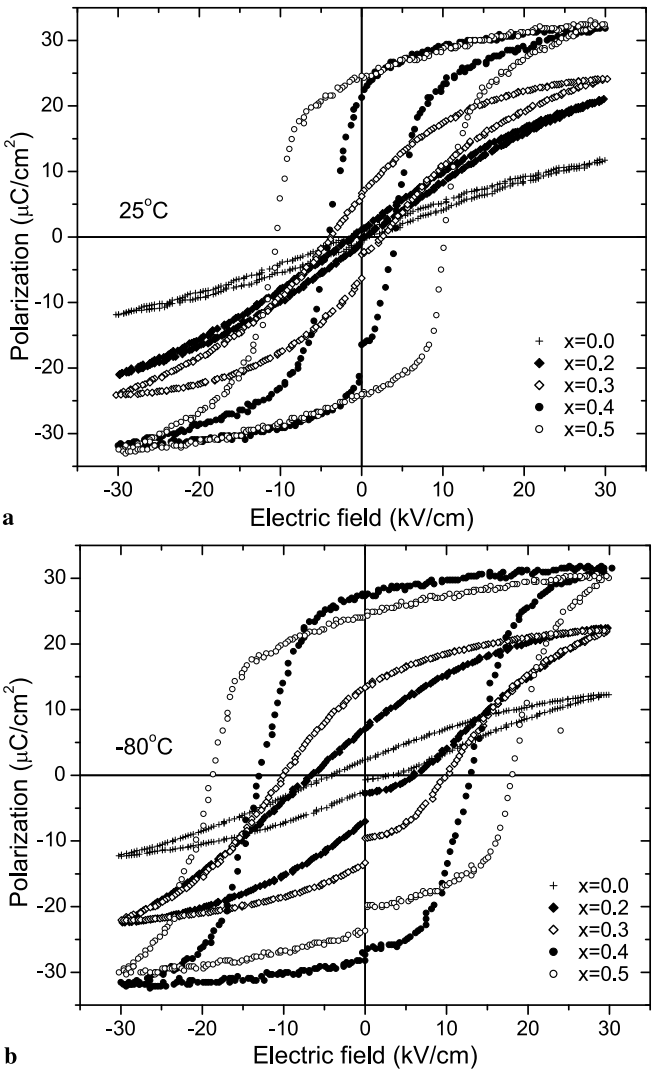

FIGURE 5 The polarization vs. electric field hysteresis loops measured from the $Pb_{0.8}Ba_{0.2}[(In_{1/2}Nb_{1/2})_{1-x}Ti_x]O_3$ ceramics at 4 Hz. (**a**) 25 °C, (**b**) −80 °C

Therefore, substitution of Pb with Ba improves the room temperature ferroelectric properties of PBINT.

All of these structure and property changes in PBINT from the PIN-PT can be traced back to the Ba-substitution. The $6s^2$ lone pair electrons on Pb cations were shown to be essential for strong ferroelectricity and the tetragonal distortion [31]. Substituting Pb on the A-site with Ba weakens the ferroelectric dipole order and the tetragonal distortion tendency. As a consequence, a lower T_{max} and a higher Ti content at MPB

Composition (x)	T_{max} (°C)	Dielectric properties at T_{max}		Dielectric properties at 25 celsius		Relaxation parameter (γ)
		ε_{max}	$\tan\delta$	ε_r	$\tan\delta$	
0.0	−5	4450	0.018	4189	0.005	1.83
0.1	−14	4820	0.018	4463	0.021	1.71
0.2	26	7591	0.029	7587	0.030	1.65
0.3	77	10177	0.032	5326	0.076	1.63
0.4	131	17376	0.036	4953	0.068	1.59
0.5	155	18541	0.049	3333	0.039	1.52

TABLE 2 Dielectric properties of the $Pb_{0.8}Ba_{0.2}[(In_{1/2}Nb_{1/2})_{1-x}Ti_x]O_3$ ceramics at 1 kHz

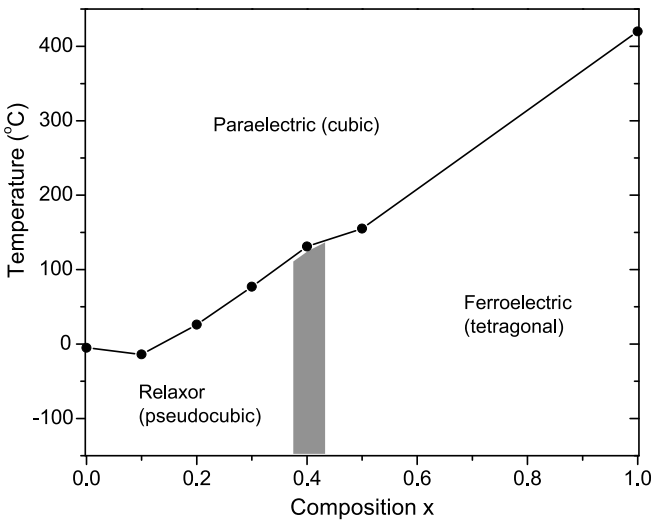

FIGURE 6 The proposed phase diagram for the $Pb_{0.8}Ba_{0.2}[(In_{1/2}Nb_{1/2})_{1-x}Ti_x]O_3$ system based on the structure analysis and properties measurement

were observed. Because of the low T_{max} in the PBINT ceramics, even at $x = 0.5$ (155 °C), the electrical dipole order has not yet frozen at room temperature, leading to a high switchable polarization. The suppression of the dielectric relaxation parameter γ in PBINT seems to be caused by Ba-substitution as well. $BaTiO_3$ appears to have the lowest γ among ferroelectric perovskite oxides [29].

The structure and properties of the $Pb_{0.8}Ba_{0.2}[(In_{1/2}Nb_{1/2})_{1-x}Ti_x]O_3$ system discussed above can be summarized into a phase diagram as shown in Fig. 6. The Curie point for $Pb_{0.8}Ba_{0.2}TiO_3$ ($x = 1.0$) is determined by assuming the solid solution follows the rule of mixture [32]:

$$T_c(°C) = 0.8 \times 490 + 0.2 \times 130\,. \quad (2)$$

Three phases are identified: the cubic paraelectric, the pseudocubic relaxor ferroelectric and the tetragonal normal ferroelectric. The cubic paraelectric phase is inferred from the general phase transition trend in the perovskite family of ferroelectric oxides [32]. The morphotropic phase boundary is denoted by the shaded area around $x = 0.4$.

4 Conclusion

Complex perovskite ceramics $Pb_{0.8}Ba_{0.2}[(In_{1/2}Nb_{1/2})_{1-x}Ti_x]O_3$ ($x = 0.0, 0.1, 0.2, 0.3, 0.4$ and 0.5) were successfully prepared via a two-step solid state reaction method. The failure of the development of long range cation order in this system indicates that Ba-substitution is effective in stabilizing the perovskite phase but not in enhancing the cation order. Compared to the PIN-PT solid solution system, replacing the Pb on the A-site with Ba leads to dramatic changes in the structure and properties. The MPB composition shifts from $x = 0.3$ for PIN-PT to $x = 0.4$ for PBINT. The T_{max} is significantly lower in PBINT than for the PIN-PT with the same Ti content (185 ~ 220 °C lower for $x = 0.1$ through 0.5). There is also a slight suppression of the dielectric relaxation parameter γ in the PBINT system. The remanent polarization P_r measured at room temperature shows a monotonic increase with Ti content in the PBINT system. While for the PIN-PT solid solution, P_r peaks at the MPB composition and then sharply decreases with further increase in Ti content in the tetragonal phase. All of these changes can be explained based on the fact that Ba cations on the A-site are weaker than Pb cations for ferroelectricity.

ACKNOWLEDGEMENTS The authors are grateful to the Thailand Research Fund (TRF), the Commission on Higher Education (CHE) and the Graduate School of Chiang Mai University for financial support.

REFERENCES

1 G.A. Smolensky, J. Phys. Soc. Japan. **28**, 26 (1970)
2 L.E. Cross, Ferroelectrics **76**, 241 (1987)
3 T.R. Shrout, A. Halliyal, Am. Ceram. Soc. Bull. **66**, 704 (1987)
4 P. Groves, J. Phys. C Solid State Phys. **19**, 5103 (1986)
5 N. Yasuda, S. Shibuya, J. Phys.: Condens. Matter **1**, 10613 (1989)
6 A. Kania, K. Roleder, G.E. Kugel, M. Hafid, Ferroelectrics **135**, 75 (1992)
7 K. Nomura, H. Terauchi, N. Yasuda, H. Ohwa, J. Kor. Phys. Soc. **32**, S989 (1998)
8 N. Yasuda, H. Ohwa, J. Ohhashi, K. Nomura, H. Terauchi, M. Iwata, Y. Ishibashi, J. Kor. Phys. Soc. **32**, S996 (1998)
9 C.A. Randall, D.J. Barber, P. Groves, R.W. Whatmore, J. Mater. Sci. **23**, 3678 (1988)
10 C. Elissalde, F. Weill, J. Ravez, Mater. Sci. Eng. B **25**, 85 (1994)
11 R.D. Shannon, Acta Cryst. **A32**, 751 (1976)
12 Y. Guo, H. Luo, T. He, Z. Yin, Solid State Commun. **123**, 417 (2002)
13 P. Groves, Ferroelectrics **65**, 67 (1985)
14 E.F. Alberta, A.S. Bhalla, Mater. Lett. **29**, 127 (1996)
15 F.G. Jones, C.A. Randall, S.J. Jang, T.R. Shrout, Ferroelectr. Lett. **12**, 55 (1990)
16 U. Kodama, M. Osada, O. Kumon, T. Nishimoto, Ceram. Bull. **48**, 1122 (1969)
17 E.F. Alberta, A.S. Bhalla, J. Kor. Phys. Soc. **32**, S1265 (1998)
18 N. Yasuda, M. Sakaguchi, Y. Itoh, H. Ohwa, Y. Yamashita, M. Iwata, Y. Ishibashi, Japan. J. Appl. Phys. **42**, 6205 (2003)
19 C. Augier, M. Phamthi, H. Dammak, P. Gaucher, J. Eur. Ceram. Soc. **25**, 2429 (2005)
20 S. Wongsaenmai, X. Tan, S. Ananta, R. Yimnirun, J. Alloys Compd., in press (2007)
21 M. Tanaka, M. Sadamoto, J. Phys.: Condens. Matter **5**, L689 (1993)
22 P. Groves, Phase Trans. **5**, 197 (1985)
23 B.P. Burton, E. Cockayne, Phys. Rev. B **60**, R12542 (1999)
24 V. Ting, Y. Liu, R.L. Withers, L. Noren, M. James, J.D. Fitzgerald, J. Solid State Chem. **179**, 551 (2006)
25 A. Halliyal, U. Kumar, R.E. Newnham, L.E. Cross, Am. Ceram. Soc. Bull. **66**, 671 (1987)
26 P. Juhas, I. Grinberg, A.M. Rappe, W. Dmowski, T. Egami, P.K. Davies, Phys. Rev. B **69**, 214101 (2004)
27 Y.H. Hu, H.M. Chan, X.W. Zhang, M.P. Harmer, J. Am. Ceram. Soc. **69**, 594 (1986)
28 H.T. Martirena, J.C. Burfoot, Ferroelectrics **7**, 151 (1974)
29 K. Uchino, S. Nomura, Ferroelectr. Lett. **44**, 55 (1982)
30 N. Vittayakorn, G. Rujijanagul, X. Tan, M.A. Marqardt, D.P. Cann, J. Appl. Phys. **96**, 5103 (2004)
31 R.E. Cohen, Nature **358**, 136 (1992)
32 A.J. Moulson, J.M. Herbert, *Electroceramics: Materials, Properties, Applications*, 2nd edn. (John Wiley & Sons, New York, 2003)

Available online at www.sciencedirect.com
ScienceDirect
Materials Letters 61 (2007) 4466–4470
materials letters
www.elsevier.com/locate/matlet

Effect of calcination conditions on phase formation and particle size of lead nickel niobate powders synthesized by using $Ni_4Nb_2O_9$ precursor

O. Khamman, R. Yimnirun, S. Ananta *

Department of Physics, Faculty of Science, Chiang Mai University, Chiang Mai 50200, Thailand

Received 24 November 2006; accepted 8 February 2007
Available online 16 February 2007

Abstract

An approach to synthesize lead nickel niobate, $Pb(Ni_{1/3}Nb_{2/3})O_3$ or PNN, powders with a modified two-stage mixed oxide synthetic route has been developed. Novel intermediate phase of nickel diniobate ($Ni_4Nb_2O_9$) was employed as a B-site precursor, with the formation of the PNN phase investigated as a function of calcination conditions by TG-DTA and XRD techniques. Morphology, particle size and chemical composition have been determined via a combination of SEM and EDX techniques. It has been found that the unreacted PbO and $Pb_{1.45}Nb_2O_{6.26}$ phases tend to form together with PNN, depending on calcination conditions. It is seen that optimization of calcination conditions can lead to a 100% yield of PNN in a cubic phase.

Keywords: Lead nickel niobate; Nickel diniobate; Perovskite; Calcination; Powders-solid-state reaction

1. Introduction

Lead nickel niobate, $Pb(Ni_{1/3}Nb_{2/3})O_3$ or PNN, one of the important compounds in the family of perovskite relaxor ferroelectrics, has been known to possess excellent dielectric broadening and electrostrictive properties [1,2]. PNN-based ceramics have been extensively investigated for their applications in multilayer capacitors, electrostrictive actuator, and electromechanical transducer devices [1–3]. However, the performance of these materials is often limited by the coexistence of a low permittivity pyrochlore phase with the perovskite phase [2,4]. Thus, there has been a great deal of interest in the preparation of single-phase PNN powders as well as in the sintering and electrical properties of PNN-based ceramics [3–7].

The mixed oxide synthetic route is probably one of the most fundamental, practical routine methods which has been used, developed and modified in both scientific research and industrial mass production for many years [5–7]. In general, PNN powders synthesized by a mixed oxide method have spatial fluctuations in their compositions. The extent of the fluctuation depends on the characteristics of the starting powders as well as on the processing schedule. Similar problem of pyrochlore formation has been encountered in the preparation of lead magnesium niobate (PMN) powders, where the use of the B-site precursor $MgNb_2O_6$ was proposed by Swartz and Shrout [8] as an effective way of producing PMN powder in high yield. The reaction sequence through which PNN is formed by solid-state reaction, where the use of the B-site precursor $NiNb_2O_6$ has been proposed in analogous to the fabrication of PMN, has been widely investigated by many researchers but with varying conclusions [5–10]. Whereas some workers have been prompted to investigate synthetic route different from the mixed oxide approach, e.g. solution combustion [11], co-precipitation [12], and hydrothermal [13]. The overall aim of the work described here is to refine the two-stage mixed oxide method further. Since, to date, the potential of the $Ni_4Nb_2O_9$ [14,15] as a key precursor for the preparation of PNN has not yet been reported. Moreover, its effect on the formation of perovskite PNN phase under various calcination conditions is very interesting and nonexistent in the literature. Thus, in this work, an attempt has been made to synthesize the lead nickel niobate powders via a rapid vibro-milling technique by employing a novel intermediate phase of nickel diniobate

* Corresponding author. Tel.: +66 53 943367; fax: +66 53 943445.
E-mail address: Suponananta@yahoo.com (S. Ananta).

0167-577X/$ - see front matter © 2007 Elsevier B.V. All rights reserved.
doi:10.1016/j.matlet.2007.02.019

($Ni_4Nb_2O_9$) as a key B-site precursor. The phase formation and morphology of the powders calcined at various conditions will be studied and discussed.

2. Experimental procedure

The starting materials were commercially available lead oxide, PbO (JCPDS file number 77–1971), nickel oxide, NiO (JCPDS file number 73–1519) and niobium oxide, Nb_2O_5 (JCPDS file number 30–0873) (Aldrich, 99% purity). These three oxide powders exhibited an average particle size in the range of 3.0–5.0 μm. The following reaction sequences are proposed for the formation of PNN:

$$4NiO(s) + Nb_2O_5(s) \rightarrow Ni_4Nb_2O_9(s) \quad (1)$$

$$12PbO(s) + 3Nb_2O_5(s) + Ni_4Nb_2O_9(s) \rightarrow 12Pb(Ni_{1/3}Nb_{2/3})O_3(s) \quad (2)$$

First, an intermediate phase of $Ni_4Nb_2O_9$ was prepared from the reaction between NiO and Nb_2O_5 at 1250 °C for 0.5 h, with heating/cooling rates of 30 °C/min applied, as reported earlier [15]. $Pb(Ni_{1/3}Nb_{2/3})O_3$ was then synthesized by the solid-state reaction of thoroughly ground mixtures of PbO, Nb_2O_5 and $Ni_4Nb_2O_9$ powders that were milled in the required stoichiometric ratio. Powder-processing was carried out in a manner similar to that employed in the preparation of other materials, as described previously [16–18]. A vibratory laboratory mill (McCrone Micronizing Mill) was carried out for 30 min with corundum cylindrical media in isopropyl alcohol (IPA). After drying at 120 °C for 2 h, the reaction of the uncalcined powders taking place during heat treatment was investigated by themogravimetric and differential thermal analysis (TG-DTA, Shimadzu), using a heating rate of 10 °C/min in air from room temperature up to 1100 °C. Based on the TG-DTA results, the mixture was calcined in air at various conditions in closed alumina crucible, in order to investigate the formation of lead nickel niobate.

All powders were subsequently examined by room temperature X-ray diffraction (XRD; Siemens-D500 diffractometer), using Ni-filtered CuK_α radiation to identify the phases formed and optimum calcination conditions for the formation of $Pb(Ni_{1/3}Nb_{2/3})O_3$ powders. Powder morphologies and particle sizes were directly imaged, using scanning electron microscopy (SEM; JEOL JSM-840A). EDX spectra were quantified with the virtual standard peaks supplied with the Oxford Instrument eXL software.

3. Results and discussion

The TG-DTA simultaneous analysis of a powder mixed in the stoichiometric proportion of $Pb(Ni_{1/3}Nb_{2/3})O_3$ is displayed in Fig. 1. The TG curve shows three distinct weight losses, i.e. ~25–150 °C,.450–700 °C and 750–1000 °C. In the temperature range from room temperature to ~150 °C, both exothermic and endothermic peaks are observed in the DTA curve, in consistent with the first weight loss. These observations can be attributed to the decomposition of the organic species (i.e. polyethylene milling jar, rubber gloves, skin, etc.) from the milling process [16–18]. Corresponding to the second fall in specimen weight, by increasing the temperature up to ~700 °C, the solid-state reaction occurred between PbO and $NiNb_2O_6$ [4–7]. The broad exothermic characteristics in the

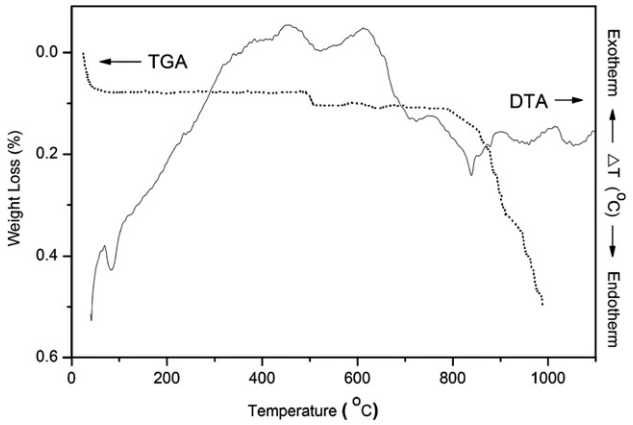

Fig. 1. TG-DTA curves for the mixture of $PbO–Nb_2O_5–Ni_4Nb_2O_9$ powder.

DTA curve represent that reaction, which has maxima at ~450 and 600 °C. Above 700 °C, the DTA curve shows that there are other small peaks at ~750, 900 and 1025 °C, however, it is to be noted that there is no obvious interpretation of these peaks. This is supported by a large fall in sample weight over the same temperature range. These data were used to define the range of calcination temperatures for XRD investigation to between 550 and 1150 °C.

To further study the phase development with increasing calcination temperature in the powders, they were calcined for 2 h in air at various temperatures, up to 1150 °C, followed by phase analysis using XRD. As shown in Fig. 2, for the uncalcined powders and the powders calcined at 550 °C, only X-ray peaks of precursors PbO (●), Nb_2O_5 (o) and $Ni_4Nb_2O_9$ (+), which could be matched with JCPDS file numbers 77–1971 [19], 30–0873 [20] and 46–0525 [21], respectively, are present, indicating that no reaction had yet been triggered during the milling or low firing processes. As the temperature increased to 600 °C, the intensity of the precursor phases of Nb_2O_5 and $Ni_4Nb_2O_9$ has been found to completely disappear, and crystalline $Pb(Ni_{1/3}Nb_{2/3})O_3$ (▼) started to appear, accompanying with PbO and $Pb_{1.45}Nb_2O_{6.26}$ as separated phases in the powder. This observation agrees well with those derived from the TG-DTA results. For the present work, there are no significant differences between the powders calcined at temperatures ranging from 600 to 800 °C. Further increase of the calcination temperature to 800 °C does not result in very much increase in the amount of $Pb(Ni_{1/3}Nb_{2/3})O_3$, whereas PbO and $Pb_{1.45}Nb_2O_{6.26}$ remain unchanged. This $Pb_{1.45}Nb_2O_{6.26}$ phase was indexable according to a cubic pyrochlore structure with lattice parameters a=1056 pm, space group *Fd3m* (no. 227), in consistent with JCPDS file numbers 84–1731 [22].

Upon calcination at 900 °C, the desired $Pb(Ni_{1/3}Nb_{2/3})O_3$ phase becomes the predominant phase and is the only detectable phase in the powders, after calcination at 1050 °C, consistent with the TG-DTA results. This $Pb(Ni_{1/3}Nb_{2/3})O_3$ phase was indexable according to a cubic perovskite structure with lattice parameters a=403 pm, space group *Pm3m* (no. 221), in consistent with JCPDS file numbers 34–0103 [23] and literature [7,13]. However, for the present study, it can be seen that at the temperature range of 1100–1150 °C, some peaks of the pyrochlore $Pb_{1.45}Nb_2O_{6.26}$ phase reappear, mixing with the major phase of $Pb(Ni_{1/3}Nb_{2/3})O_3$. This could be attributed mainly to the PbO volatilization, leading to the decomposition of the perovskite phase to the pyrochlore phase, in agreement with the TG-DTA observations at the same temperature range and also the literature [7].

Apart from the calcination temperature, the effect of dwell time was also found to be quite significant. From Fig. 3, it can be seen that the single-phase of $Pb(Ni_{1/3}Nb_{2/3})O_3$ (yield of 100% within the limitations of the XRD technique) was found to be possible in powders calcined at 1050 °C with dwell time of 0.5 h or more (Fig. 3(d,e)) and 1000 °C for at least 5 h (Fig. 3(c)). The observation that the dwell time effect may also play an important role in obtaining a single-phase perovskite product is also consistent with other similar systems [16–18]. In earlier works [3,7,9], long heat treatments at ~1000–1200 °C for at least 4 h were proposed for the formation of $Pb(Ni_{1/3}Nb_{2/3})O_3$ by a mixed oxide synthetic route with columbite $NiNb_2O_6$ precursor, although no details on phase formation

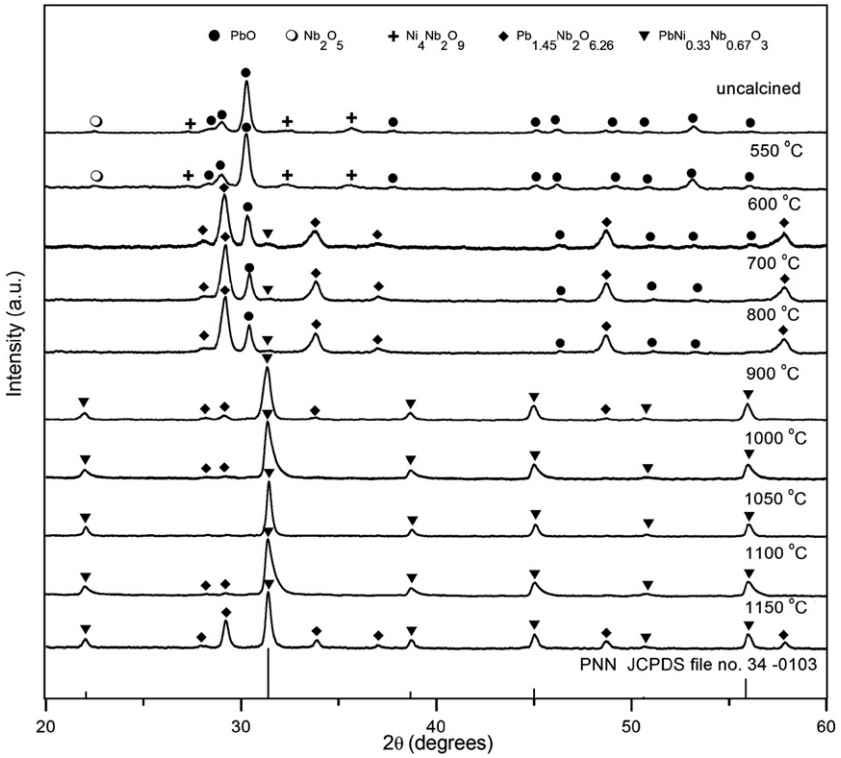

Fig. 2. XRD patterns of PNN powders calcined at various temperatures for 2 h with heating/cooling rates of 10 °C/min.

were provided. However, in the present study where corundum $Ni_4Nb_2O_9$ was employed as key precursor, it was found that there are no significant differences between the powders calcined at 1050 °C with dwell time of 0.5–2 h, as shown in Fig. 3. This observation could be attributed to the effectiveness of $Ni_4Nb_2O_9$ precursor, vibro-milling and a carefully optimized reaction. Most importantly, this study suggests that a rapid vibro-milling method can significantly lower the optimum calcination temperature and dwell time for formation of single-phase $Pb(Ni_{1/3}Nb_{2/3})O_3$ powders.

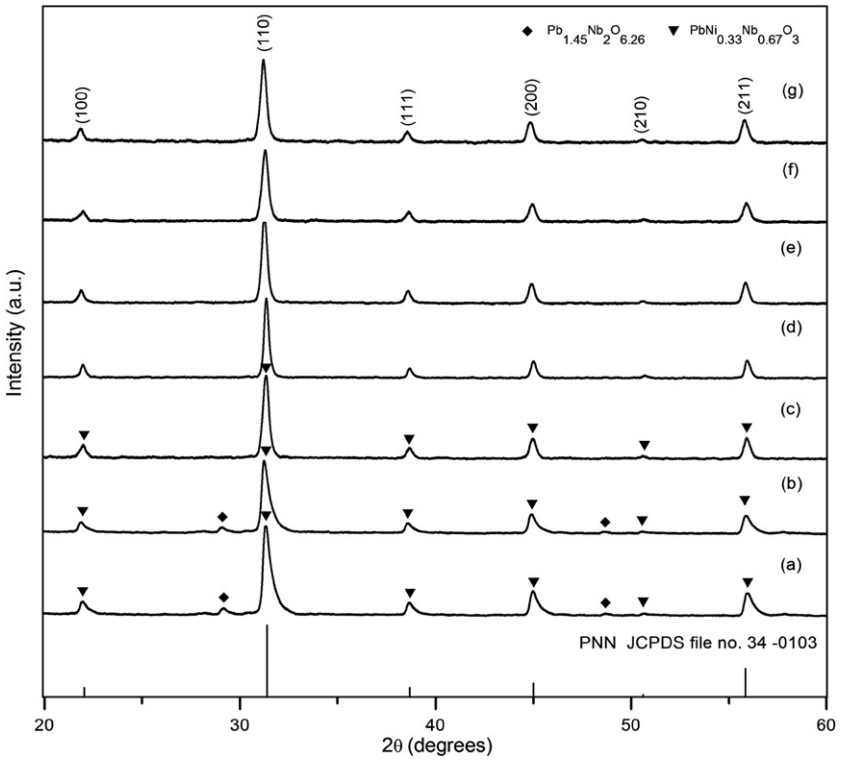

Fig. 3. XRD patterns of PNN powders calcined at 1000 °C with heating/cooling rates of 30 °C/min for (a) 3, (b) 4 and (c) 5 h; at 1050 °C with heating/cooling rates of 10 °C/min for (d) 1 and (e) 0.5 h; and at 1050 °C for 0.5 h with heating/cooling rates of (f) 20 and (g) 30 °C/min.

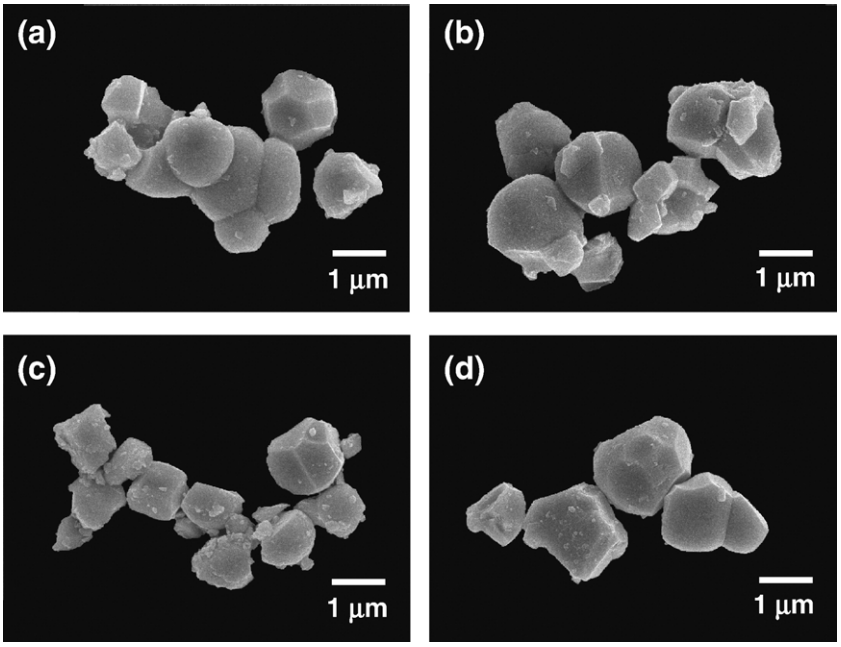

Fig. 4. SEM micrographs of the PNN powders calcined at 1050 °C for 0.5 h with heating/cooling rates of (a) 10, (b) 20 and (c) 30 °C/min; and (d) 2 h with heating/cooling rates of 10 °C/min.

In the present study, an attempt was also made to calcine $Pb(Ni_{1/3}Nb_{2/3})O_3$ powders under various heating/cooling rates. In this connection, it is shown that for the powders calcined at 1050 °C for 0.5 h, the yield of $Pb(Ni_{1/3}Nb_{2/3})O_3$ phase did not vary significantly with different heating/cooling rates, ranging from 10 to 30 °C/min (Fig. 3(e–g)). The observation that faster heating/cooling rates are required for the mixtures containing low-melting point oxide constituent (PbO), is in good agreement with early results reported in other similar systems [17,24].

Based on the TG-DTA and XRD data, it may be concluded that, over a wide range of calcination conditions, single-phase $Pb(Ni_{1/3}Nb_{2/3})O_3$ cannot be straightforwardly formed via a solid-state mixed oxide synthetic route, unless a careful design of calcination condition is performed. It is well documented that powders prepared by a conventional mixed oxide method have spatial fluctuations in their compositions. The extent of the fluctuation depends on the characteristics of the starting powders as well as the processing schedules [15–17]. It should be noted that no evidence of the pyrochlore $Pb_2Nb_2O_7$ [24], $Pb_3Nb_2O_8$ [12] and $Pb_3Nb_4O_{13}$ [25,26] was found in this study, nor was there any indication of the $Pb_{15}NiNb_{10}O_{41}$ reported by Balzer and Langbein [26] being present. The experimental work carried out here suggests that the optimal calcination conditions for single-phase $Pb(Ni_{1/3}Nb_{2/3})O_3$ (with impurities undetected by XRD technique) is 1050 °C for 0.5 h with heating/cooling rates as fast as 30 °C/min, without any addition of excess PbO or NiO [7]. Moreover, the formation temperature and dwell time for the production of $Pb(Ni_{1/3}Nb_{2/3})O_3$ powders observed in this work are also close to those reported earlier [5,6,9] but with faster heating/cooling rates. This clearly emphasizes the advantages of a combination between a corundum $Ni_4Nb_2O_9$ precursor, a rapid vibro-milling technique (only 30 min) and a carefully optimized reaction.

The morphological evolution during calcination was investigated by scanning electron microscopy (SEM). Micrographs of $Pb(Ni_{1/3}Nb_{2/3})O_3$ powders calcined at various dwell times and heating/cooling rates are illustrated in Fig 4. The influence of calcination conditions on the particle size is also given in Table 1. After calcination at 1050 °C with different dwell times and heating/cooling rates, the powders have similar morphology. In general, the particles are agglomerated and irregular in shape, with a substantial variation in particle size, particularly in samples calcined with faster heating/cooling raters (Fig. 4(c)). The results indicate that averaged particle size tend to increase with dwell times but seems to decrease with faster heating/cooling rates (Table 1).

As expected, it is seen that longer heat treatment leads to larger particle sizes and hard agglomeration (Fig. 4(d)). As shown in Fig. 4(a)–(c), as well as in Table 1, by increasing the heating/cooling rates, averaged particle size tends to decrease whilst the degree of agglomeration tends to increase. This observation could be attributed to the mechanism of surface energy reduction of the fine powders, i.e. the smaller the powder the higher the specific surface area [27]. This finding is also similar to that in $Pb(Mg_{1/3}Nb_{2/3})O_3$ powders synthesized by Wongmaneerung et al. [24]. To the authors' knowledge, the present data are the first results for the morphology–calcination relationship of $Pb(Ni_{1/3}Nb_{2/3})O_3$ powders prepared by the solid-state reaction. It is also of interest to point out that mass production of single-phase $Pb(Ni_{1/3}Nb_{2/3})O_3$ powders with the smallest particle size ~0.38 μm (estimated from SEM micrographs) can be achieved by employing a simple solid-state reaction combined with a rapid vibro-milling technique. In addition, EDX analysis using a 20 nm probe on a large number of particles of the calcined powders confirms that the parent composition is $Pb(Ni_{1/3}Nb_{2/3})O_3$ powders, in good agreement with XRD results.

4. Conclusions

The solid-state mixed oxide method via a rapid vibro-milling technique is explored in the preparation of single-phase $Pb(Ni_{1/3}Nb_{2/3})O_3$ powders by using $Ni_4Nb_2O_9$ as a novel B-site precursor. The calcination conditions have been found to show pronounced effects on phase formation and particle size of the calcined PNN powders. This work demonstrated that single-phase of lead nickel niobate powders with particle size ranging

Table 1
Particle size data of PNN powders calcined at various conditions

Calcination conditions			Particle size range (average) (±0.1 μm)
Temperature (°C)	Dwell time (h)	Rates (°C/min)	
1050	0.5	10	0.80–1.44 (1.18)
1050	0.5	20	0.58–1.87 (1.08)
1050	0.5	30	0.38–1.45 (0.92)
1050	1	10	0.70–1.70 (1.22)
1050	2	10	0.70–1.75 (1.30)

from 0.38–1.45 μm can be produced via this technique by using a calcination temperature of 1050 °C for 0.5 h, with heating/cooling rates of 30 °C/min. The resulting PNN powders exhibit similar morphology and variety of agglomerated particle sizes, depending on calcination conditions.

Acknowledgments

We thank the Thailand Research Fund (TRF), the Commission on Higher Education (CHE), the Faculty of Science and the Graduate School, Chiang Mai University for all supports.

References

[1] A.J. Moulson, J.M. Herbert, Electroceramics, 2nd ed., Wiley, Chichester, 2003.
[2] G. Haertling, J. Am. Ceram. Soc. 82 (1999) 797.
[3] F. Levassort, P. Tran-Huu-Hue, E. Ringaard, M. Lethiecq, J. Eur. Ceram. Soc. 21 (2001) 1361.
[4] T.R. Shrout, A. Halliyal, Am. Ceram. Soc. Bull. 66 (1987) 704.
[5] E.F. Alberta, A.S. Bhalla, J. Phys. Chem. Solids 63 (2002) 1759.
[6] L.C. Veitch, B.S. Thesis, The Pennsylvania State University, University Park, PA 1982.
[7] C.H. Lu, W.J. Hwang, Ceram. Int. 22 (1996) 373.
[8] S.L. Swartz, T.R. Shrout, Mater. Res. Bull. 17 (1982) 1245.
[9] E.F. Alberta, A.S. Bhalla, Mater. Lett. 54 (2002) 47.
[10] Y. Sasaki, A. Nagai, T. Yoshimoto, NIST Spec. Publ. 804 (1991) 99.
[11] M.M.A. Sekar, A. Halliyal, J. Am. Ceram. Soc. 81 (1998) 380.
[12] Y. Yoshikawa, Key Eng. Mater. 206–213 (2002) 87.
[13] C.H. Lu, W.J. Hwang, Jpn. J. Appl. Phys. 38 (1999) 5478.
[14] H. Ehrenberg, G. Wltschek, H. Weitzel, F. Trouw, J.H. Buettner, T. Kroener, H. Fuess, Phys. Rev., B 52 (1995) 9595.
[15] O. Khamman, R. Yimnirun, S. Ananta. Mater. Lett. (in press), doi:10.1016/j.matlet.2006.09.056.
[16] R. Wongmaneerung, R. Yimnirun, S. Ananta, Mater. Lett. 60 (2006) 1447.
[17] R. Tipakontitikul, S. Ananta, Mater. Lett. 58 (2004) 449.
[18] O. Khamman, W. Chaisan, R. Yimnirun, S. Anantam, Mater. Lett. (in press), doi:10.1016/j.matlet.2006.10.063.
[19] Powder Diffraction File No. 77–1971, International Centre for Diffraction Data, Newton Square, PA, 2000.
[20] Powder Diffraction File No. 33–0873, International Centre for Diffraction Data, Newton Square, PA, 2000.
[21] Powder Diffraction File No. 46–0525, International Centre for Diffraction Data, Newton Square, PA, 2000.
[22] Powder Diffraction File No. 84–1731, International Centre for Diffraction Data, Newton Square, PA, 2000.
[23] Powder Diffraction File No. 34–0103, International Centre for Diffraction Data, Newton Square, PA, 2000.
[24] R. Wongmaneerung, T. Sarakonsri, R. Yimnirun, S. Ananta, Mater. Sci. Eng., B 132 (2006) 292.
[25] A.I. Agranovskaya, Bull. Acad. Sci. U.S.S.R., Phys. Ser. 1 (1960) 1271.
[26] B. Balzer, H. Langbein, Cryst. Res. Technol. 32 (1997) 955.
[27] J.S. Reeds, Principles of Ceramic Processing 2nd ed., Wiley, New York, 1995.

Appl. Phys. A 89, 737–741 (2007)
DOI: 10.1007/s00339-007-4156-9

Applied Physics A
Materials Science & Processing

R. YIMNIRUN✉
A. NGAMJARUROJANA
R. WONGMANEERUNG
S. WONGSAENMAI
S. ANANTA
Y. LAOSIRITAWORN

Temperature scaling of ferroelectric hysteresis in hard lead zirconate titanate bulk ceramic

Department of Physics, Faculty of Science, Chiang Mai University, Chiang Mai 50200, Thailand

Received: 21 February 2007/Accepted: 4 June 2007
Published online: 28 June 2007 •

ABSTRACT The temperature scaling of the ferroelectric hysteresis was investigated in hard lead zirconate titanate (PZT) bulk ceramic. The power-law temperature scaling relations were obtained for hystersis area $\langle A \rangle$, remnant polarization P_r, and coercivity E_C in the forms of $\langle A \rangle \propto T^{-0.9650}$, $P_r \propto T^{-0.0261}$, and $E_C \propto T^{-0.8823}$, respectively, which are mostly comparable to those of its soft counterpart. The observation that P_r decayed more slowly with temperature than in soft PZT was attributed to the presence of the complex defects in hard PZT. However, the product of P_r and E_C still provided the similar scaling law on the T dependence in comparison with $\langle A \rangle$.

PACS 77.80.-e; 77.80.Fm; 77.84.-s; 77.84.Dy

1 Introduction

Acceptor-doped lead zirconate titanate ($Pb(Zr_{1-x}Ti_x)O_3$ or PZT) or commercially known as hard PZT ceramics have been employed extensively in applications that require hard piezoelectric properties, such as ultrasonic motors and high power transformers [1]. The ferroelectric characteristics of hard PZT are also different from those of the soft PZT, as a result of complex defects present [2–4]. The difference in the behaviors has also been investigated extensively [5–12]. In hard PZT, the oxygen vacancies are introduced, trapped at the domain walls, then form electric dipoles with the acceptor atoms. These dipoles called complex defects act as pinning points for the domain wall and the domain wall motion is reduced. The complex defects are absent in the soft PZT ceramics, hence the domain walls can move more easily. Therefore, hard PZT ceramics typically show higher coercivity (E_C) than soft ones [2, 3, 9, 11]. Dielectric and piezoelectric properties of the two ceramic types are also significantly different [2–7].

From both the fundamental and practical viewpoints, the temperature and thermal history have been found to impose significant effects on the ferroelectric hysteresis behavior of the hard PZT, which have also been attributed to the presence and response of the complex defects to the temperature [5, 6, 9, 12–16]. Earlier, we proposed the scaling of the area of the hysteresis with field amplitude and frequency for hard PZT bulk ceramics [17], which is interestingly very similar to that for the soft PZT bulk ceramics reported previously [18]. This observation suggested little influence of the complex defects to the dynamic behavior. However, as stated above, the complex defects are reportedly responsible for temperature-related behaviors in the hard PZT ceramics. To this connection, an investigation of the temperature scaling of dynamic hysteresis of the hard PZT ceramic with comparison to that of the soft PZT ceramic will provide insight to roles of complex defects to the temperature-dynamic hysteresis behavior. It is, therefore, the aim of this study to establish experimentally the temperature scaling of the ferroelectric hysteresis for hard PZT bulk ceramic.

✉ Fax: 6653-943-445, E-mail: rattikornyimnirun@yahoo.com

2 Experimental

The polarization–electric field (P–E) hysteresis loops of commercial hard PZT ceramic discs (APC-840, APC International, Ltd., USA) with diameter of 8 mm and thickness of 1 mm were obtained by a modified Sawyer–Tower circuit over temperature range 298–453 K with E_0 up to 40 kV/cm (f was fixed at 40 Hz). The electric field was applied to a sample by a high voltage AC amplifier (Trek 610D) with the input sinusoidal signal from a function generator (HP 3310A). The P–E loops were recorded by a digital oscilloscope (HP 54645A, 100 MHz). Each loop was obtained after 20 sampling cycle to average out the noise deformation. The hysteresis loop obtained was very consistent with that obtained by a standardized ferroelectric testing unit, RT66A (Radiant Technologies Inc., NM), which ensures the reliability of the measurements. It should be noted that the Curie temperature (T_C) of the hard PZT used was determined experimentally from dielectric measurement to be 593 K.

3 Results and discussion

Figure 1 displays the hysteresis loops profile for various electric field amplitudes E_0 at a fixed $T = 373$ K (Fig. 1a), and for various temperatures at a fixed $E_0 =$ 35 kV/cm (Fig. 1b). From the P–E loops, it is obvious that both E_0 and T play a crucial role on the hysteresis area $\langle A \rangle$. For example, in Fig. 1a, with increasing E_0, a transition from a minor loop at low field to a saturated s-shape loop at high

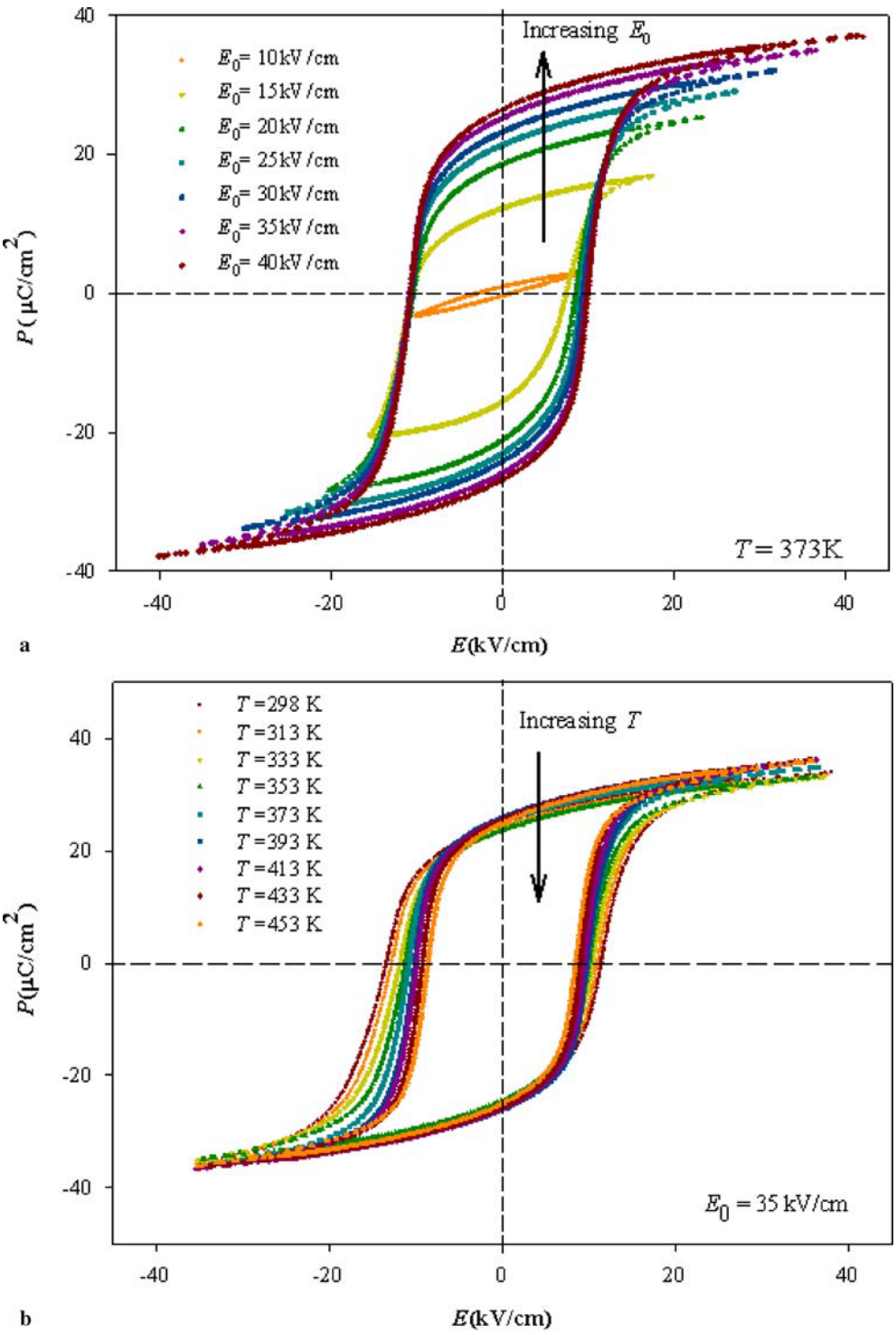

FIGURE 1 Hysteresis loops for hard PZT ceramic (**a**) at $T = 373$ K with varying E_0, and (**b**) at $E_0 = 35$ kV/cm with varying T

field occurs. This is expected because with higher field there is more electrical energy supplied into the system resulting in more 'electrical driving force' acting on electric dipole moments [3]. Consequently, the polarization has more tendencies to follow the external electric field which in turns reduces the phase lag between the polarization and the field signals. As a result, the saturated loops are obtained at the high fields instead of the minor loops at low fields. Additionally, slightly asymmetric P–E loops are also observed in the hard PZT, as displayed in Fig. 1. The observation could be attributed to the presence of the complex defects, which provide the internal bias-field [3, 5, 7, 11]. Therefore, the ferroelectric interaction between these defect dipoles, which are trapped near domain walls, and the other dipoles in the domains makes the polarization switching and domain re-orientation processes, as well as the domain wall motions, more difficult in one field direction than the other direction. This results in asymmetric loops, and the differences between E_C^+ and E_C^-, and P_r^+ and P_r^-, as observed in Fig. 1. On the other hand, as suggested in Fig. 1b, with increasing temperature, the loop area is slowly reduced in

size. This is caused by that higher temperature provides higher thermal fluctuation to the polarization order parameter which reduces the ferroelectric interaction among the dipoles [3]. Therefore, even E_0 is fixed, the polarization direction is easily tuned with the electric field at higher temperatures due to the smaller ferroelectric interaction providing a reduction in the coercivity (E_C). Interestingly, the remnant polarization (P_r) is seen to be rather stable with temperature, which is very different from what was observed in soft PZT, as reported earlier [19]. The interpretation for this observation is not obvious, but could be related to the complex defects present only in hard PZT, as will be discussed later. Nonetheless, the hysteresis loop area is still seen to reduce with increasing the temperature generally because of the strong reduction in E_C. More interestingly, the observed temperature dependence of these hysteresis parameters prompts a question whether these parameters scale with temperature the same way as in the soft PZT ceramic. For better comparison with the soft PZT case, this present study will only focus on the scaling relations for very well-saturated loops at fields above 25 kV/cm.

Figure 2 shows the relation between $\langle A \rangle$ and T in a double logarithmic form, from which one would see a similar decreasing trend for all E_0. This implies a power law relation between the hysteresis area and temperature i.e., $\langle A \rangle \propto T^{\gamma}$. By the least square-fitting method, the exponent $\gamma = -0.9650$ was obtained. As plotted in Fig. 2, the dependence of the area with temperature can be fitted (solid line) very well (with $R^2 \sim 0.97$) by

$$\langle A \rangle \propto T^{-0.9650} . \tag{1}$$

The temperature scaling relation of the hysteresis area $\langle A \rangle$ obtained for hard PZT is very much comparable to that obtained for soft PZT, as reported earlier in the form of $\langle A \rangle \propto T^{-1.1024}$ [19].

Additionally, Fig. 3 shows the relation between E_C and T in a double logarithmic plot. As being evident, the power-law temperature scaling relation seems suitable for E_C. It is found that the dependence of E_C on T can be fitted very well (with $R^2 \sim 0.99$) by

$$E_C \propto T^{-0.8823} . \tag{2}$$

When compared to that of soft PZT with a linear relation (i.e., the power exponent is equal to one) [19], the scaling relations of E_C for both types of PZT are still comparable.

Though in soft PZT ceramic the P_r was seen to scale strongly with T in the power-law form, i.e., $P_r \propto T^{-1.2322}$ [19], the P_r of hard PZT ceramic is surprisingly observed to be rather stable with temperature (with very small reduction over wide temperature range), as shown in Fig. 3. An attempt was made to fit the data and found very weak power-law decay of area with temperature in the form of

$$P_r \propto T^{-0.0261} . \tag{3}$$

It is interesting to observe that the temperature scaling behaviors for the hard PZT bulk ceramic are, to some extent, similar to those of the soft counterpart [19], particularly for $\langle A \rangle$ and E_C. By a direct comparison, the power-law exponents for the two ceramics are not significantly different. More importantly, the similar temperature scaling behaviors for the two types of ceramics suggest that though the complex defects contribute greatly to the difference on the electrical properties, they contribute only slightly to the temperature-dependent dynamic behaviors.

Nonetheless, a noticeable difference in the temperature scaling behavior of P_r between the soft and hard PZT ceramics still requires explanation. In hard PZT, P_r is seen to decrease more slowly with increasing temperature than in soft PZT. Increasing temperature provides the reduction in ferroelectric interaction between dipoles, which results in the decrease of P_r and E_C with increasing temperature in similar rates of decay, as observed in soft PZT [19]. However,

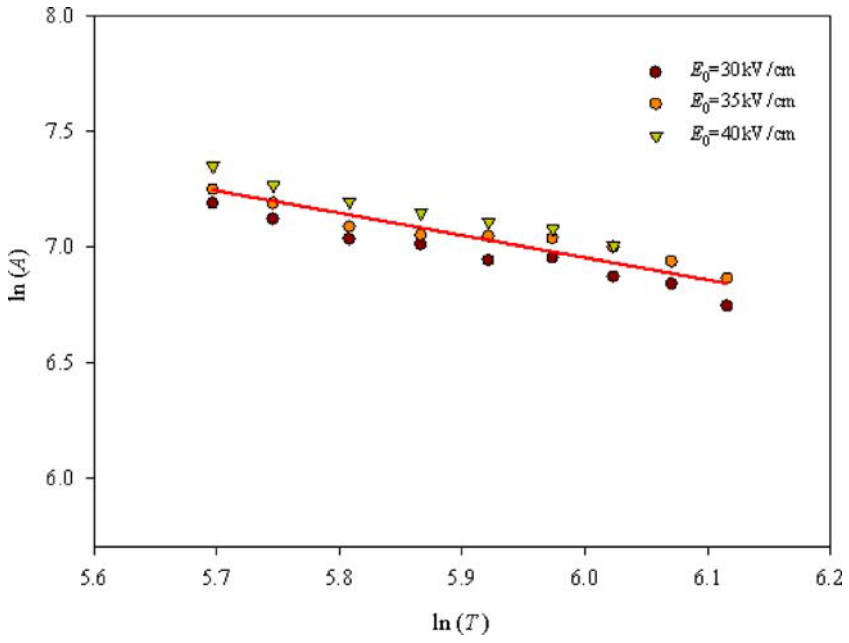

FIGURE 2 Double logarithmic plot between ln(A) and ln(T)

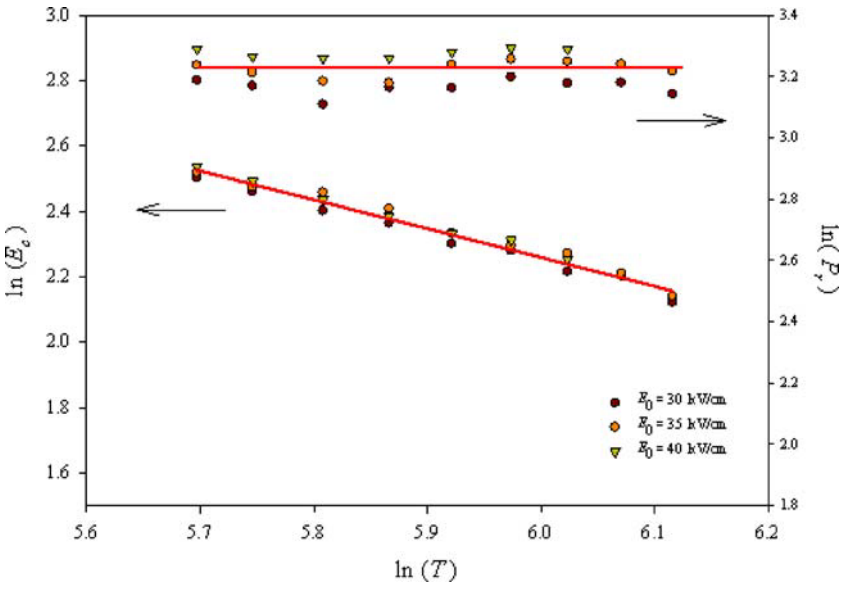

FIGURE 3 Double logarithmic plots between $\ln(P_r)$ and $\ln(T)$, and $\ln(E_C)$ and $ln(T)$

this is not the case in hard PZT as P_r is seen to decay more slowly with temperature than E_C, as seen from (2) and (3) and Fig. 1b. The reasons could be attributed to the difference in short-range ferroelectric interaction between the trapped defect dipoles and the neighboring dipoles under high field (where E_C is determined) and under zero field (where P_r is determined) conditions [5, 7, 15]. With an addition of an electrical driving force under high field condition, the majority of dipoles can switch more easily with increasing temperature, resulting in strong decay in E_C with temperature. On the other hand, without an electrical field, the thermal energy alone cannot provide enough driving force for the re-orientation of the majority of dipoles, particularly those nearby the trapped defect dipoles; hence, P_r is seen to decay very slowly with increasing temperature. The internal bias-field from the defect dipoles also causes the difference in temperature decay between E_C^+ and E_C^-, and P_r^+ and P_r^-, as observed in Fig. 1b.

Even though the temperature-scaling relations of P_r and E_C obtained for hard PZT are slightly different from those of soft PZT, particularly P_r, and as approaching saturation the hysteresis area can be roughly estimated with $(2P_r)(2E_C)$ [16, 20], it is of interest to check if the product of P_r and E_C in the case of hard PZT would still provide a similar scaling law on the T dependence in comparison with $\langle A \rangle$, as observed in soft PZT case. By using (2) and (3), it is then found that

$$(2E_C)(2P_r) \approx 4(T^{-0.9084}) . \quad (4)$$

The scaling of 'area' in this way on the temperature should have the exponent γ of -0.9084, which is very similar to that extracted from the $\ln\langle A \rangle$ and $\ln T$ plot (which the exponent γ has a value of -0.9650). Therefore, these two scaling methods seem to agree. So once the scaling of area to the temperature is found, it is possible to guess how the E_C would scale with T if the scaling relation between P_r and T is known or vice versa. The same conclusion was reached in the soft PZT ceramic case [19].

4 Conclusions

In hard PZT bulk ceramic, the power-law temperature scaling relations are obtained for hystersis area $\langle A \rangle$, remnant polarization P_r, and coercivity E_C in the forms of $\langle A \rangle \propto T^{-0.9650}$, $P_r \propto T^{-0.0261}$, and $E_C \propto T^{-0.8823}$, respectively, which are mostly comparable to those of its soft counterpart. The observation that P_r decays more slowly with temperature than in soft PZT is attributed to the presence of the complex defects in hard PZT. However, the product of P_r and E_C still provides the similar scaling law on the T dependence in comparison with $\langle A \rangle$, as also reported for soft PZT case. Most importantly, this study suggests that, while the complex defects contribute greatly to the difference in many electrical behaviors between soft and hard PZT ceramics, they show very little influence on the temperature-dependent dynamic hysteresis behavior.

ACKNOWLEDGEMENTS Financial supports from the Thailand Research Fund (TRF) and Commission on Higher Education (CHE) are gratefully acknowledged.

REFERENCES

1 K. Uchino, *Piezoelectric Actuators and Ultrasonic Motors* (Kluwer, Boston, 1997), p. 129
2 B. Jaffe, W.R. Cook, H. Jaffe, *Piezoelectric Ceramics* (Academic, New York, 1971), p. 271
3 M.E. Lines, A.M. Glass, *Principles and Applications of Ferroelectrics and Related Materials* (Clarendon, Oxford, 1977), p. 102
4 K. Uchino, *Ferroelectric Devices* (Dekker, New York, 2000), p. 145
5 K. Carl, K.H. Hardtl, Ferroelectrics **17**, 473 (1978)
6 Q.M. Zhang, H. Wang, N. Kim, L.E. Cross, J. Appl. Phys. **75**, 454 (1994)
7 T. Tsurumi, T. Sasaki, H. Kakemoto, T. Harigai, S. Wada, Japan. J. Appl. Phys. Part 1 **43**, 7618 (2004)
8 M.H. Lente, A. Picinin, J.P. Rino, J.A. Eiras, J. Appl. Phys. **95**, 2646 (2004)
9 Q. Tan, J. Li, D. Viehland, Appl. Phys. Lett. **75**, 418 (1999)
10 M. Morozov, D. Damjanovic, N. Setter, J. Eur. Ceram. Soc. **25**, 2483 (2005)
11 W. Chang, A.H. King, K. Bowman, Appl. Phys. Lett. **88**, 242 901 (2006)
12 S.K. Pandey, O. P Thakur, A. Kumar, C. Prakash, R. Chatterjee, T.C. Goel, J. Appl. Phys. **100**, 014 104 (2006)

13 Q. Tan, D. Viehland, J. Am. Ceram. Soc. **81**, 328 (1998)
14 B.S. Li, G.R. Li, Q.R. Yin, Z.G. Zhu, A.L. Ding, W.W. Cao, J. Phys. D Appl. Phys. **38**, 1107 (2005)
15 O. Lohse, D. Bolten, S. Tiedke, T. Schneller, R. Waser, Proc. IEEE-ISAF 98 **1**, 27 (1998)
16 G.L. Yuan, J.-M. Liu, S.T. Zhang, D. Wu, Y.P. Wang, Z.G. Liu, H.L.W. Chan, C.L. Choy, Appl. Phys. Lett. **84**, 954 (2004)
17 R. Yimnirun, R. Wongmaneerung, S. Wongsaenmai, A. Ngamjarurojana, S. Ananta, Y. Laosiritaworn, Appl. Phys. Lett. **90**, 112906 (2007)
18 R. Yimnirun, Y. Laosiritaworn, S. Wongsaenmai, S. Ananta, Appl. Phys. Lett. **89**, 162901 (2006)
19 R. Yimnirun, R. Wongmaneerung, S. Wongsaenmai, A. Ngamjarurojana, S. Ananta, Y. Laosiritaworn, Appl. Phys. Lett. **90**, 112908 (2007)
20 J.-M. Liu, H.P. Li, C.K. Ong, L.C. Lim, J. Appl. Phys. **86**, 5198 (1999)

Available online at www.sciencedirect.com
ScienceDirect
Current Applied Physics 8 (2008) 128–133
Current Applied Physics
An official journal of the KPS
www.elsevier.com/locate/cap
www.kps.or.kr

Development of perovskite and phase transition in lead cobalt niobate modified lead zirconate titanate system

Naratip Vittayakorn [a,*], Supamas Wirunchit [a], Sakda Traisak [a], Rattikorn Yimnirun [b], Gobwut Rujijanagul [b]

[a] *Materials Science Research Unit, Department of Chemistry, Faculty of Science, King Mongkut's Institute of Technology Ladkrabang, Bangkok 10520, Thailand*

[b] *Department of Physics, Faculty of Science, Chiang Mai University, Chiang Mai 50200, Thailand*

Received 19 December 2006; received in revised form 28 May 2007; accepted 15 June 2007
Available online 29 June 2007

Abstract

Ferroelectric lead zirconate titanate–lead cobalt niobate ceramics with the formula $(1-x)Pb(Zr_{1/2}Ti_{1/2})O_3$–$xPb(Co_{1/3}Nb_{2/3})O_3$ where $x = 0.0$–0.5 were fabricated using a high temperature solid-state reaction method. The formation process, the structure and homogeneity of the obtained powders have been investigated by X-ray diffraction method as well as the simultaneous thermal analysis of both differential thermal analysis (DTA) and thermogravimetry analysis (TGA). It was observed that for the binary system $(1-x)Pb(Zr_{1/2}Ti_{1/2})O_3$–$xPb(Co_{1/3}Nb_{2/3})O_3$, the change in the calcination temperature is approximately linear with respect to the PCoN content in the range $x = 0.0$–0.5. In addition, X-ray diffraction indicated a phase transformation from a tetragonal to a pseudo-cubic phase when the fraction of PCoN was increased. The dielectric permittivity is remarkably increased by increasing PCoN concentration. The maximum value of remnant polarization P_r (25.3 μC/cm^2) was obtained for the 0.5PZT–0.5PCoN ceramic.

PACS: 77.22.−d; 77.80.Bh; 77.84.Dy; 61.10.Nz; 77.80.Dj

Keywords: Ferroelectric; Relaxor ferroelectric; Perovskite

1. Introduction

Since the late 1960s, lead titanate:lead zirconate ceramic (generally known as $Pb(Zr_{1-x}Ti_x)O_3$ or PZT), near the tetragonal–rhombohedral morphotropic phase boundary has been considered an important material for a wide range of piezoelectric, pyroelectric and ferroelectric device applications such as transducers, computer memory and display and pyroelectric sensors [1,2]. Most commercial PZT ceramics are thus designed in the vicinity of the morphotropic phase boundary (MPB) with various doping in order to achieve optimum properties [1,2]. Recently, many piezoelectric ceramic materials have been developed from binary systems containing a combination of relaxor and normal ferroelectric materials [3] which yield high dielectric permittivities {e.g. $Pb(Zn_{1/3}Nb_{2/3})O_3$–$PbTiO_3$ (PZN–PT) [4,5], $Pb(Zr_{1/2}Ti_{1/2})O_3$–$Pb(Ni_{1/3}Nb_{2/3})O_3$ (PZT–PNN) [6]}, excellent piezoelectric coefficients {e.g. $Pb(Zn_{1/3}Nb_{2/3})O_3$–$PbTiO_3$ (PZN–PT) [4,5], $Pb(Zr_{1/2}Ti_{1/2})O_3$–$Pb(Zn_{1/3}Nb_{2/3})O_3$ (PZN–PZT) [7], $Pb(Sc_{1/3}Nb_{2/3})O_3$–$PbTiO_3$ (PSN–PT) [8,9]}, and high pyroelectric coefficients {e.g. $Pb(Ni_{1/3}Nb_{2/3})O_3$–$PbTiO_3$–$PbZrO_3$(PNN–PT–PZ) [10]}.

Lead cobalt niobate ($Pb(Co_{1/3}Nb_{2/3})O_3$, PCoN) is a typical relaxor ferroelectric characterized by a high dielectric constant, a broad diffuse phase transition near −70 °C and low firing temperature [11]. Though the paraelectric–ferroelectric transition temperature of PCoN is below room temperature, it can be easily shifted upward with the

* Corresponding author. Tel.: +66 89 700 2136; fax: +66 2 326 4415.
E-mail address: naratipcmu@yahoo.com (N. Vittayakorn).

1567-1739/$ - see front matter © 2007 Elsevier B.V. All rights reserved.
doi:10.1016/j.cap.2007.06.002

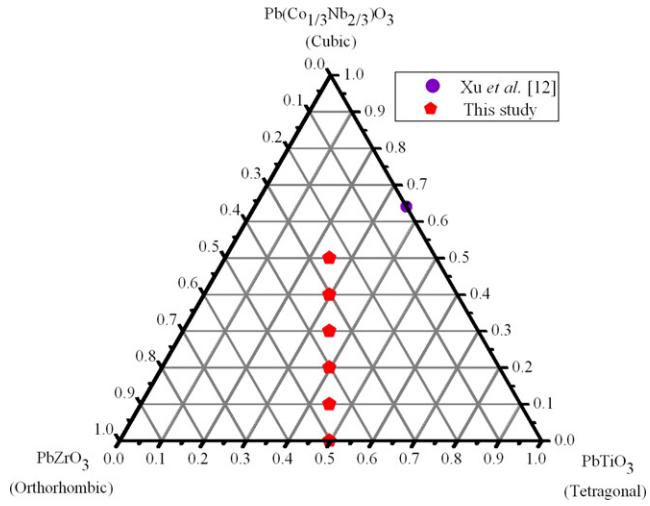

Fig. 1. Compositions studied in the $PbTiO_3$–$PbZrO_3$–$Pb(Co_{1/3}Nb_{2/3})O_3$ ternary system.

addition of $PbTiO_3$ (PT), which is a normal ferroelectric compound with a phase transition at 490 °C. So the PCoN-based relaxors are one of the most attractive materials for multilayer ceramic capacitors and electrostrictive actuators [2].

Since PCoN is a relaxor ferroelectrics with a broad dielectric peak near $T_c \approx -70$ °C and PZT (Zr/Ti = 50/50) is a normal ferroelectric with a sharp maximum permittivity at $T_c \sim 390$ °C, the curie temperature in PZT–PCoN system can be engineered over a wide range of temperature by controlling the amount of PCoN in the system. However, the PZT–PCoN ceramics have not been obtained as yet. Fig. 1 schematically shows the pseudo-ternary composition range which was studied in this work compared with other studies [2]. In order to get more information about combination of relaxor and normal ferroelectric materials and to recognize the properties of PZTCoN ceramics, this paper attempted to carry out the synthesis of the quasi-binary solid solution $(1-x)Pb(Zr_{0.5}Ti_{0.5})O_3$–$xPb(Co_{1/3}Nb_{2/3})O_3$, with $x = 0.0$–0.5 using a solid-sate reaction method and to report some properties of obtained ceramics.

2. Experimental

Ceramics of $(1-x)Pb(Zr_{0.5}Ti_{0.5})O_3$–$xPb(Co_{1/3}Nb_{2/3})O_3$(PZT–PCoN) with $x = 0$–0.5 were synthesized using the solid-state reaction method. The CoO (99.9%), Nb_2O_5 (99.9%), PbO (Fluka, >99% purity) TiO_2 (99.8%) and ZrO_2 (99%) were mixed and milled in ethyl alcohol for 18 h using a ball-milling. After drying at 120 °C for 2 h, the reaction of the uncalcined powders taking place during heat treatment was investigated by differential thermal analysis (DTA; Shimadzu) and thermogravimetry analysis (TGA; Shimadzu), using a heating rate of 10 °C/min in air from room temperature up to 1400 °C. Based on the TG–DTA results, the mixture was calcined at various temperatures ranging from 650 to 900 °C, dwell times 4 h and heating/cooling rates ranging 20 °C/min, in closed alumina crucible, in order to investigate the perovskite phase formation. The calcined powders, with polyvinyl alcohol (PVA) added as binder, were pressed into pellets of 15 mm diameter and ~2 mm thickness, which were then sintered at 1100–1200 °C in Pb-atmosphere for 4 h in a closed alumina crucible. X-ray diffraction (XRD; Philips PW 1729 diffractometer) using Cu K_α radiation was used to determine the phases formed and optimum firing temperatures for the formation of desired phase. For measuring the dielectric and ferroelectric characteristics, the specimens were polished to 1 mm thickness. After ultrasonic cleaning in ethanol bath, silver-paste was coated on the polished samples on both sides by the screen printing method, and then subsequently, fired at 650 °C for 30 min. For the dielectric properties measurement, capacitance was measured at 1 kHz using an automated measurement system consisted of an LCR meter (HP-4284, Hewlett–Packard Inc.). The dielectric constant is then calculated from $\varepsilon_r = Cd/\varepsilon_0 A$, where C is the capacitance of the sample, d and A are the thickness and the area of the electrode, respectively, and ε_0 is the dielectric permittivity of vacuum (8.854×10^{-12} F/m). The ferroelectric hysteresis loop parameters were measured with aid of a home-built Sawyer–Tower circuit.

3. Results and discussion

The TG–DTA simultaneous analysis of a powder mixed in the stoichiometric proportions of PZT–PCoN is illustrated in Fig. 2. In the temperature range from room temperature to ~350 °C, the sample shows both exothermic and endothermic peaks in the DTA curve, in consistent with a slight drop in weight loss at the same temperature range. These observations can be attributed to the decomposition of the organic species from the milling process [12,13]. The different temperature, intensities, and shapes of the thermal peaks probably are related to the different natures of the organic species and consequently, caused

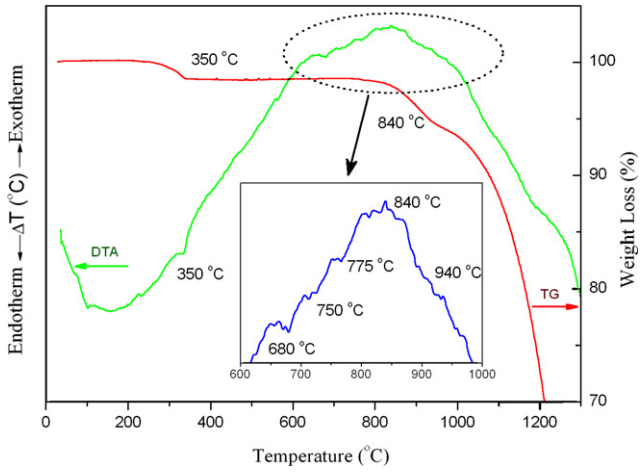

Fig. 2. DTA–TG curves for the mixture of PZT–PCoN powder.

by the removal of species differently bounded in the network [13]. In the temperature range 650–900 °C, both exothermic and endothermic peaks are observed in the DTA curve. The enlarged zone of this DTA curve shows that the endothermic peak at ~750 °C should be correlated to the phase transition of perovskite structure, because no weight loss could be found in the TG curve and that is also in accordance to literature data [14,15]. The last endothermic peak centered at ~840 °C may be caused by the decomposition of lead oxide. As a result, crystallization of PZT–PCoN powders is established above ~750 °C. Further increase in temperature or heating time will promote crystallization of perovskite phase powders. These data were used to define the range of temperatures (650–950 °C) for XRD investigation. To study the phase development with increasing calcination temperature, all compositions were calcined at various temperatures for 4 h in air with constant heating/cooling rates of 20 °C/min, followed by phase analysis using XRD technique.

XRD patterns of the calcined 0.7PZT–0.3PCoN powders at different calcination temperatures are illustrated Fig. 3. The XRD results show that the pyrochlore phase $Pb_xNb_yO_z$ pyrochlore phases was dominant at calcination temperatures below 700 °C. In the work by Chen et al. [12] it was reported that in the lead–niobium pyrochlore system the cubic $Pb_3Nb_4O_{13}$, pyrochlore phase (ICDD No. 25–443) forms first around 580 °C. At higher temperatures, it transforms to $Pb_2Nb_2O_7$, (ICDD No. 40–828) and finally to $Pb_3Nb_2O_8$, (ICDD No. 30–712) with increased calcination temperatures. At 700 °C, the pyrochlore phase began to decrease and disappeared completely at 750 °C. The yield of the perovskite phase increased significantly until at 750 °C, a single-phase of perovskite phase was formed. The studies also reflect the growth of crystallinity in the powders with the increasing heat-treatment temperatures. The results of the X-ray diffraction measurement support the DTA observation (Fig. 2) that the perovskite phase is formed at approximately 750 °C. The relationship between the relative content of perovskite phase and the calcination temperature is illustrated in Fig. 4. The relative content of perovskite phase is calculated based on the value of $(I_{Pe(110)}/(I_{Pe(110)} + I_{Py(222)}))$, where $I_{Pe(110)}$ and $I_{Py(222)}$ indicate the intensity of the (1 1 0) diffraction peak of perovskite phase and the intensity of the (2 2 2) diffraction peak of the pyrochlore phase, respectively. Based on the XRD data obtained here together with the % phase perovskite, it may be conclude that the change in the calcination temperature is approximately linear with respect to the PCoN content in the range $x = 0.0$–0.5. With an increase in x, the calcination temperature shifts up to high temperatures. The XRD patterns of $(1-x)$PZT–xPCoN ceramics with various x values are shown in Fig. 5. The patterns show single-phase perovskite-structured ceramics with $x \leqslant 0.4$. Evidence for the pyrochlore or other second phases was not detected in the patterns. Pyrochlore peaks, identified with "*" in Fig. 5, were found in the samples with $x = 0.5$. These results indicated that the presence of PCoN in the solid solution decreases the structural stability of PZT perovskite phase by its tolerance factor and electronegativity [16].

The $PbZrO_3$–$PbTiO_3$ phase diagram predicts that at room temperature $Pb(Zr_{1/2}Ti_{1/2})O_3$ falls within the tetragonal phase field near the MPB. The crystal symmetry for pure PCoN is cubic at room temperature. Below $T_{max} \approx -70$ °C, the symmetry changes to rhombohedral. Therefore, with increasing x the crystal symmetry should change due to the effects of the increased PCoN fraction and the decrease in T_C. It is well know that in the pseudo-cubic phase, the {2 0 0} profile will show a single narrow peak because all the planes of {2 0 0} share the same lattice parameters, while in the tetragonal phase, the {2 0 0} profile should be split into two peaks with the intensity height of the former being half of the latter because the

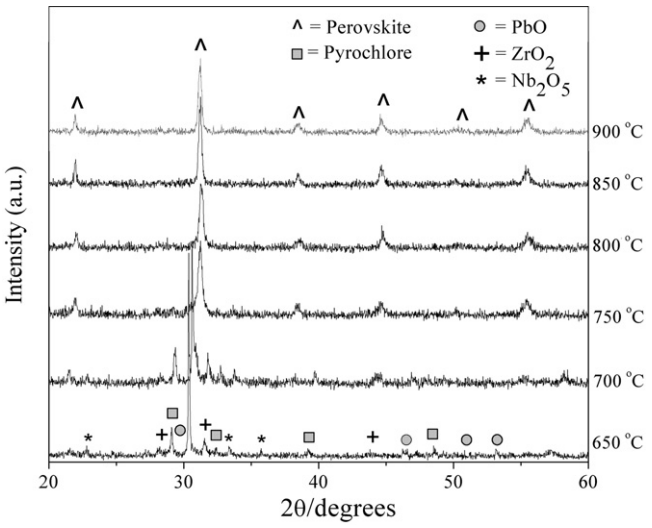

Fig. 3. XRD patterns of 0.7PZT–0.3PCoN powder calcined at various temperature for 4 h.

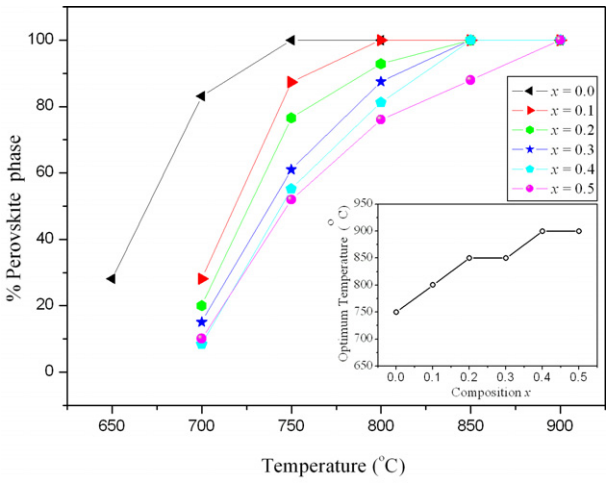

Fig. 4. Percentage of perovskite phase as a function of calcinations temperature for $(1 - x)$PZT–xPCoN powder.

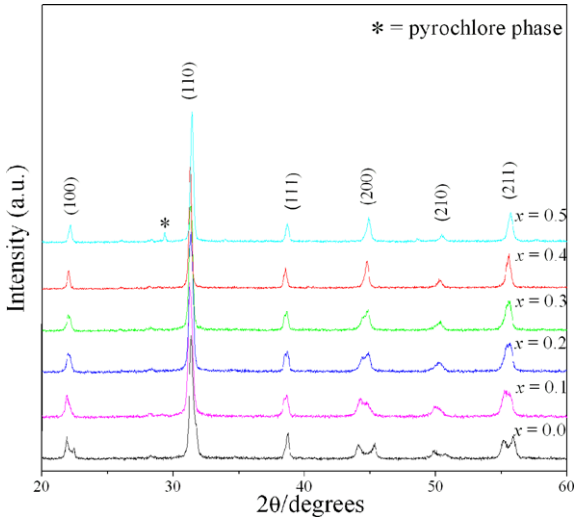

Fig. 5. XRD patterns of $(1-x)$PZT–xPCoN ceramics.

lattice parameters of (200) and (020) are the same but are slightly different from those of (002).

Based on the careful XRD study of {200} reflections in Fig. 6, we can find that a phase transformation from the tetragonal structure to the pseudo-cubic structure occurs with increasing PCoN content. The ceramics exist as tetragonal phase which is indicated by the splitting of $(002)_T$ and $(200)_T$ peaks in the 2θ range from 43.5° to 46.5° at $x = 0.10$. As PCoN content increases from $x = 0.1$ to 0.3, the ceramics coexist as tetragonal and pseudo-cubic phase revealed by the coexistence of $(002)_T$ and $(200)_R$ peaks in the 2θ range from 43.5° to 45.5°. To a first approximation, it could be said that the composition with $x = 0.1$–0.2 is close to the morphotropic phase boundary (MPB) of the $Pb(Zr_{0.50}Ti_{0.50})O_3$–$Pb(Co_{1/3}Nb_{2/3})O_3$ system, where the structure of the PZT–PCoN compositions is gradually changing from tetragonal to pseudo-cubic. Electrical data described later further supports this assumption.

The ceramics with $x = 0.50$ exist as pseudo-cubic phase revealed by the single $(200)_R$ peak. It is interesting to note that the influence of the addition of $Pb(Co_{1/3}Nb_{2/3})O_3$ on the phase transition of the $Pb(Zr_{1/2}Ti_{1/2})O_3$ system is similar to that of $Pb(Zr_{1/2}Ti_{1/2})O_3$–$Pb(Ni_{1/3}Nb_{2/3})O_3$, $Pb(Zr_{1/2}Ti_{1/2})O_3$–$Pb(Mg_{1/3}Nb_{2/3})O_3$ and $Pb(Zr_{1/2}Ti_{1/2})O_3$–$Pb(Zn_{1/3}Nb_{2/3})O_3$ systems [6,17–19].

The dielectric properties of $(1-x)$PZT–xPCoN, $x = 0.0$–0.5 are illustrated in Fig. 7. With increasing concentration of PCoN, the dielectric constant tends to increase. The effect of increasing the dielectric constant at room temperature with increasing PCoN content is interpreted to be due to the possibility of the decrease of the transition temperature to near room temperature. Because of when PCoN is added into PZT, the transition temperature of the PZT–PCoN ceramics are shifted towards the room temperature; hence the dielectric properties measured at room temperature are increased. Other authors have reported a similar behavior [6,20]. Fig. 8 shows the saturated loops of 0.9PZT–0.1PCoN samples with difference electric fields strengths. It is clearly evident that the shape of hysteresis various greatly with the electric fields strength. At 5 kV/cm electric fields strength, a near-linear relationship of P–E is observed. This result is due to the fact that the electric field is not large enough to switch any domains. At 10 kV/cm electric fields, the polarization nonlinearity is developed in both regions of the positive and negative fields. These results clearly demonstrate that the electric field strength of 10 kV/cm is of enough energy to constrain realignment of some domains in the direction of the applied fields. No evidence of pinning effect or asymmetric loop was detected in all electric fields strength. At 25 kV/cm electric field strength, the loop reveals fully developed symmetric hysteresis loop. This shows that the electric fields strength of 25 kV/cm has of enough energy to constrain realignment of all domains in the direction of the electric fields.

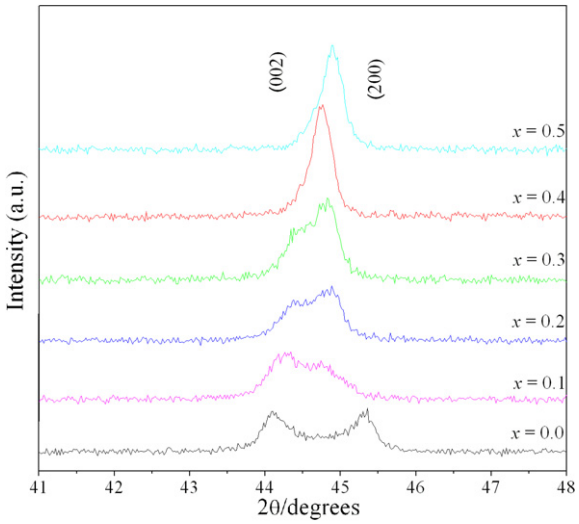

Fig. 6. XRD pattern of the (200) peak of $(1-x)$PZT–xPCoN, $x = 0.0$–0.1 ceramics.

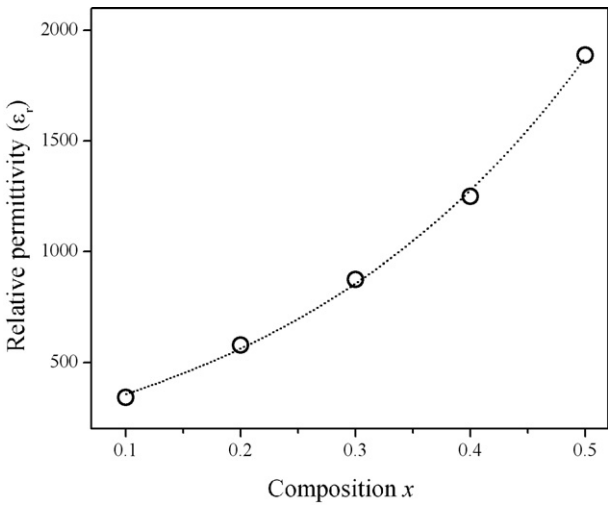

Fig. 7. Relative permittivity of $(1-x)$PZT–xPCoN as a function of compositions.

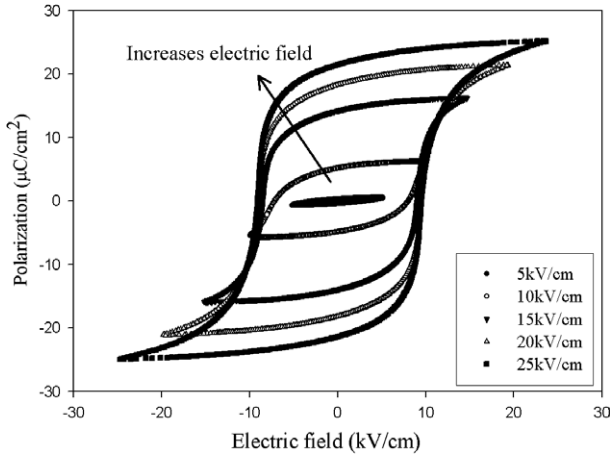

Fig. 8. Polarization of $(1-x)$PZT–xPCoN ceramics with $x = 0.1$ as a function of electric fields.

Fig. 9 illustrates the P–E curves of the samples with $x = 0.0$, 0.1 and 0.5 measured at 25 kV/cm. All compositions show symmetry in shape and reveal rectangular hysteresis loops. From the fully saturated loops, the remanent polarization P_r and coercive field E_c were determined. The values of P_r and E_c for composition $x = 0.1$ are 21.4 μC/cm^2 and 9 kV/cm, respectively, whereas for composition $x = 0.0$ the remanent polarization P_r is 15.2 μC/cm^2. At the composition $0.0 \leqslant x \leqslant 0.5$, the hysteresis loop has a typical "square" form stipulated by switching of a domain structure in an electrical field, which is typical of a phase that contains long-range cooperation between dipoles. That is characteristic of a ferroelectric micro-domain state. Room temperature values of P_r are found to be ~15.2, 21.4 and 25.3 μC/cm^2 for composition $x = 0.0$, 0.1 and 0.5 samples, respectively. The results on other compositions are also listed Table 1.

It is seen that the samples with compositions $x = 0.1$ and 0.5 exhibit the highest saturation and remnant polarization among all the ceramics studied. As indicated by the above

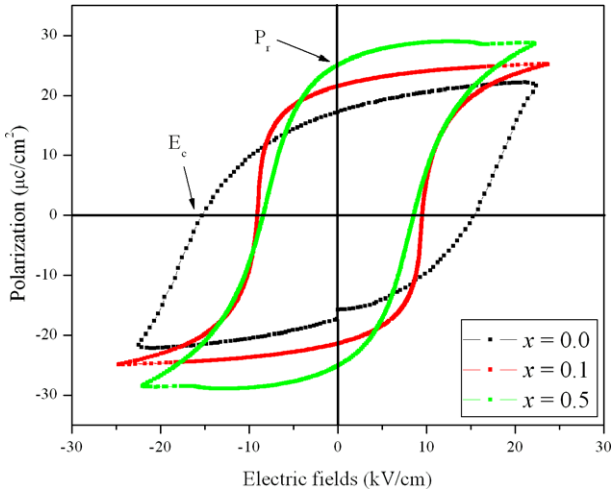

Fig. 9. Hysteresis loops of the $(1-x)$PZT–xPCoN ceramics with $x = 0.0$, 0.1 and 0.5 measured at 25 kV/cm.

Table 1
Polarization hysteresis data as a function of x in the $(1-x)$PZT–xPCoN system

Composition	P_s (μC/cm^2)	P_r (μC/cm^2)	E_c (kV/cm)
$x = 0.0$	19.3	15.2	16.7
$x = 0.1$	25.0	21.4	9.0
$x = 0.2$	10.1	9.5	9.7
$x = 0.3$	12.5	7.6	8.4
$x = 0.4$	13.9	8.6	9.8
$x = 0.5$	28.7	25.3	9.3

XRD, the composition with $x = 0.1$ contains both tetragonal and pseudo-cubic phases, so it should favor a strong ferroelectric effect due to the increased ease of reorientation during poling by transformation of a number of 180° domains into 90° ones. From the present results, it also can be revealed that the MPB coexisting in the tetragonal and pseudo-cubic phases in the present system is a broad composition region of $x \sim 0.1$, which exhibits high ferroelectric properties around the center of the MPB. Recent literature reviews [18,21] show that there are 2 MPBs in the PZT–PZN system; first, the separated tetragonal phase with rhombohedra phase at the composition 0.8PZT–0.2PZN and the second MPB showing transformation relaxor pseudo-cubic ferroelectric to normal pseudo-cubic ferroelectric at the composition 0.5PZT–0.5PZN [7]. It is interesting to note that the composition $x = 0.5$ in PZT–PCoN system may be attributed to the transition from normal ferroelectric to relaxor ferroelectric which is similar to the PZT–PZN and PZT–PNN system [6,7,21].

4. Conclusions

The effect of PCoN modification on the phase formation and transition mechanism of perovskite PZT–PCoN ceramics has been investigated for various chemical compositions. X-ray diffraction has indicated that except at $x = 0.5$, complete solid solutions occur across the entire compositional range of the $(1-x)Pb(Zr_{0.5}Ti_{0.5})O_3$–$xPb(Co_{1/3}Nb_{2/3})O_3$ system. PZT ceramic was identified by XRD as a single-phase material with a perovskite structure having tetragonal symmetry, while the mixed compositions showed a gradual change from tetragonal to pseudo-cubic symmetry, with a possible morphotropic phase boundary (MPB) between the two phases near the 0.9PZT–0.1PCoN composition. Ferroelectric and dielectric properties of the PZT–PCoN ceramics were investigated. The maximum value of remnant polarization P_r (25.3 μC/cm^2) was obtained for the 0.5PZT–0.5PCoN ceramic. Most importantly, this study showed that the addition of PCoN could improve the ferroelectric behavior in PZT ceramics.

Acknowledgements

This work was supported by the Thailand Research Fund (TRF), the Commission on Higher Education (CHE), National Research Council of Thailand (NRCT),

Thailand Graduate Institute of Science and Technology (TGIST) and King Mongkut's Institute of Technology Ladkrabang (KMITL).

References

[1] K. Uchino, Ferroelectric Devices, Marcel Dekker, Inc., New York, 2000.
[2] Y. Xu, Ferroelectric Materials and Their Application, Elsevier Science Publishers B.V., 1991.
[3] S.-E. Park, T.R. Shrout, IEEE Tr. UFFC. 44 (1997) 1140.
[4] J. Kuwata, K. Uchino, S. Nomura, Ferroelectrics 37 (1981) 579.
[5] M.L. Mulvihill, L.E. Cross, W. Cao, K. Uchino, J. Am. Ceram. Soc. 80 (1997) 1462.
[6] N. Vittayakorn, G. Rujijanagul, X. Tan, M.A. Marquardt, D.P. Cann, J. Appl. Phys. 96 (2004) 5103.
[7] H. Fan, H.-E. Kim, J. Mater. Res. 17 (2002) 180.
[8] O. Furukawn, Y. Yamashita, M. Harata, T. Takahashi, K. Inagai, Jpn. J. Appl. Phys. 24 (1985) 96.
[9] V.J. Tennery, K.W. Hang, R.E. Novak, J. Am.Ceram. Soc. 51 (1968) 671.
[10] D. Luff, R. Lane, K.R. Brown, H.J. Marshallsay, Trans. J. Br. Ceram. Soc. 73 (1974) 251.
[11] G.A. Smolenskii, A.L. Agranovskaya, Sov. Phys.-Tech. Phys. (1958) 1380.
[12] A. Ngamjarurojana, O. Khamman, R. Yimnirun, S. Ananta, Mater. Lett. 60 (2006) 2867.
[13] N. Vittayakorn, S. Wirunchit, Smart Mater. Struct. 16 (2007) 851.
[14] R. Wongmaneerung, R. Yimnirun, S. Ananta, Mater. Lett. 60 (2006) 2666.
[15] R. Wongmaneerung, T. Sarakonsri, R. Yimnirun, S. Ananta, Mater. Sci. Eng. B 130 (2006) 246.
[16] T.R. Shrout, A. Halliyal, Am. Ceram. Soc. Bull. 66 (1987) 704.
[17] N. Vittayakorn, C. Puchmark, G. Rujijanagul, X. Tan, D.P. Cann, Curr. Appl. Phys. 6 (2006) 303.
[18] N. Vittayakorn, G. Rujijanagul, X. Tan, H. He, M.A. Marquardt, D.P. Cann, J. Electroceram. 16 (2006) 141.
[19] S. Wongsaenmai, Y. Laosiritaworn, S. Ananta, R. Yimnirun, Mater. Sci. Eng. B 128 (2005) 83.
[20] N. Vittayakorn, G. Rujijanagul, T. Tunkasiri, X. Tan, D.P. Cann, J. Mater. Res. 18 (2003) 2882.
[21] H. Fan, H.-E. Kim, J. Appl. Phys. 91 (2002) 317.

Available online at www.sciencedirect.com
ScienceDirect
Materials Letters 62 (2008) 352–356
materials letters
www.elsevier.com/locate/matlet

Thermal expansion measurements in the relaxor ferroelectric PIN–PT system

Supattra Wongsaenmai [a,*], Rattikorn Yimnirun [a,c,1], Supon Ananta [a], Ruyan Guo [b], Amar S. Bhalla [b,2]

[a] Department of Physics, Faculty of Science, Chiang Mai University, Chiang Mai 50200, Thailand
[b] Materials Research Laboratory, The Pennsylvania State University, University Park, PA 16802, USA
[c] NANOTEC Center of Excellence at Chiang Mai University, Chiang Mai 50200, Thailand

Received 11 February 2007; accepted 11 May 2007
Available online 18 May 2007

Abstract

Thermal expansion was measured for the ceramic compositions $(1-x)Pb(In_{0.5}Nb_{0.5})O_3-(x)PbTiO_3$ ($x=0.0$, 0.1, 0.2 and 0.3) prepared via the wolframite method. The deviation from the straight line below Burns temperature for all the compositions was due to the dynamic polarization fluctuations. Burns temperature was determined and found to increase with increasing PT concentration. The local polarization was calculated from the thermal expansion data. The calculated local polarization and the measured reversible spontaneous polarization were compared and the relaxor behavior of the PIN–PT compositions was analyzed.

Keywords: PIN–PT; Relaxor ferroelectric; Thermal expansion; Burns temperature; Glassy polarization phase

1. Introduction

Relaxor behavior in the perovskite mixed oxides has been the topic of several reports. There are several models which attempted to explain the exact behavior of the relaxor but none can completely explain their interesting properties. The composition fluctuation model by Smolenskii [1] proposed that the different local Curie temperatures lead to broad diffuse phase transition. Cross proposed the origin of polarization mechanism analogous to the superparamagnetic cluster material [2]. The broad distribution and frequency dispersion of the dielectric properties originate from slowing down of polarization reorientation in each cluster. The glass-like behavior was considered by Viehland to extend Cross' model and was analogous to the magnetic spin glass [3]. The freezing temperature was defined as the macroscopic polarization emergence. The glassy polarization phase of relaxor ferroelectrics has been considered after Burns' and Dacol's measurements of the optic index of refraction, $n(T)$, dependence on the temperature [4–7]. The deviation from linear behavior of $n(T)$ was observed starting at Burns temperature (T_d) which is much higher than the transition temperature (T_m). This behavior was interpreted in terms of the local polar regions of randomly orientated irreversible polarization (P_d) and of very small number of unit cells, which grow with the reducing temperature. The local polarization exists above the transition temperature while disappears or is unmeasurable above Burns temperature [5]. Several other techniques, including refractive index measurements [4], Raman scattering [8], neutron powder diffraction [9], neutron elastic scattering [10], dynamic light scattering [11] and dielectric measurements [12-13] have also been used to measure Burns temperature and to explain the glass-like behavior. Thermal expansions which are related to the square of the polarization can be used to study phase transition, thermal expansion coefficient and anisotropies to estimate the dynamic polarization in the relaxor systems. Therefore, Burns temperature and local polarization can be detected by this technique [14,15].

$Pb(In_{0.5}Nb_{0.5})O_3$–PIN is a member of the relaxor family with a 1:1 stoichiometry at B-site and which can be converted from disordered state into ordered state by thermal treatment [16]. The disordered state of PIN exhibits a relaxor behavior and

* Corresponding author. Tel.: +66 53 943445.
E-mail addresses: wongsaenmai@yahoo.com (S. Wongsaenmai), rattikornyimnirun@yahoo.com (R. Yimnirun), asb2@psu.edu (A.S. Bhalla).
[1] Tel.: +66 53 943367.
[2] Tel.: +1 814 8659232.

0167-577X/$ - see front matter © 2007 Elsevier B.V. All rights reserved.
doi:10.1016/j.matlet.2007.05.029

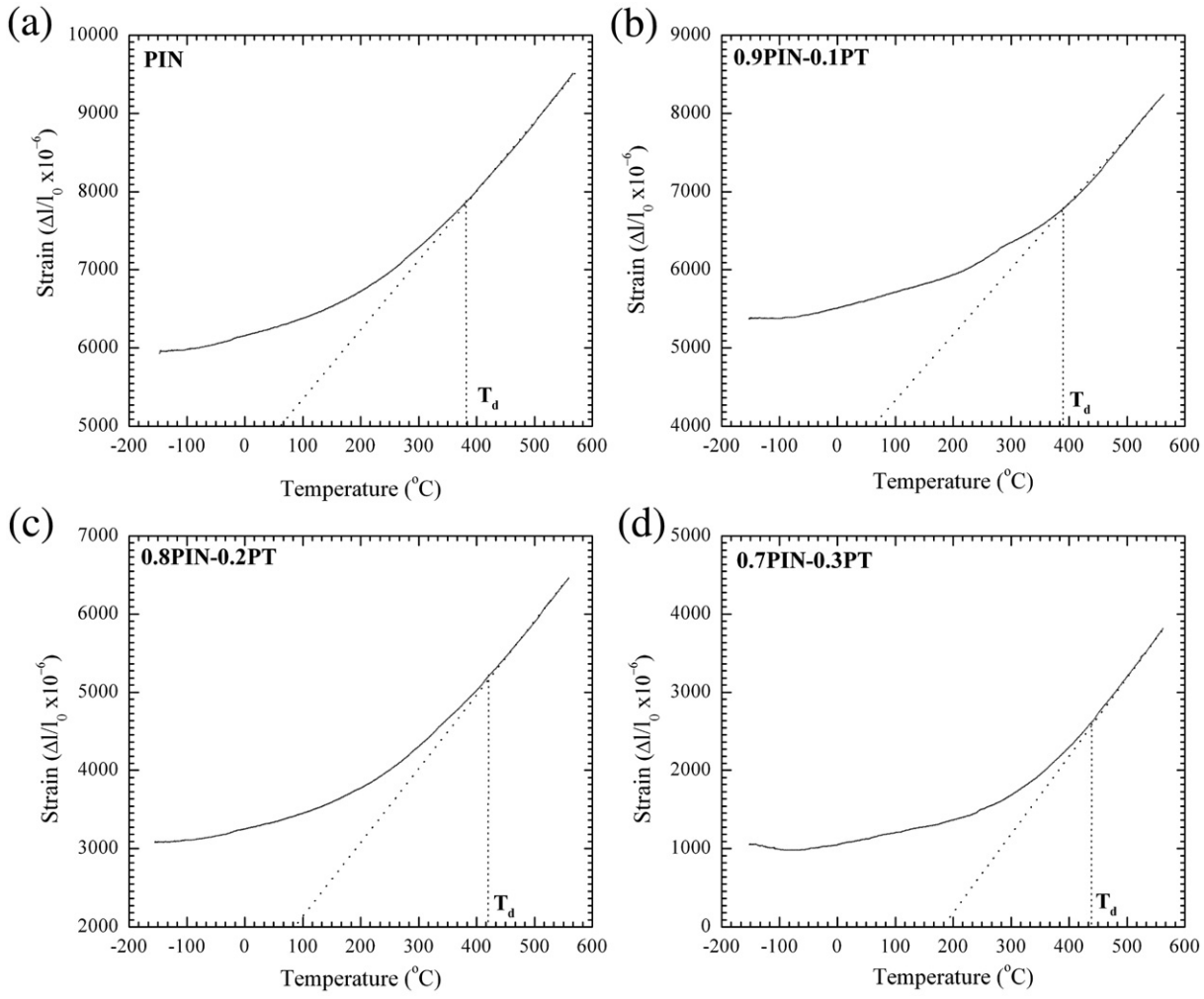

Fig. 1. Temperature dependence of the strain for $(1-x)$PIN–(x)PT system (a) $x=0.0$, (b) $x=0.1$, (c) $x=0.2$ and (d) $x=0.3$.

shows a broad dielectric maximum near 66°C [17,18]. The ordered state of PIN shows an antiferroelectric behavior with a sharp steep in the dielectric constant vs. temperature curve observed at 168°C [18,19]. There are several reports, which attempted to investigate the properties of the solid solution of relaxor ferroelectric PIN and normal ferroelectric PT, including the relaxor behavior analysis from the dielectric properties, the deviation of the Curie–Weiss law and the glass-like behavior using the Vogel–Fulcher relation [20,21]. The relaxor behavior analyzed from the thermal expansion measurement has been studied in several relaxor ferroelectric systems e.g. PMN–PT, PMN, PZN, PLZT and tungsten bronze structure family [5,7,14,22–24]. Though studies on dielectric and ferroelectric properties of the PIN-based system have been reported [25,26], there have been no thermal expansion measurement and analysis of relaxor behavior of the PIN-based system.

In this paper, the relaxor behavior of PIN–PT system was analyzed from the thermal expansion data. The glassy polarization and the relaxor behavior were studied and Burns temperature and the local polarizations were estimated. The results showed the Burns temperature between 380°C and 435°C for all of the compositions. The local polarization was calculated and compared with the reversible spontaneous polarization measurement.

2. Experimental

The powders of $(1-x)Pb(In_{0.5}Nb_{0.5})O_3$–$(x)PbTiO_3$ ($x=0.0$, 0.1, 0.2 and 0.3, abbreviated as PIN–PT) were synthesized by a two-step solid solution reaction method [27]. The wolframite $InNbO_4$ was first prepared from oxide powder of In_2O_3 and Nb_2O_5 [28]. Mixed powder was milled and calcined at 1100°C

Table 1
The parameters derived from the thermal expansion measurement of $(1-x)$PIN–(x)PT system

Composition (x)	T_m (°C) at 1 kHz	T_d (°C)	Properties at room temperature		
			$\alpha\times10^{-6}$ (°C^{-1})	P_s (μC/cm^2)	P_d (μC/cm^2)
0.0	70	380	2.2	7.6	16.0
0.1	144	391	2.9	15.2	17.7
0.2	208	420	3.4	18.7	19.9
0.3	279	435	4.0	23.3	24.1

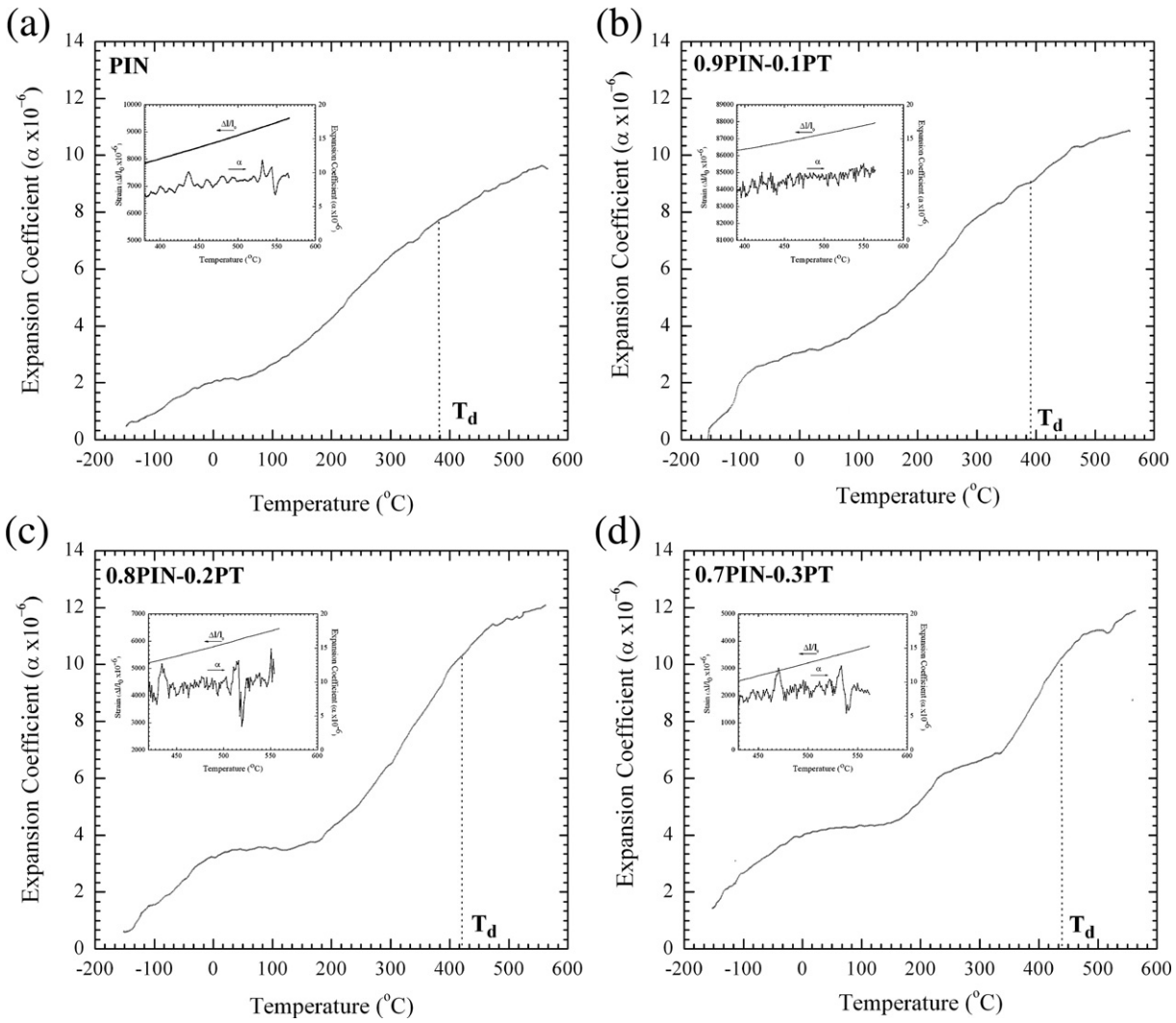

Fig. 2. Temperature dependence of thermal expansion coefficient (α) for $(1-x)$PIN–(x)PT system (a) $x=0.0$, (b) $x=0.1$, (c) $x=0.2$ and (d) $x=0.3$. (Inset shows a closer look at temperature dependence of $\Delta l/l$ and α above Burns temperature.)

temperature for 2h to obtain the intermediate precursor $InNbO_4$ [29]. The wolframite precursor was then mixed with reagent grade powder of PbO, TiO_2 for PIN–PT. Excess amounts of PbO (2%) and In_2O_3 (2%) were added at this stage. The mixtures were milled again following the intermediate precursor stage. After drying, the mixtures were calcined at temperature between 800°C and 1000°C with soaking time of 2h [30]. Pellets were pressed with 1% PVA. The pressed pellets were sintered with the soaking time of 2h in a double crucible configuration at temperature from 1100°C to 1125°C. To prevent PbO loss, the pellets were buried in protective powders.

The ceramics of PIN–PT were cut to rectangular bars with dimension 5mm × 1mm × 1mm. The effect of temperature on sample expansion (strain) was measured with a linear voltage-differential transformer (LVDT) dilatometer (Series 6500, theta industries, Inc., NY). The measurements were performed over the temperature range −145°C and 550°C with heating rate of 2°C/min, as reported in other relaxor ferroelectric systems [31,32]. However, it should also be noted that these measurements could be rate dependent, and further investigation is of interest.

3. Results and discussion

The thermal strain dependences of temperature of PIN–PT ceramics are shown in Fig. 1. There is no clear anomaly of the thermal strain at transition temperature. This behavior differs from the normal ferroelectrics which generally show an abrupt discontinuity (first orders) at the transition temperature and follow the linear relationship above transition temperature. The deviation from the straight line or linear relationship below the Burns temperature was observed for all the compositions. The values of Burns temperature were in the temperature range from 380°C to 435°C depending on PT concentration, as shown in Table 1. The Burns temperature is much higher than the transition temperature for pure PIN and other relaxor ferroelectric systems [6,25,26]. The difference between transition temperature and Burns temperature also decreases with increasing PT concentration.

Similar behavior has been reported in other quadratic relationships with the polarization such as the deviation from the straight line at transition temperature in the refractive index and birefringence measurements [33]. The increase of Burns temperature due to addition of PT was attributed to stronger correlation between the polar and slightly anisotropic normal PT ferroelectric [10]. Therefore, the increase of PT concentration leads to decrease of closeness of the

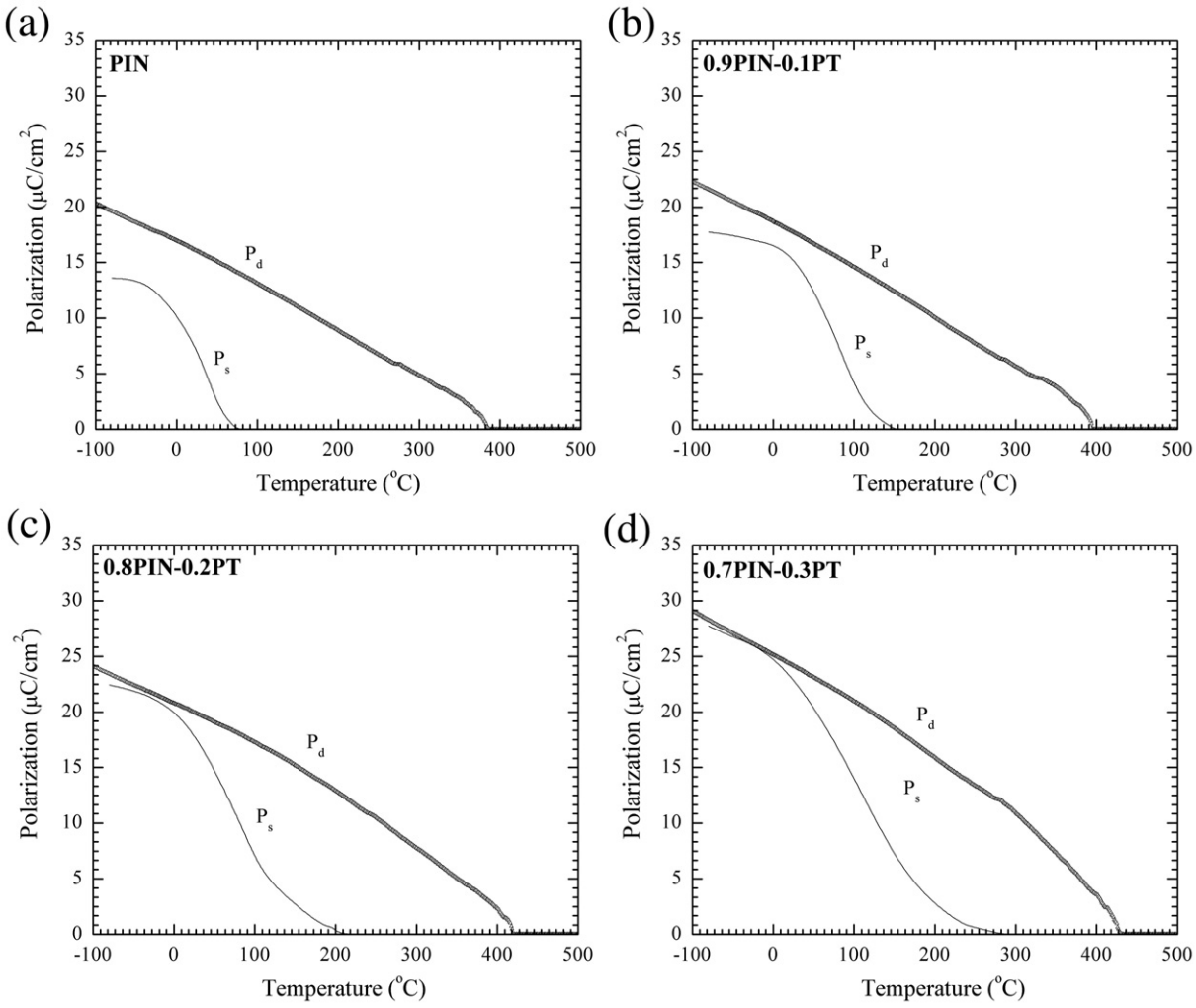

Fig. 3. Comparison of P_d and P_s of both $(1-x)$PIN–(x)PT system (a) $x=0.0$, (b) $x=0.1$, (c) $x=0.2$ and (d) $x=0.3$.

transition and Burns temperatures. This contribution follows with the decrease in relaxor ferroelectric nature in PIN ceramics which eventually decrease the degree of relaxor behavior with increasing PT concentration. At temperatures high above Burns temperature the correlation between thermal strain and temperature shows a linear relationship leading to no polarization effect.

The thermal expansion coefficient (α), defined as $\alpha_T = dx_T/dT$ [32], is calculated and listed in Table 1. The small thermal expansion coefficient values are similar to those reported for other relaxor ferroelectrics [34]. The plots of the thermal expansion coefficient vs. temperature are shown in Fig. 2. The thermal expansion coefficient gradually changes with temperature above Burns temperature, and then thermal expansion coefficient decreases more steeply below Burns temperature. Though the linear relation of strain vs. temperature above Burns temperature was shown in Fig. 1, the thermal expansion coefficients were found to change with temperature. The small fluctuations were shown in the inset of Fig. 2. The possible origin of this temperature dependence and fluctuation is not clear, but could be attributed to differential calculation error over small temperature range. Similar problem has also been reported earlier [24]. Probably, the results of the thermal expansion coefficient calculation are not suitable for defining Burns temperatures. Therefore, strain vs. temperature measurement is more suitable for Burns temperature identification.

The observation can be explained due to the results of the glassy polarization phase which occurs from charge difference of ions on the B-site in highly disordered state at the high temperature leading to the strong breaking of the translational symmetry [6]. Then, the random orientation, unstable reversible polarization and very small size of local polarization arise below Burns temperature.

The glassy polarization phase was interpreted with local polarization ($\overline{P}^2_d$) existent below Burns temperature. It is known that there is no stable and finite local polarization ($P=0$) above dielectric transition maxima temperature but there is a stable and finite square of polarization ($\overline{P}^2 \neq 0$). These dynamic local polarizations above transition temperature can be detected by the quadratic relationship with the thermal expansion behavior and can be measured. The polarization is calculated from the relationship between total thermal strain (or linear thermal expansion) and electrostriction as shown below.

$$x_{11} = \alpha(T - T_0) + (Q_{11} + 2Q_{12})\overline{P}^2 \quad (1)$$

where α is the thermal expansion coefficient, T_0 is the reference temperature and Q_{11} and Q_{12} are the electrostrictive coefficients [35]. In this paper the electrostrictive coefficient of a typical perovskite structure $PbTiO_3$ was used for the calculation of $\overline{P}^2$ [36] as it is assumed that for most materials electrostrictive coefficients are of the same range.

Fig. 3 shows the temperature dependence of the polarization. The local polarization (P_d) was calculated from Eq. (1) using the thermal strain data. The reversible spontaneous polarization (P_r) was obtained from ferroelectric (P–E) hysteresis measurement. The local polarization curves show slow decrease to zero at Burns temperature while the reversible polarization drops to zero at the transition temperature. The gradual change of reversible polarization near transition temperature is due to the distribution of polar nano-region in relaxor ferroelectric. On the other hand, the local polarization shows a gradual decrease with temperature up to the Burns temperature. The separation of both polarization curves above the transition temperature also suggests the existence of the dynamic nature of the local polarization. The value of the local polarization is closer to the reversible polarization at low temperature indicating development of stable polarization with reducing temperature. If the temperature is low enough to freeze the dynamic behavior of the polarization, the reversible polarization value will be equal to the local polarization [7]. However, it is found that the local polarization is far from the reversible polarization value at low temperature for pure PIN and the composition of $x=0.1$, suggesting the presence of enough dynamic polar regions. Similar separation of the polarizations at low temperature has also been observed in PMN and PZN [6].

4. Conclusions

The relaxor behavior of the ceramics of compositions $(1-x)Pb(In_{0.5}Nb_{0.5})O_3$–$(x)PbTiO_3$ ($x=0.0$, 0.1, 0.2 and 0.3) prepared via the wolframite method was studied by the thermal expansion measurement over the temperature range −145 °C and 550 °C. It was found that the thermal expansion exhibits a linear relation with temperature at high temperature, and starts to deviate at Burns temperature between 380 °C and 435 °C. Pure PIN shows the Burns temperature far above the transition temperature, and the difference between these temperatures is lower with increasing PT concentration. The deviation from linear behavior was interpreted with the existence of the dynamic polarization between the transition temperature and Burns temperature. The local dynamic polarization was calculated from the thermal expansion data and compared with the reversible spontaneous polarization measurement. The separation of both polarizations was very clear at high temperature, while it was closer at temperature below T_m. The results confirm that the local polarization exists in PIN–PT and increase as the temperature decreases below T_m.

Acknowledgements

This work was supported by the Thailand Research Fund (TRF), Commission on Higher Education (CHE), Graduate School of Chiang Mai University and Ministry of University Affairs, the National Nanotechnology Center (NANOTEC), NSTDA, Ministry of Science and Technology, through its program of Center of Excellence Network, Thailand, and the relaxor & metamaterials grants of NSF/DMR, USA.

References

[1] G.A. Smolenskii, Jpn. J. Appl. Phys. 28 (1970) 1970.
[2] L.E. Cross, Ferroelectrics 76 (1987) 246.
[3] D. Viehland, S.J. Jang, L.E. Cross, J. Appl. Phys. 68 (6) (1990) 2916.
[4] G. Burns, F.H. Dacol, Solid State Commun. 42 (1) (1982) 9.
[5] G. Burns, F.H. Dacol, Phys. Rev., B 28 (5) (1983) 2527.
[6] G. Burns, F.H. Dacol, Solid State Commun. 48 (10) (1983) 853.
[7] G. Burns, F.H. Dacol, Ferroelectrics 52 (1983) 103.
[8] G. Burns, F.H. Dacol, Solid State Commun. 58 (1986) 567.
[9] J. Zhao, A.E. Glazounov, Q.M. Zhang, B. Toby, Appl. Phys. Lett. 72 (1998) 1048.
[10] D. La-Orauttapong, J. Toulouse, Z.-G. Ye, W. Chen, R. Erwin, J.L. Robertson, Phys. Rev., B 67 (2003) 134110.
[11] W. Kleemann, P. Licinio, T. Woike, R. Pankrath, Phys. Rev. Lett. 86 (2001) 6014.
[12] D. Viehland, S.J. Jang, L.E. Cross, M. Wuttig, Phys. Rev., B 46 (1992) 8003.
[13] J. Dec, W. Kleemann, V. Bobnar, Z. Kutnjak, A. Levstik, R. Pirc, R. Pankrath, Europhys. Lett. 55 (2001) 781.
[14] A.S. Bhalla, R. Guo, L.E. Cross, G. Burns, F.H. Dacol, R.R. Neurgaonkar, Phys. Rev., B 36 (4) (1987) 2030.
[15] A.S. Bhalla, R. Guo, L.E. Cross, G. Burns, F.H. Dacol, R.R. Neurgaonkar, Ferroelectrics 106 (1990) 161.
[16] C.A. Randall, A.S. Bhalla, Jpn. J. Appl. Phys. 29 (2) (1990) 327.
[17] E.F. Alberta, A.S. Bhalla, Mater. Lett. 29 (1996) 127.
[18] E.F. Alberta, A.S. Bhalla, J. Phys. Chem. Solids 63 (2002) 1759.
[19] M. Iwata, S. Katagiri, H. Orihara, M. Maeda, I. Zusuki, H. Ohwa, N. Yasuda, Y. Ishibashi, Ferroelectrics 301 (2004) 179.
[20] S. Wongsaenmai, A.S. Bhalla, R. Guo, S. Ananta, R. Yimnirun, Ferroelectr. Lett. 34 (2007) 36.
[21] A.A. Bokov, M.A. Leshchenko, M.A. Malitskaya, I.P. Raevski, J. Phys., Condens. Matter 11 (1999) 4899.
[22] H. Arndt, G. Schmidt, Ferroelectrics 79 (1988) 149.
[23] G. Burns, F.H. Dacol, Ferroelectrics 104 (1990) 25.
[24] M.V. Gorev, I.N. Flerov, P.H. Sciau, V.S. Bondarev, A.G. LehMann, Ferroelectrics 307 (2004) 127.
[25] S. Wongsaenmai, R. Yimnirun, S. Ananta, J. Alloy. Compd. (in press).
[26] S. Wongsaenmai, R. Yimnirun, S. Ananta, Appl. Phys. A. (in press).
[27] S. Wongsaenmai, R. Yimnirun, S. Ananta, J. Mater. Sci. 128 (2007) 83.
[28] S. Wongsaenmai, R. Yimnirun, S. Ananta, Mater. Letter. 61 (2007) 2426.
[29] S. Wongsaenmai, O. Khamman, S. Ananta, R. Yimnirun, J. Electroceram. (in press).
[30] N. Yasuda, M. Fujie, Jnp. J. Appl. Phys. 31 (1992) 3128.
[31] D.K. Agrawal, R. Roy, H.A. Mckinstry, Mater. Res. Bull. 22 (1987) 83.
[32] V. Mueller, L. Läger, H. Beige, H.-P. Abicht, Thomas Müller, Solid State Commun. 129 (2004) 757.
[33] G. Burns, Phase Transit. 5 (1985) 261.
[34] L.E. Cross, S.J. Jang, R.E. Newhnam, S. Nomura, K. Uchino, Ferroelectrics 23 (1980) 187.
[35] L.E. Cross, Ferroelectrics 76 (1987) 241.
[36] S. Nomura, K. Uchino, Ferroelectrics 41 (1982) 117.

Japanese Journal of Applied Physics
Vol. 47, No. 2, 2008, pp. 998–1002

Synthesis and Dielectric and Ferroelectric Properties of Ceramics in $(1-x)Pb(Zr_{1/2}Ti_{1/2})O_3$–$(x)Pb(Co_{1/3}Nb_{2/3})O_3$ System

Anurak PRASATKHETRAGARN*, Naratip VITTAYAKORN[1], Supon ANANTA, Rattikorn YIMNIRUN, and David P. CANN[2]

Department of Physics, Faculty of Science, Chiang Mai University, Chiang Mai 50200, Thailand
[1]*Department of Chemistry, Faculty of Science, King Mongkut's Institute of Technology Ladkrabang, Bangkok 10520, Thailand*
[2]*Materials Science, Department of Mechanical Engineering, Oregon State University, Corvallis, OR 97331, U.S.A.*

(Received August 16, 2007; revised September 28, 2007; accepted October 26, 2007; published online February 15, 2008)

Ceramics in a PZT–PCN system with the formula $(1-x)Pb(Zr_{1/2}Ti_{1/2})O_3$–$(x)Pb(Co_{1/3}Nb_{2/3})O_3$, where $x = 0.1$–0.5, were prepared using a solid-state mixed-oxide technique (the columbite-wolframite precursor method). The phase formation behavior and microstructure were studied using X-ray diffraction (XRD) analysis and scanning electron microscopy (SEM), respectively. The dielectric and ferroelectric properties of the compounds were studied and discussed. Phase-pure perovskites of PZT–PCN ceramics were obtained over a wide compositional range. In addition, the XRD, dielectric, and ferroelectric properties confirmed that the morphotropic phase boundary (MPB) composition between the tetragonal and pseudo cubic phases of this system lied between $0.2 \leq x \leq 0.3$. [DOI: 10.1143/JJAP.47.998]

KEYWORDS: ferroelectric properties, perovskites, MPB, phase transition

1. Introduction

Lead-based perovskite-type solid solutions consisting of ferroelectric and relaxor materials have attracted more and more fundamental and practical attention because of their excellent dielectric, piezoelectric, and electrostrictive properties, which are useful in actuating and sensing applications.[1)] Recently, many piezoelectric ceramic materials have been developed from binary systems containing a combination of relaxor and normal ferroelectric materials[2)] that yield high dielectric permittivities [e.g., $Pb(Zn_{1/3}Nb_{2/3})O_3$–$PbTiO_3$ (PZN–PT)[3,4)] and $Pb(Zr_{1/2}Ti_{1/2})O_3$–$Pb(Ni_{1/3}Nb_{2/3})O_3$ (PZT–PNN)[5)]], excellent piezoelectric coefficients [e.g., $Pb(Zn_{1/3}Nb_{2/3})O_3$–$PbTiO_3$ (PZN–PT),[3,4)] $Pb(Zr_{1/2}Ti_{1/2})O_3$–$Pb(Zn_{1/3}Nb_{2/3})O_3$ (PZN–PZT),[6)] and $Pb(Sc_{1/3}Nb_{2/3})O_3$–$PbTiO_3$ (PSN–PT)[7,8)]], and high pyroelectric coefficients [e.g., $Pb(Ni_{1/3}Nb_{2/3})O_3$–$PbTiO_3$–$PbZrO_3$ (PNN–PT–PZ)[9)]]. Of the lead-based complex perovskites, lead zirconate titanate [$Pb(Zr_{1/2}Ti_{1/2})O_3$ or PZT] ceramics have been investigated from both fundamental and applied viewpoints.[10)] A solid solution of $Pb(Zr_{1-x}Ti_x)O_3$ (PZT) was found to host exceptionally high value for dielectric and piezoelectric properties for compositions close to the morphotropic phase boundary (MPB). This MPB is located at a $PbTiO_3$:$PbZrO_3$ of $\sim 1:1$ and separates the Ti-rich tetragonal phase from the Zr-rich rhombohedral phase.[10)] Furthermore, it has a high T_C of 390 °C, which allows piezoelectric devices to be operated at relatively high temperatures. Most commercial PZT ceramics are designed in the vicinity of the MPB with various doping methods in order to achieve high properties.

Lead cobalt niobate (PCN) is a perovskite relaxor ferroelectric with a broad diffuse phase transition near −70 °C.[11)] The structure is cubic at room temperature (RT). In this compound, the octahedral sites of the crystal are randomly occupied by Co^{2+} and Nb^{5+} ions.[12)] Malkov and Venevtsev have indicated that there are large deviations in the temperatures at which the permittivity is maximum (T_m) for single-crystal and ceramic samples.[13)] The effects of the DC bias on the dielectric properties have been reported as a function of temperature for single-crystal $Pb(Co_{1/3}Nb_{2/3})O_3$ with a diffuse phase transition.[14)] Although the paraelectric–ferroelectric transition temperature of PCN is below RT, it can be easily shifted upward with the addition of $PbTiO_3$ (PT), which is a normal ferroelectric compound with a phase transition at 490 °C.[15)] In addition, it is well known that the addition of PZT enhances the piezoelectric, dielectric, and ferroelectric properties in a solid solution with a relaxor ferroelectric such as PZT–PZN,[16,17)] PZT–PNN,[5)] and PZT–PMN.[18)] On the basis of this approach, solid solutions of PZT and PCN are expected to synergistically combine the properties of both the normal ferroelectric PZT and relaxor ferroelectric PCN, which could exhibit piezoelectric and dielectric properties that are better than those of the single-phase PZT and PCN.[12,19)] There have been no systematic studies on the electrical properties of ceramics within a wide composition range between PZT and PCN.

The overall purpose of this study is to determine the phase transition, grain size, and composition dependence of the dielectric properties and ferroelectric behavior of ceramics in a $(1-x)Pb(Zr_{1/2}Ti_{1/2})O_3$–$(x)Pb(Co_{1/3}Nb_{2/3})O_3$ (where $x = 0.1$–0.5) binary system prepared using the columbite-wolframite precursor method.

2. Experimental Procedure

Reagent-grade oxides of PbO, CoO, Nb_2O_5, ZrO_2, and TiO_2 (anatase-structure) were used as raw materials. The columbite $CoNb_2O_6$ and wolframite $ZrTiO_4$ precursors were weighed and introduced into the batch calculations. $CoNb_2O_6$ and $ZrTiO_4$ powders were prepared at calcination temperatures of 1100 and 1450 °C for 2 h, respectively. In the present work, $(1-x)Pb(Zr_{1/2}Ti_{1/2})O_3$–$(x)Pb(Co_{1/3}Nb_{2/3})O_3$ samples with compositions of $x = 0.1$–0.5 were prepared from $ZrTiO_4$, $CoNb_2O_6$, and PbO powders. PZT–PCN powders were synthesized using the solid-state reaction of these raw materials and mixed by a vibro-milling technique in ethanol for 1 h. PbO excess of 2.0 mol % was constantly added to compensate for lead losses during calcination and sintering.[17)] After drying, the product was calcined in an alumina crucible at a temperature of 950 °C.

*E-mail address: Prasatkhetragarn@yahoo.com

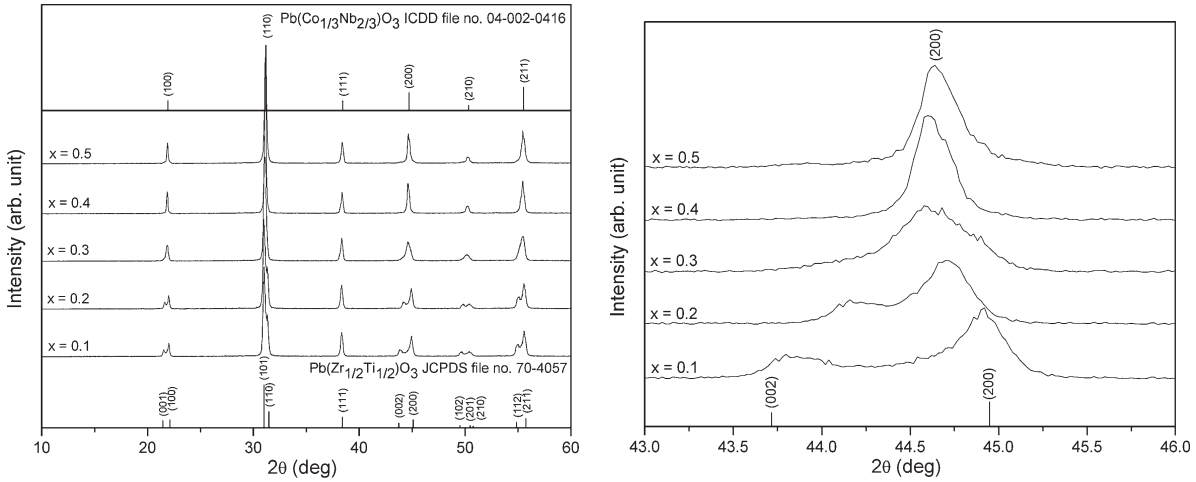

Fig. 1. XRD patterns of $(1-x)$PZT–(x)PCN ceramics, where $x = 0.1$–0.5.

The calcined powders were pressed hydraulically to form disc-shaped pellets with a diameter of 10 mm and a thickness of 1 mm, with 1 wt % poly(vinyl alcohol) (PVA) added as a binder. The pellets were sintered at 1200 °C for 2 h at a heating/cooling rate of 5 °C/min. The phase structure of the powders was analyzed via X-ray diffraction (XRD; Siemens-D500 diffractometer) analysis using Cu Kα radiation. The microstructures of the sintered samples were examined using scanning electron microscopy (SEM; JEOL JSM-840A). The dielectric properties of the samples were measured using an automated measurement system. This system consisted of an LCR meter (Hewlett-Packard HP-4284A) in connection with a Delta Design 9023 temperature chamber and a sample holder (Norwegian Electroceramics) capable of high-temperature measurement. The ferroelectric properties were examined using a simple Sawyer–Tower circuit.[18)]

3. Results and Discussion

The XRD patterns of $(1-x)$PZT–(x)PCN ceramics with various x values are shown in Fig. 1. It can be seen that a complete crystalline solution of the perovskite structure is formed throughout the entire compositional range without the presence of pyrochlore or unwanted phases. From the XRD data, the $Pb(Zr_{1/2}Ti_{1/2})O_3$ ceramic is identified as a single-phase material with a perovskite structure having tetragonal symmetry, which was matched with JCPDS file no. 70-4057. The XRD patterns of the PZT–PCN compositions show a range in symmetry between the tetragonal and pseudo cubic perovskite types.[20)] For a better comparison, ICDD file no. 04-002-0416 for $Pb(Co_{1/3}Nb_{2/3})O_3$ with pseudo cubic structural symmetry is also displayed in Fig. 1. It is clear that the crystal symmetry should change owing to the effects of increasing the PCN fraction and a corresponding decrease in T_C. It is well known that in the pseudo cubic phase, the (200) profile will show a single narrow peak, while in the tetragonal phase, the (200) profile should be split into two peaks. More interestingly, the composition at $x = 0.3$ exhibited peak broadening at a 2θ of $\sim$44–45°, indicating the structural transformation from the tetragonal phase, characterized by the shifting of the (002)/(200) peaks to the pseudo cubic phase. This observation is obviously associated with the composition showing the coexistence of two symmetries, which in this case are the tetragonal and pseudo cubic phases. To a first approximation, it could be said that the composition with $x = 0.3$ is close to the MPB of the $(1-x)$PZT–(x)PCN system, where the structure of the PZT–PCN compositions gradually changes from tetragonal to pseudo cubic. The electrical data described later on will further support this assumption.

The SEM images in Fig. 2 reveal that the addition of PCN resulted in significant changes in the microstructure of the ceramics. Some grains are observed to have irregular shapes with both open and close pores as a result of the high rate of the evaporation of PbO during the sintering.[17)] The images also show that the grain size of the ceramics varied considerably from 0.43 to 19.56 μm (Table I). However, the average grain size significantly decreased with an increase in the content of PCN. It can also be seen that the maximum density is obtained in the 0.7PZT–0.3PCN ceramics, while the minimum density is observed in the 0.5PZT–0.5PCN ceramics. Interestingly, the density results can be correlated to the microstructure because high-density 0.7PZT–0.3PCN ceramics show high degrees of grain close packing, whereas low-density 0.5PZT–0.5PCN ceramics contain many closed pores.

The dielectric properties of $(1-x)$PZT–(x)PCN, where $x = 0.1$–0.5, are illustrated in Fig. 3. At RT, with an increase in the concentration of PCN, the dielectric constant tends to increase because the transition temperature of the PZT–PCN ceramics shift across RT; hence, the value of the dielectric properties measured at RT increased, as shown in Table II. Other authors have reported a similar behavior.[5)] The temperature dependence of the dielectric constant for the compositions of the $(1-x)$PZT–(x)PCN system show broad dielectric peaks with an increase in the concentration of PCN, which indicate a diffuse phase transition. The diffuse phase transition may have been caused by a decrease in grain size; the observed difference in the degree of diffuseness could be a result of the grain size variation, as shown in Table II,[21)] and chemical inhomogenieties within the $(1-x)$PZT–(x)PCN solid solution.[20)]

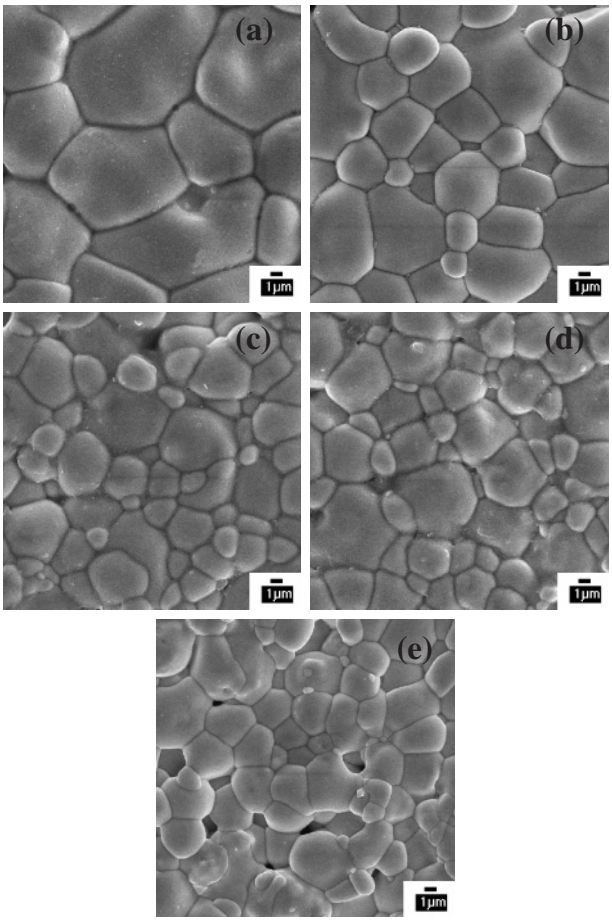

Fig. 2. SEM images of $(1-x)$PZT–(x)PCN ceramics with various compositions: $x =$ (a) 0.1, (b) 0.2, (c) 0.3, (d) 0.4, and (e) 0.5.

Table I. Physical characteristics of $(1-x)$PZT–(x)PCN ceramics, where $x = 0.1$–0.5.

Ceramics ($x = 0.1$–0.5)	Density (g/cm^3)	Grain size range (μm)	Average grain size (μm)
0.9PZT–0.1PCN	7.39 ± 0.05	4.54–19.56	7.45 ± 0.05
0.8PZT–0.2PCN	7.46 ± 0.05	2.60–12.35	4.13 ± 0.05
0.7PZT–0.3PCN	7.62 ± 0.05	0.43–9.48	2.82 ± 0.05
0.6PZT–0.4PCN	7.42 ± 0.05	0.60–10.75	2.77 ± 0.05
0.5PZT–0.5PCN	7.31 ± 0.05	0.47–9.53	2.61 ± 0.05

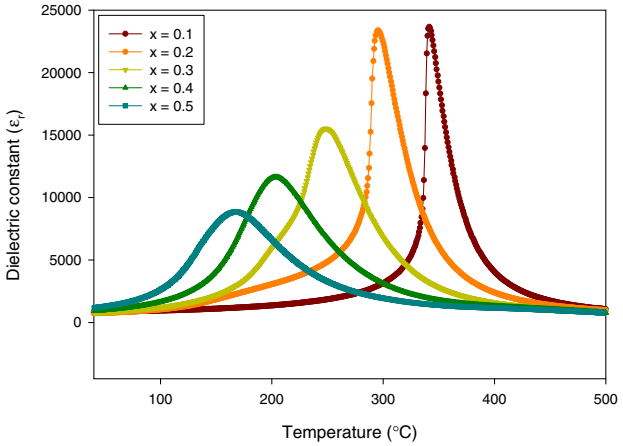

Fig. 3. (Color online) Dielectric constant (ε_r) of $(1-x)$PZT–(x)PCN ceramics at 100 kHz.

It should be noted that the formation of MPB could be clearly seen by the crystal structure analysis as described earlier. As is well known, the value of the dielectric and ferroelectric properties of a solid solution with MPB usually maximize approximately at the MPB. An anomaly at the MPB has been observed by our group in solid solution (x)PZT–$(1-x)$PNN.[5] However, no anomalies approximately at the MPB in the dielectric properties (Table II) could be found in the present work. In addition, the ferroelectric properties at approximately $x = 0.3$ are only slightly different from those of other compositions ($x = 0.2$, 0.4), rather than being "anomalously high". This could possibly be caused by a substitution of Ni^{2+} by Co^{2+} in the B-site, which shifts the MPB composition from $x = 0.2$ in the PZT–PNN system to $0.2 \leq x \leq 0.3$ in PZT–PCN. Since in this current work, we only started with compositions at 0.1 intervals, the exact MPB composition could not be clearly identified. However, as seen in Table II, the argument that the MPB composition should fall between $0.2 \leq x \leq 0.3$ in PZT–PCN is supported by all the XRD and electrical data, which show drastic decreases in the value of the electrical properties in compositions with $x > 0.3$.

The temperature dependence of the dielectric constant (ε_r) measured at 100 kHz for the $(1-x)$PZT–(x)PCN samples with $x = 0.1$–0.5 is shown in Fig. 3. In an ideal solid solution of PZT and PCN, the transition temperature is expected to vary linearly between 341 and 167 °C. As shown in Table II, the Curie temperature decreased as expected with an increase in PCN content. However, the ε_r peaks became broader with increasing PCN content at $x \geq 0.3$. It was confirmed that the composition with $0.2 \leq x \leq 0.3$ is close to the morphotropic phase boundary (MPB) of the $(1-x)Pb(Zr_{1/2}Ti_{1/2})O_3$–$(x)Pb(Co_{1/3}Nb_{2/3})O_3$ system.

Table II. Dielectric and ferroelectric properties of $(1-x)$PZT–(x)PCN ceramics, where $x = 0.1$–0.5.

Ceramics ($x = 0.1$–0.5)	T_C (°C)	Dielectric properties				Ferroelectric properties (at 25 °C)			Loop squareness (R_{sq})
		ε_{max}	ε_{RT}	γ	δ	P_r ($\mu C/cm^2$)	P_s ($\mu C/cm^2$)	E_c (kV/cm)	
0.9PZT–0.1PCN	341.40	23700	740	1.52	14.72	2.9	4.1	8.45	1.52
0.8PZT–0.2PCN	295.50	23400	800	1.68	15.73	20.1	21.6	6.84	1.91
0.7PZT–0.3PCN	248.40	15500	840	1.81	16.55	20.9	22.6	6.92	1.94
0.6PZT–0.4PCN	203.50	11600	910	1.82	16.68	18.6	20.3	6.30	1.93
0.5PZT–0.5PCN	167.50	8900	1180	1.97	16.92	14.5	15.2	6.10	1.92

To further understand the dielectric behavior of the PZT–PCN system, the ferroelectric transition can analyzed through the Curie–Weiss relationship. For normal ferroelectrics such as PZT and PCN, above the Curie temperature, the dielectric constant follows the following equation:

$$\varepsilon = \frac{c}{T - T_0}, \tag{1}$$

where c is the Curie constant and T_0 is the Curie–Weiss temperature.[10,21,23] For a ferroelectric with a diffuse phase transition such as the PZT–PCN solid solutions, the following equation applies:

$$\frac{1}{\varepsilon} \approx (T - T_m)^2, \tag{2}$$

The above equation has been shown to be valid over a wide temperature range compared with the normal Curie–Weiss law [eq. (1)].[24,25] In eq. (2), T_m is the temperature at which the dielectric constant is maximum. If the local Curie temperature distribution is Gaussian, the reciprocal permittivity can be written in the form:[5,24]

$$\frac{1}{\varepsilon} = \frac{1}{\varepsilon_m} + \frac{(T - T_m)^\gamma}{2\varepsilon_m \delta^2}, \tag{3}$$

where ε_m is the maximum permittivity, γ is the diffusivity, and δ is the diffuseness parameter. For $(1-x)$PZT–(x)PCN compositions, the diffusivity (γ) and diffuseness parameter (δ) can be estimated from the slope and intercept of the dielectric data shown in Fig. 4, and tabulated in Table II.

γ and δ are both material constants depending on the composition and structure of the material.[5] γ is the expression of the degree of dielectric relaxation, while δ is used to measure the degree of diffuseness of the phase transition. In a material with a "pure" diffuse phase transition described by the Smolenskii–Isutov relation [eq. (2)], γ is expected to be 2.[26] The mean value of the diffusivity (γ) is extracted from these plots by fitting a linear equation. The values of γ vary between 1.52 and 1.97, which confirms that diffuse phase transition occurs in the PZT–PCN system. It is important to note that in perovskite ferroelectrics, it has been established that γ and δ can be affected by microstructure features, density, and grain size.[18] For PZT-rich ceramics, γ and δ increase with an increase in PCN content, confirming the diffuse phase transitions in PZT–PCN solid solutions. It is clear that the addition of PCN increases the degree of disorder in $(1-x)$PZT–(x)PCN over the compositional range $0.1 \leq x \leq 0.5$ with the highest degree of diffuseness exhibited in the 0.5PZT–0.5PCN composition. It should also be mentioned here that different dielectric behaviors could also be caused by grain size variation,[21] as noted in Table I.

The polarization–field (P–E) hysteresis loops of $(1-x)$PZT–(x)PCN ceramics measured at 15 kV/cm are shown in Fig. 5. A series of well-developed and mostly symmetric hysteresis loops are observed for all compositions. It is seen that the remanent polarization (P_r) varies significantly across the compositional range. However, the coercive field E_c is relatively constant, as shown in Table II. The ferroelectric parameters obtained from the P–E loops are plotted in Fig. 6. The remnant polarization (P_r) and saturated polarization (P_s) increased from $P_r = 2.9\,\mu C/cm^2$ and $P_s = 4.1\,\mu C/cm^2$ in 0.9PZT–0.1PCN to reach maximum values of $P_r = 20.9\,\mu C/cm^2$ and $P_s = 22.6\,\mu C/cm^2$ in 0.7PZT–0.3PCN. At higher PCN contents, they then drop to $P_r = 14.5\,\mu C/cm^2$ and $P_s = 15.2\,\mu C/cm^2$ in 0.5PZT–0.5PCN. However, it should be noted that the P_r (2.9 $\mu C/cm^2$) for the composition $x = 0.1$ in the present work is

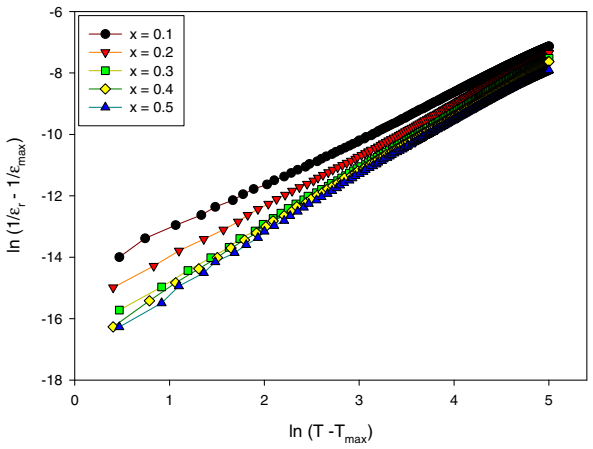

Fig. 4. (Color online) Variation of $\ln(1/\varepsilon_r - 1/\varepsilon_{max})$ vs $\ln(T - T_{max})$ of $(1-x)$PZT–(x)PCN ceramics.

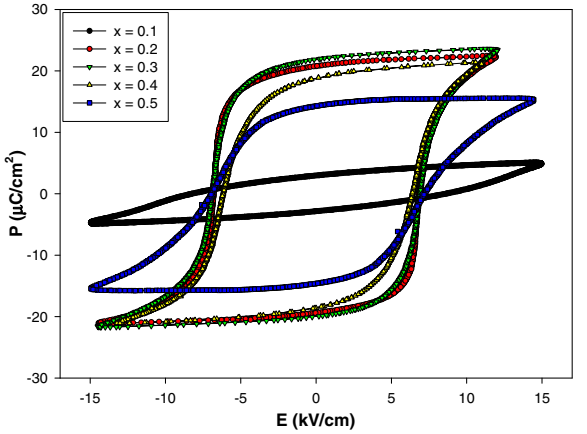

Fig. 5. (Color online) Effect of composition (x) on P–E hysteresis loops for $(1-x)$PZT–(x)PCN ceramics with $x = 0.1$–0.5.

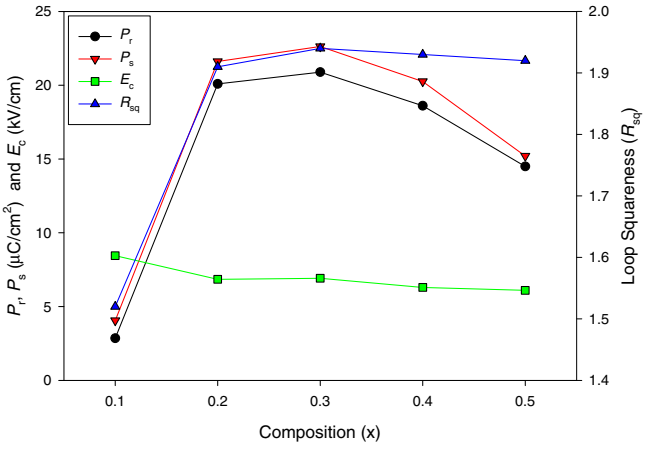

Fig. 6. (Color online) Remnant polarization (P_r), saturation polarization (P_s), coercive field (E_c), and loop squareness (R_{sq}) of $(1-x)$PZT–(x)PCN ceramics.

lower than the P_r ($\sim 15\,\mu C/cm^2$) in a previous study,[20] probably due to the fact that the solid-state conventional mixed oxide method used in the previous study[20] yielded two MPB compositions at $x = 0.1$ and 0.5, which is different from the columbite–wolframite method used in this study, which showed only one MPB composition at approximately $0.2 \leq x \leq 0.3$. It is well known that ferroelectric values, such as P_r, P_s, and E_c, show maximum values approximately at the MPB composition.

An empirical relationship between remnant polarization (P_r), saturation polarization (P_s) and polarization at the fields above the coercive field was derived by Haertling and Zimmer.[27] This permits the quantification of changes in the hysteresis behavior for the $(1-x)$PZT–(x)PCN samples through the following equation:

$$R_{sq} = \frac{P_r}{P_s} + \frac{P_{1.1E_c}}{P_s}, \quad (4)$$

where R_{sq} is the squareness of the hysteresis loop and $P_{1.1E_c}$ is the polarization at an electric field equal to 1.1 times the coercive field (E_c). For an ideal hysteresis loop, R_{sq} is equal to 2.0. As listed in Table II, the loop squareness parameter R_{sq} increased from 1.52 in 0.9PZT–0.1PCN to reach the maximum value of 1.94 in 0.7PZT–0.3PCN before decreasing to 1.92 in the 0.5PZT–0.5PCN composition. This observation is in good agreement with the *P–E* hysteresis loops, as depicted in Fig. 5. The results imply that the addition of 30 mol % PCN into PZT results in an optimized square *P–E* loop.

4. Conclusion

In this study, ceramics within the $(1-x)Pb(Zr_{1/2}Ti_{1/2})O_3$–$(x)Pb(Co_{1/3}Nb_{2/3})O_3$ solid solution system (where $x = 0.1$–0.5) were successfully prepared using a solid-state mixed-oxide technique. The PZT ceramic was identified by XRD analysis as a single-phase tetragonal perovskite, while the addition of PCN resulted in a gradual shift from tetragonal symmetry to pseudo cubic symmetry, with a possible MPB between the two phases located near the 0.7PZT–0.3PCN composition. However, the dielectric and ferroelectric properties did not show anomalously high value for the dielectric and ferroelectric properties at the 0.7PZT–0.3PCN composition, indicating that the MPB composition shifted to $0.2 \leq x \leq 0.3$ in the PZT–PCN system.

Acknowledgements

This work was supported by the Commission on Higher Education (CHE), the Thailand Research Fund (TRF), the Faculty of Science, and the Graduate School of Chiang Mai University.

1) A. J. Moulson and J. M. Herbert: *Electroceramics: Materials, Properties, Applications* (Wiley, Chichester, U.K., 2003).
2) S.-E. Park and T. R. Shrout: IEEE Trans. Ultrason. Ferroelectr. Freq. Control **44** (1997) 1140.
3) J. Kuwata, K. Uchino, and S. Nomura: Ferroelectrics **37** (1981) 579.
4) M. L. Mulvihill, L. E. Cross, W. Cao, and K. Uchino: J. Am. Ceram. Soc. **80** (1997) 1462.
5) N. Vittayakorn, G. Rujijanagul, X. Tan, M. A. Marquardt, and D. P. Cann: J. Appl. Phys. **96** (2004) 5103.
6) H. Fan, G.-T. Park, J.-J. Choi, J. Ryu, and H.-E. Kim: J. Mater. Res. **17** (2002) 180.
7) O. Furukawa, Y. Yamashita, M. Harata, T. Takahashi, and K. Inagaki: *5th Meet. Ferroelectric Materials and Their Applications, Kyoto, 1985*, Jpn. J. Appl. Phys. **24** (1985) Suppl. 24-3, p. 96.
8) V. J. Tennery, K. W. Hang, and R. E. Novak: J. Am. Ceram. Soc. **51** (1968) 671.
9) D. Luff, R. Lane, K. R. Brown, and H. J. Marshallsay: Trans. J. Br. Ceram. Soc. **73** (1974) 251.
10) L. E. Cross: Mater. Chem. Phys. **43** (1996) 108.
11) G. A. Smolenskii and A. L. Agranovskaya: Sov. Phys. Tech. Phys. **3** (1958) 1380.
12) T. Kudo, T. Yazaki, F. Naito, and S. Sugaya: J. Am. Ceram. Soc. **53** (1970) 326.
13) B. A. Malkov and Y. N. Venevtsev: Izv. Akad. Nauk Neorg. Mater. **13** (1977) 1468 [in Russian].
14) V. D. Saĺniov, Y. S. Kuźminov, and Y. N. Venevtsev: Izv. Akad. Nauk Neorg. Mater. **7** (1971) 1277 [in Russian].
15) C. Xu, Z. Duan, X. Wang, D. Yang, and K. Chen: J. Cryst. Growth **281** (2005) 543.
16) N. Vittayakorn, C. Puchmark, G. Rujijanagul, X. Tan, and D. P. Cann: Curr. Appl. Phys. **6** (2006) 303.
17) N. Vittayakorn, G. Rujijanagul, T. Tankasiri, X. Tan, and D. P. Cann: Mater. Sci. Eng. B **108** (2004) 258.
18) R. Yimnirun, S. Ananta, and P. Laoratanakul: J. Eur. Ceram. Soc. **25** (2005) 3235.
19) T. Hachiga, S. Fujimoto, and N. Yasuda: J. Phys. D **20** (1987) 1291.
20) N. Vittayakorn, S. Wirunchit, S. Traisak, R. Yimnirun, and G. Rujijanagul: Curr. Appl. Phys. **8** (2008) 128.
21) R. Yimnirun, S. Ananta, and P. Laoratanakul: Mater. Sci. Eng. B **112** (2004) 79.
22) I. W. Chen, P. Li, and Y. Wang: J. Phys. Chem. Solids **57** (1996) 1525.
23) G. H. Haertling: J. Am. Ceram. Soc. **82** (1999) 797.
24) A. Halliyal, U. Kumar, R. E. Newnham, and L. E. Cross: Am. Ceram. Soc. Bull. **66** (1987) 671.
25) R. D. Shannon and C. T. Prewitt: Acta Crystallogr., Sect. B **25** (1969) 925.
26) Y.-M. Chiang, D. P. Birnie, and W. D. Kingery: *Physical Ceramics* (Wiley, Chichester, U.K., 1997) p. 522.
27) G. H. Haertling and W. J. Zimmer: Am. Ceram. Soc. Bull. **45** (1966) 1084.

J. Phys. D: Appl. Phys. **41** (2008) 085406 (5pp) doi:10.1088/0022-3727/41/8/085406

Changes in dielectric properties of $Pb(In_{1/2}Nb_{1/2})O_3$-$PbTiO_3$ ceramics under compressive stress applied parallel and perpendicular to an electric field

M Unruan, S Wongsaenmai, Y Laosiritaworn, S Ananta and R Yimnirun[1]

Department of Physics, Faculty of Science, Chiang Mai University, Chiang Mai, 50200, Thailand

E-mail: rattikornyimnirun@yahoo.com

Received 16 November 2007, in final form 25 January 2008
Published 12 March 2008
Online at stacks.iop.org/JPhysD/41/085406

Abstract

The influences of compressive stress on the dielectric properties of $(1-x)Pb(In_{1/2}Nb_{1/2})O_3$–$xPbTiO_3$ ($x = 0.1$–0.5) ceramics was investigated in this study. The dielectric properties were measured under compressive stress applied parallel and perpendicular to electric field. The results clearly showed that the superimposed compression stress had pronounced effects on the dielectric properties of PIN–PT ceramics. In general, with increasing compressive stress the dielectric constant of the ceramics increased and decreased when the stress was applied parallel and perpendicular, respectively, to the electric field direction. The dielectric loss tangent, however, decreased in both stress cases. The observations were mainly interpreted in terms of competing influences of the domain switching through non-180° domain walls, clamping of domain walls, de-ageing and the stress-induced decrease in the switchable part of spontaneous polarization.

(Some figures in this article are in colour only in the electronic version)

1. Introduction

There has been a great deal of interest in lead indium niobate, $Pb(In_{1/2}Nb_{1/2})O_3$ (PIN), because it can be obtained in a disordered state and can be made to exhibit a transition from the disordered state to the ordered state by long-time thermal annealing. In the disordered state, PIN is a relaxor ferroelectric (RFE) with rhombohedral symmetry. On the other hand, the ordered PIN structure is antiferroelectric (AFE) with orthorhombic symmetry [1]. However, the temperature related to the maximum dielectric constant (T_{max}) of PIN in the RFE phase is low (at 1 kHz, $T_{max} = 66\,^{\circ}C$) [2, 3]. Thus, to enhance the dielectric properties of PIN (as well as increasing T_{max}), lead titanate, $PbTiO_3$ (PT) is added to PIN with compositions $(1-x)$PIN–xPT (for $x = 0.1$–0.5).

Piezoelectric and ferroelectric ceramics are widely used in devices such as actuators and transducers. However, when they are used in devices specified above, these ceramics are often subjected to self-induced or environmental stresses [4–6]. A prior knowledge of the effects of stresses on the material properties is crucial for proper design of a device and for suitable selection of materials for a specific application [7–9]. Therefore, it is very important to obtain experimental data, as well as to better understand how these materials behave under stress [10–12]. Recently, the compressive stress dependence of dielectric properties has been studied in materials such as $BaTiO_3$ (BT), $Pb(Zr_{0.52}Ti_{0.48})O_3$ (PZT), $Pb(Mg_{1/3}Nb_{2/3})O_3$ (PMN), $Pb(Mg_{1/3}Nb_{2/3})O_3$–$PbTiO_3$ (PMN–PT), $Pb(Mg_{1/3}Nb_{2/3})O_3$–$Pb(Zr_{0.52}Ti_{0.48})O_3$ (PMN–PZT) and $Pb(Zr_{0.52}Ti_{0.48})O_3$–$BaTiO_3$ (PZT–BT) [13–22]. The results clearly showed that the effects of stress on the dielectric properties depended significantly on ceramic compositions and stress levels. Practically, there have been many previous reports on the electrical properties of PIN and PT ceramics, but there has been no systematic study on the influence of an applied stress on the dielectric properties of the PIN–PT ceramics. Earlier investigation has

[1] Author to whom any correspondence should be addressed.

Table 1. Characteristics of PIN–PT ceramics with optimized processing conditions (measured at 10 kHz) [28, 29].

Ceramic	Sintering temperature (°C)	Density (g cm^{-3})	T_{max} (°C)	Room-temperature stress-free dielectric properties	
				ε_r	tan δ
0.9PIN–0.1PT	1100	7.78	134	2275	0.105
0.8PIN–0.2PT	1125	7.85	213	863	0.053
0.7PIN–0.3PT	1125	7.81	292	689	0.028
0.6PIN–0.4PT	1125	7.85	355	1132	0.049
0.5PIN–0.5PT	1125	7.80	398	483	0.083

already revealed the significance of stress-induced ferroelectric phase transition in PIN-based materials [23]. Therefore, it is the aim of this study to determine the dielectric properties of the $(1-x)$PIN–xPT ceramics as a function of compressive stress. Comparison between the changes in the dielectric properties under compressive stress applied parallel and perpendicular to the electric field direction is reported.

2. Experimental method

In this study, $(1-x)Pb(In_{1/2}Nb_{1/2})O_3$–$xPbTiO_3$ (for $x = 0.1$–0.5) ceramics were prepared from the two stage mixed-oxide method. First, $InNbO_4$ was first prepared from oxide powders of Nb_2O_5 and In_2O_3. The powders were mixed by a rapid vibratory mill for 30 min in alcohol. After drying, the mixture was calcined at 1100 °C for 2 h to obtain the intermediate precursor $InNbO_4$ [24]. Next, the precursor was mixed with an appropriate amount of PbO and TiO_2 by a rapid vibratory mill for 30 min. For optimization purposes, the mixtures were calcined at temperatures between 800 and 900 °C for 2 h. After calcination, the powders were pressed hydraulically to form disc-shaped pellets of 10 mm in diameter and 3 mm thick, with 3 wt% polyvinyl alcohol as a binder. Finally, the disc-shaped pellets were sintered in air at temperatures between 1100 and 1125 °C for 2 h. The sintering temperature was determined from the maximum density and phase purity. The sintering temperature of 1100 °C was the optimized condition for 0.9PIN–0.1PT, and 1125 °C for the other compositions, as listed in table 1. The detailed preparation process is given elsewhere [25]. Before studying the dielectric properties under compressive stress, the sintered specimens were cut as rectangular bars (typical dimensions $6\times2\times2$ mm^3) and lapped to obtain parallel faces. After coating with silver paint as an electrode at the faces, the specimens were heated at 750 °C for 12 min to ensure contact between the electrode and the surface of the ceramic.

To study the effects of stress on the dielectric properties of the ceramic, the compressometer was constructed for simultaneous applications of the mechanical stress and the electric field [26]. The compressometer cell, consisting of a cylindrical brass cell with a heavy brass base, a brass ram and a precisely guided loading platform, provided true uniaxial stress during mechanical loading. The compressive stress was supplied by the servohydraulic load frame and the applied stress level was monitored with the pressure gauge of the load frame. Measurements were performed as a function of mechanical pre-stress applied discretely [27]. For the case of the compressive stress applied parallel to the electric field direction, the specimen bar was carefully placed between the two alumina blocks and the electric field was applied to the specimen via the copper shims attached to the alumina blocks. For the case of stress perpendicular to the electrical field, the electrodes were applied on the other two opposite faces with silver wire attached to the electrodes for electrical measurement. The low-field dielectric properties were measured by an LCR-meter (Instrek LCR-821) with an applied voltage of 1 V. The room temperature (25 °C) capacitance and the dielectric loss tangent were determined at a frequency of 10 kHz. The dielectric constant was then calculated from a parallel-plate capacitor equation, e.g. $\varepsilon_r = Cd/\varepsilon_0 A$, where C is the capacitance of the specimens, d and A are, respectively, the thickness and the area of the electrode and ε_0 is the dielectric permittivity of vacuum (8.854×10^{-12} F m^{-1}). In addition, it should also be noted that the dielectric properties could be affected by the collapse of the structure of silver paint electrode under compressive stress. Therefore, a careful examination of the specimens' electrodes was taken after the measurements, and there was no clear evidence of the collapse of the electrodes. This is probably due to the relatively low stress level used.

3. Results and discussion

Since this work reports the dielectric properties of PIN–PT ceramics under the application of compressive pre-stress, the following paragraph is only served as preliminary information on structural and dielectric characteristics under stress-free conditions, which are important in the discussion of the influence of stress on the dielectric properties of the ceramics. More information on the above mentioned characteristics can be found in previous publications [28, 29]. By the x-ray diffraction method, the phase and structural information of the PIN–PT ceramics was established [29]. In general, pseudo-cubic symmetry was observed at low PT contents ($x = 0.1$, 0.2 and 0.3). However, by the influence of PT, the tetragonal symmetry had developed in the compositions $x = 0.4$ and 0.5. The dielectric constant (ε_r) was also measured as functions of both temperature and frequency, as previously described in detail in previous publications [28, 29]. In compositions $x = 0.4$ and 0.5, the dielectric properties were nearly independent of frequency, except in the vicinity of the phase transformation temperature; a typical characteristic of normal ferroelectrics. At low PT contents, the dielectric behaviour was shifted towards that of relaxor materials. The dielectric properties of the compositions with $x \leqslant 0.3$ exhibited a diffuse phase transition with dielectric peak broadening. As listed in table 1, the high value of dielectric constant under stress-free conditions at room temperature is obtained in ceramic composition with $x = 0.4$ because of its vicinity to the morphotropic phase boundary (MPB) of the PIN–PT system, as reported earlier [1, 28, 29]. In addition, the high room temperature dielectric constant for $x = 0.1$ composition is due to the fact that dielectric maximum temperature (T_{max})

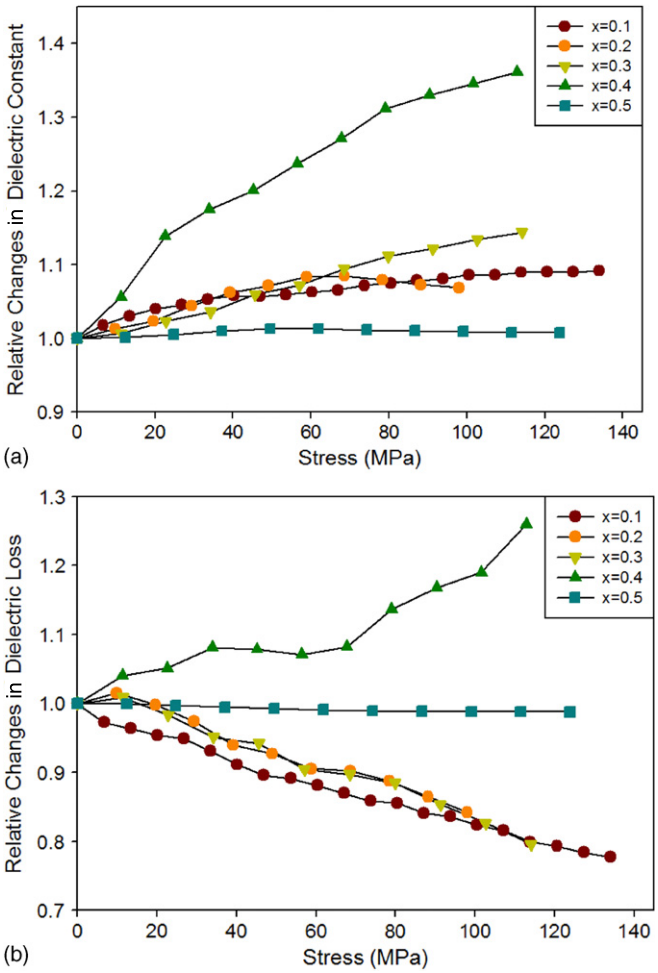

Figure 1. (*a*) Relative changes in dielectric constant (ε_r) and (*b*) relative changes in dielectric loss tangent ($\tan\delta$) with compressive stress applied parallel to the electric field direction for $(1-x)$PIN–xPT ceramics (measured at 25 °C and 10 kHz).

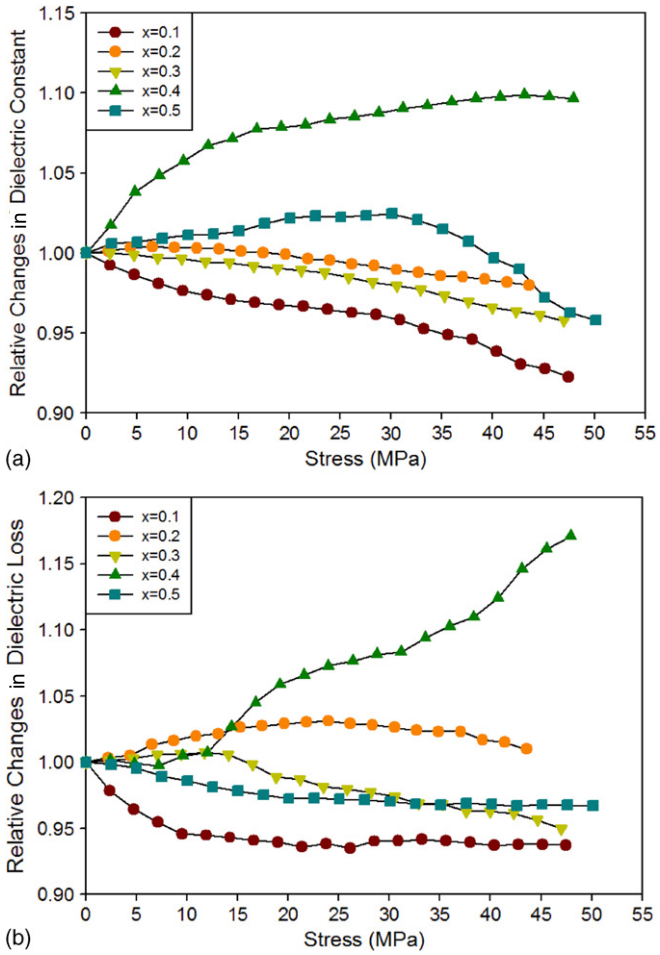

Figure 2. (*a*) Relative changes in dielectric constant (ε_r) and (*b*) relative changes in dielectric loss tangent ($\tan\delta$) with compressive stress applied perpendicular to the electric field direction for $(1-x)$PIN–xPT ceramics (measured at 25 °C and 10 kHz).

of 134 °C is much closer to room temperature than T_{max} of other compositions. Hence, the dielectric peak is on the rise in this composition, and results in a higher room temperature dielectric constant value than that of other compositions.

The room temperature dielectric properties at 10 kHz of $(1-x)$PIN–xPT ceramics as a function of compressive stress are depicted in figures 1 and 2. For better comparison, the dielectric properties of each composition under stress are normalized to the stress-free values. In addition, the measurements were performed with the mechanical stress increased to maximum stress, then gradually removed to zero. The results showed only slightly different dielectric properties between loading and unloading conditions, which differ from results previously observed in other ceramic systems and PIN–PT with poled specimens, likely caused by the stress-induced depoling mechanism at high stress [21, 30–32]. Therefore, the averaged changes in the dielectric properties with stress are plotted in figures 1 and 2. Clearly, there are observable changes in both the dielectric constant and the dielectric loss tangent with stress, in both cases of the compressive stress being applied either parallel or perpendicular to the electric field direction.

For the case of stress parallel to the electric field direction, as depicted in figures 1(*a*) and (*b*), the changes in the dielectric properties with stress can be divided into three groups. As shown in figure 1(*a*), for the pseudo-cubic compositions ($x = 0.1$–0.3), the dielectric constant increases noticeably (5–12%) when the stress reaches 100 MPa. On the other hand, the dielectric loss tangent ($\tan\delta$) is seen to decrease significantly (20–25%) with increasing stress, as displayed in figure 1(*b*). Interestingly, for the tetragonal composition ($x = 0.5$), the dielectric properties (both dielectric constant and dielectric loss tangent) show very little change with stress. More interestingly, the dielectric properties of the composition with $x = 0.4$, which is very close to the MPB of PIN–PT system (at $x \sim 0.37$ [33]), increase significantly with the applied stress (30% at maximum stress). It is also noticed that the changes in the dielectric properties with the compressive stress obtained in this study are in parts similar to those for BT, PZT, PMN–PZT and PMN–PT systems in earlier investigations [13, 14]. Other investigations on commercial hard and soft PZT ceramics also observed similar changes in the dielectric properties with the compressive stress applied parallel to the electric field direction [20, 21, 31].

For the case of stress applied perpendicular to the electric field direction, as depicted in figures 2(*a*) and (*b*), the changes in the dielectric properties with stress are significantly different from the parallel stress case. As shown in figure 2(*a*), for the pseudo-cubic compositions ($x = 0.1$–0.3), the dielectric constant decreases with the applied stress, as opposed to the parallel stress case. Interestingly, for the tetragonal compositions ($x = 0.5$), the dielectric constant first increases with stress, then decreases with further increase in the applied stress. On the other hand, the dielectric constant of the near MPB composition $x = 0.4$ still shows an increasing trend with applied stress. It is of interest to observe that the changes in the dielectric loss tangent with stress of all compositions are similar to those in the case of the parallel stress, as shown in figure 2(*b*). For the case of the compressive stress applied perpendicular to the direction of the electric field, only a few previous experimental works have been carried out on some commercial hard and soft PZT ceramics, and PMN–PT ceramics [21, 30, 31, 34]. Interestingly, the results observed in this study are in general very similar to those obtained earlier in PZT and PMN–PT ceramics mentioned above.

To understand these experimental results, at least qualitatively, various effects have to be considered. When a compressive stress is applied to the ferroelectric materials, the domain structure in the material will change to maintain the domain energy at a minimum because the stress will move some of the polarization away from its polar direction; during this process some of the domains engulf other domains or change shape irreversibly. Under a stress, the domain structure of ferroelectric ceramics may undergo domain switching through non-180° domain walls, de-ageing and clamping of domain walls [15, 18, 21, 31].

The experimental observations, both the drastic change and the very little change cases, can be attributed to competing influences, in an opposite way, of the intrinsic contribution of domains and the extrinsic contribution of re-polarization and growth of micro-polar regions. Under the applied compressive stress, the non-180° domain wall density increases. Hence the increase in the dielectric constant is observed. The de-ageing mechanism, which also increases the dielectric constant [14–16, 21], is also expected to play a role here. Therefore, a combination of the domain switching and the de-ageing mechanisms is believed to be a reason for the increase in the dielectric constant. On the other hand, the stress clamping of domain walls, which results in a decrease in domain wall mobility, and the stress-induced decrease in the switchable part of spontaneous polarization are expected to play a role in the decrease of the dielectric constant [14, 21, 31]. In addition, the continuous decrease in the dielectric constant can also be attributed to the switching of 90° domains, which causes the significant decrease in the dielectric constant. With all these possible mechanisms stated, one can easily understand the experimental results obtained. In the case of parallel stress, a combination of the domain switching and the de-ageing mechanisms is believed to be a reason for the increase in the dielectric constant in all compositions, as shown in figure 1(*a*). In addition, a large increase in the dielectric constant of the near MPB composition, i.e. 0.6PIN–0.4PT, is attributed to more domain states in the composition which combines six possible domain states from the tetragonal phase with 8 possible domain states from the pseudo-cubic (or rhombohedral) phase [7], hence a much larger non-180° domain wall density and a larger change are observed. This mechanism still dominates in the case of the perpendicular stress for the same composition, which results in an increase in the dielectric constant, while the other compositions show a slight decrease in the dielectric constant when the stress is applied perpendicular to the direction of the electric field, as depicted in figure 2(*a*). This observation suggests that the stress clamping of domain walls and the stress-induced decrease in the switchable part of spontaneous polarization play a key role in controlling the change in the dielectric constant with the stress applied in the perpendicular direction to the electric field. It should also be noticed that the dielectric constant of 0.5PIN–0.5PT are rather stable under applied stress when compared with the near MPB 0.6PIN–0.4PT composition. This suggests the influence of different structures. As stated above, the 0.6PIN–0.4PT composition contains mixed tetragonal–rhombohedral phases with more possible domain states (14), while the 0.5PIN–0.5PT contains mainly tetragonal phases with only six domain states, hence much smaller changes in dielectric properties. In addition, since the measurements were carried out at room temperature, which is far below the transition temperature of 398 °C for the 0.5PIN–0.5PT composition, the domain is much less mobile and the change in the dielectric properties is also much less. This also explains why the change in the dielectric properties with the applied stress of this composition is much less than that of other non-MPB compositions with much lower transition temperatures. In addition, a little decrease in the dielectric constant after a full cycle of stress application has been observed and attributed to the stress-induced decrease in the switchable part of spontaneous polarization at high stress and the irreversible 90° domain switching [15, 31].

The cause of the stress dependence of the dielectric loss tangent is a little more straightforward. In both the parallel and the perpendicular stress cases, as observed in figures 1(*b*) and 2(*b*), the clamping of the domain walls under compressive stress results in a decrease in domain wall mobility and reduces the dielectric loss tangent in the $x = 0.1$–0.3 compositions [21, 31]. This is a reversible effect with the domain wall mobility returning to near the original values when the applied stress is removed, as stated earlier that the dielectric properties return to near their original values after a stress cycle. On the other hand, it should be noted that a noticeable increase in the dielectric loss tangent of the 0.6PIN–0.4PT composition is observed, as seen in figures 1(*b*) and 2(*b*). Similarly to the dielectric constant changes with stress, this is mainly attributed to more available domain states of 14 and hence more domain wall mobility in this near MPB composition. Moreover, the de-ageing mechanism is also expected to play a role in the increase in dielectric response with stress in this composition. During the ageing process, some of the domain walls become pinned by impurities and structural imperfections. When a large enough stress is applied to the aged samples, it causes structural changes and redistribution of impurities. As a